UiO : University of Oslo

Fabio Zeiser

Uncertainty quantification for nuclear level densities and γ-ray strength functions from the Oslo method and beyond

Thesis submitted for the degree of Philosophiae Doctor

Department of Physics
Faculty of Mathematics and Natural Sciences

2021

Series of dissertations submitted to the
Faculty of Mathematics and Natural Sciences, University of Oslo
No. 2369

ISSN 1501-7710

Cover: Hanne Baadsgaard Utigard.
Print production: Reprosentralen, University of Oslo.

Handling instructions

Despite their brevity, the stories in this book are full-fledged writings. Their advantage is, that one saves time with them, since they do not require our attention for weeks or months. While the soft-boiled egg is cooking or until the number you are dialing answers (provided it is engaged, of course), read a one-minute story. Feeling unwell or shattered nerves are not an obstacle. [. . .]
Attention!
If there is something you don't understand, reread the story in question. If you still don't understand then the fault lies with the author.
There are no dim-witted people, only badly written one-minute stories.

Használati utasítás

A mellékelt novellák rövidségük ellenére is teljes értékű írások. Előnyük, hogy az ember időt spórol velük, mert nem igényelnek hosszú hetek-hónapokra terjedő figyelmet. Amíg a lágy tojás megfő, amíg a hívott szám (ha foglaltat jelez) jelentkezik, olvassunk el egy Egyperces Novellát. Rossz közérzet, zaklatott idegállapot nem akadály. [. . .]
Figyelem!
Aki valamit nem ért, olvassa el újra a kérdéses írást. Ha így sem érti, akkor a novellában a hiba.
Nincsenek buta emberek, csak rossz Egypercesek!

István Örkény, *Egyperces novellák (One-minute stories)*

Abstract

Nuclear level densities (NLD) and γ-ray strength functions (GSF) are essential average characteristics of the atomic nucleus. They describe the number of levels in an excitation energy interval and electromagnetic transition probabilities, respectively. There has been significant progress in the theoretical descriptions, but experimental information is necessary to "gauge" the quality of different models. Furthermore, the NLD and GSF are important ingredients to cross-section calculations, which are used in a variety of applications spanning from nuclear energy and nuclear medicine to astrophysics and the quest of understanding how our universe was formed.

This thesis contributes to the understanding and quantification of uncertainties in measurements of NLDs and GSFs with a focus on the so-called Oslo method. We have developed a new Python library, OMpy, which reimplements the data analysis software used in the Oslo method. It enables, for the first time, a complete propagation of statistical errors from the raw data to the final results and permits the treatment of several types of systematic errors. Moreover, it enhances research reproducibility through a transparent documentation and facilitates the publication of all steps of the analysis.

For the interpretation of any measurement it is important to characterize the measurement devices. Therefore, we have determined the energy response of the recently commissioned γ-ray detector array OSCAR at the Oslo Cyclotron Laboratory.

We have conducted an experiment to find the NLD and GSF of ^{240}Pu. The particular challenges of the (d, p) reaction on a heavy target nucleus are explored, it is shown to violate an assumption of the Oslo method, and a new procedure to mitigate this problem is presented. Moreover, special challenges in the cross-section calculations for actinides are discussed.

We present the new code gledeli, which puts measurements on NLDs and GSFs in a broader perspective, as it facilitates the simultaneous analysis of several experimental techniques. The combined fits are particularly suitable for the evaluation of theoretical descriptions and to find recommended NLD and GSF parametrizations, that can be used in cross-section calculations.

Finally, the work on actinide targets has lead us to the development of a novel technique to estimate prompt-fission γ rays. We use the (d, p) reaction as a surrogate for fast-neutron induced fission to study the spectral characteristics as a function of excitation energy. This reaction enables us to report on the average multiplicity, and the total and average γ-ray energy emitted in the fission of the compound nuclei $^{234}\mathrm{U}^*$ and $^{240}\mathrm{Pu}^*$.

Acknowledgements

First and foremost I would like to thank my supervisors Gry M. Tveten, Ann-Cecilie Larsen and Sunniva Siem. Gry has been a role model to me: smart, thorough and curiously thinking outside the box. During the past years she has not only been my supervisor, but also a friend and we shared the office, good memories and considerable amounts of *kanelboller*. Blindern has never been the same after you left for new endeavours. I would like to thank Ann-Cecilie for the many, sometimes heated, debates on all details of our work. I think science lives from this. Sunniva has always been a positive and encouraging and it is difficult to overrate her efforts that make this group thrive. I am very grateful for the confidence all of you have had in me and the freedom you gave me to find my own perspective.

This thesis has been a journey and much of it would not have been possible without the efforts of my collaborators. Luckily, I met Jørgen E. Midtbø and Erlend Lima along my path. Jørgen has been a great source of inspiration. He started the work on OMpy, whereas I came in from the other end and I think we have reasons to be proud of the final product. I was able to win Erlend for our project, without whom I would still write programs that distress my future me and cut garlic cloves instead of crushing them.

It was both a great pleasure and I have learned a lot from Dorthea Gjestvang, whom I co-supervised on her Master thesis. I was glad to see how she embraced the work Sunniva Rose and I started on prompt-fission γ-rays and relieved, because she would, one after the other, tackle all problems Sunniva and I had only touched upon. I would like to thank Sunniva Rose for her enthusiasm and for encouraging us to move forward, where I could have spent years on all the small details.

Anders Kvellestad patiently helped me to distill our problems. I wish I would have started to work with him much earlier. To date, he is still the only person I follow on twitter, mostly because of the now well-known fact that he has a *samfunnskritiske funksjon*.

I would like to express my gratitude to Gregory Potel and Stephan Oberstedt on both personal and scientific accounts. To Kristine Beckmann for sharing joy and sadness with me. It was a pleasure to get to know and work with Frank L. Bello Garrote, Magne Guttormsen, Vetle W. Ingeberg and all other members of the nuclear physics group at UiO.

The past four years have not only been a scientific, but also a personal development. Of my many "mentors", I am most indebted to Morten, who included me in his family and taught me how to enjoy winter even if you, literally, end up setting up your tent in a snow storm. Pär continued to push me on cross-country skiing and found an open door to a woodshed when we turned

up at the wrong cabin after a night where maybe just should have stayed *værfast*. Wictor believed in us and proved that it does not need a PhD to be *lurere enn Luhr*, but that working on a PhD is not a hindrance either. The isolated crag you found this spring probably saved my sanity.

I can still recall the time when I said that it was never my ambition, but if I ever become a *professor*, it is due to the spirit and energy of Philippe, Maclau and Isak. *Axé Capoeira.*

I would like to thank Viola for making me fall in love with Hungarian, and Johannes for choosing Hungarian courses with me instead of Swedish – who would ever have a use for Swedish, I naively thought back then. *Ez a világ a legtökéletesebb az összes lehetséges világok között – Diese Welt ist die vollkommenste aller möglichen Welten.*

My family has been a strong support all along. I would not stand here without my brother, the philosophical discussions during the time we actually should have spent on our homework, and all the care and chocolate pudding we received by *Frau Schnorr*. My father nourished my curiosity and gave me the freedom to discover the world. My mother, who always believed in me. I am incredibly grateful that you were able to visit me here and share the simple pleasures of life, pitting cherry-stones.

A special thanks to Synnøve. With you it was a joy, not a burden, to stay at home this spring – so much that I never returned to Blindern over the summer.

List of Papers

This thesis is based on following six papers:

Paper I

Midtbø, J. E.[†], Zeiser, F.[†], Lima, E. Larsen, A. C. Tveten, G. M. Guttormsen, M. Bello Garrote, F. L. Kvellestad, A. and Renstrøm, T. "A new software implementation of the Oslo method with rigorous statistical uncertainty propagation". Accepted for publication in: *Computer Physics Communications*. arXiv: 1904.13248.
Erratum: Published after submission, CPC Vol. 262 (2021) 107795. DOI: 10.1016/j.cpc.2020.107795.

Paper II

Zeiser, F., Tveten, G. M., Bello Garrote, F. L., Guttormsen, M., Larsen, A. C., Ingeberg, V. W., Görgen, A. and Siem, S. "The γ-ray energy response of the Oslo Scintillator Array OSCAR". To appear in: *NIM A*. Vol. 985, (2021) 164678, DOI: 10.1016/j.nima.2020.164678. arXiv: 1708.04101

Paper III

Zeiser, F., Potel, G., Tveten, G. M., Larsen, A. C., Guttormsen, M., Laplace, T. A., Siem, S., Bleuel, D. L., Goldblum, B. L., Bernstein, L. A., Bello Garrote, F. L., Crespo Campo, L., Eriksen, T. K., Hadynska-Klek, K., A. Görgen K., Midtbø, J. E., Renstrøm, T., Sahin, E., Tornyi, T., Voinov, A. and Wiedeking, M. "Impact of restricted spin-ranges in the Oslo Method: The example of $(\mathrm{d},\mathrm{p})^{240}\mathrm{Pu}$". Accepted for publication in: *Proceedings of the Compound Nuclear Reactions Workshop, Berkeley 2018*. arXiv: 1902.02966

Paper IV

Zeiser, F., Tveten, G. M., Potel, G., Larsen, A. C., Guttormsen, M., Laplace, T. A., Siem, S., Bleuel, D. L., Goldblum, B. L., Bernstein, L. A., Garrote, F. L. Bello, Campo, L. Crespo, Eriksen, T. K., Görgen, A., Hadynska-Klek, K., Ingeberg, V. W., Midtbø, J. E., Sahin, E., Tornyi, T., Voinov, A., Wiedeking, M. and Wilson, J. "Restricted spin-range correction in the Oslo method: The example of nuclear level density and γ-ray strength function from $^{239}\mathrm{Pu}(\mathrm{d},\mathrm{p}\gamma)^{240}\mathrm{Pu}$". In: *Physical Review C*. Vol. 100 (2019) 024305, DOI: 10.1103/physrevc.100.024305. arXiv: 1904.02932

Paper V

Zeiser, F. and Kvellestad, A. "gledeli: Gamma-ray strength function and nuclear LEvel DEnsity LIkelihoods". *Manuscript in preparation*

Paper VI

Rose, S. J.[‡], Zeiser, F.[‡], Wilson, J. N., Oberstedt, A., Oberstedt, S., Siem, S., Tveten, G. M., Bernstein, L. A., Bleuel, D. L., Brown, J. A., Crespo Campo, L., Giacoppo, F., Görgen, A., Guttormsen, M., Hadyńska, K., Hafreager, A., Hagen, T. W., Klintefjord, M., Laplace, T. A., Larsen, A. C., Renstrøm, T., Sahin, E., Schmitt, C., Tornyi, T. G. and Wiedeking, M. "Energy dependence of the prompt γ-ray emission from the (d, p)-induced fission of $^{234}U^{*}$ and $^{240}Pu^{*}$". In: *Physical Review C*. Vol. 96 (2017) 014601 DOI: 10.1103/PhysRevC.96.014601. arXiv: 1707.01651

[†] These authors are shared first authors with equal contributions.
[‡] These authors are corresponding authors with equal contributions.

Contents

Acknowledgements v

List of Papers vii

Contents ix

1 Introduction 1
- 1.1 Research questions . . . 2
- 1.2 Thesis outline . . . 2

2 Background 5
- 2.1 Level density . . . 5
  - 2.1.1 Empirical models . . . 5
- 2.2 γ-ray strength function . . . 9
  - 2.2.1 Simplifications: Brink–Axel hypothesis . . . 11
  - 2.2.2 Empirical models . . . 13
- 2.3 Microscopic models . . . 16
  - 2.3.1 The Shell model . . . 17
  - 2.3.2 Hartree-Fock method and QRPA . . . 19
- 2.4 Experiments . . . 20
  - 2.4.1 Oslo method . . . 21
  - 2.4.2 Singles γ-ray, two-step and multi-step cascade spectra . . . 22
  - 2.4.3 Nuclear resonance fluorescence . . . 23
  - 2.4.4 Neutron and proton resonance capture . . . 25
  - 2.4.5 Cross sections and evaporation spectra . . . 28
  - 2.4.6 Other experiments . . . 31

3 Summary of Papers 33

4 Summary and outlook 37
- 4.1 Future research . . . 39

Papers 44

I A new software implementation of the Oslo method with rigorous statistical uncertainty propagation 45

II The γ-ray energy response of the Oslo Scintillator Array OSCAR 67

III Impact of restricted spin-ranges in the Oslo Method: The example of $(d, p)^{240}Pu$ 75

IV Restricted spin-range correction in the Oslo method: The example of nuclear level density and γ-ray strength function from $^{239}Pu(d, p\gamma)^{240}Pu$ 85

V gledeli: Gamma-ray strength function and nuclear LEvel DEnsity LIkelihoods 97

VI Energy dependence of the prompt γ-ray emission from the (d, p)-induced fission of $^{234}U^*$ and $^{240}Pu^*$ 113

Appendices 125

A Derivations of the photo-excitation strength function 127

B Supplement to Paper II 131

Bibliography 135

Chapter 1

Introduction

Muss ich mir den subatomaren Raum vorstellen als etwas grosses, ~~ruhiges~~, dunkles, in das man hinabsteigen kann?

Do I have to imagine subatomic space as something huge ~~and silent~~ and dark that you can climb down into?

Peter Fischli und David Weiss *Findet mich das Glück? (Will happiness find me?)*

Almost 40 years after the first application of what has become known as the *Oslo method* [1–4] we have to ask ourselves: *Is there still anything new to discover?* The honest answer has to be that we do not know – otherwise it would not be a discovery – but there are still many important questions to pursue.

The nucleus is a complex quantum mechanical object, but it has been shown that many aspects are well described by average statistical quantities. The Oslo method is an experimental technique that has been at the forefront of the determination of the level density and γ-ray strength function of the atomic nucleus. The initial works have been dedicated exclusively to basic science, the understanding of the nucleus [1, 2, 5–8]. In this respect, the discovery of a strong enhancement in the emission probabilities of low-energy γ rays is regarded as a breakthrough of the Oslo method [9].

As the technique matured, the question of how the results from the Oslo method would impact applications has gained more attention. Nuclear level densities and γ-ray strength functions are essential inputs to the calculation of neutron capture cross-sections, which are a measure for the probability that a nucleus absorbs a neutron and subsequently emits γ-rays. The delicate balance between neutron capture and fission is crucial for the control of the chain reactions that are at the heart of nuclear energy production. A more precise knowledge of neutron capture cross-sections may become more important as the industry pushes towards reactors driven by fast-neutron reactions, where direct cross-section measurements are extremely challenging [10–12].

Another intriguing challenge is to reconstruct how our universe was formed from the abundance of different elements that we can observe today. In stellar environments no elements heavier than iron can be formed through fusion, such that they must have been created through a fine balance between neutron and proton capture, and nuclear decays. If we determine the key inputs to cross-section calculations more precisely by applying i.e. the Oslo method, we can improve our knowledge of the formation of our universe [13–15]. This is a strong claim, and of course, there are other aspects involved; the astrophysical conditions, i.e. where, with how strong neutron fluxes and at what temperatures

the reactions proceeded will arguably have the strongest impact. However, given the recent progress on the determination of the astrophysical sites, the discovery of a neutron-star merger event by the LIGO/Virgo collaboration in 2017 [16], a precise understanding of the nuclear input is essential [15]. However, "with great power must also come – great responsibility".[1]

If we intend to minimize the uncertainties in applications like the above, we need a detailed understanding and quantification of the uncertainties that arise from the experimental measurements and their analysis. A milestone for the Oslo method has been the work of Schiller et al. in 1999/2000 [3]. The authors developed a formalism for a simultaneous fit of the level density and γ-ray strength function to the experimental data that does not require prior assumptions on the parametrization of results. The principle is still used today. Furthermore, they provided an approximation of the uncertainties of this method. Larsen et al. followed this up with an analysis of possible systematic errors in the Oslo method [4]. Given the significant progress in computation power during the past 20 years, it is time to revisit the matter and proceed from approximations to a rigorous quantification of the statistical – and where possible also systematic – uncertainties.

1.1 Research questions

This leads to the following research question for this thesis:

- How can we achieve a *full and justifiable quantification* of the statistical and systematic uncertainties in the Oslo Method?
- Are there limits to the applicability of the Oslo Method?

From my work on actinide targets, the following questions came in addition:

- Can we improve the data processing for actinide targets, where a considerable amount of data is rejected due to the opening of the fission channel?
- What is the impact of our results on neutron capture cross-sections calculations, especially for actinide targets?

1.2 Thesis outline

This thesis is structured as follows. In Chapter 2 I review the foundation and scientific context of this thesis, that is the definition, models and experiments to determine the level density and γ-ray strength function. Chapter 3 provides a short description of the publications that form this thesis. In Chapter 4 I summarize the main findings and present an outlook on further research questions.

[1] This is a quote from S. Lee's *Spider-Man*, but very similar phrases are known e.g. from W. Churchill and T. Roosevelt.

Finally, a reprint of the six articles included in the thesis is provided. Paper I presents a reimplementation of the software for the Oslo method with a focus on the rigorous statistical uncertainty quantification. Paper II characterizes the γ-ray energy response of the new detector array OSCAR. Papers III and IV analyze a specific assumption of the Oslo method, quantify the bias in a case where it is not fulfilled and propose a new correction method. Paper V shifts the focus from the analysis with the Oslo method and demonstrates how we can improve our knowledge of level densities and γ-ray strength functions from the combination of several experimental methods. Finally, in Paper VI a new technique is explored to obtain prompt-fission γ rays from data that has to be rejected in the Oslo method.

Chapter 2

Background

> *Remember that all models are wrong; the practical question is how wrong do they have to be to not be useful.*
>
> — George Box, *Empirical Model-Building and Response Surfaces*

2.1 Level density

Describing a nucleus is a quantum mechanical many-body problem with no easy solution. However, for many applications it has been fruitful to describe the nucleus in terms of macroscopic statistical or phenomenological models. One quantity that is often described through a statistical approach is the nuclear level density ρ, which is a measure for the number of levels N in an energy region ΔE. It is inversely related to the average spacing D between the levels,

$$\rho = \frac{N}{\Delta E} = \frac{1}{D}. \tag{2.1}$$

Note that each level is degenerate with $2J+1$ magnetic substates, such that the state density is given by $\rho^{(\text{state})}(J) = (2J+1)\rho(J)$. From quantum mechanics, it is known that the excited levels are not truly discrete, but have a certain width Γ, which can be related to their lifetime τ through a Fourier transformation resulting in $\Gamma = \hbar/\tau$ [17] [18, p. 412ff]. Nevertheless, the low excitation energy region is usually referred to as the *discrete region*, which can be justified as the width Γ is negligible in comparison to the average level spacing D. With increasing excitation energy E_x, the level spacing D decreases whilst the width Γ increases, until the levels eventually form a *continuum*. This thesis is concerned with the region in-between, the so-called *quasi-continuum*, where the levels do not overlap yet. There, the states are built up by complex enough wave-functions that a statistical treatment is usually sufficient for applications like cross-section calculations.

2.1.1 Empirical models

In the following, I will introduce some of the most widely used phenomenological models for the level density. More details can be found e.g. in the *Reference Input Parameter Library (RIPL3)* [19] and references therein. A graphical comparison of the different models is given for ^{164}Dy in Fig. 2.1.

Backshifted Fermi Gas Model

Already in 1936 Bethe [20] derived the state and level density for non-interacting Fermi gases. I describe Bethe's model in Paper V:

> In 1936 Bethe proposed a level density formula assuming that neutrons and protons form a gas of non-interacting fermions [20]. The model was later amended slightly, allowing the excitation energy E_x to be shifted by a constant E_1 for better fits to observables like the density from discrete levels. The shift is proposed to be connected to the breaking of Cooper pairs, see eg. Ref. [21], even though this differs from an exact derivation based on the Bardeen-Cooper-Schrieffer theory [22, 23]. The level density ρ of the backshifted Fermi gas (BSFG) is given by [24]
>
> $$\rho(E_x) = \frac{1}{12\sigma\sqrt{2\pi}} \frac{\exp\left(2\sqrt{aU}\right)}{a^{1/4}U^{5/4}}, \tag{2.2}$$
>
> where $U = E_x - E_1$ is the effective (backshifted) excitation energy and a is the so-called level density parameter. The spin-cut parameter σ is an energy dependent parameter related to the spin-parity distribution and will be discussed in [Sec. 2.1.1]. At $U = 25/(16a)$, Eq. (2.2) has a minimum and we adopt the procedure of Ref. [25] to set $\rho(E_x)$ constant below this energy to avoid unphysical results.

Implicitly, I have assumed here that the level density parameter a does not depend on the excitation energy E_x, which is consistent with the initial derivation of the (BS)FG model. However, one observes that nuclei closer to magic numbers are best fit by a lower a, which indicates the importance of shell effects. This is also relevant for the dependence of a on the excitation energy E_x as shell effects gradually play a lesser role for higher E_x. A phenomenological description of $a(E_x)$ was first proposed in Ref. [26] and the concept is in agreement with microscopical calculations, see Ref. [19] and references therein. For the works included in this thesis, we only require and obtain information on the level density ρ up to approximately the neutron separation energy S_n. In this regime, the effect of the variation of a on the level density $\rho(E_x)$ is negligible. To minimize the number of free parameters, we therefore use the BSFG formula with a constant a. For Fig. 2.1, I have used the parameters E_1 and a compiled in Ref. [25], together with the Fermi gas spin-cutoff which will be introduced in Eq. (2.7).

Constant Temperature Model

In most recent works of the Oslo group the constant temperature model is used, which I describe in Paper V:

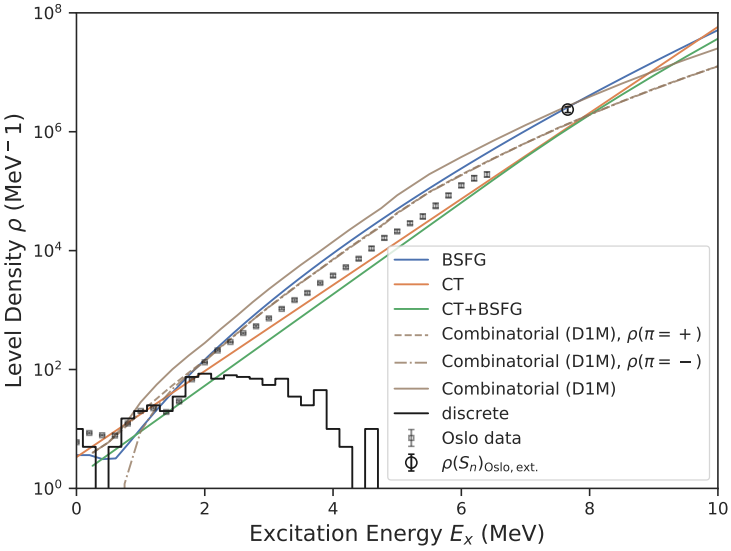

Figure 2.1: Level density of ^{164}Dy obtained from empirical parameterizations [25], theoretical calculations [32] and extracted with the Oslo method [Paper I, 33] . The combinatorial model explicitly takes into account the parity dependence and shows that parity equilibration a good approximation above ≈ 2 MeV. Also shown is $\rho(S_n)$ obtained from the average s-wave resonance spacing D_0 that is used as a normalization constrain in the Oslo method.

> The Constant Temperature (CT) model has been proposed by Ericson [27] essentially in realization that the level density ρ obtained from discrete levels is fit well by [19, 24, 27, 28]
>
> $$\rho(E_x) = \frac{1}{T} \exp \frac{E_x - E_0}{T}, \tag{2.3}$$
>
> where the *temperature* of the nucleus T is assumed to be constant over the whole energy range, and E_0 is a shift parameter. For applied purposes, Gilbert and Cameron [24] suggested a combined formula with the CT model for low energies and the BSFG for higher energies. However, works by the Oslo group suggest the usage of the CT formula even up to the neutron separation energy S_n, see e.g. Refs. [29–31] and references therein.

The parameters T and E_0 for Fig. 2.1 are taken from the compilation of Ref. [25].

Composite Gilbert Cameron Model

As stated above, Gilbert and Cameron [24] suggested a level density formula, which combines the CT and BSFG model at low and high energies, respectively. Different approaches exist on how exactly the models should be combined, but they all impose a continuity of absolute values and first derivatives at the matching point E_m [19, 24, 34]. Usually, E_m is below the neutron separation energy S_n, but unless it is far below S_n, the results from the Oslo method are not able to distinguish between the composite Gilbert Cameron model (CT+BSFG) and a *pure* CT model. In Fig. 2.1 I show this model with the default parametrization from TALYS v1.9 [35], where $E_m = 6.6$ MeV, which is 1 MeV below S_n.

Spin-Parity distribution

Up to now, we have implicitly treated the level density ρ only as a function of the excitation energy E_x.[1] From the definition of the level density ρ, we find that it should also depend on the total angular momentum J (conventionally called *spin*) and the parity π. However, the phenomenological models assume that the level density $\rho(E_x, J, \pi)$ can be factorized as follows

$$\rho(E_x, J, \pi) = \rho(E_x) g(E_x, J, \pi), \tag{2.4}$$

where $g(E_x, J, \pi)$ is the spin-parity distribution, which is assumed to have a Gaussian-like functional form. I describe $g(E_x, J, \pi)$ in Paper V:

> The spin-parity distribution $g(E_x, J, \pi)$ is usually assumed to have following form [20, 24, 36]
>
> $$g(E_x, J, \pi) = \frac{1}{2} g(E_x, J), \tag{2.5}$$
>
> $$g(E_x, J) = \exp \frac{J^2}{2\sigma^2} - \exp \frac{(J+1)^2}{2\sigma^2} \approx \frac{2J+1}{2\sigma^2} \exp - \frac{(J+1/2)^2}{2\sigma^2}, \tag{2.6}$$
>
> For a derivation, see App. E. of Ref. [24], which refines the arguments used in Refs. [20, 36]. The parity dependence is usually neglected in the empirical models [25], resulting in the equiparity assumption of Eq. (2.5).
>
> Various descriptions exist for the spin-cut parameter σ, which determines the width of the spin distribution $g(E_x, J)$. Although the BSFG model provides a formula for σ, alternatives are commonly used as they provide e.g. a better description of the distribution of known discrete states [19, 22, 25, 37].

In the articles presented here, two different spin-cutoff formulas are used (and we implemented several other choices in OMpy):

[1] In some contexts this is called the *total* level density, but I will avoid this name, as others use it to refer to the state density.

- In Papers III and IV we use the spin-cutoff σ of Ref. [38] (as referenced in Ref. [25]) which is based on the rigid body moment of inertia,

$$\sigma^2(E_{\mathrm{x}}) = 0.0146A^{5/3}\frac{1+\sqrt{4aU(E_x)}}{2a}, \tag{2.7}$$

  where A is the mass number of the nucleus.

- At low E_x, typically at ≈1–2 MeV, the spin cut-off σ can also be obtained from an average of the spins J of known levels. To reconcile a potential discrepancy to the spin-cutoff σ calculated from Eq. (2.7) we have chosen the same approach as in Refs. [19, 34] for Paper I: We interpolate σ^2 linearly between the value obtained at an average energy E_d for the discrete region and the Fermi gas expression for S_n. Note that we have chosen Eq. (2.7) as the model for the spin-cutoff $\sigma(S_n)$, which differs from the functional form used in Refs. [19, 34] for $\sigma(S_n)$. Below E_d, the spin-cutoff σ is assumed to be constant.

The parametrization of the spin-cutoff σ is a major systematic uncertainty in the normalization of the results from the Oslo method, as I also mention in Paper I. So far, there are no experiments that can provide reliable information on the spin-cutoff σ for heavy nuclei, or the spin distribution $g(E_x, J)$ itself, between the discrete region and the separation energy S_n. With OMpy, it is now at least very easy to rerun the analysis for a set of reasonable models for σ.

It should be noted that $g(E_x, J, \pi)$ is the *intrinsic* distribution of levels with spin J and parity π in the nucleus. This is in general different from the distribution of levels that are *populated* in a given reaction (denoted $g_{\mathrm{pop}}(E_x, J, \pi)$ in Papers I, III and IV). The difference is striking in reactions like nuclear resonance fluorescence or for the population of a nucleus through β-decay of the parent, as strong selection rules limit the available J^π states. In other cases, like for (d, p) reactions, the population of different spin-parities crucially depends on the beam energy and may be proportional to the intrinsic spin-parity distribution. Papers III and IV discuss challenges for the Oslo method when the beam energy in the (d, p) reaction is below the Coulomb barrier for the ^{240}Pu target.

2.2 γ-ray strength function

The γ-ray strength function[2] f is a measure for the average transition probability between states in the nucleus. We will here adopt a slightly modified definition[3] of Bartholomew et al. [39, Eq. (1.1)] for a transition with energy E_γ and

[2] I may refer to f also just as (γ-ray) strength, and strength function. In literature it is also called radiative- or photon strength function.

[3] In contrast Eq. (2.8), Bartholomew et al. [39] uses a *asymmetric* definition, where the partial transition widths $\Gamma_\gamma(\cdot)$ are defined as transitions from the higher- to the lower energy level not only for decays, but also for excitations. We conceptually prefer a *symmetric* definition, but show the equivalence below, which follows from a corresponding change in the level density.

multipolarity XL,

$$f_{XL}(E_\gamma, E_i, J_i^\pi, J_f^\pi) = \frac{\left\langle \Gamma_\gamma^{(XL)}(E_i, J_i^\pi \to E_f, J_f^\pi) \right\rangle}{E_\gamma^{2L+1}} \underbrace{\rho(E_i, J_i, \pi_i)}_{\frac{1}{D(E_i, J_i, \pi_i)}, \text{ see (2.1)}}, \tag{2.8}$$

where $E_f = E_i \pm E_\gamma$ for absorption and emission of a photon, respectively, and the variables for the initial and final states have the subscript i and f. The average $\langle\cdot\rangle$ over the partial widths[4] $\Gamma_\gamma^{(XL)}(E_i, E_f, J_i^\pi, J_f^\pi)$ should be taken over many levels with the same spin-parity at the energy of the initial state. It should be clear from the context whether f denotes the γ-ray strength or the final state. A transition with multipolarity XL can be either of electric ($X = E$) or magnetic type ($X = M$) and has the multipole order L (where $L = 1$ is dipole, ...).

Note that other definitions exist in literature [39, 40], like $f = \langle\Gamma_\gamma\rangle\rho$ or $f = \langle\Gamma_\gamma\rangle\rho/(E_\gamma^{2L+1}A^{2/3})$, with the A being the mass number; the choice of Bartholomew et al. [39] divides out the "obvious" E^{2L+1} energy dependence of the transition probabilities [18, p. 595] due to the properties of the electromagnetic operator.

In general, one distinguishes between the strength from photo-excitation ("upward") processes $\vec{f}$, usually from the ground state of a target nucleus, and the strength from γ decay ("downward") $\overleftarrow{f}$. The above equation Eq. (2.8) for f transforms automatically in Bartholomew's definition of $\overleftarrow{f}$

$$\overleftarrow{f}_{XL}(E_\gamma, E_i, J_i^\pi, J_f^\pi) = \frac{\left\langle \Gamma_\gamma^{(XL)}(E_i, J_i^\pi \to E_f, J_f^\pi) \right\rangle}{E_\gamma^{2L+1}} \rho(E_i, J_i, \pi_i), \tag{2.9}$$

where $E_f = E_i - E_\gamma$. Using the principle of detailed balance [18, p. 602], it also transforms into Bartholomew's definition of $\vec{f}$,[5]

$$\begin{aligned}
\vec{f}_{XL}(E_\gamma, E_i = 0, J_i^\pi, J_f^\pi) &= \frac{\left\langle \Gamma_\gamma^{(XL)}(E_i, J_i^\pi \to E_i, J_f^\pi) \right\rangle}{E_\gamma^{2L+1}} \rho(E_f, J_i, \pi_i) \\
&= \frac{\left\langle \Gamma_\gamma^{(XL)}(E_f, J_f^\pi \to E_i, J_i^\pi) \right\rangle}{E_\gamma^{2L+1}} \frac{\rho(E_f, J_f, \pi_f)}{\rho(E_i, J_i, \pi_i)} \rho(E_i, J_i, \pi_i) \\
&\approx \frac{\left\langle \Gamma_\gamma^{(XL)}(E_f, J_f^\pi \to E_i, J_i^\pi) \right\rangle}{E_\gamma^{2L+1}} \rho(E_f, J_f, \pi_f),
\end{aligned} \tag{2.10}$$

[4] They are not to be confused with the *total* radiative width for the decay of a state i, $\Gamma_\gamma = \sum_f \Gamma_\gamma(i \to f)$.

[5] Note a slight inconsistency here that I was not able to resolve: The principle of detailed balance relates the ratios of transition widths between an initial and final state and the *state* densities, $\Gamma_{i\to f}/\rho_f^{(\text{state})}$, not *level* density ρ. The difference might be that we now regard transition widths between levels, not states.

where $E_f = E_\gamma$ (and one would now average over the final levels).

In practice, the photo-excitation strength function $\vec{f}$ is usually calculated via the photoabsorption cross-section[6] σ (see Appendix A) [39, 41–43],

$$\vec{f}_{XL} = \frac{1}{(2L+1)(\pi\hbar c)^2}\frac{\sigma_{XL}}{E_\gamma^{2L-1}}. \tag{2.11}$$

Finally, the γ-ray strength function f can also be related to the transmission coefficient $T \sim 2\pi\Gamma\rho$ [18, p. 389], using Eq. (2.9),

$$\overleftarrow{f}_{XL} = \frac{T_{XL}}{2\pi E_\gamma^{2L+1}}. \tag{2.12}$$

In many situations it is interesting to model partial decay widths given a model of the (average) strength function $\overleftarrow{f}$. For brevity, let me denote the partial decay width by Γ_{part}. Inverting Eq. (2.9) one finds

$$\langle\Gamma_{\text{part}}\rangle = \frac{\overleftarrow{f}_{XL}(E_\gamma, E_i, J_i, \pi_i)E_\gamma^{2L+1}}{\rho(E_i, J_i, \pi_i)}. \tag{2.13}$$

The equation above provides only the average behavior. Assuming an extreme configuration mixing of the wave-functions, Porter and Thomas [44] found that the ratio of each partial width *independently* follows a χ^2 distribution with $\nu = 1$ degrees of freedom, which is also called Porter-Thomas distribution,

$$\frac{\Gamma_{\text{part}}}{\langle\Gamma_{\text{part}}\rangle} \sim \chi^2_{\nu=1}. \tag{2.14}$$

This is in good agreement with many experiments, see e.g. Refs. [45–49] and can be derived from random-matrix theory [50]. However, Porter and Thomas [44] already noted that the independence assumption probably breaks down for transitions to low-lying states, which are much less *complex* than the states at higher excitation. Several recent experiments [51, 52] have found violations of the Porter-Thomas distribution that cannot be explained by random-matrix theory, even after inclusion of coupling of different channels [53].

2.2.1 Simplifications: Brink–Axel hypothesis

Faced with the challenge of calculating neutron widths, Brink [54, p. 101ff] came up with following simplification in his dissertation: He assumed that the "upward" and "downward" γ-ray strengths of the giant electric dipole resonance (GDR) are equivalent. To be precise, Brink's assumption was on the cross sections, not the γ-ray strength function. However, as can be seen in Eq. (2.11) these are closely related. In addition, Brink assumed a parametrization of the cross-section that is independent of the spin-parity and excitation energy of the initial and final

[6] Cross sections, the spin-cut, and the standard deviation of a Gaussian are denoted with σ, but it should be clear from the context what I refer to.

states, but depends only on the transition energy $E_\gamma = E_i - E_f$. Later, the idea was extended to include also other transitions than the GDR, like the M1 scissors or pygmy dipole resonance. With this assumption, we can simplify our notation for the strength function

$$f_{XL}(E_\gamma) = \vec{f}_{XL}(E_\gamma, E_i, J_i^\pi, J_f^\pi) = \overleftarrow{f}_{XL}(E_\gamma, E_i, J_i^\pi, J_f^\pi). \tag{2.15}$$

The assumption of the spin independence may have been motivated by the observation of Hughes and Harvey [55] that the average total radiative widths $\langle \Gamma_\gamma \rangle$ seem independent of the ground-state spin of the target nucleus in (n, γ) reactions.

It is not immediately clear that the Brink hypothesis should hold true, especially given the peculiar asymmetry of the initial versus final level density in Eqs. (2.9) and (2.10). However, it is quite common to apply at least the spin independence of the Brink hypothesis in cross-section calculations and comparisons of the γ-ray strength function from different experiments (see e.g. Refs. [56–59]). Brink's thesis remained unpublished until recently, but the results were referred to in an article of Kinsey [41]. Seven years after the dissertation, Axel [42] was the first to widely use the hypothesis of Brink in the calculation of strength functions and radiative widths. The hypothesis then started to be referred to as the Brink–Axel hypothesis.

The Brink–Axel hypothesis is usually invoked when using the Oslo method. Some aspects of it can also be verified through the application of the Oslo method. The independence of the decay strength function from the excitation energy E_x in the quasi-continuum has e.g. been shown in Refs. [60, 61] using the Oslo method. Furthermore, a study that compares the strength of the $M1$ scissors resonance obtained with the Oslo method and nuclear resonance fluorescence strongly suggests that the "upward" and "downward" strengths are equal [59]. This is also confirmed in the analysis of two-step and multi-step cascade spectra [62, 63] and other experiments [64].

The hypothesis is, however, also highly debated and there are known limitation. The low energy part of the strength function is not accessible in the photo-excitation of the ground state, as the level spacing is relatively high for the lowest excited states. Analogously to the remark on the Porter-Thomas fluctuations, transitions between low-lying states may in addition not be well represented by a statistical model, as structure effects play a larger role. In contrast to the photo-excitation, the decay may probe the low energy part of the strength function in transitions between the closely spaced quasi-continuum states. In light of these differences, one can argue that the Brink–Axel hypothesis is violated [65, 66] – or that the concept of the photo-excitation strength function is not applicable in this region. Still, other recent works [67, 68] exhibit a violation of the Brink–Axel hypothesis also for higher energies (most notably, Ref. [68], which does not depend on a specific level density or strength function model) or attempt to determine limits of its applicability [58].

2.2.2 Empirical models

In the following, I will briefly describe some of the models that are often used for the γ-ray strength function. The parameters for these models are usually determined by a fit to data, or if no measurements are available, one resorts to (semi-)empirical predictions. The goal of the description here is to give an impression of the manifold of models, rather than a theoretical justification; given the variety of approaches, the final justification for the (semi-)empirical models is usually given by the match with the data, not by the consistency of the approach. For more details, the reader is referred to Refs. [19, 69] and references therein.

Standard Lorentzian

In his Doctoral thesis, Brink [54] proposed the standard Lorentzian (SLO) for the electric dipole strength $\breve{f}_{E1}$. Nowadays, modifications of this model are usually used for the $E1$ strength, but it is still commonly used to describe $M1$ and $E2$ modes [19]. Let us recall the description given in Paper V:

> The γ-ray strength function $f(E_\gamma)$ is dominated by dipole radiation [66, 70–80] and the most prominent feature in the region up to about 20 MeV is known as the giant (electric) dipole resonance (GDR). One of the simplest models for the GDR explains it as a collective motion of protons against neutrons. The resonance can then be described by a damped harmonic oscillator, leading to the standard Lorentzian (SLO) [39, 54, 81]
>
> $$f^{(\mathrm{SLO})}(E_\gamma) = \frac{1}{3\pi\hbar^2c^2}\sigma\Gamma\frac{E_\gamma\,\Gamma}{(E_\gamma^2 - E^2)^2 + E_\gamma^2\Gamma}, \tag{2.16}$$
>
> where σ, Γ and E are the cross section, width and energy of the resonance, respectively, and the factor $1/(3\pi\hbar^2c^2) \approx 8.674 \times 10^{-8}\mathrm{mb}^{-1}\mathrm{MeV}^{-2}$. For deformed nuclei, the GDR has a double peaked structure, which is interpreted as independent oscillations along each of the deformation axes.

An interesting observation for the SLO model is that it does not depend on the initial excitation energy E_i, but only on the γ-ray energy E_γ, thus $\vec{f}^{(\mathrm{SLO})} = \breve{f}^{(\mathrm{SLO})}$. Note also that the shape of $f^{(\mathrm{SLO})}$, given in Eq. (2.16), resembles a relativistic Breit-Wigner cross-section, but using Eq. (2.11) it can be shown that there is a different energy dependence ($\times E^4$).

The family of Lorentzian models

The SLO has two main shortcomings: It mismatches experimental data and (semi-)microscopic calculations in the low-energy region ($\lesssim$ 1–2 MeV), and it cannot simultaneously represent data around the GDR and the neutron separation energy S_n (see e.g. Refs. [19, 82–84] and references therein). This has motivated the development of other strength function models, which generalize the Lorentzian shape and lead to a "family" [69] of Lorentzians. The new models

have improved the agreement with the observables. A comparison of four of these models is given in Fig. 2.2.

The first extension of the SLO was proposed by Kadmenskiĭ, Markushev and Furman (KMF) [85]. Based on the theory of Fermi liquids, they predict that the width Γ should not be constant, but depend on the γ-ray energy E_γ, as well as on the temperature of the final states T_f,

$$\Gamma_{\mathrm{KMF}}(E_\gamma, T_f) = \frac{\Gamma}{E^2}(E_\gamma^2 + 4\pi^2 T_f^2), \tag{2.17}$$

As the KMF strength function is built on the Fermi gas model, the temperature is defined as $T_f = \sqrt{E_x - E_\gamma}/a$. The resulting strength function is given by [19, 85]

$$f_{\mathrm{KMF}}(E_\gamma, T_f) = \frac{1}{3\pi\hbar^2 c^2} 0.7\sigma\Gamma E \frac{\Gamma_{\mathrm{KMF}}(E_\gamma = 0, T_f)}{(E_\gamma^2 - E^2)^2}. \tag{2.18}$$

Whilst this improves the low energy behavior of the strength function, it poses two problems. First, the γ-ray strength function no longer obeys the Brink–Axel hypothesis, or specifically, the final state temperature dependence leads to $\vec{f}_{\mathrm{KMF}} \neq \overleftarrow{f}_{\mathrm{KMF}}$. However, as there is no fundamental reason why the Brink–Axel hypothesis has to hold, this could be considered a consequence rather than a shortcoming of the model. The second problem is more severe: The strength function has a singularity at the resonance energy, $E_\gamma = E$, such that it cannot be used to fit GDR data.

To remedy the deficiency at low energy, whilst keeping a tractable form in the GDR region, Kopecky and Uhl [83] introduced the generalized Lorentzian (GLO), using the KMF model as a basis,

$$f_{\mathrm{GLO}}(E_\gamma, T_f) = \frac{1}{3\pi\hbar^2 c^2}\sigma\Gamma\left[\frac{E_\gamma \Gamma_{\mathrm{KMF}}(E_\gamma, T_f)}{(E_\gamma^2 - E^2)^2 + E_\gamma^2 \Gamma_{\mathrm{KMF}}(E_\gamma, T_f)^2}\cdot \right. \\ \left. + \frac{0.7\Gamma_{\mathrm{KMF}}(E_\gamma = 0, T_f)}{E^3}\right]. \tag{2.19}$$

The GLO provides better fits to the data, but still underestimates the strength around S_n for heavier nuclei. This led to a modification called the enhanced generalized Lorentzian (EGLO) where the width Γ_{KMF} used in the GLO model is further modified for nuclei with $A \geq 148$ [19, 86].

There are yet other Lorentzian models, like the generalized Fermi liquid model (GFL) [87] and modified Lorentzian model (MLO) [82, 88–90]. It seems like authors in the field choose rather freely between the different models for the $E1$ strength function. On the one hand, the choices may seem arbitrary, or defined solely on the basis of which model fits for the nucleus under study. On the other hand, this approach might be justified, as it is not given that there is a single empirical model that can describe nuclei in all mass regions. Thus, to evaluate the models, it would be helpful to implement all of them in a code

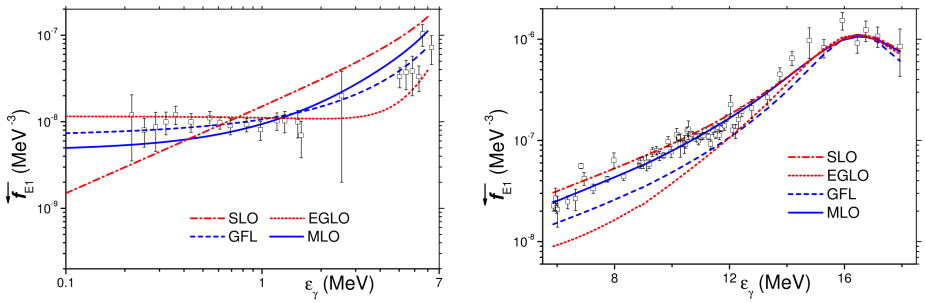

Figure 2.2: Comparison of different $E1$ γ-ray strength function models fit in RIPL3 [19] experimental data from (a) ^{144}Nd [91] in the low energy region and to (b) ^{90}Zr [92] around the GDR. The strength function is plotted for a fixed temperature T_f. Reprinted from Ref. [19] with permission from Elsevier.

like gledeli presented in Paper V and automatically perform the analysis with each model. At best, the results of all models should then be published – also those that did not fit well – such that a final recommendation for the model choice can be based on a larger scale. This has partly been performed in RIPL3 [19], but the database does not include data from sources like the Oslo method and nuclear resonance fluorescence experiments, which are important for the low energy tail.

Single-particle strength

Probably the first widely used model on the strength of electromagnetic transitions was developed by Weisskopf [93] in 1951 and refined by Blatt and Weisskopf [18, p. 278ff, 627, 647, 653] in their standard work *Theoretical Nuclear Physics* the year after. It is based on the extreme assumption of the independent-particle model, in which nucleons interact with each other only through a mean-field. This leads to a nuclear wave function which is composed of a separable product of single-particle wave functions. The γ radiation (or absorption) is then ruled by the transition of a single particle, in the original formulation a proton. A very similar expression is obtained for neutrons, at least for $E1$ transitions, see Ref. [94, p. 387] and Ref. [95, 97f]. With some approximations, the transition probability λ is determined as [18, p. 627]

$$\lambda_{XL} = C_{XL} E_\gamma^{2L+1} R^{2L}, \tag{2.20}$$

where C_{XL} is a constant that depends on the multipolarity XL (see Blatt and Weisskopf [18, p. 627] for details) and R is the nuclear radius. Equation (2.20) is also known as the Weisskopf estimate for transition strengths.

Using $\Gamma = \hbar\lambda$ and Eqs. (2.9) and (2.10), we find that the strength function f depends only on the constant C_{XL}, the radius R, and the level density $\rho(E_>)$, where $E_>$ is the excitation energy at the upper level. For transitions between

highly excited states of the nucleus Blatt and Weisskopf [18, p. 644ff] further argue that the transition probability must be divided amongst the levels, which adds a factor $1/\rho(E_>)$ to the strength function, such that it effectively becomes constant for a given XL,

$$f_{XL} = \frac{\langle\Gamma\rangle_{XL}}{E^{2L+1}}\rho(E_>) = \frac{C_{XL}E^{2L+1}R}{E^{2L+1}}\rho(E_>) \overset{\text{high } E_x}{\rightarrow} \frac{C_{XL}E^{2L+1}R}{E^{2L+1}\rho(E_>)}\rho(E_>) = const. \tag{2.21}$$

They roughly estimate the applicability of this model up about 25 MeV for nuclei with $Z \sim 50$.

Although many authors use an SLO for $M1$ and $E2$ transitions, which is recommended by RIPL3 [19] for the latter, it is still not uncommon to see the single-particle model used for those transition types, see e.g. Refs. [57, 63, 96]. I want to conclude this section with the modest remark of Weisskopf [93] on his own model:

> The assumptions made in deriving these estimates are extremely crude and they should be applied to actual transitions with the greatest reservations. [...] In spite of these difficulties it may be possible that the order of magnitude of the actual transition probabilities is correctly described by these formulas. We have published these exceedingly crude estimates only because of the rather unexpected agreement with the experimental material which was pointed out to us by many workers in this field.

2.3 Microscopic models

The empirical descriptions of the level density and γ-ray strength function are most important for common applications like the cross-section calculations that are used e.g. in nuclear energy, shielding and nuclear medicine. Major libraries like JEFF-3.3 [97] and JENDL-4.0 [98] apply the models listed above, or very similar descriptions. Remaining discrepancies to experimental data are simply minimized by rescaling the calculations. Despite their heavy usage, the empirical models have three significant drawbacks. First, they are mostly descriptive and provide only a very limited understanding of the nucleus. Second, some collective phenomena in nuclei, like the $M1$ scissors resonance, have no global description for the parameters; for other modes, like $M1$ spin-flip resonance, only very crude descriptions exists, see Ref. [66, 99] and references therein. Finally, the phenomenological parameterizations most likely do not extrapolate well for nuclei far from stability, which are relevant for astrophysics [100]. For this reason, microscopic calculations have enjoyed an increased popularity [69, 84, 100, 101]. Sometimes one explicitly uses the term *semi*-microscopic calculations when the underlying microscopic theory is altered with some empirical description to improve the fit with experimental observables. In the following, I will briefly

review some of the most successful theoretical description for mid-mass and heavy nuclei.

The common starting point for most microscopic descriptions of the nucleus is the time-independent many-body Schrödinger equation,

$$\hat{H}|\psi\rangle = E|\psi\rangle, \tag{2.22}$$

with the Hamiltonian

$$\hat{H} = \sum_i -\frac{\hbar^2}{2m}\nabla_i^2 + \sum v_{i(j,\dots)}, \tag{2.23}$$

The potential v is usually simplified to include only mean-field v_i and two-body interactions v_{ij}. In the equations above, $|\psi\rangle$ is a many-body wave function of the nucleus and E is its excitation energy.

2.3.1 The Shell model

Probably the most well known approach to solve this problem is the Shell model, which in a simple form is now taught even at introductory nuclear physics courses. Although the principles were already known from atomic physics, the success of the nuclear shell model started only after the introduction of the spin-orbit interaction in the potential by Goeppert Mayer [102, 103] and Jensen [104]. In their excellent review on the Shell model, Caurier et al. [105] summarize the effect as follows:

> In modern language this proposal amounts to assuming that the main effect of two-body nucleon-nucleon interactions is to generate a spherical mean field. The wave function of the ground state of a given nucleus is then the product of one Slater determinant for the protons and another for the neutrons, obtained by filling the lowest subshells (or "orbits") of the potential. This primordial shell model is nowadays called the *independent-particle model* (IPM) or *naive shell model*.

In the shell model, the state energies E (and thus the level density ρ) are obtained by a diagonalization of the Hamilton matrix. The new basis – the eigenstates $|\psi'\rangle$ – can be used to calculate the γ-ray strength function f, which is schematically given by $f_{XL} \propto \langle\Gamma_\gamma\rangle \propto \langle\psi'_f|\hat{O}_{XL}|\psi'_i\rangle$. In practice, this turns out to be a challenging problem for calculations that go beyond a mean-field approach and one has to resort to phenomenological interactions and/or restrict ("truncate") the model space. A common approximation for "heavier" nuclei ($A > 20$) is to assume an inert core and only allow interactions between particles in some valence orbitals above the core.

The Lanczos method [106] and even more so the Monte-Carlo Shell Model (MCSM) [107] have proven to be relatively efficient ways to calculate approximate energies and wave functions for light to mid-mass nuclei ($A \approx 60-140$), see e.g. Refs. [108–114] and references therein. Nevertheless, in this mass-region

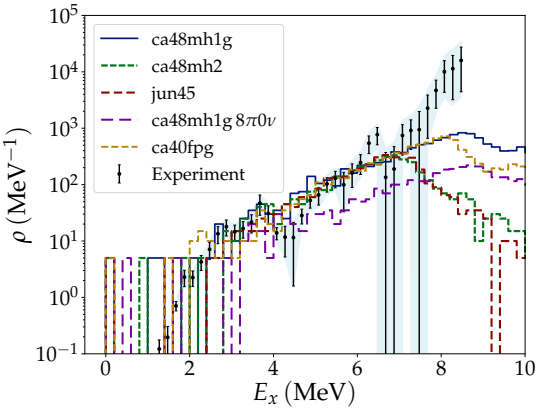

Figure 2.3: Level density of ^{70}Ni from the Oslo Method ("experiment") compared to Shell model calculations with different interactions. Reprinted with permission from Larsen et al. [115]

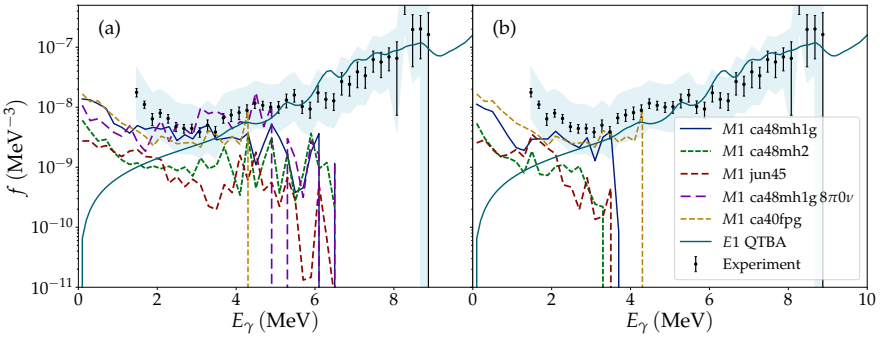

Figure 2.4: γ-ray strength function of ^{70}Ni from the Oslo Method ("experiment") compared to shell model calculations for f_{M1} with different interactions, and QTBA for f_{E1}. Pannel (a) shows the f_{M1} Shell model strength from all $M1$ transitions, whereas (b) only includes transitions from initial levels with $J_i^\pi = [5^-, 6^-, 7^-]$. Reprinted with permission from Larsen et al. [115]

it is common to apply a truncation to an inert core plus a single major shell. If one disregards so-called intruder orbitals, all other orbitals of the one shell have the same parity. Therefore, the selection rules imply that the $E1$ strength cannot be calculated from this approach. However, the calculation can provide the $M1$ strength, and this type of shell model calculations have been used e.g. as a theoretical backing of the *low-energy enhancement* in the γ-ray strength function [109, 111, 114, 115]. Figures 2.3 and 2.4 compare the level density and γ-ray strength function of ^{70}Ni from the Oslo method to Lanczos method based Shell model calculations with different interactions [115].

Another technique with a similar name, the Shell model Monte Carlo (SMMC) method [116, 117], has been very actively developed by Alhassid and collaborators [117–121]. In contrast to the methods presented above, the SMMC level density is estimated without the construction of eigenstates. Thus, the strength function cannot be calculated in this approach. On the other hand, it is tractable for considerably higher valence spaces and thus allows the calculation for heavier nuclei, which are, in general, further off the core. This has enabled the calculation of the level densities of spherical and deformed nuclei as heavy as $^{143-150,152}$Nd, $^{149-155}$Sm and ^{162}Dy [119–121].

2.3.2 Hartree-Fock method and QRPA

In the near future, none of the above methods will be feasible for large scale calculations of level densities and γ-ray strength functions across the nuclear chart. The need for these as input to abundance calculations in nuclear astrophysics has motivated the development of level density models based on the Hartree-Fock (HF) method. In Ref. [122] the level density is calculated using a Skyrme force with the Bardeen-Cooper-Schrieffer (BCS) formalism to account for pairing correlations. Based on the ground-state HF-BCS single-particle level scheme, the level density is approximated from the partition function. The authors of Ref. [122] refer to this as the "statistical approach". A drawback of the approximation is that the resulting level density is smooth even at low energies, where gaps are expected due to wider spacing of the discrete states [122, 123]. In addition, the parity dependence of the level density cannot be resolved [123]. These problems were solved by the application of a combinatorial method [124, 125] instead of the "statistical method" on the single-particle level scheme [32, 123]. In these works, a generalization of the HF formalism, the Hartree–Fock–Bogolyubov (HFB) method has been used instead of BCS to account for pairing. In the latter work, Ref. [32], the underlying force has also been changed to a recently updated Gogny-D1M interaction which can explicitly treat some collective properties which were previously included by an empirical enhancement [32, 126].

The major gain of this type of microscopic calculations is certainly for very heavy nuclei and for nuclei further away from stability. The difference between the average level spacing calculated from the HF–BSC+statistical and HFB+combinatorial models and experimental data from neutron experiments is between a factor of 2 and 3 [32, 122, 123]. This is comparable, even if slightly worse than the agreement with the phenomenological BSFG model, *with a global parametrization* of the level density parameter a and backshift E_1 [32, 127]. Note that the empirical models in Papers III to V are parametrized taking into account the experimental average level spacings, thus the agreement can be arbitrarily good, but this information is only available for a subset of the stable nuclei.

The $E1$ γ-ray strength function can be found by applying the quasi-particle random-phase approximation (QRPA) based on the HF-BCS and HFB calculations with the Skyrme or Gogny+D1M force, respectively [100, 128, 129]. Through the usage of an axially-symmetric deformed QRPA calculation, Goriely

et al. [101] have recently also been able to determine the $M1$ strength function based on the Gogny+D1M interaction. On top of the calculations, some empirical corrections are applied: An energy shift of about 2 MeV to mimic the inclusion of higher order particle-hole excitations in the QRPA calculation, a broadening of the strength with a Lorentzian to substitute a damping of the collective motion, and for calculations before Ref. [101], also empirical deformation effects. Alternatively, a QRPA calculation with explicit coupling to phonons can be used to obtain the $E1$ strength function [130–132]. The result of this approach is shown in Fig. 2.4 for ^{70}Ni, where the calculations include the quasi-particle time blocking approximation (QTBA) [115, 133].

2.4 Experiments

So far, I have introduced different phenomenological and microscopic models for the nuclear level density ρ and γ-ray strength function f. In this section, I will briefly review experimental techniques that are used to measure level densities and γ-ray strengths. More information on the strength function can be found in two recent reviews by Goriely et al. [69] and Ref. [134]. They were initiated by the IAEA and lead to an online database with a collection of experimental data and theoretical estimations. To my knowledge there are no recent reviews on the experimental or theoretical progress of level density calculations, but Refs. [135, 136] give a good description of the methods developed until the start of the 1980s.

I have started this chapter with Box's realization that "all models are wrong", or as he rephrases it in the same book, that models are only approximations of the "truth" [137, p. 74, 424]. We may reflect over this also for experiments. The level density and γ-ray strength are not directly observable, so a "measurement" is to be understood in the sense that information about them is inferred from an experiment. This process usually involves a considerable amount of assumptions, such as the validity of the Brink–Axel hypothesis. Still, apart from internal consistency, experiments are the only way to evaluate the quality of the phenomenological and microscopic models.

A prime example for the sustained value of experimental measurements in this field is the discovery of the low-energy enhancement ("upbend") of the strength function in 2004 [8] through the Oslo method: A striking 50 years after the GDR was found [138, 139] and rather soon after also explained [140], there were still unexpected features in the γ-ray strength function. Even though the discovery initially caused a lot of skepticism, see e.g. Refs. [141–143], it led to the refinement of several empirical and theoretical models and to the development of a new experimental technique, the Ratio method [144]. A good review of the discovery and present status of the low-energy enhancement is given in the PhD thesis of Midtbø [145].

2.4.1 Oslo method

The Oslo method allows to simultaneously obtain the level density ρ and decay γ-ray strength function $\overleftarrow{f}$ below the particle separation thresholds. In Paper I we describe OMpy, a reimplementation of the software used during the data analysis with a focus on uncertainty propagation and we provide an updated review of the all steps of the method. The starting point is an E_x–E_γ matrix of excitation energy tagged spectra of the γ decay. These are traditionally obtained from coincidence measurements of charged particles and γ-rays from inelastic scattering or a transfer reaction like (d, p). Recent modifications have extended the range of possible nuclei that can be studied through the usage of inverse reactions [146] or β-decay as a population mechanism [147].

The primary γ-rays from the reaction, i.e. the first γ-rays emitted for each cascade, are extracted by an iterative subtraction method [148] from the E_x–E_γ matrix, which contains all γ-rays of the cascades. It assumes the formation of a compound nucleus, and that the spin-parity dependent population probabilities g_{pop} for the employed reaction, e.g. (d, p), are independent of the excitation energy.

The resulting matrix is called the primary, or first-generation, γ-ray matrix and it is usually denoted by $P(E_x, E_\gamma)$. Using Bohr's compound nucleus picture [149] and the Brink–Axel hypothesis, it can be decomposed into the product of the level density $\rho(E_x)$ and the γ-ray strength function $f(E_\gamma)$, (see App. C of Paper I for a derivation)

$$P(E_x, E_\gamma) \approx C_{E_x} \rho(E_f = E_x - E_\gamma) E_\gamma^3 f(E_\gamma), \tag{2.24}$$

where we consider decays from an initial excitation energy bin E_x with γ-ray energy E_γ, so that we receive the level density at the final states' bin $E_f = E_x - E_\gamma$; C_{E_x} is a normalization constant for each excitation energy bin E_x. In addition, we have assumed the dominance of dipole radiation, which is supported by many experiments and theory [66, 70–80].

The solutions to Eq. (2.24) have been shown to be invariant under a continuous transformation with three parameters [3]. To get the "physical solution" the results are normalized to (at least) three other types of information.[7] Usually, that is: i) the level density ρ at low excitation energies ($\lesssim 2$ MeV) from discrete states measured through spectroscopy, ii) the level density $\rho(S_n)$ derived from the average s-wave neutron resonance spacing D_0 and the spin-parity distribution $g(E_x)$, and iii) the average total radiative width from s-wave capture $\langle \Gamma_{\gamma,0} \rangle$. Additionally, for most experiments, an extrapolation of the level density ρ is required from the highest E_x bin $\approx$1 – 2 MeV below S_n to the normalization point $\rho(S_n)$. The extrapolation is performed with a level density model. In recent years the CT model has been favored, as it matches better with the

[7] One normalization parameter is common, two are independent for ρ and f. Usually, the discrete levels are binned in more than two bins, so in principle they would be sufficient to infer two of the normalization parameters unambiguously.

Oslo data than a BSFG model[8] [29–31]. Another extrapolation is needed in the determination of the absolute scale of the γ-ray strength function.

In summary, the main controversial assumptions are i) the form of the spin-parity dependent population probabilities g_{pop}, ii) the Brink–Axel hypothesis and (see discussion in Section 2.2.1) iii) the parametrization of the intrinsic spin distribution g, which is used in the normalization. The impact of g can be treated as a systematic uncertainty by using different sensible results from phenomenological models and microscopic calculations. A recent development to mitigate the normalization uncertainties, the *Shape method*, will be presented briefly in Section 2.4.6. For a debate on the Brink–Axel hypothesis, see Section 2.2.1.

For many mid-mass nuclei the assumption of the spin-parity dependent population probabilities has been tested by comparison of the results of two different reactions, like $(^3\text{He}, \alpha)$ and $(^3\text{He}, ^3\text{He}')$, for the same residual nucleus [59, 150–152]. This is an indirect test: If the assumption is not fulfilled, one would expect that the results for different reactions disagree. However, they seem to be rather consistent. For very heavy nuclei, which have a broad intrinsic spin distribution, the situation is not as clear. In several actinide nuclei an ad hoc correction to the normalization was necessary in order to recover a somewhat consistent γ-ray strength f [153–155]. The consequences of a breakdown of the assumption on the spin-parity population g_{pop} for $(\text{d}, \text{p})^{240}\text{Pu}$ is analyzed in more detail in Paper III, where we show that the ad hoc correction has serious short-comings. This is further developed in Paper IV, where we attempt to mitigate the effects of the assumption.

The biggest advantage of the Oslo method is that it allows to extract information on both level density and γ-ray strength function, and it is feasible to perform the fits without prior knowledge on the parametrization of the functions. Therefore it is ideally suited to search for new features, as has been demonstrated with the low-energy enhancement.

2.4.2 Singles γ-ray, two-step and multi-step cascade spectra

Another way to infer information about level densities ρ and decay γ-ray strength functions $\tilde{f}$ is from singles γ-ray [156, 157], two-step cascade (TSC) [62, 65, 141, 158] and multi-step cascade (MSC) [63, 143, 159] spectra. Apart from one case, these spectra have been obtained from (n, γ) reactions [69]. Level densities and γ-ray strength functions cannot be obtained directly, but are inferred from a comparison of the spectra with model calculations using a statistical decay code.

There are major differences in the experimental setups which have been applied for the acquisition of the (singles), TSC and MSC spectra, that propagate to the data analysis. For TSC, slow neutron capture has been used, which populates several resonances at around the neutron binding energy S_n at the

[8] The composite Gilbert Cameron model has not been attempted in the extrapolation. Probably it was seen as a disadvantage, as it introduces more parameters, which would not be easy to fit with the previous software implementation. With OMpy, they could easily be introduced as nuisance parameters and marginalized in the results.

same time, and the resulting γ-ray spectra have been measured with a few high resolution Ge detectors. The setup is simple enough that corrections due to Compton effect, cross-talk, etc. can apparently be applied as a background subtraction process in the beginning of the analysis [141, 158]. The MSC spectra have been obtained following the population of isolated resonances of known spin and parity, leading to a well determined initial state. The data available sofar has been obtained with the DANCE γ-ray calorimeter [160]. Due to the close configuration and high segmentation of the detector, it is challenging to account for the detector response by an unfolding procedure. Instead, every γ-ray cascade that was modeled to build up the MSC spectra is fed through a Monte Carlo simulation of the detectors and the results are compared to the raw data.

Singles, TSC and especially MSC spectra have a high sensitivity to different level density and γ-ray strength function models and parameters. However, none of the parameter searches and model comparisons have been fully automated yet using e.g. a gradient-descent based or gradient-free optimization. Whilst this may be possible for the singles and TSC spectra, the detector simulations necessary for MSC spectra are very time consuming and the likelihoods to obtain MSC data are complicated or a priori not known, hampering an automated search [63]. The drawback of calculations with a limited number of attempted parametrizations can e.g. be seen for studies of the low-energy enhancement in ^{96,98}Mo. Whereas earlier TSC [141] and MSC [143, 161] analyses reported that a pronounced low-energy enhancement in these nuclei is incompatible with their analysis, a recent reanalysis allowed for significantly higher strengths at low energy [159], now consistent with the Oslo method results [150]. The difference was attributed to "significantly different PSFs [γ-ray strength function] shapes compared to those tested in Refs. [143, 161]." [159].

2.4.3 Nuclear resonance fluorescence

The resonant absorption and subsequent reemission of photons below the particle emission threshold is called Nuclear Resonance Fluorescence (NRF) and it is a tool to study the photo-excitation strength function $\vec{f}$. The photoabsorption cross-section σ can be converted to the strength function $\vec{f}$ using Eq. (2.11). For more details on the experiments and data analysis, see the reviews in Refs. [69, 162–165] and references therein.

NRF excites the nucleus mostly through dipole and, with less intensity, quadrupole photons. The multipolarity XL of the decay radiation and the spins of the exited states can be deduced from angular correlation measurements. In addition, the parity can be determined when using polarized beams or Compton polarimeters. The average absorption cross-section σ is the sum of the *elastic scattering* cross-section $\sigma_{\gamma\gamma}$, i.e. direct decay to the ground-state ($f = 0$), and the *inelastic scattering* $\sigma_{\gamma\gamma'}$, where the decay proceeds through one or more intermediate state(s) ($f \neq 0$). These partial cross-sections can be obtained from Eq. (A.5) (including the discussing below Eq. (A.6)) by multiplication with the branching ratio Γ_f/Γ_γ. [69]

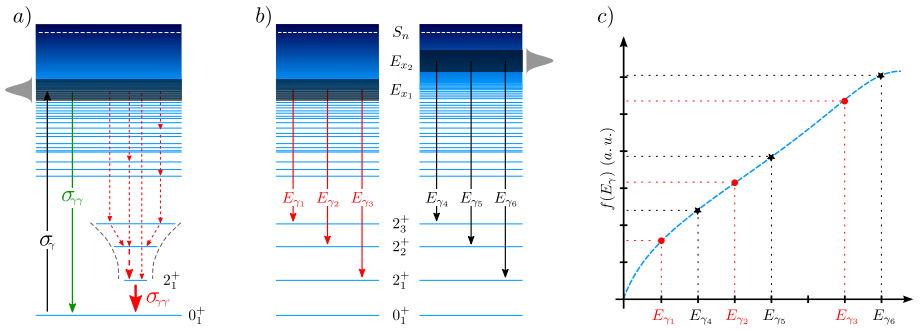

Figure 2.5: Sketch of two different experimental methods to determine the γ-ray strength function. (a) Shows a NRF method to determine the photo-excitation strength $\vec{f}$ from the elastic cross-section (green arrow) and the approximate contribution of the inelastic cross-section (red arrows). In (b) the extraction of the ratio of the decay strength functions $\overleftarrow{f}$ from decays to different low-lying excited (here, 2^+) states is displayed for two different excitation energies $E_{x,i}$. The ratios are combined in (c) to obtain the shape of $\overleftarrow{f}$. Reprinted with permission from Pietralla, Isaak, and Werner [165].

There are two main challenges for NRF when extracting the absorption cross-sections and thus γ-ray strengths. First, the branching ratio to the ground-state $\Gamma_{f=0}/\Gamma_\gamma$ has to be determined in order to relate the elastic scattering cross-section $\sigma_{\gamma\gamma}$ to the absorption cross-section σ. For experiments with a broader incident spectrum, like those obtained a γELBE, the inelastic scattering contribution need to be determined from statistical γ-cascade simulations [69]. The approach and problems correspond to those described in Section 2.4.2. When a quasi-monochromatic beam is used, as e.g. at the HIγS facility, the different contributions to the cross section may be determined from measurements of direct decays ($\sigma_{\gamma\gamma}$) and, in addition, the decay through other low-lying state(s) ($\sigma_{\gamma\gamma'}$). This is schematically displayed in Fig. 2.5a. Under the assumption that all inelastic decay cascades proceed through low-lying state(s), displayed as different 2^+ states, the inelastic scattering cross-section $\sigma_{\gamma\gamma'}$ can be determined from the intensity of decays of the first excited state [68, 165, 166].

The population at higher excitation energies, thus higher level densities, poses an additional problem. In this region, the fraction of weak transitions that may not be resolved increases. They need to be taken into account if one wants to obtain the (full) average strength function and not only the strength to excite some selected states. However, one needs to subtract the contribution of background events before one can integrate all transitions, including those that are unresolved ones, i.e. the whole spectrum. This background of unresolved γ-rays stems e.g. from Thomson and Compton scattering in the target and constitutes a large fraction of the detected coincidence events. It can be simulated with a particle transport code like Geant4 [167] and subsequently taken into

account in an "effective" detector response, see Ref. [168] and Ref. [169, p. 62]. However, this poses a question on the systematic uncertainties of this approach.

Recently, an approach has been developed by Isaak el al. [68, 166], that adds the possibility to measure the decay strength $\overleftarrow{f}$ in the same NRF experiment used to determine $\vec{f}$. It is based on the **Ratio method**, [144] that was initially applied to γ rays following a (d, p) reactions and is sketched in Fig. 2.5 (b, c). Using $\gamma-\gamma$ coincidence measurements one can gate on decays of known low-lying levels $E_{\mathrm{low},i}$ and study the intensity I_i of the γ rays $E_{\gamma,i}$ feeding these. Only γ-ray combinations that sum up to the beam energy E_{beam} within the experimental resolution are accepted, $E_{\mathrm{beam}} \approx E_x \approx E_{\mathrm{low},i} + E_{\gamma,i}$. If the low-lying levels $E_{\mathrm{low},i}$ have the same spin-parity, the ratio r of the intensities for different γ rays are directly proportional to the ratio of the strength-function (and the energy factors $E_{\gamma,i}^{2L+1}$). By combining the ratios r for different excitation energies, the γ-ray strength function can be determined up to a common normalization factor. As mentioned above, this was initially performed for (d, p)^{95}Mo, where it confirmed the presence of the low-energy enhancement in $\overleftarrow{f}$ [144]. The special aspect of the $\gamma-\gamma$ coincidence measurements with a polarized beam performed by Isaak el al. [68, 166] is that they were able to study the photo-excitation $\vec{f}$ and decay strengths $\overleftarrow{f}$ in the same experiment, thus eliminating systematic uncertainties due to different reaction mechanisms. At present, only ^{128}Te has been studied with this new $(\vec{\gamma}, \gamma\gamma)$ technique[9]. For that nucleus, the authors find that the results "cannot be described quantitatively within the ansatz of the statistical model. The results indicate that the BA [Brink–Axel] hypothesis is not fulfilled" [68]. It is expected that this type of experiments will contribute significantly to the debate on the validity of the Brink–Axel hypothesis.

2.4.4 Neutron and proton resonance capture

Let us start with the a description of the **average level spacing** D and **average total radiative width** $\langle\Gamma_\gamma\rangle$ given in Paper V:

> Neutron capture experiments provide two important observables, the average level spacing D, which is simply the inverse of the level density ρ, and the average total radiative width $\langle\Gamma_\gamma\rangle$, which is a convolution of the γ-ray strength function f and the level density ρ.
>
> The observables are grouped according to the angular momentum ℓ transferred by the neutron, where $\ell = 0$ is called s-wave capture[a]. From the spacing of resonances in s-wave capture D_0 one receives the level density ρ at the neutron binding energy S_n for the accessible levels (assuming experiments with thermal neutrons, so that their kinetic energy is negligible),
>
> $$D_0 = \frac{1}{\sum \rho(S_n, J = J_t \pm 1/2, \pi_t)}, \tag{2.25}$$

[9] Sometimes it is denoted as $(\vec{\gamma}, \gamma'\gamma'')$ which makes it even more explicit that the γ rays from the decay are not identical to the initial photon.

“

where J_t and π_t are the target nucleus ground state spin and parity, respectively, and the addition of $1/2$ is due to the intrinsic spin of the neutron. For $J_t^\pi = 0^+$, which is the ground-state spin-parity for even-even nuclei, D_0 provides the spacing of $J^\pi = 1/2^+$ levels in the residual nucleus (recalling that $J \geq 0$). [...]

After neutron capture, the nucleus is in an excited state with $E_x \approx S_n$ and the decay is dominated by γ-ray emission[b]. The width of the decay following s-wave capture $\langle \Gamma_{\gamma 0} \rangle$ is given by

$$\langle \Gamma_{\gamma 0}(S_n) \rangle \approx \frac{D_0}{2} \int_0^{S_n} \mathrm{d}E_\gamma \left[f(E_\gamma) E_\gamma^3 \times \sum_{J_i} \sum_{J_f=|J_i-1|}^{J_i+1} \rho(S_n - E_\gamma, J_f, \pi_t) \right], \tag{2.26}$$

where the first sum runs over all possible residual nucleus spins $J_i = |J_t \pm 1/2|$ and the second sum runs over all final spins J_f, assuming a dominance of dipole radiation. For more information and a derivation of this equation, see eg. App. D in Ref. [171], which is based on [18, p. 649], and Sec. 2.3 in Ref. [170] and references therein. In addition, we have assumed that the radiative width is dominated by the compound nuclear processes, which suggested by many experiments [170, 172, 173].

[a]Most data exists for s-wave capture, which will be used in the following, but the equations can be generalized for other angular momentum transfers, like p-wave capture ($\ell = 1$).

[b]The neutron widths are typically about 1–2 orders of magnitude smaller than the total radiative width Γ_γ for excitation energies E_x only slight above the neutron emission threshold S_n, see e.g. the discussion in Ref. [18, p. 471] and data tabulated in Ref. [170]. Internal conversion is negligible for high transition energies and other decay modes, like β decay, change the isotope.

”

There are two major compilations of the average level spacings D and average total radiative widths $\langle \Gamma_\gamma \rangle$, the *Atlas of neutron resonances* by Mughabghab [170] and the RIPL3 library [19], which date to 2018 and 2009 in the most recent versions cited here, respectively. Mughabghab [170] also provides a list over individual resonances and their total width Γ_γ, along with recommended values for average total width $\langle \Gamma_\gamma \rangle$ for some nuclei where no direct measurements exists. It should be noted that there are significant differences in the evaluated values and uncertainties for some nuclei – even when apparently the same resonance data is used. Unfortunately, neither of the two libraries describes the evaluation procedures in more detail.

Neutron resonance capture can also be used to determine the decay γ-ray strength function $\bar{f}$ at around the neutron separation energy S_n. Two methods, the **direct resonance capture** (DRC) and **average resonance capture** (ARC) have been used very actively between the 1960s and ’90s, see Refs. [69, 174–176] and references therein.

In DRC one measures the decay intensities I_γ, i.e. the number of γ rays per neutron capture for several resonances *individually*. The measurements are either preformed directly, or by comparing the count rates to a calibration standard like ^{197}Au [174]. The partial widths $\Gamma_\gamma^{(XL)}(E_i, J_i^\pi \to E_f, J_f^\pi)$ are obtained from the intensities I_γ by multiplication with the total radiative width Γ_γ. The strength function $\overleftarrow{f}$ is then calculated from Eqs. (2.8) and (2.9) by division of the energy factor and D_0. The values of Γ_γ and D_0 are usually obtained from other experiments or evaluations as described above. The data exhibit large fluctuations due to counting statistics and the Porter-Thomas distribution, which are reduced by averaging over several resonances. Note that a certain degree of averaging is also required from the definition of the strength function. As before, the majority of information is for s-wave capture but the relations can be expressed analogously for p-wave (and d-wave) capture. [175, 176]

In contrast to DRC, in ARC neutron beams with a broader energy profile are used with full widths half maximums (FHWM) between 150 eV and 24 keV . This leads to the simultaneous measurement of many resonances and consequently an improved, intrinsic statistical averaging. However, whilst the initial states in DRC were (usually) well determined and from single resonances, the mixture of different resonances in ARC inhibits the conversion of the intensities I_γ to partial width $\Gamma_\gamma^{\text{part}}$ via the total radiative width Γ_γ. This is because Γ_γ is an inherent property of each single resonance and whilst a general trend might be obtained, it varies in particularly also for resonances of different spins. Despite the difficulties, the strength function can still be extracted up to a common factor stemming from the lack of Γ_γ. Different approaches exists in literature, but the latest works of Kopecky et al. [84, 176–178] normalize to the average strength from DRC measurements wherever available. [176]

Both techniques allow for the discrimination of the γ-ray multipolarity XL through the usage of spin-parity assignments of the initial and final states. This means that for DRC, the averaging can, in principle, be performed for groups of the same initial and final spins, provided that there are enough resonances, see Ref. [175] and references therein. In ARC however, where multiple initial spins J_i are populated simultaneously, statistical factors for the detection of different transitions need to be taken into account assuming Brink-Hypothesis, i.e. the independence of the γ-ray strength function from spins of initial and final states [175, 179, 180].

The first compilation of γ-ray strength functions from neutron resonances was published in 1981 by McCullagh, Stelts, and Chrien [174]. Since then, many updates have emerged (see e.g. Refs. [69, 84, 99, 175–178, 181]), both as new data from DRC and ARC experiments became available, but also because previous results were reevaluated due to their dependence on external data for D_0, Γ_γ and the spin-parity assignments. In some compilations the authors attempted to account for missing resonances due to small intensities in Porter Thomas fluctuations, but in the most recent compilation of 2019, Kopecky and Goriely [176] rely on that the effect is small when many transitions have been measured.

Recently, attempts have been published to obtain the γ-ray strength from **thermal capture γ-rays**. The procedure is very similar to DRC, but it is not possible to average over initial resonances, which leads to very strong fluctuations. Two independent compilations appeared in quick succession: Firestone was responsible for the evaluations in [69][10] and Kopecky [182] used a slightly different approach and other data sources. The later provides a direct comparison of the strength function for each nucleus to the HFB+QRPA calculations of Goriely et al. [101] with the Gogny+D1M force. At the current stage, the large scatter of the data poses questions to the added value of the new technique.

The authors of the γ-ray strength function database [69] have also compiled data for **average proton resonance capture**, which resembles very much the ARC technique. However, according to Goriely et al. [69] the publications often do not describe enough information for a proper analysis of systematic and statistical uncertainties.

2.4.5 Cross sections and evaporation spectra

In a statistical treatment of nuclear reactions the cross sections in the unresolved resonance region can be calculated using a formalism developed by Hauser and Feshbach [183]. Level densities and γ-ray strength functions, or more generally, γ-ray and particle transmission coefficients are input to the Hauser-Feshbach calculations. Therefore, information on them can be inferred from a comparison of calculations to experimental cross-section measurements. For applications described below that involve the Hauser-Feshbach theory, an appropriate optical potential has to be known, but this is often rather well determined for stable nuclei.

The Hauser-Feshbach formalism has been applied to the calculation of **particle evaporation spectra**. This enables the study of level densities in the quasi-continuum below the particle separation threshold and, under certain conditions, also above. The essential ideas of this method are given in Ref. [18, p. 365ff] and a review of the refinements and applications is provided in Ref. [184]. Practically, the spin-parity distribution has to be known and the resulting level density is obtained up to a normalization constant, which is usually determined by a comparison to known low-lying levels [184, 185]. Furthermore, one needs an appropriate optical potential, and the experimental condition and analysis have to be optimized to minimize the contribution of non-compound reactions [184, 186] or they need to be modeled explicitly, see e.g. Refs. [187, 188]. There are several examples that have shown a good agreement between the level densities obtained with the Oslo method and from particle evaporation spectra [185, 189, 190] . Recently the uncertainty due to the non-compound reactions has been removed by measuring low-energy γ rays in coincidence with particle spectra in the ^{64}Ni(^{9}Be, αn)^{68}Zn reaction [191]. Direct reaction or multistep have been excluded by gating on the coincidence of γ rays from transitions of known discrete

[10] Summary figures are provided in the article, but the data is not part of the online database.

levels in the residual nucleus ^{68}Zn that are primarily populated by the compound reaction.

In an excitation energy range that is usually some MeV above S_n, so that the levels already start to overlap, $\Gamma > D$, but below the "true" continuum, the level width can be determined from so-called **Ericson fluctuations** [192–194]. Ericson showed, that the "average period" of the autocorrelation function of the total neutron cross-section fluctuations is related to the average level width Γ [184]. Deviations from the average are determined by the level spacing D and thus by the level density ρ. The corresponding equations can be solved for the level density, but the final calculations require knowledge of the spin-cutoff parameter, see e.g. Ref. [195]. In addition, width fluctuation corrections might be necessary [196–198].

The **fluctuation analysis** was developed further for lower excitation energies E_x, where the levels do not overlap yet, but cannot be resolved by counting due to the detector resolution ΔE, so $\Gamma < D < \Delta E$. Originally, the technique was applied to study the level density through β-delayed particle spectra, but has later been extended to inelastic electron and proton scattering. In the derivation it is assumed that the level spacings and partial decay widths follow the Wigner and Porter-Thomas distributions, respectively. More information can be found in the outstanding (also in literary terms) review of Hansen, Jonson, and Richter [199] and the recent review of Neumann-Cosel and Tamii [200] and references therein. As the employed reactions are selective to certain spin-parities, only partial level densities are obtained. Nevertheless, this can provide very valuable information. Through the study of the giant resonances by this method, Kalmykov et al. [201] obtained e.g. the level spacings D for $2^{\pm}$ states, independently for each parity, between $E_x = 6-11$ MeV from inelastic scattering of ^{90}Zr. As before, total level densities, i.e. summed over all spins, can then be obtained assuming a given spin distribution, see e.g. Ref. [70].

Another important source of information – and an application – for level densities and γ-ray strength functions are **cross-section calculations**. In the resonance region the (phenomenological) R-matrix formalism was developed, but it provides "only" a parametrization for cross sections when experimental data exists (apart from very light nuclei, where the R matrix can be calculated directly) [202–205]. Above the resolved resonance the Hauser-Feshbach formalism is used, which for mid-mass and heavy nuclei holds approximately for incident neutron energies E_n in the range of some keVs to a few tens of MeVs. Note however, that there are some recent developments that allow for the Hauser-Feshbach calculations to extend to lower energies by adding "statistical" resonances [206]. An example of the separation in the different regions is given in Fig. 2.6. Amongst all channels, the neutron capture cross-section $\sigma_{(\mathrm{n},\gamma)}$ depends most strongly on the level density and γ-ray strength function. This was employed e.g. in Ref. [83] to infer properties of the $E1$ strength function at low energies. In the strength function database [69] also Maxwellian-averaged neutron capture cross-sections have been considered for model selection.

In the last 5 – 10 years, the calculation of neutron [13–15, 146, 147, 154, 155, 208–214] and proton [212, 215] capture cross-sections have become a popular

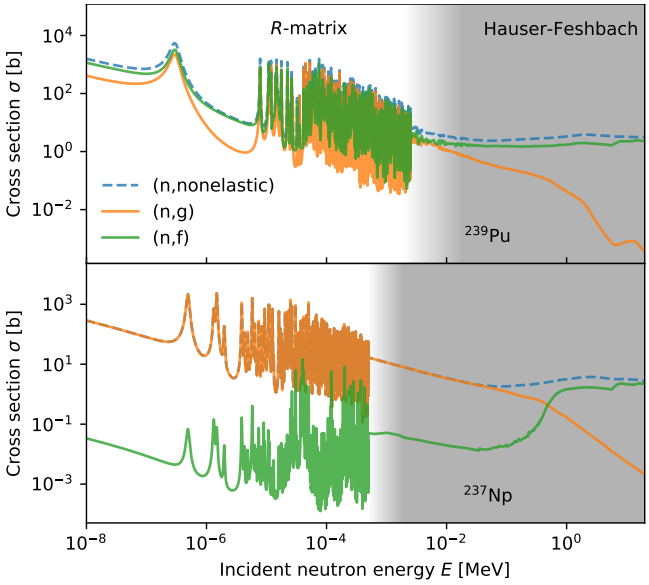

Figure 2.6: Non-elastic, absorption and fission cross-section for incident neutrons on ^{239}Pu (upper panel) and ^{237}Np (lower panel). The analysis regions for the R-matrix and Hauser-Feshbach formalism are highlighted. Data extracted from ENDF/B-VIII.0 [207].

application for the results of the Oslo method, especially for nuclei where direct measurements are impeded due to unstable target nuclei. Alternatively, the target might be stable, but measurements in the fast neutron region ($\sim 1-10$ MeV) are challenging due to a lack of appropriate monoenergetic neutron sources. Amongst the initial ideas of this thesis was that the level density and γ-ray strength function of ^{240}Pu should be used to calculate the neutron capture cross-section of ^{239}Pu. However, for actinides the fission channel (n,f) is open in addition to (n,γ), which leads to considerable challenges. As the total cross-section in the calculations is determined from the optical model, a change in the cross-sections of one channel will effect also all other open channels. From Fig. 2.6 we see that fission dominates over capture for ^{239}Pu in the energy range where the Hauser-Feshbach framework is applicable[11]. The fission cross-section is sensitive to even very small deviations in the fission barrier parameters. Due to the interdependence of the different channels, this means that the parameters for fission have to be tuned carefully even if one "just" wants to calculate capture cross-sections. In general, one needs to fit all parameters (level densities, strength-functions, fission barriers, etc.) simultaneously to arrive at a consistent description of all cross-sections, see e.g. Refs. [97, 207, 216–218]. This is beyond the scope of this thesis, although the results of Paper IV may of course be

[11] The figure provides only *evaluated* cross-sections, but they agree well with measurements (for simplicity not plotted here).

valuable input for an evaluation.

After having seen some of the challenges in cross-section calculations for actinide nuclei, it is insightful to discuss the results on ^{237}Np(n, γ) [154] and ^{242}Pu(n, γ) [155], which compare the cross-section calculations to direct measurements. Especially the former is sometimes used to state that calculations based on the level density and γ-ray strength function obtained with the Oslo method have "demonstrated [the] ability to reproduce known neutron capture rates in heavier mass nuclei" [13]. Due to the pairing energy, fission is suppressed at low energies in the odd-odd residual nucleus ^{238}Np and only starts to dominate the non-elastic cross sections above $E_n \approx 0.5$ MeV, see Fig. 2.6. So despite of the arguments raised above, the detailed treatment of the fission channel in the calculation of the capture cross-section might be negligible for $E_n \ll 0.5$ MeV. However, it should be noted that the optical model used in Ref. [154] was modified in an ad hoc manner without conservation of the behavior of the total neutron cross section. Thus, unless one performs a reevaluation of all cross-sections, it seems safest to use the results of the Oslo method for non-fissionable nuclei and to keep in mind the influence of the optical model. Depending on the nucleus other parameters may also be important, like coupled-channels calculations for deformed nuclei.

Finally, I want to discuss a novel approach to model (n,γ) cross sections for unstable nuclei developed by Escher et al. [219] and recently applied also in Ref. [220]. It uses (d, p) as a surrogate reaction for the (n,γ) reaction. The central idea is that the neutron capture cross section $\sigma_{(\mathrm{n},\gamma)}$ can be expressed in the Hauser-Feshbach formalism as a product of the compound nucleus (CN) formation cross-section $\sigma^{(\mathrm{CN})}$ and the probability of γ decay $G_\gamma^{(CN)}$ from the compound states, [183, 221]

$$\sigma_{(\mathrm{n},\gamma)}(E_n) = \sum_{J,\pi} \sigma^{(\mathrm{CN})}(E_x, J, \pi) G_\gamma^{(CN)}(E_x, J, \pi), \tag{2.27}$$

where the excitation energy E_x can be related to the incident neutron energy E_n. The CN formation can be calculated reasonably well from the optical model for (n,γ), and from a breakup-fusion formalism for (d, p), see e.g. Ref. [221, 222] and references therein. Using these calculations, Escher et al. [219] inferred $\sigma_{(\mathrm{n},\gamma)}$ from a Bayesian fit to a selection of measured proton$-\gamma$ coincidences. In the fit, the level density and γ-ray strength function served as parameters. The comparison of the calculated cross-sections of Refs. [219, 220] to direct measurements looks very promising, but it is difficult to judge the impact of their work, as no information of the prior and posterior distributions of the fitted parameters is provided.

2.4.6 Other experiments

Above the particle separation threshold, the photo-excitation cross-section and γ-ray strength $\vec{f}$ can be measured using **photonuclear reactions**, see Eq. (2.11). These measurements are very important, as they map the GDR. In 2019, the

IAEA has released a major update of their data library, which addresses different experiments, their analysis and in particular also the discrepancies between the results obtained at different facilities [134].

Furthermore, the decay strength function $\overleftarrow{f}$ has been studied with **inelastic electron** or **proton scattering**, where the nucleus is excited by the exchange of a virtual photon, see the reviews in Refs. [69, 200, 223] and references therein. Amongst the most prominent contributions of these experiments is the first experimental report of the $M1$ scissors resonance. This excitation mode had been predicted several year earlier by Iudice and Palumbo [224] and Iachello [225], based on the work of Bohr and Mottelson [226], and the experimental confirmation was performed using an $(\mathrm{e}, \mathrm{e}')$ reaction [136, 227]. Note that the recent database [69] for γ-ray strength functions contains only very few datasets from inelastic scattering experiments.

Finally, I want to highlight a recent development in the **Ratio method**, which was initially applied to obtain the decay strength $\overleftarrow{f}$ from $\gamma-\gamma$ coincidences following a (d, p) reaction [144, 228], but subsequently also in $(\mathrm{p}, \mathrm{p}')$ [76], $(\vec{\gamma}, \gamma\gamma)$ [68, 166] (see Section 2.4.3, where the Ratio method is briefly introduced), and (p, γ) [229] reactions. Based on the work of Wiedeking et al. [144] we have introduced the **Shape method** [230] to obtain the γ-ray strength function (again, apart from the absolute normalization) also from experiments with worse γ-ray resolution. We have demonstrated that the technique can in many cases be applied to the same data that is used in the Oslo method and thus serve as an intrinsic normalization of the "slope" parameter of the γ-ray strength and, as they are coupled, also of the level density [231].

Chapter 3

Summary of Papers

Paper I A new software implementation of the Oslo method with rigorous statistical uncertainty propagation

In this article we present a complete reimplementation of the software used for the Oslo method. The new library OMpy supersedes a collection of codes that have become known as the oslo-method-software. We review all steps of the Oslo method and present derivations of the essential equations. The library focuses primarily on a rigorous propagation of statistical uncertainties, where the differences to the oslo-method-software are discussed thoroughly. It also facilitates a transparent tracking of several systematic uncertainties. To verify the implementation of OMpy we apply it to a previously published dataset on ^{164}Dy and data that was synthetically generated by a Monte Carlo decay code. As a step towards transparency and reproducibility, all functions are documented automatically and the whole analysis is published and can be re-run online at CodeOcean.

Paper II The γ-ray energy response of the Oslo Scintillator Array OSCAR

Every experiment requires that we understand our measurement devices. The interaction of γ rays with the detector and surrounding materials is called the detector response. A precise knowledge of it is necessary for the *unfolding* of γ-ray spectra, which is the first step of the Oslo method and other experiments like the extraction of prompt-fission γ rays (Paper VI). In this article we use the Monte Carlo particle transport code Geant4 to characterize the response of the newly commissioned γ-ray detector array OSCAR, which consists of 30 large volume $LaBr_3(Ce)$ crystals. The results are verified by a comparison to measurements from calibration sources and in-beam γ rays.

Paper III Impact of restricted spin-ranges in the Oslo Method: The example of $(d, p)^{240}$Pu

The Oslo method makes strong assumptions on the probability to populate levels of different spin-parities. Whilst these assumptions may be fulfilled for mid-mass nuclei, recent studies suggest that there may be complications when using a (d, p) reaction to populate on actinide nuclei due to a low spin transfer. In this proceedings we present a quantitative study of the effect on the example of a ^{239}Pu$(d, p)^{240}$Pu experiment with a deuteron beam energy of 12 MeV, which is below the Coulomb barrier. The analysis is performed on synthetic datasets with known input level density and γ-ray strength function that can be compared to the results when applying the Oslo method. We find a good agreement between input and results only when the assumptions of the Oslo method are fulfilled. We quantify

the deviations that arise when we use more realistic calculations of the population cross-section for this reaction. Furthermore, we show that the mismatch persists when using a correction method, which was proposed in [Guttormsen et al., PRL **16**, 109 (2012)] and that has been applied to all previous Oslo method analyses of actinide nuclei.

Paper IV Restricted spin-range correction in the Oslo method: The example of nuclear level density and γ-ray strength function from ^{239}Pu(d, pγ)^{240}Pu

This article expands on Paper III and we develop new solution to correct for the low spin transfer of the sub-Coulomb barrier (d, p) reaction. The level density and γ-ray strength function for the residual nucleus ^{240}Pu are obtained from an iterative procedure in which we compare the results of applying the Oslo method on experimental and synthetic data. We show that the results modified by the new iterative method provide a better fit to the experimental data, but highlight also the challenges of the procedure that we have adopted.

Moreover, we provide a more detailed discussion on the spin-parity resolved population cross-sections that are the basis of the decay simulations of the iterative method. They are obtained from Green's Function Transfer calculations, which treat the (d, p) reaction as a compound nucleus formation of the target with a neutron emitted from deuteron breakup. It is shown that this dominates for a sub-Coulomb reaction over the "standard" compound reaction mechanism as obtained with the reaction code TALYS, and the resulting population probability is compared to the intrinsic spin-parity distribution.

Paper V gledeli: Gamma-ray strength function and nuclear LEvel DEnsity LIkelihoods

Despite the extremely high relevance of nuclear level densities and γ-ray strength functions for nuclear theory and applications, there exists to date no common framework to evaluate the results of different types of experiments. Here, we introduce gledeli, a modular framework for γ-ray strength function and nuclear level density likelihoods. In this first application of gledeli we include three observables, i) particle$-\gamma$ coincidences from the Oslo method ii) neutron capture data (D_0 and $\langle\Gamma_\gamma\rangle$), and iii) photonuclear cross-sections. Due to the flexibility of the approach other observables can be included in future versions. On the example of ^{162}Dy, we demonstrate how a simultaneous Bayesian fit to many experimental observables can contribute to find recommended level densities and strength functions, as suggested in the recent IAEA database project for γ-ray strength functions [Goriely et al., EPJA **55**, 172 (2019)], or serve as a guideline in the comparison to microscopic calculations.

Paper VI Energy dependence of the prompt γ-ray emission from the (d, p)-induced fission of ^{234}U* and ^{240}Pu*

This article features an exploratory analysis of prompt-fission γ rays obtained at the Oslo Cyclotron Laboratory. The data is extracted from

the same experiment as in Paper III (and a similar ^{233}U(d, p) experiment), but for the Oslo method we have to reject all fission events. We now demonstrate that this data can be used to obtain valuable information on prompt-fission γ-rays. We show for the first time how the (d, p)-induced fission can be used to obtain γ-ray spectra for different excitation energies in the fissioning compound nuclei ^{234}U and ^{240}Pu. With this surrogate reaction we can measure spectral characteristics like the γ-ray multiplicity, and the average and total emitted γ-ray energy for an excitation energy range comparable to fast-neutron induced fission, which is very challenging to measure directly. Above the fission barrier, no significant change in the γ-ray characteristics as a function of the excitation energy of the fissioning nucleus is observed, even though an additional $\sim$5 MeV is potentially available to fission fragments. The results are compared to model calculations with the fission code GEF and experimental data on thermal-neutron induced fission, and possible differences from using the (d, p) reaction are highlighted.

Chapter 4

Summary and outlook

> *When I say "honesty and transparency are not enough," I'm not dissing honesty and transparency. I'm just saying you can be as honest and transparent as anybody, but you're still not gonna move forward if you're trying to use a bathroom scale to weigh a feather – and the feather is resting loosely in the pouch of a kangaroo that is vigorously jumping up and down.*
>
> — Andrew Gelman, *Blog post on his article "Honesty and transparency are not enough"*

Obtaining reliable information on nuclear level densities and γ-ray strength functions remains a challenge for experimental and theoretical nuclear physics. They are essential ingredients for cross-section calculations, which are used in various fields ranging from nuclear energy and nuclear medicine to the understanding of the formation of our universe from astrophysical observations.

This thesis started with a review of the concepts and definitions behind the level density and γ-ray strength function in Chapter 2. I have introduced common empirical descriptions and briefly summarized the state of experiments and (semi-)microscopic calculations. The focus here has been on how experiments may be used as a tool for inference and testing of different models and parametrizations of the level density and strength function. I have also tried to highlight the challenges and assumptions that are involved in the different experiments, as a proper knowledge of the limitations is necessary when comparing different experiments either between each other or to theoretical calculations.

A major part of this thesis was dedicated to the exploration and quantification of the statistical uncertainties in the Oslo method. In Paper I we introduce OMpy, which is a reimplementation of the software used in the Oslo method with a focus on a complete propagation of the statistical uncertainties. A considerable effort has been devoted to the development and clear documentation of all functions of the software. The code facilitates a transparent and reproducible analysis. To stand by our goals, we have published the whole analysis of the article such that it can be re-run online at CodeOcean. However, as remarked by Gelman, "honesty and transparency are not enough". Therefore, OMpy does not remain a naive translation of the old programs, but we have attempted to improve and justify the statistical treatment of the data at every stage. The propagation of systematic uncertainties is facilitated where alternative models exists. Finally, the package has also been verified on simulated data with known input level densities and strength functions.

After this first general overview of all aspects of the Oslo method, the next three articles treat specific challenges. The interpretation of any experimental measurement requires that we have a precise knowledge of our measurement devices. In Paper II we characterized the γ-ray energy response of the recently commissioned $LaBr_3(Ce)$ array OSCAR. We used the Monte Carlo particle transport code Geant4 to simulate the interaction of γ-rays with the detectors and show that there is an excellent agreement between our simulations and experimentally obtained γ-ray spectra. In Appendix B we have extended the comparison of the detector efficiency to higher energies with data that was recently obtained in the Master thesis of Paulsen [232].

In Papers III and IV the level density and γ-ray strength function of ^{240}Pu were obtained. We explored a limit of the Oslo method and tested an assumption that is essential for the first-generation method and the decomposition into the level density and γ-ray strength function. Strictly speaking, the first-generation method is only applicable if a reaction populates approximately the same fraction of levels of a given spin-parity in the whole excitation energy range. Furthermore, it is usually assumed that levels are populated proportionally to the intrinsic spin distribution in order to extract and normalize the level density and γ-ray strength function. Through the analysis of synthetic data that was generated from the statistical decay code RAINIER [57] we have shown that the Oslo method provides consistent results if the assumption is fulfilled. However, the two articles have also demonstrated in a first quantitative study that the assumption fails for the $(d, p)^{240}$Pu experiment that we performed, as the deuteron beam energy was below the Coulomb barrier leading to a more selective reaction. For lower and mid-mass nuclei the beam energies are usually above the Coulomb barrier, such that this is not expected to be a problem. Moreover, we observed that the problem persists when using a modified normalization procedure that was applied in previous analyzes of actinide nuclei. We have developed a new iterative method to correct for the population cross-section and highlighted the challenges that remain despite of this procedure.

In Paper V we looked at the challenge of obtaining information on level densities and γ-ray strength functions from a broader perspective and introduced gledeli, a modular code for Gamma-ray strength function and LEvel DEnsity LIkelihoods. The idea arose from the realization that there are a variety of different experimental techniques available that can be used to infer and test information on level densities and γ-ray strength function, but often only one observable is used at a time. Instead, we propose to explore the parameter-space with a likelihood that contains all available experimental data for a given nucleus. For the example of ^{162}Dy we have combined experimental data from the Oslo method (the first generation matrix), neutron capture data (D_0 and $\langle\Gamma_\gamma\rangle$) and photonuclear cross-sections. Using the powerful scanners implemented in the ScannerBit package [233] of GAMBIT [234] we were able to obtain simultaneous fits of the profile likelihoods and posterior distributions for all parameters of two competing level density and strength function models.

In the last part of this thesis, I have examined additional challenges and perspectives when working with actinide targets. One of the initial goals was

to improve neutron capture cross-section calculations through the usage of experimentally determined level densities and γ-ray strength functions. However, as explained in Section 2.4.5, for actinides the fission channel is open in addition to neutron capture. The complex interplay of all open channels requires e.g. that fission parameters are simultaneously refit if one replaces the input level densities and γ-ray strength functions. This is a formidable task and beyond the scope of this thesis, but the results of Paper IV can be used to inform future cross-section evaluations.

The Oslo method requires that we remain selective on γ decay, thus events with a trigger in the fission detectors have to be rejected. Despite several attempts to use the fission-vetoed data for excitation energies above the onset of the (sub-barrier) fission of ^{240}Pu, I was not able to find a satisfactory solution, but excluded this region for the analysis in Paper IV. In hindsight, we see that this might be explained by a failure of the first-generation method and thus of the Oslo method for this energy region, as we find that there is a major change in the populated spin-parities that we calculated in Paper IV at around the same energy as the inset of sub-barrier fission.

However, finally the search for improvements on the data processing for actinide targets resulted in the development of a novel technique to study prompt-fission γ rays. In Paper VI we performed an exploratory analysis of the (d,p) induced fission to reveal spectral characteristics of prompt-fission γ rays as a function of the excitation energy. The reaction serves as a surrogate for neutron induced fission and enables us to study an excitation energy range comparable to fast-neutron induced fission. This knowledge is important for next generation reactors, but challenging to obtain directly due to the lack of appropriate mono-energetic neutron sources that could cover the full energy range. We extracted the fission gated γ-ray spectra and important summary statistics: the average multiplicity, and the average and total γ-ray energy emitted per fission for the compound nuclei ^{234}U and ^{240}Pu. From our data we find no significant change of the γ-ray spectra above the fission barrier.

4.1 Future research

I conclude with a collection of possible measures that go beyond the results presented in this thesis:

- The study of prompt-fission γ rays with the (d,p) reaction provides extremely useful data on the spectral characteristics. In Paper VI we had to resort to a crude approximation of the neutron contribution, but the new experiments performed with OSCAR can use the superior timing resolution of the $LaBr_3$(Ce) detectors to discriminate neutrons by time-of-flight[1]. Furthermore, the difference between (d,p) and (n,γ) reactions

[1] This is shown in the Master thesis of D. Gjestvang, whom I have co-supervised, and it is subject to her forthcoming publication *Measurement and simulation of prompt-fission γ rays from the (d, p)-induced fission of* ^{241}Pu*

should be studied in more detail to improve the understanding of the impact of the reaction mechanism.

- The impact of the population cross-section should be studied for the previously conduced actinide experiments, as well as other experiments if the beam energies are close to or below the Coulomb barrier.
- OMpy has been written with modularity in mind and the users are encouraged to test new methods and functionalities:
  - I have proposed to couple OMpy to PyFBU [235], a python based implementation of the *Fully Bayesian Unfolding* [236], and provided a basic example for this online. In contrast to the currently implemented unfolding routine in OMpy, this allows to extract the full correlation of unfolded spectra. The application of PyFBU for the Oslo method and fission data is now studied in more detail in two Master theses.[2]
  - As explained in Paper I, the current version (v1.1.0) of OMpy assumes a common uncertainty of 30% for each datapoint in the normalization of the level densities and γ-ray strength function. This somewhat arbitrary assumption is lifted in a forthcoming update[3] which introduces a class that treats the uncertainty of each data point as nuisance parameter.
- A transparent publication of the full analysis together with the articles can improve the reproducibility of the research, and promote reuse and testing of new models and theories. In this thesis two new libraries were developed and presented, OMpy and gledeli, that facilitate this process for the study of level densities and γ-ray strength functions.
- The recently completed IAEA database project for γ-ray strength functions [69] was supposed to compile *and* establish recommended strength functions for users. The latter goal was not achieved, due to the lack of a full uncertainty analysis for all datasets and a common framework to treat different experiments. I propose to couple gledeli to a Hauser-Feshbach code and a decay code like RAINIER. This should open the possibility to describe the likelihood of data from any experiment using a common level density and γ-ray strength function model.
- For the case of the particle$-\gamma$ coincidence data, the coupling of gledeli to a decay code would also enable us to turn assumptions of the Oslo method (that hold or do not hold) into parameters. Instead of using the first-generation spectra, one could for example generate and compare the all-generations spectra to data directly, using population cross-sections as an additional input to the simulations.

[2] V. Valsdottir has graduated on "Exploring Fully Bayesian Unfolding for γ-ray Spectra" in August 2020 (to be published) and J. Due at the time of writing continues this work.

[3] V. W. Ingeberg et. al. "Nuclear level density and γ-ray strength function of ^{67}Ni", (working title), *Manuscript in preparation.*

- To learn more about the validity of level density and γ-ray strength function models for different mass-regions, OMpy and/or gledeli should be applied to all previously published results. If a database was created with the raw-data for all experiments and meta-data like the extraction limits for the Oslo method, the analysis for all nuclei could in addition easily be re-run for all major updates, such as the implementation of a new unfolding mechanism. Furthermore, it would facilitate the comparison of existing and the test of new models across the nuclear chart.

- It would be extremely helpful to create an update review and compilation of level densities *and* γ-ray strength functions, similar to the recently conducted IAEA projects [69, 134]. For many experiments and applications, the knowledge of these two quantities is inherently coupled and this should be preserved for consistent results. Again, packages like OMpy and gledeli facilitate the publication of coupled results through a full list of samples from the posterior distributions.

Papers

Paper I

A new software implementation of the Oslo method with rigorous statistical uncertainty propagation

Midtbø, J. E.†, Zeiser, F.†, Lima, E., Larsen, A. C., Tveten, G. M., Guttormsen, M., Bello Garrote, F. L., Kvellestad, A., Renstrøm, T.

Accepted for publication in *Computer Physics Communications*, arXiv: 1904.13248.
Erratum: Published after submission, CPC Vol. 262 (2021) 107795. DOI: 10.1016/j.cpc.2020.107795.
† These authors are shared first authors with equal contributions.

A new software implementation of the Oslo method with rigorous statistical uncertainty propagation

Jørgen E. Midtbø[a,*], Fabio Zeiser[a,**], Erlend Lima[a], Ann-Cecilie Larsen[a], Gry M. Tveten[a,b], Magne Guttormsen[a], Frank Leonel Bello Garrote[a], Anders Kvellestad[a], Therese Renstrøm[a]

[a] *Department of Physics, University of Oslo, N-0316 Oslo, Norway*
[b] *Expert Analytics AS, 0160 Oslo, Norway*

Abstract

The Oslo method comprises a set of analysis techniques designed to extract nuclear level density and average γ-decay strength function from a set of excitation-energy tagged γ-ray spectra. Here we present a new software implementation of the entire Oslo method, called `OMpy`. We provide a summary of the theoretical basis and derive the essential equations used in the Oslo method. In addition to the functionality of the original analysis code, the new implementation includes novel components such as a rigorous method to propagate uncertainties throughout all steps of the Oslo method using a Monte Carlo approach. The resulting level density and γ-ray strength function have to be normalized to auxiliary data. The normalization is performed simultaneously for both quantities, thus preserving all correlations. The software is verified by the analysis of a synthetic spectrum and compared to the results of the previous implementation, the `oslo-method-software`.

PROGRAM SUMMARY

Program Title: `OMpy` [1]
Code Ocean Capsule: [DOI follows with publication]
Licensing provisions: GPLv3
Programming language: Python, Cython
Reference of previous version: `oslo-method-software`
Does the new version supersede the previous version?: Yes
Reasons for the new version: Facilitate modular program flow and reproducible results in a transparent and well-documented code base. Updated uncertainty quantification: formerly a stage-wise normalization without built-in uncertainty propagation.
Summary of revisions: Complete reimplementation; ensemble based uncertainty quantification throughout whole method; fitting based on well-tested external libraries; corrections for the normalization procedure; auto-documentation with `Sphinx`
Nature of problem: Extraction of the nuclear level density and average γ-ray strength function from a set of excitation-energy tagged γ-ray spectra including the quantification of uncertainties and correlations of the results.
Solution method: The level density and γ-ray strength function can be obtained simultaneously using a set of analysis techniques called the Oslo method. To propagate the uncertainty from the counting statistics, we analyze an ensemble of perturbed spectra, which are created based on the experimental input. One obtains a set of level densities and γ-ray strength functions for each realization from a fit process. The fitting metric (χ^2) is degenerate, but the degeneracy is removed by a *simultaneous* normalization of the level density and γ-ray strength function to external data, such that all correlations are preserved.

Keywords: Oslo method; Nuclear level density; γ-ray strength function; Degenerate inverse problem

1. Introduction

One long-standing challenge in nuclear physics is to precisely determine nuclear properties at excitation energies above the discrete region and up to the particle threshold(s). This region is often referred to as the *quasicontinuum* and represents an excitation-energy range where the quantum levels are very closely spaced. That leads to a significant degree of mixing (complexity) of their wave functions, but they are still not fully overlapping as in the continuum region. For the quasicontinuum, it is fruitful to introduce average quantities to describe the excited nucleus: instead of specific levels, the level density $\rho(E_x)$ as a function of excitation energy E_x is used, and instead of specific reduced transitions strengths $B(XL)$ between a given initial and final state, the average decay strength represented by the γ-ray strength function (γSF) is applied.

* jorgenem@gmail.com
** fabio.zeiser@fys.uio.no
erlenlim@fys.uio.no

In addition to their key role in describing fundamental nuclear properties, both the level density and the γ-ray strength function are vital components for calculating cross sections and reaction rates for explaining the nucleosynthesis of heavy elements in astrophysics [2, 3]. The ability to calculate cross sections may also help in the design of next generation nuclear reactors, where direct cross section measurements are missing or have too high uncertainties for the given application [4–7].

The Oslo method [8–11] allows for extracting the level density ρ and the γSF simultaneously from a data set of particle γ-ray coincidences. It has been implemented in a collection of programs known as the `oslo-method-software` [12], and the analysis has been successfully applied to a range of nuclei in widely different mass regions [13–16]. However, the Oslo method consists of several non-linear steps. This makes an analytical propagation of statistical and systematic uncertainties very difficult, and thus hampers a reliable uncertainty quantification for the final results. The statistical uncertainty propagation from unfolding the γ spectra and the determination of the primary γ-ray distribution has so far not been addressed in a fully rigorous way. In lieu of this, an approximate uncertainty estimation has been used, which is described in Ref. [11]. Moreover, uncertainties related to the absolute normalization of the level density ρ and γSF have been discussed in Ref. [17], but there was no automatized way to include this in the final results. Approximate ways to include normalization uncertainties have been suggested and used, see e.g. Ref. [18], but they do not account for correlations between parameters as they were not available within the `oslo-method-software`.

In this work, we approach the problem of uncertainty propagation using a Monte Carlo technique. By generating an ensemble of perturbed input spectra, distributed according to the experimental uncertainties, and propagating each ensemble member through the Oslo method, we can gauge the impact of the count statistics on the final results. The resulting level density and γ-ray strength function have to be normalized to external data. We have implemented a new simultaneous normalization for both quantities, thus preserving all correlations between them.

In the following, we present `OMpy`, the new implementation of the Oslo method. We discuss the various steps of the method and present our new uncertainty propagation and normalization routine. The code is tested by the analysis of a synthetic spectrum. The capability of the new method is illustrated by applying it to experimental data and a comparison to the previous implementation.

2. Usage of `OMpy`

`OMpy` is designed to facilitate a more complete uncertainty propagation through the whole Oslo method and at the same time simplify the user interface and enhance the reproducibility of the analysis. This section will focus on the latter two goals. `OMpy`, as well as all the Jupyter notebooks and datasets used to create the figures in this article, is available online [1] [+ Code Ocean [DOI follows with publication]].

The documentation of the interface of `OMpy` is created automatically from its source code with the `sphinx-automodapi` package and is available from ompy.readthedocs.io. A detailed example of the usage is provided in the `getting-started` Jupyter notebook. Taking a step beyond just listing the version number, we have set up a `docker` container to ensure also the reproducibility of the software environment in which the user runs the analysis. The notebooks can be run interactively online without installation through Binder [19], although a limit on the available computation power can lead to considerable computation times for cases with large ensembles. For larger calculations we recommend the Code Ocean [DOI follows with publication] capsule.

As most operations within the Oslo method will require working on binned quantities like γ-ray spectra or level densities, or a collection of spectra into matrices, we have created the `Vector` and `Matrix` classes. These store the count data as one- or two-dimensional `NumPy` [20, 21] arrays, together with an array giving the energy calibration for each axis. The classes also contain a collection of convenience functions e.g. for saving and loading files to disk, rebinning and plotting.

3. The Oslo method

The starting point for the Oslo method is an E_x-E_γ *coincidence matrix*, i.e. a set of γ-ray spectra each stemming from an identified initial excitation energy E_x. A standard way to construct this input matrix is from coincidence measurements of γ rays and charged ejectiles following inelastic scattering or transfer reactions with light ions. An array of γ-ray detectors measures the energy E_γ of the emitted γs, while a particle telescope determines the excitation energy E_x using the energy deposited from the outgoing charged particles. (For a detailed description, see e.g. Ref. [17] and references therein.) Recently, other methods have been developed that obtain the coincidence matrix from γ rays in β-decay [22] or in an inverse kinematics setup [23]. An example of a coincidence matrix for ^{164}Dy from a standard Oslo method experiment [14, 24] at the Oslo Cyclotron Laboratory is shown in panel (a) of Fig. 1.

The first step of the Oslo method is to *unfold*, i.e., deconvolute the γ-ray spectra for each excitation energy to compensate for the detector response (Compton scattering, pair production, etc.). This is implemented in the `Unfolder` class using an iterative unfolding method described in Ref. [25]. We reiterate the main points of the procedure in Appendix A. There we also describe a routine to select the best iteration, which has already been implemented in the `oslo-method-software` but not yet published elsewhere. The unfolded ^{164}Dy spectrum is shown in Fig. 1 (b).

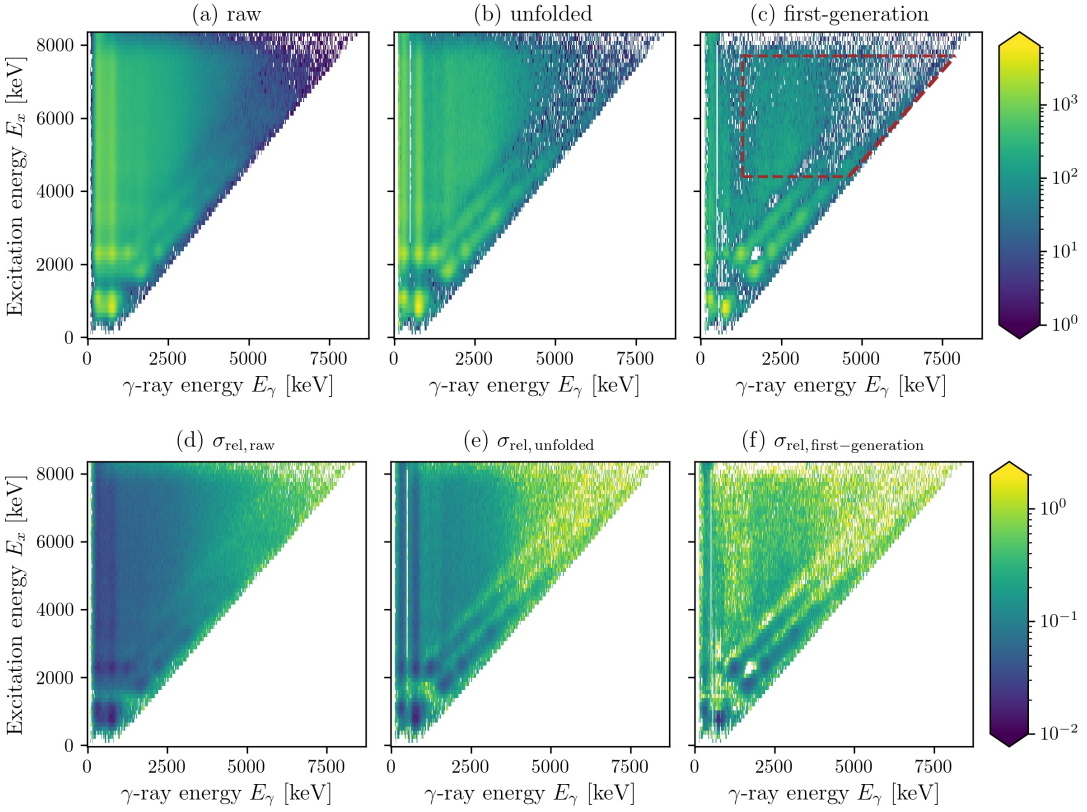

Figure 1: Raw (a), unfolded (b) and first-generation (c) matrices for the ^{164}Dy dataset [14, 24], as well as the respective relative standard deviation matrices (d-f) obtained with the ensemble propagation technique for $N_{\mathrm{ens}} = 50$ realizations. The dashed lines in panel (c) highlight the fit limits for ρ and f.

The second step is the determination of the *first-generation*, or *primary*, γ-ray spectrum for each excitation energy. In the `FirstGeneration` class an iterative procedure is applied as described in Ref. [26]. We recapitulate the procedure in Appendix B, including a small addition to minimize fluctuations in higher order iterations. The resulting first-generation γ-ray matrix is shown in panel (c) of Fig. 1. The main assumption of the first-generation method is that the γ-ray spectra following the populations of levels within the excitation energy bin E_x by the inelastic or transfer reaction are the same as when this excitation energy bin is populated via γ-ray decay from higher lying levels [17]. Although this plausible at first sight, it requires that the spin-parity distribution of the populated levels is approximately independent of the excitation energy [17, 27].

The next step of the Oslo method consists of fitting the first-generation spectra by a product of two one-dimensional functions, namely the *nuclear level density* $\rho(E_x)$ and the *γ-ray transmission coefficient* $\mathcal{T}(E_\gamma)$. The method relies on the relation

$$P(E_x, E_\gamma) \propto \rho(E_f = E_x - E_\gamma)\mathcal{T}(E_\gamma), \tag{1}$$

where we look at deexcitations from an initial excitation energy bin E_x to the final bin E_f, such that the γ-ray energy is $E_\gamma = E_x - E_f$. Here, $P(E_x, E_\gamma)$ is a matrix of first-generation spectra $FG(E_\gamma)_{E_x}$ normalized to unity for each E_x bin.[1] Furthermore, if we assume that the γ decay at high E_x is dominated by dipole radiation, the transmission coefficient is related to the dipole *γ-ray strength function* $f(E_\gamma)$ (or γSF) by the relation

$$\mathcal{T}(E_\gamma) = 2\pi E_\gamma^3 f(E_\gamma). \tag{2}$$

[1] Note that we follow the standard notation for the Oslo method, where $P(E_x, E_\gamma)$ is the conditional probability $p(E_\gamma|E_x)$ for the first γ-ray transition with energy E_γ to come from an initial excitation energy E_x.

A derivation of Eq. (1) is shown in Appendix C, where the main assumptions underpinning this decomposition are:

- The compound nucleus picture: We assume that the γ decay from an excited nuclear state is independent of how the excited state was formed. This goes back to Bohr's theory for compound nuclei [28] and is supported by many experiments [14, 29–36].
- Dominance of dipole radiation: It is assumed that the decay it dominated by dipole radiation. This is strongly supported by data and theory, see e.g. Refs. [36–47].
- The generalized Brink-Axel hypothesis: The γ-ray strength function $f(E_\gamma)$ is independent of the initial and final states, i.e., it is the same for excitations and decays between any initial and final state that are separated by the energy E_γ [40, 48–54].
- The population cross-section: To obtain the "summed" level density $\rho(E_f) = \sum_J \rho(E_f, J)$ in Eq. (1) the population cross-section has to be approximately proportional to the intrinsic spin distribution $g(E_x, J)$ (and we assume parity equilibration, i.e. $\rho(E_x, J, \pi = +) \approx \rho(E_x, J, \pi = -)$). When the employed reaction is very spin selective, like in β-decay, a weighted sum of the level densities is obtained instead, see Eq. (C.14).

Finally, we have to normalize the nuclear level density $\rho(E_x)$ and γ-ray strength function $f(E_\gamma)$ (or equivalently, the γ-ray transmission coefficient $\mathcal{T}(E_\gamma)$). It was shown by Schiller et al. [11] that the solution to Eq. (1) is invariant under a Lie group G of transformations by three continuous real valued parameters A, B and α:

$$\rho(E_f = E_x - E_\gamma), f(E_\gamma) \xrightarrow{G} Ae^{\alpha E_f}\rho(E_f), Be^{\alpha E_\gamma} f(E_\gamma). \tag{3}$$

However, we stress that the degrees of freedom are limited to those given by G – i.e., all shape features of ρ and f beyond the exponential prefactor given by G are uniquely determined by the fit. It is important to note that the α parameter, which influences the slope (in a log plot) of the functions, is common to ρ and f. Hence, their normalizations are coupled together in the Oslo method. To obtain the physical solution, the level density and γSF need to be normalized to auxiliary data. Typically, one uses s-wave resonance spacings, D_0, from neutron capture experiments as well as discrete levels to fix the level density normalization, and augment this by average total radiative width data, $\langle\Gamma_\gamma\rangle$, to normalize the γSF. This will be discussed in more detail in the next sections.

4. Uncertainty propagation by ensemble

We use an approach based on the Monte Carlo (MC) technique to estimate the statistical uncertainties in the Oslo method by creating an ensemble of randomly perturbed copies of the data set under study. To illustrate the method, we have chosen an experimental data set for ^{164}Dy. The data was obtained in Ref. [24] and we will compare our results to the reanalysis published by Renstrøm et al. [14].

The random variables are the experimental number of counts in each bin i in the raw E_x-E_γ coincidence matrix R. We assume that they are independent and follow a Poisson distribution with parameter λ_i. The Poisson distribution $\mathcal{P}_\lambda$ is given as

$$\mathcal{P}_\lambda = p(k|\lambda) = \frac{\lambda^k e^{-\lambda}}{k!} \tag{4}$$

We take the number of counts k_i in bin i of R as an estimate for the Poisson parameter λ_i. Note that it is an unbiased estimator for λ_i, since the expectation value $\langle k\rangle = \lambda$. To generate a member matrix R_l of the MC ensemble, the counts in each bin i are replaced by a random draw from the distribution $\mathcal{P}_{k_i}$. By this procedure, we obtain $N_{\rm ens}$ matrices representing different realizations of the experiment. Defining $\vec{r}_i = (r_i^{(1)}, r_i^{(2)}, \ldots, r_i^{(N_{\rm ens})})^T$ as the vector of all $N_{\rm ens}$ realizations m of bin i we can calculate the sample mean $\langle\vec{r}_i\rangle$,

$$\langle\vec{r}_i\rangle = \frac{1}{N_{\rm ens}}\sum_{l=1}^{N_{\rm ens}} r_i^{(m)}, \tag{5}$$

and standard deviation σ_i,

$$\sigma_i = \sqrt{\frac{1}{N_{\rm ens}}\sum_{l=1}^{N_{\rm ens}}\left(r_i^{(m)} - \langle\vec{r}_i\rangle\right)^2}. \tag{6}$$

Of course, in the case of the raw matrix R, the standard deviation is trivial because it is given by the Poisson distribution ($\sigma = \sqrt{\lambda}$). But the technique also allows us to estimate the standard deviation at later stages in the Oslo method – after unfolding, after the first-generation method and even after fitting the level density and γ-ray transmission coefficient. In Fig. 1 we show the relative standard deviations $\sigma_{{\rm rel},i} = \sigma_i/r_i$ in the raw (d), unfolded (e) and first-generation (f) matrices of the ^{164}Dy dataset based on $N_{\rm ens} = 50$ ensemble members.

It should be noted that we usually analyze spectra with a (possibly time-dependent) background. In this case we measure two raw spectra, the total and the background spectra, which independently follow a Poisson distribution. In `OMpy`, both spectra can be read in and perturbed independently. The background subtracted spectra R' are then generated for each realization. When the number of background counts are large enough, this may lead to bins in R' with negative number of counts. With the current default, these are removed before further processing at the cost of a potential bias towards higher level densities ρ and strength functions f (see the discussion in Sec. 7). The generation of the all ensembles matrices (including application of the unfolding and first-generation method) is handled by the `Ensemble` class.

5. Decomposition into level density and γ-ray strength function

With the first-generation matrices and their standard deviation at hand, we may proceed with the fitting of ρ and $\mathcal{T}$ for each ensemble member. First, we select a suitable bin size ΔE, typically $100-300$ keV depending on the detector resolution, and rebin the first-generation matrix along both the E_x and E_γ axes to this bin size. The matrix of experimental decay probabilities $P_{\rm exp}(E_x, E_\gamma)$ is obtained by normalizing the spectrum in each E_x bin to unity. For the fit of ρ and $\mathcal{T}$, we take the function value in each bin as a free parameter. For a given pair of trial functions $(\rho, \mathcal{T})$, the corresponding matrix $P_{\rm fit}(E_x, E_\gamma)$ is constructed by

$$P_{\rm fit}(E_x, E_\gamma) = C_{E_x}\rho(E_x - E_\gamma)\mathcal{T}(E_\gamma), \tag{7}$$

where C_{E_x} is a normalization coefficient so that $\sum_{E_\gamma} P_{\rm fit}(E_x, E_\gamma) = 1\ \forall E_x$. We fit $P_{\rm fit}$ by a χ^2 minimization approach, minimizing the weighted sum-of-squared errors

$$\chi^2 = \sum_{E_x, E_\gamma} \left(\frac{P_{\rm exp}(E_x, E_\gamma) - P_{\rm fit}(E_x, E_\gamma)}{\sigma_{P_{\rm exp}}(E_x, E_\gamma)} \right)^2. \tag{8}$$

It is important to use a weighted sum rather than simply a sum of the residuals, to suppress the influence of bins with large uncertainties. This in turn makes uncertainty estimation important. As already mentioned, a shortcoming of the original Oslo method implementation [11] in the `oslo-method-software` has been the estimation of the uncertainty $\sigma_{P_{\rm exp}}(E_x, E_\gamma)$ in the denominator of the χ^2 fit. Due to the lack of a complete statistical uncertainty propagation, one has had to resort to an approximate uncertainty estimation. It was based on a Monte Carlo scheme similar to the present work, but where only the first-generation spectrum is perturbed as if each entry was direct count data. This is discussed in detail in Ref. [11]. In `OMpy`, we have access to a proper uncertainty matrix $\sigma_{P_{\rm exp}}$. We checked that most bins of the first-generation matrices approximately follow a normal distribution. However, they are distributed with a larger and varying standard deviation as compared to what one would have received if the first generation entries were count data directly and followed the expectation value $\langle k \rangle = \lambda$. The approximate adherence to the normal distribution justifies the use of a χ^2 minimization as a likelihood maximization.

The χ^2 minimization is carried out by numerical minimization in the `Extractor` class. This is a different implementation than in the `oslo-method-software`, where the minimum is found by iteratively solving a set of equations to obtain a solution satisfying $\partial\chi^2/\partial\rho = 0$, $\partial\chi^2/\partial\mathcal{T} = 0$ for each bin of ρ and $\mathcal{T}$ [11]. After testing several off-the-shelf minimizers, we have found that the modified Powell's method in the `SciPy` package works well [55, 56].

The normalized first-generation matrix $P(E_x, E_\gamma)$ is compared to the fitted matrix in Fig. 2 for one ensemble member of the ^{164}Dy dataset. In Fig. 3 we show the corresponding level density ρ and γ-ray strength function f, where the latter is obtained from $\mathcal{T}$ using Eq. (2).

5.1. Testing the sensitivity on the initial values

The presently used minimization routine requires an initial guess for the trial functions $(\rho, \mathcal{T})$. In principle, the choice of the trial functions may have a significant effect on the results if the minimizer is prone to get caught in local minima. Ref. [11] proposes to set the initial ρ to a constant, arbitrarily chosen as 1, for all excitation energies E_x, and $\mathcal{T}(E_\gamma)$ as the projection of $P_{\rm exp}(E_x, E_\gamma)$ on the E_γ-axis. In `OMpy`, we have implemented several choices to test the stability of the solutions towards other initial guesses. For the cases shown here, no significant impact on the final results was observed.

Our default choice for the initial guess on ρ has been motivated by a long lasting discussion on whether the level density ρ follows the back-shifted Fermi gas (BSFG) equation [57, 58] or a constant temperature (CT) model [58, 59] below the neutron separation energy S_n , see Ref. [60, 61] and references therein. In recent years, the results of the Oslo method have strongly suggested a close-to CT-behavior. As this is equivalent to the initial guess for ρ in Ref. [11] (after a transformation G (see Eq. (3)), we set the default initial guess to a BSFG-like solution. More specifically, we draw from a uniform distribution centered around a BSFG-like initial guess for each ensemble member. Fig. 3 demonstrates that the resulting fit is still best described by the CT-model, but it is now very unlikely that this is due to a failure of the minimizer. The initial guess for $\mathcal{T}$ is still chosen as in Ref. [11], but with the same randomization with a uniform distribution as for the level density ρ.

Besides the two alternatives named above, we have also tested a rather exotic initial guess for ρ given by a quadratic function with a negative coefficient for the second-degree. This contrasts any expectation that the level density ρ increases as a function of the excitation energy E_x. However, even for this choice, the solution is stable.

5.2. Uncertainty estimation

Given the degeneracy of the χ^2, it is nontrivial to estimate the uncertainty in the solutions of ρ and $\mathcal{T}$. The `oslo-method-software` implements the approach of Ref. [11], where the uncertainty is estimated from the standard deviation of the solutions $(\rho^{(m)}, \mathcal{T}^{(m)})$ for each realization of the first-generation matrix $P^{(m)}_{\rm exp}$. This may lead to erroneously high uncertainties, as any transformation G gives an equally good solution to a given $P^{(m)}_{\rm exp}$. To illustrate this, we could imagine that the $P^{(m)}_{\rm exp}$'s only differ by a very small noise term. Due to the noise term the solutions will not be identical. In addition, we recapitulate that any given $P^{(m)}_{\rm exp}$ can be equally well fit by ρ as with any allowed transformation G such as 10ρ or 100ρ. Instead

of a negligible standard deviation one receives a standard deviation solely based on the degeneracy of the solutions. So far, we have observed that the minimization results are more stable as one might expect for the scenario outlined here (provided that the initial guess is not randomized). This is probably due to the way the minimizer explores the parameter space. Nevertheless, for the standard usage of `OMpy` we provide the functionality to estimate the uncertainty of solutions ρ and $\mathcal{T}$ after normalization of each ensemble of $(\rho^{(m)}, \mathcal{T}^{(m)})$. This will be explained in more detail in the next section.

5.3. Fit range

Using the Oslo method we have to restrict the fit range for the $P(E_x, E_\gamma)$ matrix. The area below $E_x^{\min}$ exhibits discrete transitions, thus does not adhere to the statistical nature of the γ-ray strength function f and is therefore excluded. To remain selective on the γ-decay channel, we can only use $P(E_x, E_\gamma)$ up to a maximum excitation energy $E_x^{\max}$ around the neutron separation energy S_n. Finally, we also constrain the minimum γ-ray energy to $E_\gamma^{\min}$, which usually attributed to a deficiency of the unfolding or first-generation method for low γ-ray energies. The limits are highlighted in Fig. 1 (c) and only this valid region of $P(E_x, E_\gamma)$ is sent to the minimizer.

6. Normalization of ρ and γSF

At first glance, the results bear little resemblance to a level density or γSF. That is because the fit has not yet been normalized. Thus, the solution shown in Fig. 3 is just one of an infinite set of solutions to the fit. In this section we will discuss how auxiliary data can be used to find the transformation G that gives the physical solutions.

6.1. Auxiliary experimental data

For the level density ρ, there are often two different types of auxiliary datasets available. At low energies, the discrete levels are known from spectroscopy. They can be compared to the fitted level density from the Oslo method after applying the same binning. One can also account for the detector resolution by applying e.g. a Gaussian smoothing to the histogram. At higher excitation energies, typically ∼1-3 MeV, the spectroscopy data fails to resolve all levels [60]. The user will thus have to set a sensible region in the low energy regime for the comparison.

The second piece of information stems from neutron resonance experiments, e.g. the average s-wave resonance spacings D_0. They provide information about the level density $\rho(E_x = S_\mathrm{n}, J_\mathrm{t} \pm 1/2, \pi_\mathrm{t})$ at the neutron separation energy S_n, where J_t and π_t are the ground-state spin and parity of the target nucleus, i.e. the $A-1$ nucleus [60]. With the Oslo method we obtain the total level density

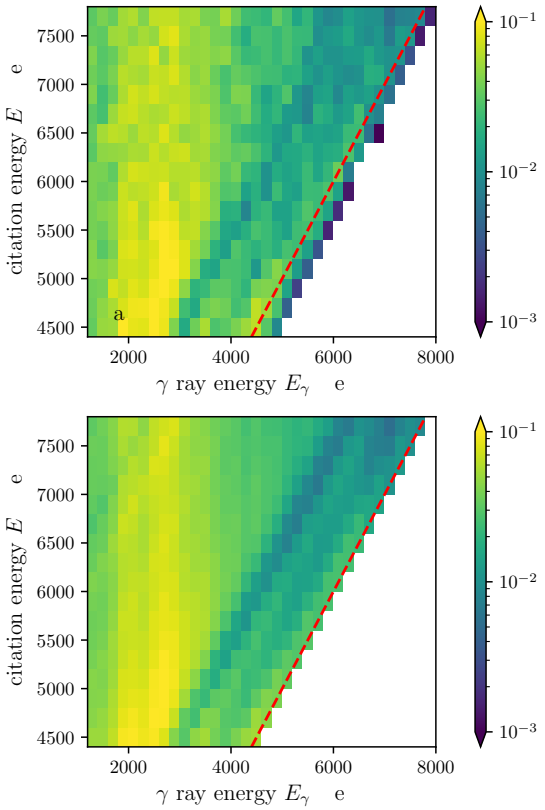

Figure 2: One realization of the normalized first-generation matrix $P(E_x, E_\gamma)$ (a) compared to its fit (b) by the product of the level density $\rho(E_x)$ and γSF $f(E_\gamma)$ (see Fig. 3). The dashed line indicates the maximum γ-ray energy $E_\gamma = E_x$. Counts to the right of this diagonal are due to the detector resolution or noise only and have been excluded from the fit. Note that pannel (a) is similar to Fig. 1c, but rebinned to 200 keV and for one realization instead of the mean of the ensemble.

$\rho(E_x) = \sum_{J,\pi} \rho(E_x, J, \pi)$. If one knows the fraction of $J_\mathrm{t} \pm 1/2, \pi_\mathrm{t}$ levels, one can estimate $\rho(S_n)$ by from D_0 by [11]

$$\rho(S_n) = \frac{1}{D_0} \frac{2}{g(E_x, J_\mathrm{t} + 1/2) + g(E_x, J_\mathrm{t} - 1/2)}, \qquad (9)$$

where $g(E_x, J, \pi)$ is the spin-parity distribution of the nucleus at E_x and the factor of 2 comes from the assumption of equiparity, i.e. $g(E_x, J, \pi) = g(E_x, J)/2$. Note that the $J_\mathrm{t} - 1/2$ term vanishes for $J_\mathrm{t} = 0$. For the spin-parity distribution $g(E_\mathrm{x}, I)$ it is common to use a form proposed in Ref. [62, Eq. (3.29)]; however the exact parametrization is a major source of systematic uncertainties in the normalization, thus several suggestions are implemented in `OMpy`.

The usage of $\rho(S_n)$ for the normalization is further complicated by restricted fit-regions for $P(E_x, E_\gamma)$ (see

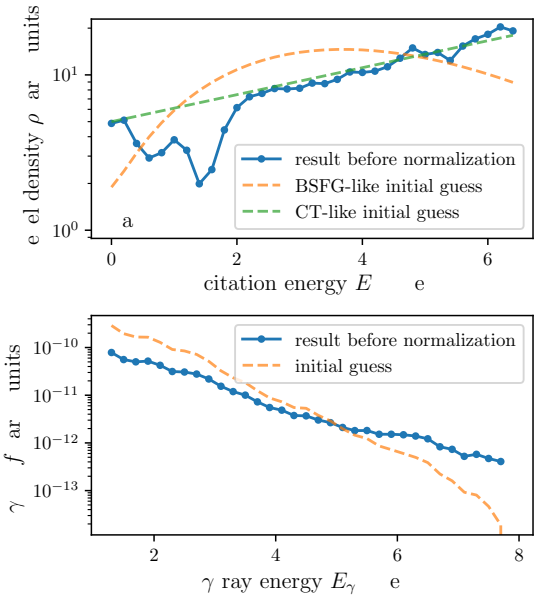

Figure 3: Level density $\rho(E_x)$ and γSF $f(E_\gamma) = \mathcal{T}(E_\gamma)/(2\pi E_\gamma^3)$ from the fit in Fig. 2. No transformation has been applied to the fit. Even though the initial guess for ρ was chosen from a BSFG-like function, the results are better described by the CT model above ~ 2 MeV. The initial guess is shown before the randomization with a uniform distribution.

Sec. 5.3). These limit the extraction of the level density ρ up to $E_x^{\max}$-$E_\gamma^{\min}$, which is often about 1-3 MeV below S_n. Consequently, we cannot directly normalize the fitted level density ρ to $\rho(Sn)$ obtained from D_0. To utilize this information, we have to extrapolate ρ and compare the extrapolation at S_n. The exact form of the extrapolation is another systematic uncertainty. Generally, the constant temperature (CT) model [62] fits well with the level density data obtained from the Oslo method [63],

$$\rho_{\mathrm{CT}}(E_x) = \frac{1}{T}\exp\frac{E_x - E_0}{T}, \tag{10}$$

where the temperature T and the energy shift E_0 are free parameters of the model. We obtain them by a fit to ρ in a suitable energy range.

The convolution of the level density ρ and γ-ray strength function f (or equivalently $\mathcal{T}$) can be further constrained by the average total radiative width $\langle\Gamma_\gamma(S_n)\rangle$ from neutron-capture experiments (see e.g. Ref. [60]) on a target nucleus with ground-state spin J_t using the following equation:

$$\langle\Gamma_{\gamma\ell}(S_n)\rangle = \frac{D_l}{2}\int_0^{S_n} dE_\gamma \left[f(E_\gamma)E_\gamma^3\rho(S_n - E_\gamma) \times \sum_{J_i}\sum_{J_f=|J_i-1|}^{J_i+1} g(S_n - E_\gamma, J_f)\right], \tag{11}$$

where the first sum runs over all possible residual nucleus spins J_i, i.e. from $\min|J_t \pm 1/2 \pm \ell|$ to $J_t + 1/2 + \ell$ and the second sum runs over all final spins J_f accessible with dipole radiation starting from a given J_i. Often only s-wave information is available, corresponding to $\ell = 0$ in the notation above, and the measurements are performed with low energy neutrons, such that $E_x \approx S_n$; for brevity it is then common to write $\langle\Gamma_\gamma\rangle$ for $\langle\Gamma_{\gamma\ell}(S_n)\rangle$. A derivation of Eq. 11 is given in Appendix D. Currently, we approximate $\langle\Gamma_\gamma\rangle$ using the integral involving the level density ρ for all excitation energies E_x, although the integral at low energies can be replaced by a sum over decays to the known discrete levels for more precise calculations. Note that we also have to extrapolate the γ-ray strength function to be able to use this equation. Due to its shape, a log-linear function is often fitted to the results.

6.2. Likelihood

In the following, we will define the likelihood $\mathcal{L}(\boldsymbol{\theta})$ that is used to find the proper normalizations. Let $\mathcal{L}_i(\boldsymbol{\theta})$ denote the likelihood for a given solution $(\rho, \mathcal{T})$ of Eq. (7) to match the normalization information i (i.e. discrete levels, D_0, $\langle\Gamma_\gamma\rangle$) after the transformation G with the parameters $\boldsymbol{\theta} = (A, B, \alpha)$. Due to the extrapolation of the level density ρ mentioned above, we have to introduce two nuisance parameters T and E_0, so we extend $\boldsymbol{\theta}$ to include (A, B, α, T, E_0). To reduce the computational complexity, we extrapolate the γ-ray strength function by the best-fit values for a given set of transformations (α, B). The total likelihood $\mathcal{L}(\boldsymbol{\theta})$ is then given by

$$\mathcal{L}(\boldsymbol{\theta}) = \prod_i \mathcal{L}_i(\boldsymbol{\theta}). \tag{12}$$

We assume that the experimental D_0 and $\langle\Gamma_\gamma\rangle$ data are normal distributed, thus maximizing the log-likelihood is equivalent to minimizing a sum of χ_i^2's. Note that the measurement of the discrete levels is of course not stochastic; however, the count data we use to determine ρ for the

comparison is. More explicitly, we have

$$\ln \mathcal{L}_i(\boldsymbol{\theta}) = K_i - \frac{1}{2}\sum_i \chi_i^2, \tag{13}$$

$$\chi^2_{\text{discrete}} = \sum_j \left(\frac{\rho_{j,\text{discrete}} - \rho_{j,\text{Oslo}}(\boldsymbol{\theta})}{\sigma_j} \right)^2, \tag{14}$$

$$\chi^2_{D_0} = \left(\frac{D_{0,\text{exp}} - D_{0,\text{CT}}(\boldsymbol{\theta})}{\sigma_{D_{0,\text{exp}}}} \right)^2 + \sum_j \left(\frac{\rho_{j,\text{CT}} - \rho_{j,\text{Oslo}}(\boldsymbol{\theta})}{\sigma_j} \right)^2, \tag{15}$$

$$\chi^2_{\langle\Gamma_\gamma\rangle} = \left(\frac{\langle\Gamma_\gamma\rangle_{\text{exp}} - \langle\Gamma_\gamma\rangle_{\text{Oslo}}(\boldsymbol{\theta})}{\sigma_{\langle\Gamma_\gamma\rangle_{\text{exp}}}} \right)^2, \tag{16}$$

where $K_i = \ln(1/(2\pi\sigma_i))$ is a constant as long as the standard deviation(s) σ_i does not depend on $\boldsymbol{\theta}$. The subscript *exp* denotes the experimental data. The sums in Eq. (14) and (15) run over all data points used in the evaluation, and for $\chi^2_{D_0}$ we invert Eq. (9) to obtain D_0 from the level density (extrapolated with the CT model). The second term of Eq. (15) arises due to the fit of the nuisance parameters of the CT model (T, E_0) to the Oslo method data, here labeled ρ_{Oslo}.

As discussed in Sec. 5.2, the degeneracy of the solutions ρ and f prevents us from directly inferring their parameter uncertainties in the fit of the first generation matrix P_{exp}. However, clearly the data points of ρ and $\mathcal{T}$ have a statistical uncertainty that should propagate to inform the posterior distribution of $\boldsymbol{\theta}$. We choose to model this by setting σ_j somewhat arbitrarily to a relative uncertainty of 30%. We propose to test the implications in a future work e.g. by comparing inferred D_0's for datasets where D_0 is known but on purpose not included in the χ^2 fit of Eq. (15). Note that with this specification of the standard deviations σ_j, the K_i become $\boldsymbol{\theta}$-dependent:

$$K_i = \sum_j \ln \frac{1}{\sqrt{2\pi}\sigma_j} = \sum_j \ln \frac{1}{\sqrt{2\pi \times 0.3\rho_{j,\text{Oslo}}(\boldsymbol{\theta})}}. \tag{17}$$

The likelihood can easily be extended if other information shall be taken into account. In several recent works on the Oslo method, experimental data on $\langle\Gamma_\gamma\rangle$ was not available, but roughly estimated from systematics (see e.g. Ref. [18, 64]). With the new possibilities of `OMpy` we would instead recommend to constrain α and B by adding a term to the total likelihood that describes the match with other measured strength function data (usually above S_n).

6.3. Implementation

We sample this likelihood with the Bayesian nested sampling algorithm `MultiNest` [65, 66] using the `PyMultiNest` module [67]. For a more efficient calculation, we first find an approximate solution (more accurately the maximum-likelihood estimator) $\hat{\boldsymbol{\theta}}$ with the differential evolution minimizer of `SciPy` [55, 68]. This is by default used to create weakly informative priors for A, B and α and T. For A and B we use a normal distribution truncated at 0 (negative values of ρ or f are not meaningful), a default mean μ given by $\hat{\boldsymbol{\theta}}$ and a broad width of 10μ. For α and the nuisance parameter T (entering through the level density extrapolation model) we use log-uniform priors spanning one order of magnitude around $\hat{\boldsymbol{\theta}}$. For the second nuisance parameter E_0 we choose a normal distribution with mean 0 and width 5 MeV, which is truncated below (above) -5 and 5 MeV, respectively. The latter choice is well justified regarding the range of reported values of E_0 in Ref. [69].

This simultaneous normalization is implemented in the `NormalizerSimultan` class, which relies on composition of the `NormalizerNLD` and `NormalizerGSF` classes handling the normalization of the level density ρ and γ-ray strength function f. To facilitate a comparison with the `oslo-method-software` calculations, one can also run a sequential normalization first using Eq. (14) and (15) through `NormalizerNLD` and then the resulting ρ as input to the normalization through `NormalizerGSF`, see Eq. (11). It should be stressed though that the normalization through the likelihood calculations in `OMpy` will still differ from the approach taken in the `oslo-method-software`. The latter allowed only to receive best-fit estimates of the transformation parameters A, B and α. Any subsequent uncertainty estimation due to the normalization itself was up to the users. We also note that an advantage of the simultaneous approach is that one obtains the correlations between A, B and α such that uncertainties in the normalization of ρ directly propagate to the estimation transformation parameters for f.

From the `MultiNest` fit we obtain the posterior probability distribution for the parameters $\boldsymbol{\theta}$, given as (equally-weighted) samples $\boldsymbol{\theta}_i$.[2] The normalization uncertainty for the solution $(\rho^{(m)}, f^{(m)})$ of the realization m can then be mapped out by creating a normalized sample $(\rho^{(m)}, f^{(m)})_i$ for each $\boldsymbol{\theta}_i$ using Eq. (3). By repeating this procedure for all realizations m of the ensemble, we also recover the uncertainty due to the counting statistics. This is performed in the `EnsembleNormalizer` class.

7. Systematic uncertainties

The previous sections described the necessary tools to evaluate the statistical uncertainties due to the counting statistics and the normalization procedure. It is important to keep in mind that there are also systematic uncertainties linked to the analysis, which are summarize below:

a) *Removal of negative counts in raw matrix*: When subtracting the background from the raw matrix, we often receive a matrix with negative counts in some bins. This is clearly linked to the Poisson statistics in regions with a low signal to background ratio. If one

[2] For brevity, we drop the index m on $\boldsymbol{\theta}$, but the normalization is performed for each realization m individually.

simply removes the negative counts, one potentially biases the mean of the level density and γ-ray strength points derived from these bins. It was previously observed that negative counts in the raw matrix can cause technical challenges in the currently implemented unfolding method, with some bins obtaining extreme negative values after several iterations. For the background subtraction, it might be a more reasonable fix to redistribute the negative counts to bins within the resolution. This is implemented by `Matrix.fill_negative` as an alternative to the default method, `Matrix.remove_negative`, which removes all negative counts. For the ^{164}Dy, there is a high signal to background ratio, thus the background subtraction does not have this problem. In cases with a worse background ratio, both methods could be compared. If they result in significant differences, further analysis is needed to find the optimal procedure.

b) *Removal of negative counts in unfolded and first-generation matrix*: The unfolding and first-generation methods can result in negative counts which can not be linked to the Poisson statistics any longer. It is thus not clear whether it is better to keep the negative counts or to redistribute them in the fashion described above. Again, the problem was negligible in the ^{164}Dy dataset, but has to be treated carefully if the methods lead to more bins with such a behavior. To retrieve the matrices before removal of the negative counts, the user can simply replace or deactivate the `remove_negative` methods of the `Unfolder` and `FirstGeneration` classes.

c) *Unfolding method*: There are two main sources of systematic uncertainties, the iterative unfolding method itself, and the detector response functions. The latter can be gauged by obtaining an ensemble of different detector response functions that capture the breadth of physically reasonable configurations (e.g. auxiliary software such as `GEANT4` [70]). Each member of the raw matrices $R^{(m)}$ is then unfolded with one (or each) of the different detector response functions. The former uncertainty is more difficult to quantify. In this special case, alternative methods exist already and one approach could be to implement an alternative unfolding algorithm (e.g. Ref. [71]). The `oslo-method-software` attempts to quantify the systematic uncertainty from unfolding and the first-generation matrix following an *ad hoc* numerical procedure described in Ref. [11]. A proper treatment that pays tribute to the full complexity of the problem is outside the scope of the present work.

d) *Population cross-section*: As mentioned in Sec. 3, the first-generation method assumes that the spin-parity distribution of the populated levels $g_{\rm pop}$ is similar for the whole excitation energy range studied. At best, $g_{\rm pop}$ approximates the spin-parity distribution g of the levels in the nucleus itself. This is often believed to be the case for low and mid-mass nuclei, where the beam energy is chosen such that the compound cross-section dominates over the direct cross-section. More details can be found in Refs. [17, 72] for challenges if the intrinsic spin-parity distribution $g(E_x, J, \pi)$ is very different from the (normalized) population cross-section $g_{\rm pop}(E_x, J, \pi)$.

e) *Decomposition and the Brink-Axel hypothesis*: The decomposition of the first-generation matrix into the level density $\rho(E_x)$ and γ-ray strength function $f(E_\gamma)$ relies on a generalization of the Brink-Axel hypothesis [48, 49], where the strength function is assumed to be approximately independent of E_x, J and π (see Eq. (C.5)). The validity of the assumption has been tested within the Oslo method by comparison of the γ-ray strength function f extracted from different initial and final excitation energy bins, see Refs. [50, 51] and references therein for further works.

f) *Intrinsic spin-parity distribution*: Both the normalization of the level density ρ at S_n via D_0 and the absolute scaling of the γ-ray strength function via $\langle\Gamma_\gamma\rangle$ rely on the knowledge of the intrinsic spin-parity distribution $g(E_x, J, \pi)$ of the nucleus, see Eq. (9) and Eq. (11). It it difficult to measure the spin-parity distribution $g(E_x, J, \pi)$ in the (quasi)continuum and there are various different empirical parametrization and theoretical calculations, see e.g. Refs. [58, 69, 73, 74] and Refs. [75–78] respectively.

g) *Lack of D_0 and $\langle\Gamma_\gamma\rangle$*: In several recent cases where the Oslo method has been applied, experimental values of D_0 and/or $\langle\Gamma_\gamma\rangle$ were not available, see e.g. Refs. [14, 18, 36, 64]. In these works, D_0 and/or $\langle\Gamma_\gamma\rangle$ were estimated from the values of nearly nuclei. With `OMpy` it is now easier to adopt the normalization procedure via the likelihood $\mathcal{L}(\boldsymbol{\theta})$ in Eq. (12) instead. One can either remove terms where the experimental information is missing, allowing for a larger degeneracy of the solutions, or add different constrains, like a measure of how well the γ-ray strength function $f(E_\gamma)$ matches other measured γ-ray strength function data, which often exists above S_n.

h) *Bin sizes and fit ranges*: Several decisions have to be made on the bin sizes and fit ranges, for example in the normalization of the level density ρ to the known level scheme, see Sec. 6.1. The user can test different sensible regions for this comparison.

In this work, only the impact of the negative counts, items a and b have been studied. In many cases it is challenging to evaluate the impact of the assumptions on the data. Whenever the uncertainty is linked to models, algorithms, parameter sets or alike, and alternative choices exists (items c, d, f, h), it is possible to utilize `OMpy`'s error propagation functionality. This was illustrated for

the unfolding of the data in item c. More information on items e and f can be found in Ref. [17].

8. Discussion and comparison

In Fig. 4 we show the level density ρ and γ-ray strength function f of ^{164}Dy resulting from the simultaneous normalization of $N_{\rm ens} = 50$ realizations. Each realization m is transformed with $N_{\rm samp} = 100$ samples from the normalization parameters $\boldsymbol{\theta}_i$. The combined uncertainty of the normalization and counting statistics is visualized through the 16th, 50th, and 84th percentiles which together form the median and a 68% credible interval. Additionally, we show one randomly selected sample $(\rho^{(m)}, f^{(m)})_i$ including its extrapolation. The results are compared to the analysis of Renstrøm et al. [14] which used the `oslo-method-software`, and we display both the uncertainty that is quoted due to the counting statistics and the total uncertainty, that includes the normalization. Note that we discussed in Sec. 5.2 that this split into the uncertainty due to counting statistics and due to normalization is, strictly speaking, not possible – hence, the quoted decomposition is an approximation.

It is gratifying to see that overall, both analyses provide similar results. In Fig. 4a, the level density below ~ 2 MeV exhibits the same structure of bumps attributable to the discrete level structure, and at higher E_x the curves are practically identical. Similarly, for the γSF in Fig. 4b, the data is mostly compatible within the error-bars. The median of the results from `OMpy` has slightly steeper slope and the uncertainties are somewhat more evenly distributed across the whole energy range.

Some deviation between the results is expected due to the different fitting method and software implementations. Moreover, different fit-regions may lead to different estimations of the normalization parameters θ, which in turn give different slopes (and absolute values) for ρ and the γSF. Usually, there will be several sensible fit-regions. With `OMpy`, the user could create a wrapper that loops through the different fit-regions. The mean and spread of the results can be analyzed using the same ensemble based approach as above.

Another way to verify the results of `OMpy` is to simulate decay data for a given ρ and the γSF and compare these to the analysis with `OMpy` from the simulated data. We have used the Monte-Carlo nuclear decay code `RAINIER` v1.5 [80, 81] to create decay data from a ^{164}Dy-like nucleus. To create an artificial level scheme, we used the first 20 known discrete levels [60] and for higher energies created levels following the CT model and spin-distribution described in Renstrøm et al. [14]. The γSF has been modeled with the parameters from the same publication. Then, we simulate the experiment by populating 2×10^6 levels below S_n and recording the decay γs for each event. For simplicity, we have assumed here that we populate the levels proportionally to the intrinsic spin distribution of the nucleus. Finally, we use the response functions of the ^{164}Dy experiment to convert the recorded γ rays to a matrix of synthetically generated events that substitute the experimentally determined raw matrix in the further analysis with `OMpy`. The full setting file can be found with the supplementary material online.

In Figure 5 we compare the results of `OMpy` to the input level density ρ and γSF from RAINIER. The fitted level density ρ slightly over-pronounces the structures of the discrete levels at low excitation energies. From a practical point of view this is not a significant problem, as the Oslo method is used for an analysis of the quasicontinuum region, so at energies $\gtrsim 2$ MeV. There, we observe a perfect match between the input and the fitted level density. The resulting γSF is in very good agreement with the input γSF. There are small deviations at the lowest and highest energies that can easily be understood. The apparent discrepancy of the input γSF below ~ 2 MeV can be explained by a failure of the first-generation method due to strong populations of discrete states and is directly visible in the comparison of the unfolded to first-generation matrix (see supplementary material online). The region could have been excluded from the comparison, but we aimed for the same extraction region as for the experimental ^{164}Dy data set. The mismatch propagates to a wrong extrapolation of the γSF towards lower energies. The two resonance-like structures at $\sim$6 and 7 MeV overcompensate for the mismatch of the level density at the lowest excitation energies.

One of the main motivations for `OMpy` was to improve the uncertainty analysis in the Oslo method. Throughout the article we have highlighted several improvements to the theoretical framework for propagating the uncertainties compared to the `oslo-method-software`. The most fundamental source of uncertainties in the analysis is the count statistics. For each experiment a balance between the run-time costs and the possibility to gather more data has to be found. Therefore, we find it instructive to study the impact of a reduced number of counts for the ^{164}Dy experiment. We create a new raw matrix, which we draw from a Poisson distribution with a mean of 1/10th of the original data (an arbitrary choice corresponding to 1/10th of the run actual time) and otherwise perform the same analysis as above. Both analyses are compared in Fig. 6, and overall we find a good agreement of the median values.

There is one major difference in the analysis that leads to different uncertainty estimates. In the case with the reduced number of counts we have to use a lower maximum excitation energy $E_x^{\rm max}$ in the fit to $P(E_x, E_\gamma)$. As a consequence, the extracted level density ranges only up to about 4.5 MeV instead of 6.5 MeV, increasing the uncertainty in the determination of the normalization parameters. The increased uncertainty of the slope parameter α is directly visible for the level density ρ. For the γSF we additionally require a suitable fit to the experimental $\langle\Gamma_\gamma\rangle$, so a different slope α will also affect the absolute scaling B. This results in the normalized γSFs *tilting* around a γ-ray energy of about 5 MeV, where the exact location of the

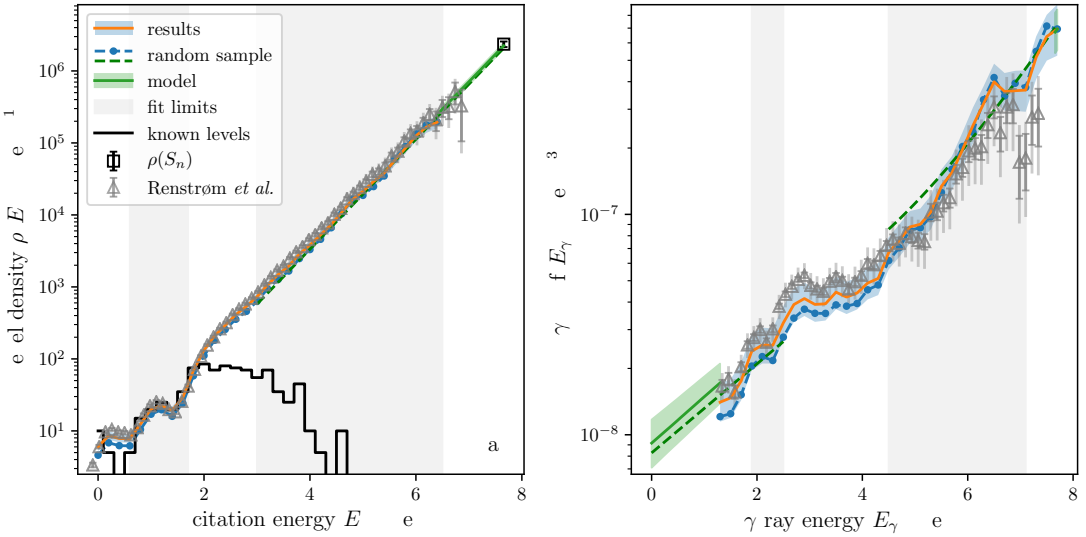

Figure 4: Extracted level density ρ (a) and γSF f (b) for ^{164}Dy. The fit is similar to that shown in Fig. 3, but the normalization according to Eq. (3) has been applied. We display the median and 68% credible interval obtained from the counting and normalization uncertainties (orange line and blue shaded band, respectively) together with one randomly selected sample of ρ and f (blue dots). The median and 68% credible interval for the extrapolation is given by the green line and shaded band. In addition, the extrapolation used together with the random sample is indicated by the dashed line. The data points within the grey area denoted *fit limits* are used for the normalization and extrapolations, such that we match the binned known levels (black line) [79], $\rho(S_n)$ calculated from D_0 [60] (and $\langle\Gamma_\gamma\rangle$ [60]). The results are compared to the analysis of Renstrøm et al. [14] which used the `oslo-method-software`, displaying both the uncertainty that is quoted due to the count statistics (inner error bar) and the total uncertainty, including the normalization (outer error bar) (see text for more details).

tilting point depends on the nucleus. The normalization uncertainty thus leads to increasing relative uncertainties of the γSF for lower γ-ray energies E_γ. This contrasts to the naive expectation that the relative uncertainties should increase with E_γ, as the number of counts that determine each γSF bin decrease. Finally, we foresee that the updated framework for the uncertainty analysis may have a significant impact when further processing of the results from the Oslo method. An example of this is given in Renstrøm et al. [14], where the authors fit of the strength of the peak at ~ 3 MeV in the γSF which assumed to be a $M1$ scissors mode.

9. Extension of `OMpy`

`OMpy` is written with modularity in mind. We want it to be as easy as possible for the user to add custom functionality and interface `OMpy` with other libraries. For example, in Sec. 7 we discussed that it may be of interest to try other unfolding algorithms than the one presently implemented. To achieve this, one just has to write a wrapper function with the same return structure as the callable `Unfolder` class. Then one provides the new wrapper to `Ensemble` instead of the `Unfolder` class and all matrices will be unfolded with the new algorithm.

It is our hope and goal that `OMpy` will be used as much as possible. Feedback and suggestions are very welcome. We encourage users who implement new features to share them by opening a pull request in the Github repository.

10. Conclusions and outlook

We have presented `OMpy`, a complete reimplementation of the Oslo method in Python. The capabilities of the code have been demonstrated by comparison with a synthetic data set modeled with the decay code `RAINIER`. We have also compared `OMpy` to the analysis for ^{164}Dy with the previous implementation of the Oslo method, the `oslo-method-software` and in general find a good agreement. However, we have refined the uncertainty quantification of the analysis using an ensemble-based approach. We are now able to simultaneously take into account statistical uncertainties from the counting statistics and the normalization to external data and preserve the full correlation between the resulting level density ρ and γSF.

Acknowledgements

We would like to thank V. W. Ingeberg for a beta test and his feedback on the software. This work was supported by the Research Council of Norway under project

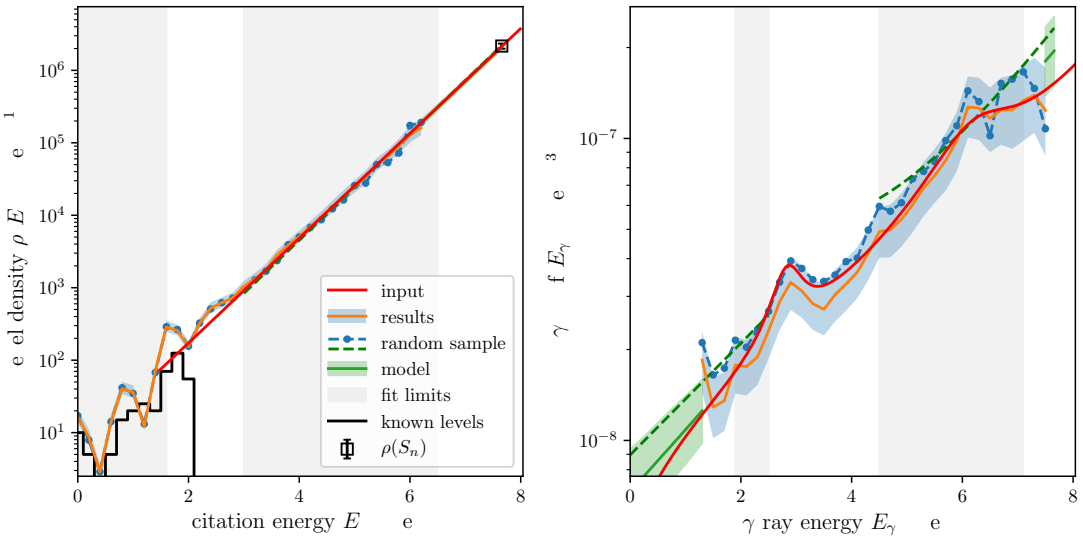

Figure 5: Extracted level density ρ (a) and γSF f (b) from synthetic data for a ^{164}Dy-like nucleus. In the quasicontinuum region the analysis with `OMpy` (labeled results) agrees well with the input level density and γ-ray strength function model.

Grants No. 263030, 262952 and 23054. A.C.L. gratefully acknowledges funding from the European Research Council, ERC-STG-2014 Grant Agreement No. 637686.

Appendix A. Unfolding

Here we explain the unfolding technique presented in Ref. [25], which is used both in the original Oslo method implementation in the `oslo-method-software` and in `OMpy`. Let the detector response be modelled as a conditional probability density function

$$p(E_\gamma|E'_\gamma), \tag{A.1}$$

encoding the probability that a γ ray with true energy E'_γ is detected with energy E_γ. Given a true γ-ray spectrum $U(E_\gamma)$, the folded spectrum $F(E_\gamma)$, i.e. the spectrum seen by the detector, is then given by

$$F(E_\gamma) = \int p(E_\gamma|E'_\gamma)U(E'_\gamma)\,\mathrm{d}E'_\gamma. \tag{A.2}$$

By discretizing into energy bins of width ΔE_γ, it becomes a matrix equation

$$\vec{F} = P\vec{U}, \tag{A.3}$$

where P is the response matrix of discrete probabilities $P_{kl} = p(E_{\gamma,k}|E'_{\gamma,l})\Delta E_\gamma$. The unfolding procedure amounts to solving this equation for $\vec{U}$. However, a straightforward matrix inversion is ill-advised, as it will often lead to singularities or produce large, artificial fluctuations in $\vec{U}$ [82, 83]. Instead, the approach taken in the Oslo method is to use an iterative technique that successively approximates $\vec{U}$. Letting $\vec{R}$ denote the measured spectrum, the algorithm is

1. Start with a trial function $\vec{U}_0 = \vec{R}$ at iteration $i = 0$
2. Calculate the folded spectrum $\vec{F}_i = P\vec{U}_i$
3. Update the trial function to $\vec{U}_{i+1} = \vec{U}_i + (\vec{R} - \vec{F}_i)$
4. Iterate from 2 until $\vec{F}_i \approx \vec{R}$.

Note that the `oslo-method-software` uses a custom tailored combination of the additive updating procedure of step 3, and a ratio approach, $\vec{U}_{i+1} = \vec{U}_i \circ (\vec{R} \oslash \vec{F}_i)$, where the Hadamard products stand for an element wise product. We obtain equally good results by adopting only the additive updating in `OMpy`. The updating procedure may sometimes lead to a negative number of counts in the unfolded spectra. For negative counts close to zero, it is not clear whether these should be kept or discarded, as it is not clear whether they originate from the statistical nature of the data. In some cases, one observes some bins with large, negative counts which hints at a failure of the method. These cases should be analyzed carefully before the results are processed further. The current default is to remove the negative counts at the end of the unfolding.

A too large number of iterations does not improve the results significantly, but introduces strong fluctuations in the unfolded spectrum. After the publication of Ref. [25]

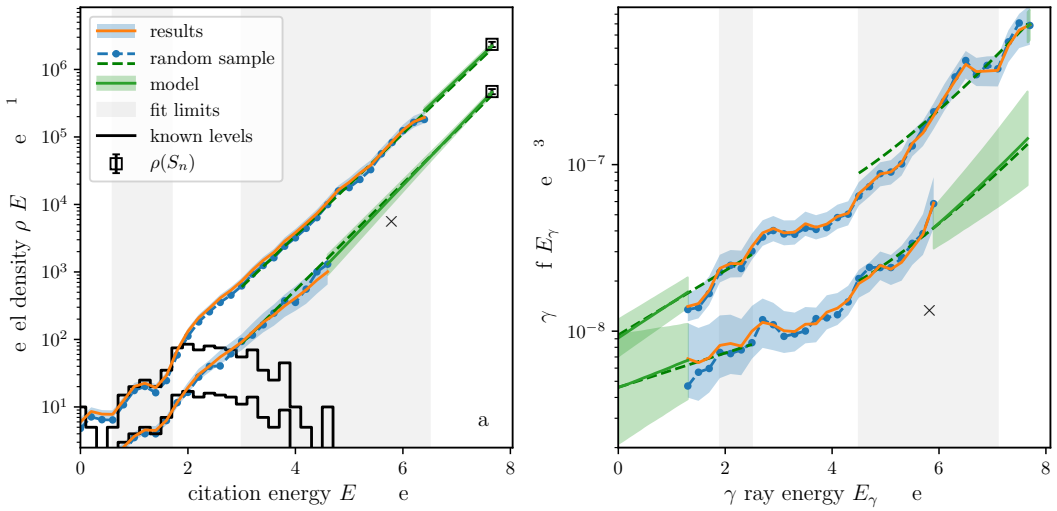

Figure 6: Similar to Fig. 4 we show the extracted level density ρ (a) and γSF f (b) for the ^{164}Dy experiment, but here it is compared to a case with only 1/10th of the data. The level density ρ (a) and γSF from the case with reduced number of counts have been scaled down by a factor of 5 in the plot to facilitate the visual comparison with the original analysis. For each case, one randomly selected sample including its extrapolation is shown in addition to the median and a 68% credible interval.

a criterion for step 4 has been added to the `oslo-method-software`, which is also used in `OMpy`. A predefined number (usually around 30-200) iterations is run and the best iteration is selected based on a weighted sum over each vector element of the root-mean-square error of $\vec{F}_i - \vec{R}$ and the relative level of fluctuations in $\vec{U}_i$ compared to the fluctuations of the raw spectrum $\vec{R}$. The relative fluctuations are estimated as $|(\vec{U}_{i,l} - \langle\vec{U}_i\rangle)/\langle\vec{U}_i\rangle|_1$, where $\langle\vec{U}_i\rangle$ is a smoothed version of the spectrum $\vec{U}_i$.

In addition to this, the user can choose to use a further refinement to the unfolding method known as Compton subtraction [25]. It is used to further control the fluctuations in the unfolded spectrum. The basic concept behind it is to use the previously unfolded spectrum to decompose $\vec{R}$ into parts corresponding to the full-energy, single and double escape and annihilation peaks, and the "rest" which comes from Compton scattering and similar processes. Each of these parts, save for the full-energy peak, are then smoothed with the detector resolution before they are subtracted from $\vec{R}$. The resulting spectrum normalized to maintain the number of counts. The idea is that this gives an unfolded spectrum with the same statistical fluctuations as in the original spectrum $\vec{R}$.

Appendix B. The first-generation method

In this appendix we describe the idea behind the first-generation method of Ref. [26] and its implementation in `OMpy`. Let $FG(E_\gamma)_{E_x}$ denote the first-generation γ-ray spectrum, i.e., the intensity distribution of γ-ray decay from a given excitation energy E_x, as function of γ-ray energy E_γ. Generally, the nucleus will decay from E_x down to the ground state by emitting a cascade of γ rays, which forms the *total* γ-ray spectrum. The total, or all-generations γ-ray spectrum, denoted $AG(E_\gamma)_{E_x}$, can be viewed as a superposition of the first-generation spectrum and a weighted sum of the all-generations spectra of excitation energies below,

$$AG(E_\gamma)_{E_x} = FG(E_\gamma)_{E_x} + \sum_{E'_x<E_x} w(E'_x)_{E_x} \underbrace{n(E'_x)_{E_x} AG(E_\gamma)_{E'_x}}_{\langle AG(E_\gamma)_{E'_x}\rangle}. \quad \text{(B.1)}$$

Here, $w(E'_x)_{E_x}$ is a weight factor that gives the decay probability from E_x to E'_x, and $n(E'_x)_{E_x}$ is a normalization factor which corrects for the varying cross section to populate the E'_x bins. Note that the normalization factor $n(E'_x)_{E_x}$ times the all-generations spectrum $AG(E_\gamma)_{E'_x}$ gives the spectra of γ rays $\langle AG(E_\gamma)_{E'_x}\rangle$ emitted from the E'_x bin for each single population.

Normalization and multiplicity estimation

The normalization factor $n(E'_x)_{E_x}$ can be estimated from the singles spectra $S(E_x)$, which contain the number of reactions populating the excitation energy bin E_x and

thus the number of γ-ray cascades out of this level,

$$n(E'_x)_{E_x} = \frac{S(E_x)}{S(E'_x)}. \tag{B.2}$$

However, usually it is determined from the total γ-ray spectrum by the relation

$$n(E'_x)_{E_x} = \frac{\langle M(E'_x)\rangle N(E_x)}{\langle M(E_x)\rangle N(E'_x)}, \tag{B.3}$$

where $\langle M(E_x)\rangle$ and $N(E_x)$ denote the average γ-ray multiplicity and the total number of counts, respectively, at excitation energy E_x. This reformulation uses the fact that $S(E_x) = N(E_x)/M(E_x)$. In `OMpy` there are two ways to determine the average multiplicity $\langle M(E_x)\rangle$. The initial idea, the *total multiplicity estimation* is given in Ref. [8] as

$$\langle M(E_x)\rangle = \frac{E_x}{\langle E_\gamma\rangle}, \tag{B.4}$$

where $\langle E_\gamma\rangle$ is the weighted-average γ-ray energy at excitation energy E_x. Due to the detector threshold, we are usually not able to measure all γ rays, and this will artificially increase $\langle E_\gamma\rangle$. To solve this problem, a *statistical multiplicity estimation* has been added to the `oslo-method-software` and is adapted in `OMpy`. The underlying ideas is that in heavier nuclei, like in the rare-earth region, γ rays from entry states at higher excitation energy will decay down to the yrast-line, where it enters at an energy denoted here as $E_{\rm yrast}$. From there, the γ rays follow a non-statistical decay to the ground state. For heavy nuclei, there are many levels at low excitation energies, such that is is assumed here that the yrast transitions will proceed with many γ rays of so low energy, that they are usually below the detector threshold. In that case, we can replace the excitation energy in Eq. (B.4) by the *apparent* excitation energy $\tilde{E}_x = E_x - E_{\rm yrast}$. A challenge in this method is to correctly estimate the entry energy $E_{\rm yrast}$. Thus we recommend to use the *total multiplicity estimation* whenever the experimental conditions allow for it.

Weight function and iteration

The weight function $w(E'_x)$ encodes the probability for the nucleus to decay from E_x to E'_x, and is in fact nothing but the normalized first-generation spectrum for E_x,

$$w(E'_x)_{E_x} = \frac{FG(E_x - E'_x)_{E_x}}{\sum_{E'_\gamma} FG(E'_\gamma)_{E_x}}. \tag{B.5}$$

By rewriting Eq. (B.2), we obtain

$$FG(E_\gamma)_{E_x} = AG(E_\gamma)_{E_x} - \sum_{E'_x<E_x} n(E'_x)_{E_x} \frac{FG(E_x - E'_x)_{E_x}}{\sum_{E'_\gamma} FG(E'_\gamma)_{E_x}} AG(E_\gamma)_{E'_x}. \tag{B.6}$$

This is a self-consistent set of equations for the FG spectra, which we solve by an iterative procedure, starting with a set of trial functions $FG(E_\gamma)_{E_x}$ and iterating until convergence is reached. In `OMpy`, the trial functions are chosen as constant functions, i.e. with the same value for all E_γ. In the original implementation of the first-generation method, the trial functions are instead chosen based on a Fermi gas level density model [60, 84]. We have checked with `OMpy` that this gives identical results as with constant functions. The iterative procedure may sometimes lead to a negative number of counts in the resulting first generation spectra. As for the unfolding method, it is not clear whether they originate from the statistical nature of the data or from inaccuracies in the iterative procedure. The current default solution in `OMpy` is to remove negative bins from the obtained FG spectra. However, as described in Section 7, the user can choose to rather redistribute the negative counts to neighboring bins using the `Matrix.fill_negative` option. In cases where a few bins obtain large, negative counts, we advise the user to carefully analyze the results before processing them further.

Based on the development in `oslo-method-software` a small variation was added to `OMpy` to ensure better convergence for higher iteration numbers. Starting from iteration 5, each iteration i of the FG spectra is calculated at $FG_i = 0.7FG'_i + 0.3FG_{i-1}$, where FG'_i is the spectrum from the analytical solution of (B.6). This is comparable to a fixed learning rate in machine learning algorithms.

Appendix C. Derivation of the Oslo method equation

Here, we derive the relationship between the distribution of primary γ rays, and the strength function and level density. The derivation is based on Weisskopf [85, p. 214–217], and Blatt and Weisskopf [86, p. 342, 649], but generalizes the equations to take into account angular momentum conservation. This corresponds to the Hauser-Feshbach theory of statistical reactions [87], but we apply several simplifications, like the Brink-Axel hypothesis, such that we can arrive at the *Oslo method equation*, Eq. (1).

We start with Bohr's independence hypothesis [28] for the cross section σ in a nuclear reaction $a + A \rightarrow {\rm CN}^* \rightarrow c+C$.[3] Let us denote all quantum numbers of the entrance channel, the compound nucleus and the exit channel by α, i and f, respectively. The cross section is then given by [86, p. 342], [28]

$$\sigma(\alpha, f) = \sigma_{\rm CN}(\alpha) G_{\rm CN}(i, f), \tag{C.1}$$

where the compound nucleus formation cross-section $\sigma_{\rm CN}$ depends only on the entrance channel α. Following Bohr, the decay probability of the compound nucleus $G_{\rm CN}$ depends only on the branching ratios of the compound nucleus level i to a specific channel f, but not on the entrance

[3] More precisely, we assume that our reaction, e.g. a (d, p) reaction, leads to a compound nucleus CN*, which subsequently decays by γ-ray emission.

channel. In the Oslo method, we select only excitation energies E_x below the particle separation threshold, so the compound nucleus can decay by γ-rays only. The decay probability $G_{\rm CN}$ of the state i is then simply the γ-ray branching ratio to a specific final state f with energy E_f and the spin-parity J_f^π,

$$G_{\rm CN} = \frac{\Gamma_\gamma(i \to f)}{\Gamma_\gamma}, \tag{C.2}$$

where $\Gamma_\gamma(i \to f)$ is a partial, and $\Gamma_\gamma = \sum_f \Gamma_\gamma(i \to f)$ is the total radiative width for the level i.

The spectrum of the decay radiation $n(i,f)\mathrm{d}E_f$ from the compound nucleus level i is then given by the summation (or integration) of $\sigma(\alpha, f)$ over an interval dE_f (up to a constant due to the flux of a and density of A which would cancel out later):

$$\begin{aligned} n(i,f)\mathrm{d}E_f &= \sum_{f \text{ in } E_f} \sigma(\alpha, f) = \sigma_{\rm CN}(\alpha) \sum_{f \text{ in } E_f} \frac{\Gamma_\gamma(i \to f)}{\Gamma_\gamma} \\ &= \sigma_{\rm CN}(\alpha) \sum_{XL} \frac{\langle \Gamma_\gamma(i \to f) \rangle}{\Gamma_\gamma^{(L)}} \rho_{\rm avail}(E_f), \\ &= \sigma_{\rm CN}(\alpha) \sum_{XL} \frac{f_{XL}(E_\gamma) E_\gamma^{2L+1}}{\Gamma_\gamma^{(L)} \rho(E_x, J_i^\pi)} \rho_{\rm avail}(E_f) \\ &= C_{\alpha,i} \sum_{XL} \frac{f_{XL}(E_\gamma)}{\Gamma_\gamma^{(L)}} E_\gamma^{2L+1} \rho_{\rm avail}(E_f), \end{aligned} \tag{C.3}$$

where $\rho_{\rm avail}$ is density of accessible final levels at E_f, $C_{\alpha \to i}$ is a constant that depends only on the entrance channel (which determines the compound nucleus state i), and we have replaced the average partial radiative width $\langle \Gamma_\gamma(i \to f) \rangle$ by γ-ray strength-function[4] f_{XL}.

The γ-ray strength function f_{XL} for a given multipolarity XL and for decays from an initial level i to final level f is defined as [88]

$$f_{XL}(E_x, J_i^\pi, E_\gamma, J_f^\pi) = \frac{\left\langle \Gamma_{\gamma XL}(E_x, J_i^\pi, E_\gamma, J_f^\pi) \right\rangle}{E_\gamma^{2L+1}} \rho(E_x, J, \pi) \tag{C.4}$$

where $\langle \cdots \rangle$ denotes an average over individual transitions in the vicinity of E_x (in practice defined by the energy binning resolution). This can be simplified using the dominance of dipole radiation ($L = 1$) and a common generalization of the Brink-Axel hypothesis [48, 49], where the strength function is assumed to be approximately independent of E_x, J and π,

$$\begin{aligned} \sum_{XL} f_{XL}(E_x, J_i^\pi, E_\gamma, J_f^\pi) &\overset{\text{dipole}}{\approx} f_1(E_x, J_i^\pi, E_\gamma, J_f^\pi) \\ &\overset{\text{Brink-Axel}}{\approx} f_1(E_\gamma) \end{aligned} \tag{C.5}$$

where we define the total dipole strength function f_1 as the sum of the electric and magnetic dipole strength, f_{E1} and f_{M1}, respectively, $f_1 = f_{E1} + f_{M1}$.

If we again use the dominance of dipole radiation in Eq. (C.3) (which leads to $\Gamma_\gamma \approx \Gamma_\gamma^{(L=1)}$), and assume parity equilibration of the level density, i.e. $\rho(E_x, J, +) \approx \rho(E_x, J, -)$ we can write

$$\begin{aligned} n(i,f)\mathrm{d}E_f &\approx C_{\alpha,i} E_\gamma^3 \\ &\times \left(\frac{f_{E1}(E_\gamma)}{\Gamma_\gamma} \sum_{J_f = J_i - 1}^{J_f = J_i + 1} \rho(E_f, J_f, -\pi_i) \right. \\ &\left. + \frac{f_{M1}(E_\gamma)}{\Gamma_\gamma} \sum_{J_f = J_i - 1}^{J_f = J_i + 1} \rho(E_f, J_f, \pi_i) \right) \\ &= C'_{\alpha,i} E_\gamma^3 f_1(E_\gamma) \sum_{J_f = J_i - 1}^{J_f = J_i + 1} \rho(E_f, J_f, \mathrm{eq}), \end{aligned} \tag{C.6}$$

where $\rho(E_x, J_f, \mathrm{eq})$ denotes the level density of one parity, the notation emphasizing the assumption of parity equilibration[5] and $C'_{\alpha,i} = C_{\alpha,i}/\Gamma_\gamma$. We may write the partial level density $\rho(E_x, J, \mathrm{eq})$ as

$$\rho(E_x, J, \mathrm{eq}) = \frac{1}{2} g(E_x, J) \rho(E_x), \tag{C.7}$$

where g denotes the intrinsic spin distribution of the nucleus and $\rho(E_x) = \sum_{J^\pi} \rho(E_x, J, \pi)$ is the "summed" (or "total") nuclear level density. With this, we can further simplify the sum over the final levels in Eq. (C.6):

$$\begin{aligned} &\sum_{J_f = J_i - 1}^{J_f = J_i + 1} \rho(E_f, J_f, \mathrm{eq}) \\ &= \frac{\rho(E_f)}{2} \sum_{J_f = J_i - 1}^{J_f = J_i + 1} g(E_f, J_f) \approx \frac{3\rho(E_f)}{2} g(E_f, J_i), \end{aligned} \tag{C.8}$$

which is a good approximation except for the case of $J_i = 0$ (and $J_i = 1/2$), where the selection rules allow only transitions to $J_f = 1$ ($J_i = \{1/2, 3/2\}$) states.

Next, we write $n(i,f)\mathrm{d}E_f$ more explicitly as $I(E_i, J_i^\pi, E_\gamma)$ and exploit probability conservation,

$$\begin{aligned} P_{J_i^\pi}(E_i, E_\gamma) &= \frac{I(E_i, J_i^\pi, E_\gamma)}{\sum_{E_\gamma} I(E_i, J_i^\pi, E_\gamma)} \\ &= C_{E_i, J_i^\pi} E_\gamma^3 f_1(E_\gamma) \rho(E_i - E_\gamma) g(E_i - E_\gamma, J_i) \end{aligned} \tag{C.9}$$

where $P_{J_i,\pi_i}(E_i, E_\gamma)$ is the probability to decay from an initial excitation energy bin E_i with a γ ray of energy E_γ,

[4] To keep standard notation we will denote both the γ-ray strength function and the final level by f. It should be clear from the context what we refer to.

[5] The selection rules dictate that dipole radiation changes the angular momentum J by at most one unit. For $M1$, the parity is unchanged, while for $E1$ it flips. This determines the density of available final levels for the decay. In the case of $J_i = 1/2$ the sum runs over $J_f = \{1/2, 3/2\}$, and in the case of $J_i = 0$, the sum only runs over $J_f = 1$, since $J = 0 \to J = 0$ transitions are forbidden.

the subscripts J_i and π_i limit the initial levels to of a given spin and parity, respectively, and C_{E_i,J_i^π} is a normalization constant. Note that the normalization constant $C'_{\alpha,i}$ cancels out (which includes compound nucleus cross-section $\sigma_{\rm CN}$, the total radiative width Γ_γ, and the density of intrinsic levels $\rho(E_i, J_i^\pi)$).

The final step is to generalize this equation for the case where levels of different spins and parities are populated. Naively, we may just sum over the decays $P_{J_i^\pi}$ from all initial levels J_i^π

$$\begin{aligned}\sum_{J_i^\pi} P_{J_i^\pi} &\approx C_{E_i} E_\gamma^3 f_1(E_\gamma)\rho(E_i - E_\gamma)\sum_{J_i^\pi} g(E_i - E_\gamma, J_i)\\ &= C_{E_i} E_\gamma^3 f_1(E_\gamma)\rho(E_i - E_\gamma),\end{aligned} \tag{C.10}$$

from which we would already recover the standard Oslo method equation for a suitable normalization constant C_{E_i}. However, we have to note that the normalization constants C_{E_i,J_i^π} in Eq. (C.9) depend on the spin and parity, and cannot be factored out. As we will see, this can be solved under the assumption that the cross-section $\sigma_{\rm CN}$ to create the compound nucleus at different spin-parities J_i^π is proportional to number of levels in the nucleus (i.e. it is not spin-selective, but proportional to intrinsic spin distribution),

$$\begin{aligned}\sigma_{\rm CN}(\alpha \to E_i, J_i^\pi) &\approx \sigma_{\rm CN}(E_i)\rho(E_i, J_i, \pi_i)\\ &= \sigma_{\rm CN}(E_i)\rho(E_i)g(E_i, J_i, \pi_i).\end{aligned} \tag{C.11}$$

Using Eq. (C.6) to (C.8), the (cross-section weighted) sum over the decay spectra from all populated levels is

$$\begin{aligned}I(E_x, E_\gamma) &= \sum_{J_i^\pi} I(E_x, E_\gamma, J_i^\pi)\\ &= \sum_{J_i^\pi} \frac{\sigma_{\rm CN}(E_i)\rho(E_i, J_i, \pi_i)}{\Gamma_\gamma \rho(E_i, J_i, \pi_i)} f_1(E_\gamma) E_\gamma^3 \rho_{\rm avail}(E_f)\\ &\approx \frac{\sigma_{\rm CN}(E_i)}{\Gamma_\gamma} f_1(E_\gamma) E_\gamma^3 \frac{3\rho(E_f)}{2} \sum_{J_i^\pi} g(E_x, J_i)\\ &= 3\frac{\sigma_{\rm CN}(E_i)}{2\Gamma_\gamma} f_1(E_\gamma) E_\gamma^3 \rho(E_x - E_\gamma).\end{aligned} \tag{C.12}$$

In principle, we also have to average over the excitation energy bin E_x. However, as the level density ρ and the total average radiative width Γ_γ are assumed to vary only slowly with energy, this will not lead to any changes in the equation above. The normalized spectrum is given by

$$\begin{aligned}P(E_x, E_\gamma) &= \frac{I(E_x, E_\gamma)}{\sum_{E_\gamma} I(E_x, E_\gamma)}\\ &= C_{E_x} f_1(E_\gamma) E_\gamma^3 \rho(E_f = E_x - E_\gamma),\end{aligned} \tag{C.13}$$

for a normalization constant C_{E_x} that depends only on the excitation energy.

In the case of a more spin-selective population of the compound nucleus, like in β-decay one receives a weighted sum of the level densities. If we denote the normalized population of the levels per for each excitation energy by $g_{\rm pop}(E_x, J, \pi) = \sigma_{\rm CN}(E_x, J, \pi)/\sum_{J^\pi}\sigma_{\rm CN}(E_x, J, \pi)$, Eq. (C.12) can be generalized as

$$\begin{aligned}&P(E_x, E_\gamma)\\ &= C_{E_x} f_1(E_\gamma) E_\gamma^3 \rho(E_f = E_x - E_\gamma)\sum_{J^\pi} \frac{g_{\rm pop}(E_x, J, \pi)}{g(E_x, J)}.\end{aligned} \tag{C.14}$$

In summary, we have shown that the Oslo method equation arises naturally from the Bohr's independence hypothesis for the compound nucleus under the assumption of i) the dominance of dipole radiation, ii) parity equilibration of the level density and iii) a compound nucleus cross-section $\sigma_{\rm CN}$ that is proportional to the spin distribution of intrinsic levels.

Appendix D. Calculation of $\langle\Gamma_\gamma\rangle$

In this appendix we derive Eq. (11) used to calculated the average total radiative width $\langle\Gamma_\gamma\rangle$ from the level density ρ and γ-ray strength function f. The derivation is based on Eqs. (7.19-7.23) in Ref. [86] and p. 106 in Ref. [49]. It bases on the same arguments as Appendix C, but for ease of readability, we reitterate the main points.

The radiative width Γ_γ denotes the probability for a state to decay by γ-ray emission. In the multipolar expansion it is written as

$$\Gamma_\gamma = \sum_L (\Gamma_{EL} + \Gamma_{ML}), \tag{D.1}$$

where EL and ML denote the electric and magnetic components of the radiation of order L, respectively. To simplify the derivation, we will now assume the dominance of dipole radiation, such that

$$\Gamma_\gamma = \Gamma_{E1} + \Gamma_{M1}. \tag{D.2}$$

We will continue with the derivations for the $E1$ radiation, but similar equations hold for $M1$. Analogeously to Eq. (C.3), we can express Γ_{E1} as the sum of the partial decay widths $\Gamma_{E1,i\to f}$ from the initial level i to allowed final levels f,

$$\Gamma_{E1} = \Gamma_{\gamma,E1}(E_x, J_i, \pi_i) = \sum_f \Gamma_{E1,i\to f}, \tag{D.3}$$

where the initial level is at the excitation energy E_x and has the spin J_i and parity π_i. The angular momentum and parity of the final states is given by the usual selection rules.

We now rewrite the partial widths $\Gamma_{E1,i\to f}$ in terms of the strength function f, using the definition of f, Eq. (C.4), and the generalized Brink-Axel hypothesis, Eq. (C.5),

$$\Gamma_{E1,i\to f} \to \langle\Gamma_{E1}(E_\gamma, E_x)\rangle = \frac{f_{E1}(E_\gamma)E_\gamma^3}{\rho(E_x, J_i, \pi_i)} \tag{D.4}$$

where $\rho(E_x, J_i, \pi_i)$ is the density of the initial levels, and the energy difference to the final state(s) is given by $E_\gamma = E_x - E_f$.

Next, we replace the the sum in Eq. (D.3) by an integral, where we note that the number of partial widths $\langle\Gamma_{E1}(E_\gamma, E_x)\rangle$ is proportional to the level density at the final states

$$\sum_{J_f}\sum_{\pi_f}\rho(E_x - E_\gamma, J_f, \pi_f), \tag{D.5}$$

such that the average total radiative width $\langle\Gamma_{\gamma,E1}(E_x, J_i, \pi_i)\rangle$ is given by

$$\begin{aligned}&\langle\Gamma_{\gamma,E1}(E_x, J_i, \pi_i)\rangle \\ &= \int_0^{E_x} dE_\gamma \,\langle\Gamma_{E1}(E_\gamma, E_x)\rangle \sum_{J_f}\sum_{\pi_f}\rho(E_x - E_\gamma, J_f, \pi_f) \\ &= \int_0^{E_x} dE_\gamma \,\frac{f_{E1}(E_\gamma)E_\gamma^3}{\rho(E_x, J_i, \pi_i)} \sum_{J_f=|J_i-1|}^{J_i+1}\rho(E_x - E_\gamma, J_f, \bar{\pi}_i)\end{aligned} \tag{D.6}$$

where the $E1$ operator requires a change of parity for the final state, here denoted as $\bar{\pi}_i$. The same selection rules as given in footnote 5 have been applied, but we do not use the approximation of Eq. (C.8), as many nuclei have a initial spin J_i of 0 or 1/2. Further, we assume parity equilibration of the level density, i.e. $\rho(E_x, J, +) \approx \rho(E_x, J, -)$, and express the level density $\rho(E_x, J, \pi)$ through the spin-distribution $g(E_x, J)$, Eq. (C.7),

$$\begin{aligned}&\langle\Gamma_{\gamma,E1}(E_x, J_i, \pi_i)\rangle = \frac{1}{\rho(E_x, J_i, \pi_i)} \\ &\times \int_0^{E_x} dE_\gamma \left[f_{E1}(E_\gamma)E_\gamma^3\rho(E_x - E_\gamma) \sum_{J_f=|J_i-1|}^{J_i+1} \frac{g(E_x - E_\gamma, J_f)}{2}\right].\end{aligned} \tag{D.7}$$

At this point, to obtain the expression for $M1$ radiation, one only needs to exchange the $E1$ strength function f_{E1} by the $M1$ strength function f_{M1}. Using Eq. (D.2), we find

$$\begin{aligned}&\langle\Gamma_\gamma(E_x, J_i, \pi_i)\rangle = \frac{1}{2\rho(E_x, J_i, \pi_i)} \\ &\times \int_0^{E_x} dE_\gamma \left[\big[f_{E1}(E_\gamma) + f_{M1}(E_\gamma)\big]E_\gamma^3\rho(E_x - E_\gamma)\right. \\ &\left.\times \sum_{J_f=|J_i-1|}^{J_i+1} g(E_x - E_\gamma, J_f)\right].\end{aligned} \tag{D.8}$$

This is equivalent to Eq. (2.11) in Ref. [88] under the assumptions listed above. One can determine $\langle\Gamma_\gamma(E_x, J_i, \pi_i)\rangle$ from neutron capture experiments, where usually slow neutrons are used, thus $E_x \approx S_n$. This is shown e.g. in Ref. [89], but we will repeat the derivation to get a comprehensive picture. The intrinsic spin of the neutron is 1/2, so with capture of order ℓ on a target (denoted with the subscript t) the entry states in the residual nucleus have the possible spins $J_i = J_t \pm 1/2 \pm \ell$ and parity $\pi_i = \pi_t(-1)^\ell$. For s-wave capture on a target nucleus with $J_t = 0$, there is only one possible J_i, and we can directly compare the experimental measurements to the calculations using (D.8). For $J_t > 0$, often only the average over all resonance of different J_i is reported. Using the level density $\rho(S_n, J_i)$ of the accessible J_i's, we find

$$\begin{aligned}&\langle\Gamma_{\gamma\ell}(S_n)\rangle = \frac{\sum_{J_i}\rho(S_n, J_i)\langle\Gamma_\gamma(S_n, J_i, \pi_i)\rangle}{\sum_{J_i}\rho(S_n, J_i)} \\ &= \frac{D_l}{2}\int_0^{S_n} dE_\gamma \left[f(E_\gamma)E_\gamma^3\rho(S_n - E_\gamma)\right. \\ &\left.\times \sum_{J_i}\sum_{J_f=|J_i-1|}^{J_i+1} g(S_n - E_\gamma, J_f)\right],\end{aligned} \tag{D.9}$$

where we substituted $\sum_{J_i}\rho(S_n, J_i)$ by the average neutron resonance spacing D_l and used the assumption of the dominance of the dipole decay to rewrite the sum of the average $M1$ and $E1$ strengths as $f(E_\gamma)$. Note that transitions for the highest γ-ray energies go to discrete states, not a quasi(-continuum). Thus, this integral is an approximation, and more precise calculations could distinguish between a sum over transitions to discrete states and the integral for the (quasi-)continuum region.

References

[1] J. E. Midtbø, F. Zeiser, E. Lima, Vetle W. Ingeberg, M. RK, oslocyclotronlab/ompy: Ompy v1.0.0, 2020. doi:doi:10.5281/ZENODO.3740074.

[2] M. Arnould, S. Goriely, K. Takahashi, The r-process of stellar nucleosynthesis: Astrophysics and nuclear physics achievements and mysteries, Physics Reports 450 (2007) 97–213. doi:doi:10.1016/j.physrep.2007.06.002.

[3] A. Larsen, A. Spyrou, S. Liddick, M. Guttormsen, Novel techniques for constraining neutron-capture rates relevant for r-process heavy-element nucleosynthesis, Progress in Particle and Nuclear Physics 107 (2019) 69–108. doi:doi:10.1016/j.ppnp.2019.04.002.

[4] Nuclear data high priority request list of the nea (req. id: H.32), http://www.oecd-nea.org/dbdata/hprl/hprlview.pl?id=451, 2018. URL: http://www.oecd-nea.org/dbdata/hprl/hprlview.pl?ID=451.

[5] Nuclear data high priority request list of the nea (req. id: H.33), http://www.oecd-nea.org/dbdata/hprl/hprlview.pl?id=452, 2018. URL: http://www.oecd-nea.org/dbdata/hprl/hprlview.pl?ID=452.

[6] M. Salvatores et al., Uncertainty and target accuracy assessment for innovative systems using recent covariance data evaluations, Technical Report Volume 26, OECD/NEA WPEC, 2008. URL: https://www.oecd-nea.org/science/wpec/volume26/volume26.pdf.

[7] H. Harada, et al., Uncertainty and target accuracy assessment for innovative systems using recent covariance data evaluations, Technical Report Volume 31, NEA/NSC/WPEC/-DOC(2014)446, OECD/NEA WPEC, 2014. URL: https://www.oecd-nea.org/science/wpec/volume31/volume31.pdf.

[8] J. Rekstad, A. Henriquez, F. Ingebretsen, G. Midttun, B. Skaali, R. Øyan, J. Wikne, T. Engeland, T. F. Thorsteinsen, E. Hammaren, E. Liukkonen, A study of the nuclear structure at high energy and low spin, Phys. Scr. T5 (1983) 45–50. doi:doi:10.1088/0031-8949/1983/t5/007.

[9] L. Henden, L. Bergholt, M. Guttormsen, J. Rekstad, T. Tveter, On the relation between the statistical γ-decay and the level density in 162dy, Nuclear Physics A 589 (1995) 249–266. doi:doi:10.1016/0375-9474(95)00133-l.

[10] T. Tveter, L. Bergholt, M. Guttormsen, E. Melby, J. Rekstad, Observation of fine structure in nuclear level densities and γ-ray strength functions, Physical Review Letters 77 (1996) 2404–2407. doi:doi:10.1103/physrevlett.77.2404.

[11] A. Schiller, L. Bergholt, M. Guttormsen, E. Melby, J. Rekstad, S. Siem, Extraction of level density and γ strength function from primary γ spectra, Nucl. Instrum. Methods Phys. Res. A 447 (2000) 498–511. doi:doi:10.1016/s0168-9002(99)01187-0.

[12] M. Guttormsen, F. Zeiser, J. E. Midtbø, V. W. Ingeberg, A.-C. Larsen, oslocyclotronlab/oslo-method-software: Oslo method v1.1.2, doi.org/10.5281/zenodo.2318646, 2018. doi:doi:10.5281/zenodo.2318646.

[13] A. C. Larsen, J. E. Midtbø, M. Guttormsen, T. Renstrøm, S. N. Liddick, A. Spyrou, S. Karampagia, B. A. Brown, O. Achakovskiy, S. Kamerdzhiev, D. L. Bleuel, A. Couture, L. C. Campo, B. P. Crider, A. C. Dombos, R. Lewis, S. Mosby, F. Naqvi, G. Perdikakis, C. J. Prokop, S. J. Quinn, S. Siem, Enhanced low-energy γ-decay strength of Ni70 and its robustness within the shell model, Physical Review C 97 (2018). doi:doi:10.1103/physrevc.97.054329.

[14] T. Renstrøm, H. Utsunomiya, H. T. Nyhus, A. C. Larsen, M. Guttormsen, G. M. Tveten, D. M. Filipescu, I. Gheorghe, S. Goriely, S. Hilaire, Y.-W. Lui, J. E. Midtbø, S. Péru, T. Shima, S. Siem, O. Tesileanu, Verification of detailed balance for γ absorption and emission in dy isotopes, Physical Review C 98 (2018). doi:doi:10.1103/physrevc.98.054310.

[15] T. Renstrøm, H.-T. Nyhus, H. Utsunomiya, R. Schwengner, S. Goriely, A. C. Larsen, D. M. Filipescu, I. Gheorghe, L. A. Bernstein, D. L. Bleuel, et al., Low-energy enhancement in the γ-ray strength functions of ge73,74, Physical Review C 93 (2016). URL: http://dx.doi.org/10.1103/PhysRevC.93.064302. doi:doi:10.1103/physrevc.93.064302.

[16] T. A. Laplace, F. Zeiser, M. Guttormsen, A. C. Larsen, D. L. Bleuel, L. A. Bernstein, B. L. Goldblum, S. Siem, F. L. Bello Garrote, J. A. Brown, et al., Statistica properties of ^{243}Pu, and ^{242}Pu(n,γ) cross section calculation, Physical Review C 93 (2016) 014323. doi:doi:10.1103/physrevc.93.014323.

[17] A. C. Larsen, M. Guttormsen, M. Krtička, E. Běták, A. Bürger, A. Görgen, H. T. Nyhus, J. Rekstad, A. Schiller, S. Siem, et al., Analysis of possible systematic errors in the oslo method, Phys. Rev. C 83 (2011) 034315. doi:doi:10.1103/physrevc.83.034315.

[18] I. K. B. Kullmann, A. C. Larsen, T. Renstrøm, K. S. Beckmann, F. L. B. Garrote, L. C. Campo, A. Görgen, M. Guttormsen, J. E. Midtbø, E. Sahin, S. Siem, G. M. Tveten, F. Zeiser, First experimental constraint on the os191(n,γ) reaction rate relevant to s -process nucleosynthesis, Physical Review C 99 (2019). doi:doi:10.1103/physrevc.99.065806.

[19] P. Jupyter, M. Bussonnier, J. Forde, J. Freeman, B. Granger, T. Head, C. Holdgraf, K. Kelley, G. Nalvarte, A. Osheroff, M. Pacer, Y. Panda, F. Perez, B. Ragan-Kelley, C. Willing, Binder 2.0 - reproducible, interactive, sharable environments for science at scale, in: Proceedings of the 17th Python in Science Conference, SciPy, 2018. doi:doi:10.25080/majora-4af1f417-011.

[20] T. E. Oliphant, A guide to NumPy, volume 1, Trelgol Publishing USA, 2006.

[21] S. van der Walt, S. C. Colbert, G. Varoquaux, The NumPy array: A structure for efficient numerical computation, Computing in Science & Engineering 13 (2011) 22–30. doi:doi:10.1109/mcse.2011.37.

[22] A. Spyrou, S. N. Liddick, A. C. Larsen, M. Guttormsen, K. Cooper, A. C. Dombos, D. J. Morrissey, F. Naqvi, G. Perdikakis, S. J. Quinn, et al., Novel technique for constraining r -process (n,γ) reaction rates, Physical Review Letters 113 (2014). doi:doi:10.1103/physrevlett.113.232502.

[23] V. W. Ingeberg, S. Siem, M. Wiedeking, K. Sieja, D. L. Bleuel, C. P. Brits, T. D. Bucher, T. S. Dinoko, J. L. Easton, A. Görgen, M. Guttormsen, P. Jones, B. V. Kheswa, N. A. Khumalo, A. C. Larsen, E. A. Lawrie, J. J. Lawrie, S. N. T. Majola, K. L. Malatji, L. Makhathini, B. Maqabuka, D. Negi, S. P. Noncolela, P. Papka, E. Sahin, R. Schwengner, G. M. Tveten, F. Zeiser, B. R. Zikhali, First application of the oslo method in inverse kinematics, The European Physical Journal A 56 (2020). doi:doi:10.1140/epja/s10050-020-00070-7.

[24] H. T. Nyhus, S. Siem, M. Guttormsen, A. C. Larsen, A. Bürger, N. U. H. Syed, G. M. Tveten, A. Voinov, Radiative strength functions in dy 163 , 164, Physical Review C 81 (2010). doi:doi:10.1103/physrevc.81.024325.

[25] M. Guttormsen, T. Tveter, L. Bergholt, F. Ingebretsen, J. Rekstad, The unfolding of continuum γ-ray spectra, Nucl. Instrum. Methods Phys. Res. A 374 (1996) 371–376. doi:doi:10.1016/0168-9002(96)00197-0.

[26] M. Guttormsen, T. Ramsøy, J. Rekstad, The first generation of γ-rays from hot nuclei, Nucl. Instrum. Methods Phys. Res. A 255 (1987) 518–523. doi:doi:10.1016/0168-9002(87)91221-6.

[27] F. Zeiser, G. Potel, G. M. Tveten, A. C. Larsen, M. Guttormsen, T. A. Laplace, S. Siem, D. L. Bleuel, B. L. Goldblum, L. A. Bernstein, F. L. Bello Garrote, L. Crespo Campo, T. K. Eriksen, K. Hadynska-Klek, A. G. K., J. E. Midtbø, T. Renstrøm, E. Sahin, T. Tornyi, A. Voinov, M. Wiedeking, Impact of restricted spin-ranges in the oslo method: The example of (d,p)^{240}Pu, Proceedings of the Compund Nuclear Reactions Workshop, Berkeley 2018. (2018). arXiv:arXiv:1902.02966, submitted.

[28] N. Bohr, Neutron capture and nuclear constitution 137 (1936) 344–348. doi:doi:10.1038/137344a0.

[29] A. Wallner, B. Strohmaier, H. Vonach, Extraction of nuclear level densities from neutron spectra emitted in proton-induced reactions on lead isotopes and bi, Physical Review C 51 (1995) 614–622. URL: http://dx.doi.org/10.1103/PhysRevC.51.614. doi:doi:10.1103/physrevc.51.614.

[30] A. V. Voinov, S. M. Grimes, C. R. Brune, M. J. Hornish, T. N. Massey, A. Salas, Test of nuclear level density inputs for hauser-feshbach model calculations, Physical Review C 76 (2007). doi:doi:10.1103/physrevc.76.044602.

[31] A. V. Voinov, B. M. Oginni, S. M. Grimes, C. R. Brune, M. Guttormsen, A. C. Larsen, T. N. Massey, A. Schiller, S. Siem, Nuclear excitations at constant temperature, Physical Review C 79 (2009). doi:doi:10.1103/physrevc.79.031301.

[32] A. P. D. Ramirez, A. V. Voinov, S. M. Grimes, Y. Byun, C. R. Brune, T. N. Massey, S. Akhtar, S. Dhakal, C. E. Parker, Level density and mechanism of deuteron-induced reactions on fe 54,56,58, Physical Review C 92 (2015). doi:doi:10.1103/physrevc.92.014303.

[33] R. Sherr, F. P. Brady, Spectra of (p, α) and (p, p$\prime$) reactions and the evaporation model, Physical Review 124 (1961) 1928–1943. doi:doi:10.1103/physrev.124.1928.

[34] B. V. Zhuravlev, A. A. Lychagin, N. N. Titarenko, V. G. Demenkov, V. I. Trykova, Nuclear level densities in 47V, 48V, 49V, 53Mn, and 54Mn from neutron evaporation spectra, Physics of Atomic Nuclei 74 (2011) 335–340. doi:doi:10.1134/s1063778811030173.

[35] M. Guttormsen, R. Chankova, U. Agvaanluvsan, E. Algin, L. A. Bernstein, F. Ingebretsen, T. Lönnroth, S. Messelt, G. E. Mitchell, J. Rekstad, et al., Radiative strength functions in mo 93 – 98, Physical Review C 71 (2005). doi:doi:10.1103/physrevc.71.044307.

[36] A. C. Larsen, M. Guttormsen, N. Blasi, A. Bracco, F. Camera, L. C. Campo, T. K. Eriksen, A. Görgen, T. W. Hagen, V. W. Ingeberg, B. V. Kheswa, S. Leoni, J. E. Midtbø, B. Million, H. T. Nyhus, T. Renstrøm, S. J. Rose, I. E. Ruud, S. Siem, T. G. Tornyi, G. M. Tveten, A. V. Voinov, M. Wiedeking, F. Zeiser, Low-energy enhancement and fluctuations of γ-ray strength functions in 56,57Fe: test of the brink–axel hypothesis, Journal of Physics G: Nuclear and Particle Physics 44 (2017) 064005. doi:doi:10.1088/1361-6471/aa644a.

[37] S. Bassauer, P. von Neumann-Cosel, A. Tamii, γ strength function and level density of pb208 from forward-angle proton

scattering at 295 MeV, Physical Review C 94 (2016). doi:doi:10.1103/physrevc.94.054313.

[38] B. B. Kinsey, G. A. Bartholomew, Dipole and quadrupole transition probabilities in neutron-capture gamma radiation, Physical Review 93 (1954) 1260–1278. doi:doi:10.1103/physrev.93.1260.

[39] J. Kopecky, Quadrupole radiation strength in neutron capture, Technical Report ECN–99, Netherlands, 1981. URL: https://inis.iaea.org/search/search.aspx?orig_q=RN:13649709.

[40] J. Kopecky, R. Chrien, Observation of the $m1$ giant resonance by resonance averaging in ^{106}Pd, Nuclear Physics A 468 (1987) 285–300. doi:doi:10.1016/0375-9474(87)90518-5.

[41] R. Chrien, J. Kopecky, The nuclear structure of 239u, Nuclear Physics A 414 (1984) 281–300. doi:doi:10.1016/0375-9474(84)90645-6.

[42] C. Winter, K. P. Lieb, Strength functions of primary transitions following thermal neutron capture in strontium, Zeitschrift für Physik A - Atomic Nuclei 332 (1989) 397–405. doi:doi:10.1007/bf01292425.

[43] R. Vennink, J. Kopecky, P. Endt, P. Glaudemans, Investigation of the 56fe(n, γ)57fe and 58fe(n, γ)59fe reactions, Nuclear Physics A 344 (1980) 421–445. doi:doi:10.1016/0375-9474(80)90400-5.

[44] M. D. Jones, A. O. Macchiavelli, M. Wiedeking, L. A. Bernstein, H. L. Crawford, C. M. Campbell, R. M. Clark, M. Cromaz, P. Fallon, I. Y. Lee, M. Salathe, A. Wiens, A. D. Ayangeakaa, D. L. Bleuel, S. Bottoni, M. P. Carpenter, H. M. Davids, J. Elson, A. Görgen, M. Guttormsen, R. V. F. Janssens, J. E. Kinnison, L. Kirsch, A. C. Larsen, T. Lauritsen, W. Reviol, D. G. Sarantites, S. Siem, A. V. Voinov, S. Zhu, Examination of the low-energy enhancement of the γ -ray strength function of fe56, Physical Review C 97 (2018). doi:doi:10.1103/physrevc.97.024327.

[45] G. Rusev, N. Tsoneva, F. Dönau, S. Frauendorf, R. Schwengner, A. P. Tonchev, A. S. Adekola, S. L. Hammond, J. H. Kelley, E. Kwan, H. Lenske, W. Tornow, A. Wagner, Fine structure of the giant m1 resonance in zr90, Physical Review Letters 110 (2013). doi:doi:10.1103/physrevlett.110.022503.

[46] A. C. Larsen, N. Blasi, A. Bracco, F. Camera, T. K. Eriksen, A. Görgen, M. Guttormsen, T. W. Hagen, S. Leoni, B. Million, H. T. Nyhus, T. Renstrøm, S. J. Rose, I. E. Ruud, S. Siem, T. Tornyi, G. M. Tveten, A. V. Voinov, M. Wiedeking, Evidence for the dipole nature of the low-energy γ enhancement from 56Fe, Physical Review Letters 111 (2013). doi:doi:10.1103/physrevlett.111.242504.

[47] A. Simon, M. Guttormsen, A. C. Larsen, C. W. Beausang, P. Humby, J. T. Burke, R. J. Casperson, R. O. Hughes, T. J. Ross, J. M. Allmond, R. Chyzh, M. Dag, J. Koglin, E. McCleskey, M. McCleskey, S. Ota, A. Saastamoinen, First observation of low-energy γ-ray enhancement in the rare-earth region, Physical Review C 93 (2016). doi:doi:10.1103/physrevc.93.034303.

[48] D. M. Brink, Ph.D. thesis, Ph.D. thesis, University of Oxford, 1955. URL: https://ora.ox.ac.uk/objects/uuid:334ec4a3-8a89-42aa-93f4-2e54d070ee090.

[49] P. Axel, Electric dipole ground-state transition width strength function and 7-mev photon interactions, Phys. Rev. 126 (1962) 671–683. doi:doi:10.1103/physrev.126.671.

[50] M. Guttormsen, A. C. Larsen, A. Görgen, T. Renstrøm, S. Siem, T. G. Tornyi, G. M. Tveten, Validity of the generalized brink-axel hypothesis in np 238, Physical Review Letters 116 (2016). doi:doi:10.1103/physrevlett.116.012502.

[51] L. Crespo Campo, M. Guttormsen, F. L. Bello Garrote, T. K. Eriksen, F. Giacoppo, A. Görgen, K. Hadynska-Klek, M. Klintefjord, A. C. Larsen, T. Renstrøm, E. Sahin, S. Siem, A. Springer, T. G. Tornyi, G. M. Tveten, Test of the generalized brink-axel hypothesis in ni64,65, Physical Review C 98 (2018). doi:doi:10.1103/physrevc.98.054303.

[52] F. Bečvář, P. Cejnar, R. E. Chrien, J. Kopecký, Test of photon strength functions by a method of two-step cascades, Physical Review C 46 (1992) 1276–1287. doi:doi:10.1103/physrevc.46.1276.

[53] M. Krtička, F. Bečvář, J. Honzátko, I. Tomandl, M. Heil, F. Käppeler, R. Reifarth, F. Voss, K. Wisshak, Evidence for m1 scissors resonances built on the levels in the quasicontinuum of dy163, Physical Review Letters 92 (2004). doi:doi:10.1103/physrevlett.92.172501.

[54] C. W. Johnson, Systematics of strength function sum rules, Physics Letters B 750 (2015) 72–75. doi:doi:10.1016/j.physletb.2015.08.054.

[55] E. Jones, T. Oliphant, P. Peterson, others, SciPy: Open source scientific tools for Python, 2001. URL: http://www.scipy.org/.

[56] M. J. D. Powell, An efficient method for finding the minimum of a function of several variables without calculating derivatives, The Computer Journal 7 (1964) 155–162. doi:doi:10.1093/comjnl/7.2.155.

[57] H. A. Bethe, An attempt to calculate the number of energy levels of a heavy nucleus, Physical Review 50 (1936) 332–341. doi:doi:10.1103/physrev.50.332.

[58] A. Gilbert, A. G. W. Cameron, A composite nuclear-level density formula with shell corrections, Canadian Journal of Physics 43 (1965) 1446–1496. doi:doi:10.1139/p65-139.

[59] T. Ericson, A statistical analysis of excited nuclear states, Nuclear Physics 11 (1959) 481–491. doi:doi:10.1016/0029-5582(59)90291-3.

[60] R. Capote, M. Herman, P. Obložinský, P. Young, S. Goriely, T. Belgya, A. Ignatyuk, A. Koning, S. Hilaire, V. Plujko, et al., Ripl – reference input parameter library for calculation of nuclear reactions and nuclear data evaluations, Nuclear Data Sheets 110 (2009) 3107–3214. doi:doi:10.1016/j.nds.2009.10.004, data extraced from RIPL-3 online database https://www-nds.iaea.org/RIPL-3/, accessed 10.05.2015.

[61] M. Guttormsen, B. Jurado, J. N. Wilson, M. Aiche, L. A. Bernstein, Q. Ducasse, F. Giacoppo, A. Görgen, F. Gunsing, T. W. Hagen, et al., Constant-temperature level densities in the quasi-continuum of th and u isotopes, Phys. Rev. C 88 (2013) 024307. doi:doi:10.1103/physrevc.88.024307.

[62] T. Ericson, The statistical model and nuclear level densities, Advances in Physics 9 (1960) 425–511. URL: http://dx.doi.org/10.1080/00018736000101239. doi:doi:10.1080/00018736000101239.

[63] M. Guttormsen, M. Aiche, F. L. Bello Garrote, L. A. Bernstein, D. L. Bleuel, Y. Byun, Q. Ducasse, T. K. Eriksen, F. Giacoppo, A. Görgen, et al., Experimental level densities of atomic nuclei, The European Physical Journal A 51 (2015). doi:doi:10.1140/epja/i2015-15170-4.

[64] A. C. Larsen, M. Guttormsen, R. Schwengner, D. L. Bleuel, S. Goriely, S. Harissopulos, F. L. Bello Garrote, Y. Byun, T. K. Eriksen, F. Giacoppo, A. Görgen, T. W. Hagen, M. Klintefjord, T. Renstrøm, S. J. Rose, E. Sahin, S. Siem, T. G. Tornyi, G. M. Tveten, A. V. Voinov, M. Wiedeking, Experimentally constrained (p,γ)y89 and (n,γ)y89 reaction rates relevant to p-process nucleosynthesis, Physical Review C 93 (2016). doi:doi:10.1103/physrevc.93.045810.

[65] F. Feroz, M. P. Hobson, M. Bridges, MultiNest: an efficient and robust bayesian inference tool for cosmology and particle physics, Monthly Notices of the Royal Astronomical Society 398 (2009) 1601–1614. doi:doi:10.1111/j.1365-2966.2009.14548.x.

[66] F. Feroz, M. P. Hobson, E. Cameron, A. N. Pettitt, Importance nested sampling and the multinest algorithm (2013). arXiv:http://arxiv.org/abs/1306.2144v2.

[67] J. Buchner, A. Georgakakis, K. Nandra, L. Hsu, C. Rangel, M. Brightman, A. Merloni, M. Salvato, J. Donley, D. Kocevski, X-ray spectral modelling of the AGN obscuring region in the CDFS: Bayesian model selection and catalogue, Astronomy & Astrophysics 564 (2014) A125. doi:doi:10.1051/0004-6361/201322971.

[68] R. Storn, K. Price, Differential evolution – a simple and efficient heuristic for global optimization over continuous spaces, Journal of Global Optimization 11 (1997) 341–359. URL: http://dx.doi.org/10.1023/A:1008202821328. doi:doi:10.1023/a:1008202821328.

[69] T. von Egidy, D. Bucurescu, Systematics of nuclear level density parameters, Phys. Rev. C 72 (2005) 044311. doi:doi:10.1103/physrevc.72.044311.

[70] S. Agostinelli, J. Allison, K. Amako, J. Apostolakis, H. Araujo, P. Arce, M. Asai, D. Axen, S. Banerjee, G. Barrand, F. Behner, L. Bellagamba, J. Boudreau, L. Broglia, A. Brunengo, H. Burkhardt, S. Chauvie, J. Chuma, R. Chytracek, G. Cooperman, G. Cosmo, P. Degtyarenko, A. Dell'''Acqua, G. Depaola, D. Dietrich, R. Enami, A. Feliciello, C. Ferguson, H. Fesefeldt, G. Folger, F. Foppiano, A. Forti, S. Garelli, S. Giani, R. Giannitrapani, D. Gibin, J. G. Cadenas, I. González, G. G. Abril, G. Greeniaus, W. Greiner, V. Grichine, A. Grossheim, S. Guatelli, P. Gumplinger, R. Hamatsu, K. Hashimoto, H. Hasui, A. Heikkinen, A. Howard, V. Ivanchenko, A. Johnson, F. Jones, J. Kallenbach, N. Kanaya, M. Kawabata, Y. Kawabata, M. Kawaguti, S. Kelner, P. Kent, A. Kimura, T. Kodama, R. Kokoulin, M. Kossov, H. Kurashige, E. Lamanna, T. Lampén, V. Lara, V. Lefebure, F. Lei, M. Liendl, W. Lockman, F. Longo, S. Magni, M. Maire, E. Medernach, K. Minamimoto, P. M. de Freitas, Y. Morita, K. Murakami, M. Nagamatu, R. Nartallo, P. Nieminen, T. Nishimura, K. Ohtsubo, M. Okamura, S. O'Neale, Y. Oohata, K. Paech, J. Perl, A. Pfeiffer, M. Pia, F. Ranjard, A. Rybin, S. Sadilov, E. D. Salvo, G. Santin, T. Sasaki, N. Savvas, Y. Sawada, S. Scherer, S. Sei, V. Sirotenko, D. Smith, N. Starkov, H. Stoecker, J. Sulkimo, M. Takahata, S. Tanaka, E. Tcherniaev, E. S. Tehrani, M. Tropeano, P. Truscott, H. Uno, L. Urban, P. Urban, M. Verderi, A. Walkden, W. Wander, H. Weber, J. Wellisch, T. Wenaus, D. Williams, D. Wright, T. Yamada, H. Yoshida, D. Zschiesche, Geant4—a simulation toolkit, Nuclear Instruments and Methods in Physics Research Section A: Accelerators, Spectrometers, Detectors and Associated Equipment 506 (2003) 250–303. doi:doi:10.1016/s0168-9002(03)01368-8.

[71] G. Choudalakis, Fully bayesian unfolding (2012). arXiv:201.4612v4.

[72] F. Zeiser, G. M. Tveten, G. Potel, A. C. Larsen, M. Guttormsen, T. A. Laplace, S. Siem, D. L. Bleuel, B. L. Goldblum, L. A. Bernstein, F. L. Bello Garrote, L. Crespo Campo, T. K. Eriksen, A. Görgen, K. Hadynska-Klek, V. W. Ingeberg, J. E. Midtbø, E. Sahin, T. Tornyi, A. Voinov, M. Wiedeking, J. Wilson, Restricted spin-range correction in the oslo method: The example of nuclear level density and γ-ray strength function from ^{239}Pu$(d, p\gamma)^{240}$Pu, Physical Review C 100 (2019) 024305. doi:doi:10.1103/physrevc.100.024305.

[73] T. von Egidy, D. Bucurescu, Experimental energy-dependent nuclear spin distributions, Phys. Rev. C 80 (2009) 054310. doi:doi:10.1103/physrevc.80.054310.

[74] T. Von Egidy, H. Schmidt, A. Behkami, Nuclear level densities and level spacing distributions: Part II, Nuclear Physics A 481 (1988) 189–206. doi:doi:10.1016/0375-9474(88)90491-5.

[75] S. Goriely, S. Hilaire, A. J. Koning, Improved microscopic nuclear level densities within the hartree-fock-bogoliubov plus combinatorial method, Physical Review C 78 (2008). doi:doi:10.1103/physrevc.78.064307.

[76] Y. Alhassid, L. Fang, H. Nakada, Heavy deformed nuclei in the shell model monte carlo method., Physical Review Letters 101 (2008). doi:doi:10.1103/physrevlett.101.082501.

[77] R. Sen'kov, V. Zelevinsky, Nuclear level density: Shell-model approach, Physical Review C 93 (2016). doi:doi:10.1103/physrevc.93.064304.

[78] Y. Alhassid, G. F. Bertsch, S. Liu, H. Nakada, Parity dependence of nuclear level densities, Physical Review Letters 84 (2000) 4313–4316. doi:doi:10.1103/physrevlett.84.4313.

[79] Data extracted from the endsf database using nndc's chart of nuclides, http://www.nndc.bnl.gov/chart/, accessed on 01.08.2020, 2020.

[80] L. Kirsch, L. Bernstein, RAINIER: A simulation tool for distributions of excited nuclear states and cascade fluctuations, Nuclear Instruments and Methods in Physics Research Section A: Accelerators, Spectrometers, Detectors and Associated Equipment 892 (2018) 30–40. doi:doi:10.1016/j.nima.2018.02.096.

[81] F. Zeiser, L. E. Kirsch, fzeiser/rainier: Rainier v1.5.0, 2020. doi:doi:10.5281/ZENODO.3689461.

[82] J. Kaipio, E. Somersalo, Statistical inverse problems: Discretization, model reduction and inverse crimes, Journal of Computational and Applied Mathematics 198 (2007) 493–504. doi:doi:10.1016/j.cam.2005.09.027.

[83] V. Blobel, Unfolding, in: Data Analysis in High Energy Physics, Wiley-VCH Verlag GmbH & Co. KGaA, 2013, pp. 187–225. doi:doi:10.1002/9783527653416.ch6.

[84] H. A. Bethe, Nuclear physics b. nuclear dynamics, theoretical, Reviews of Modern Physics 9 (1937) 69–244. doi:doi:10.1103/revmodphys.9.69.

[85] V. F. Weisskopf, The statistical theory of nuclear reactions, in: Lecture Series on Nuclear Physics, LA-24, 1943, pp. 207–286. doi:doi:10.2172/12678451.

[86] J. M. Blatt, V. F. Weisskopf, Theoretical Nuclear Physics, Wiley [u.a.], New York, 1952.

[87] W. Hauser, H. Feshbach, The inelastic scattering of neutrons, Physical Review 87 (1952) 366–373. doi:doi:10.1103/physrev.87.366.

[88] G. A. Bartholomew, E. D. Earle, A. J. Ferguson, J. W. Knowles, M. A. Lone, Gamma-ray strength functions, Advances in Nuclear Physics (1973) 229–324. doi:doi:10.1007/978-1-4615-9044-6_4.

[89] A. Voinov, M. Guttormsen, E. Melby, J. Rekstad, A. Schiller, S. Siem, γ -ray strength function and pygmy resonance in rare earth nuclei, Physical Review C 63 (2001) 044313. doi:doi:10.1103/physrevc.63.044313.

Paper II

The γ-ray energy response of the Oslo Scintillator Array OSCAR

II

Zeiser, F., Tveten, G. M., Bello Garrote, F. L., Guttormsen, M., Larsen, A. C., Ingeberg, V. W., Görgen, A., Siem, S.

Published in *Nuclear Instruments and Methods in Physics Research Section A: Accelerators, Spectrometers, Detectors and Associated Equipment*, September 2020 (online), 1 January 2021 (print) Volume 985, Article no. 164678 DOI: 10.1016/j.nima.2020.164678. arXiv: 1708.04101

Nuclear Inst. and Methods in Physics Research, A 985 (2021) 164678

Contents lists available at ScienceDirect

Nuclear Inst. and Methods in Physics Research, A

journal homepage: www.elsevier.com/locate/nima

The γ-ray energy response of the Oslo Scintillator Array OSCAR

F. Zeiser *, G.M. Tveten[1], F.L. Bello Garrote, M. Guttormsen, A.C. Larsen, V.W. Ingeberg, A. Görgen, S. Siem

Department of Physics, University of Oslo, N-0316 Oslo, Norway

ARTICLE INFO

Keywords:
Geant4
Response function
Lanthanum-bromide
Gamma-ray detector array
Monte Carlo Simulation
Detector modeling

ABSTRACT

The new Oslo Scintillator Array (OSCAR) has been commissioned at the Oslo Cyclotron Laboratory (OCL). It consists of 30 large volume (⌀ 3.5 × 8 inches) $LaBr_3$(Ce) detectors that are used for γ-ray spectroscopy. The response functions for incident γ rays up to 20 MeV are simulated with Geant4. In addition, the resolution, and the total and full-energy peak efficiencies are extracted. The results are in very good agreement with measurements from calibration sources and experimentally obtained mono-energetic in-beam γ-ray spectra.

1. Introduction

The Oslo Cyclotron Laboratory (OCL) at the University of Oslo has commissioned the new Oslo SCintillator ARray (OSCAR) in 2018, replacing the NaI(Tl) scintillator array CACTUS [1]. The $LaBr_3$(Ce) detectors of OSCAR significantly improve the timing and energy resolution and intrinsic efficiency, which will not only provide better experimental conditions for the type of experiments most commonly carried out at OCL, but also open the door to novel studies. Since the early 1980's, the OCL has contributed substantially to experimental studies of nuclear properties in the quasi-continuum with the Oslo method [2–4]. As the first step of the analysis it uses a common technique in nuclear physics and high energy physics called unfolding to calculate the emitted γ-ray spectrum from the measured spectrum [1,5,6]. This requires an accurate knowledge of the γ-ray response of OSCAR. In this article, we present simulations of the response and verify them by comparison to experimentally determined calibration sources and in-beam γ-ray spectra. The simulations are written in C++ using the GEometry ANd Tracking 4 (Geant4) library [7] v10.06, which is a standard tool for particle transport simulations in nuclear and particle physics experiments. The focus will be on the determination of the response between ≈100 keV and 10 MeV, as this is the energy range used in most common applications planed for OSCAR, the Oslo method and the study of prompt fission γ rays.

2. Setup

OSCAR consists of a total of 30 large volume BriLanCe™ 380 $LaBr_3$(Ce) scintillating crystals manufactured by Saint-Gobain. The crystals are cylindrical with a diameter of 3.5 inches and a length of 8 inches. The detectors are coupled to Hamamatsu R10233-100 photo multiplier tubes (PMT) with active voltage dividers (LABRVD) [8] and placed in an aluminum housing. They are powered by 6 iseg NHS 60 20n power supplies. The signals are processed by 14-bit, 500 MHz, XIA Pixie-16 modules and written to disk for subsequent offline analysis. An article dedicated to the detector characteristics and digital electronics will follow [9].

The detectors are mounted in a football shaped frame, see Fig. 1, where the distance to the center is adjusted by the choice of distance rods. For this work, we used the closest configuration with a face-to-center distance d between detector and source of $d \approx 16.3$ cm, which results in a solid angle coverage of 57% of 4π. A table with the positions and labels of the OSCAR detectors is provided in Appendix.

The γ-ray detector array encompasses the beam-line and target chamber, in which the sources are placed, as well as the SiRi particle telescope [10] and for some experiments the NIFF PPAC fission fragment detector [11].

3. Implementation of the simulation

3.1. Geometry

The implemented geometry includes the full setup of the array, including the OSCAR detectors and their support structure, SiRi, NIFF, two alternative target chambers, the beam-line, the target holder and the target frame or radioactive calibration source itself. The full model v2.0.0 is available on github and as Ref. [12]. Most components can be (de)activated via macros at runtime to reflect the experimental

* Corresponding author.
E-mail address: fabio.zeiser@fys.uio.no (F. Zeiser).
[1] Present address: Expert Analytics AS, N0160 Oslo, Norway.

https://doi.org/10.1016/j.nima.2020.164678
Received 26 August 2020; Received in revised form 17 September 2020; Accepted 17 September 2020
Available online 19 September 2020

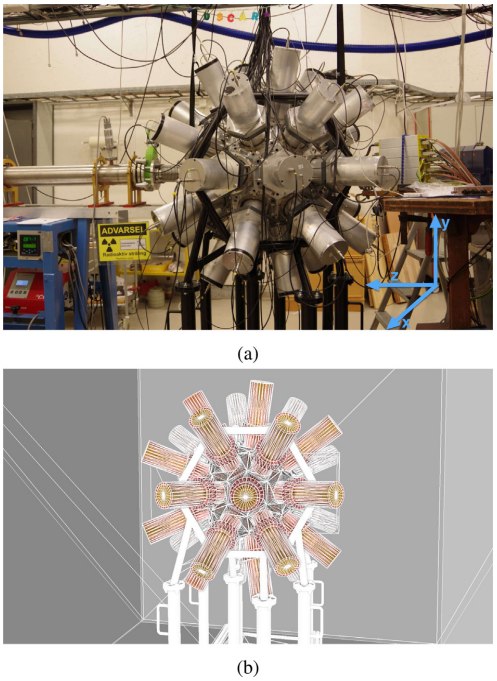

(a)

(b)

Fig. 1. (a) A photo of the new array OSCAR and (b) its geometry implementation in Geant4. The axes used in the Geant4 implementation are included as an overlay.

conditions or to speed up the calculations. The standard configuration of the experiments is available via `setup_normal_run.mac` and does not include NIFF and the calibration source, as in-beam spectra on very thin metal foils are used. By default, we use the spherical target chamber installed in 2018.

To maintain a high performance of the simulations we have used the Constructed Solid Geometry (CSG) wherever feasible. Thus, the radioactive source, the detectors including their encapsulation and housing, and the football-like shaped aluminum frame, a truncated icosahedron, are implemented as CSG solids. The polar angle θ and azimuth angle ϕ of the 30 detectors are fixed by the truncated icosahedron geometry and given in Table A.1 in the Appendix; the beamline runs through the remaining two faces. As common practice, the z-axis is chosen along the beam direction, and the y-axis points upwards. The face-to-center distance d between detector and source can be physically adjusted by different spacer rods; in the simulations d can be adjusted for each detector individually with a macro command, or they may even be removed totally, which facilitates updating the response matrix for experiments in a non-standard configuration. By default, all 30 detectors are placed at a distance of $d \approx 16.3$ cm.

An older cylindrical target chamber is dedicated to actinide experiments and is implemented via CSG solids. The new spherical target chamber, including the wheel with the target holders, has a much more complex geometry, such that we used the Computer-Aided Design (CAD) drawings instead. Similarly, the support structure of the frame is implemented with the CAD geometry.

All CAD drawings are imported as GDML files after conversion with GUIMesh v1 [13]. We preprocessed the drawings slightly, removing several small elements like sealing rings, which are not expected to effect the γ rays significantly, but may increase the computation time considerably. Each element of the setup is implemented through an individual Geant4 *parallel world geometry* to facilitate the navigation and avoid boundary problems. The *layered mass geometry* ensures that a particle at any given point only sees the topmost parallel world with a volume defined at the point, or if no parallel world is defined it seems the basic *mass world*. We use following top to bottom hierarchy:

1. `ParallelWorld Targets on Wheel`: Target frames placed on the target wheel,
2. `ParallelWorld SiRi`: A CAD implementation of SiRi particle telescopes (a more primitive CSG implementation exists),
3. `ParallelWorld Frame Outer`: The support structure of the frame,
4. `ParallelWorld Target Chamber`: The spherical target chamber including the target wheel,
5. `massWorld` The *normal* world, where all CSG volumes are defined.

The rectangular calibration sources are modeled given the manufacturer specifications of Eckert & Ziegler through a 0.5 cm^3 acrylic glass cube of the support material, embedding an Amberlite™ IR-120 sphere containing the active material with a radius of 0.5 mm.

All commands related to the geometry are in the `/OCL` macro directory and its sub-directories and are documented online. The geometry is constructed in a modular fashion, such that it is easy to reuse parts of the code when the $LaBr_3$(Ce) detectors are used at another experimental facility.

3.2. Physics processes and event generation

We have chosen the QGSP_BIC_HP reference physics list, which implements standard electromagnetic interactions through G4EmStandardPhysics and neutron interactions through data driven high precision cross-sections. All events are generated at the target position at the center of the sphere using the General Particle Source (GPS). For the calibration sources we use the Radioactive Decay Module in addition. Whilst the active area of the calibration source is approximated by a small spherical source of the carrier material, we used a small (≈ 3 mm^2) isotropic planar source roughly corresponding to the beam size for the cyclotron at the target position. The scintillation process can be simulated with G4OpticalPhysics, but is not included in the simulations by default, as it significantly increases the computation time without any impact on the energy collection.

3.3. Scoring and data analysis

The energy deposited in each crystal is recorded as an n-tuple and stored as a ROOT [14] tree. For the further analysis, we combine the histograms for all detectors to a cumulative response of OSCAR. As Geant4 does not model the electronic response of the system and inclusion of the scintillation process for large scale simulations is prohibited by the computation time, we initially get histograms with spikes at the full-energy peak, single escape, etc. These are folded by a Gaussian to mimic the statistical behavior and non-uniformity of the scintillation photon collection, the PMT and the signal processing electronics. The full width at half maximum (FWHM) is determined by fits to 15 peaks from following radioactive sources: ^{60}Co, ^{133}Ba, ^{137}Cs, ^{152}Eu and ^{241}Am. The variation of the FWHM as a function of the γ-ray energy E_γ is fitted by

$$\mathrm{FWHM}(E_\gamma)\,[\mathrm{keV}] = \sqrt{a_0 + a_1 E_\gamma + a_2 E_\gamma^2}, \tag{1}$$

with the best fit values $a_0 = 60.64(73)$, $a_1 = 0.458(02)$, and $a_2 = 2.6555(17) \times 10^{-4}$, assuming E_γ is given in keV.

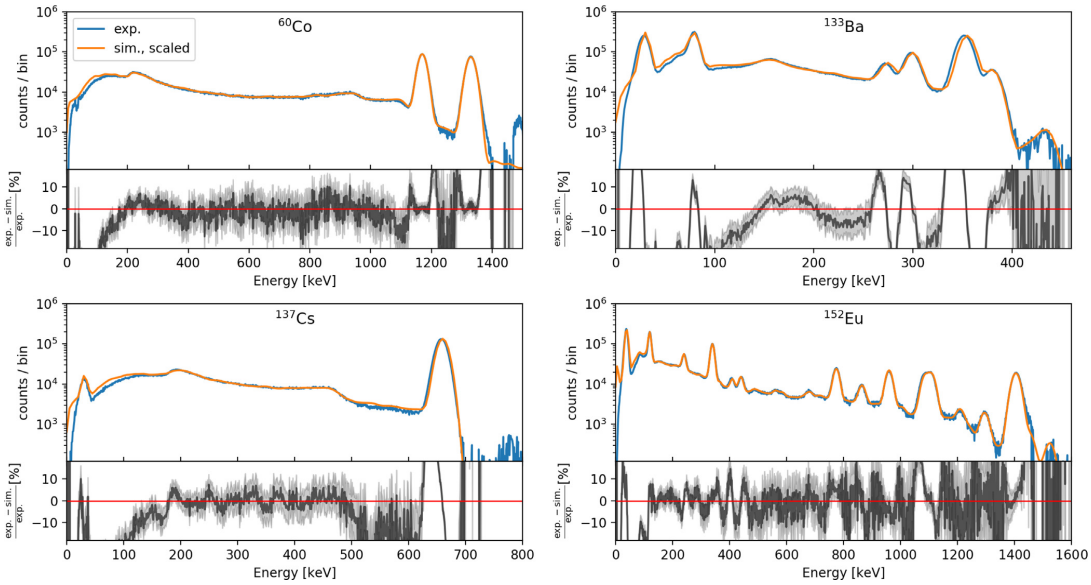

Fig. 2. Experimental source spectra (blue) compared to the simulations (orange) for ^{60}Co (top left), ^{133}Ba (top right), ^{137}Cs (bottom left) and ^{152}Eu (bottom right). The simulations are scaled to the same number of decays as the experimental spectra. The lower panels show the relative difference between experiment. Note that the displayed energy ranges are different for each isotope. (For interpretation of the references to color in this figure legend, the reader is referred to the web version of this article.)

4. Results and verification

4.1. Calibration sources

The response has been simulated for 2×10^5 decays of ^{60}Co, ^{133}Ba, ^{137}Cs and ^{152}Eu (the activity of the ^{241}Am is not known) and is compared to the experimental measured spectra in Fig. 2. The simulations are scaled to same number of decays as in the experimental data, using the activity and measuring time of the sources. We use a quadratic energy calibration fitted to 15 peaks of all four sources and subtract the background. This generally works quite well, although small deficiencies are visible in the ^{60}Co and ^{152}Eu spectra between ≈1.4 and 1.5 MeV, where the strong internal radiation of the $LaBr_3$(Ce) detectors is not correctly subtracted due to a small drift of the calibration. The simulations give an excellent reproduction of the calibration spectra with an average deviation below 5% for γ-ray energies E_γ above 200 keV.

Between 50 and 200 keV the deviations reach up to about 20%. We expect larger deviations in this area, as low energy γ rays are easily attenuated, thus require an even more precise implementation of the geometry. In the most common application of OSCAR, the Oslo method, usually γ rays between ≈1 and 10 MeV are studied. Newer applications, like the study of prompt fission γ rays, may also study the γ-ray response above ≈100 keV. However, when the low energy region (≤100 keV) is of interest, it might be important to include details like the cables leading to SiRi and the target wheel, small screws, as well as sealing rings, which were removed from the CAD drawings to improve the computation time, see Section 3.1. Furthermore, non-linearities in the detector response will become relevant at these energies. It can also be noted that the magnitude of the deviation depends on the exact source spectrum, thus we cannot find a generally applicable correction function that could be used on top of the simulations. Below ≈30 to 50 keV, the above considerations on the geometry are valid as well, but in addition the onset of the detector threshold (which cannot be simulated with Geant4) will lead to a loss of counts in the experimental spectra.

The full-energy peak efficiency ϵ_{fe} of the setup has been analyzed and is displayed in Fig. 3. The results depend on the choice of the fit function and minimization routine, and we estimate this systematic uncertainty to ≈3–5%. Our main goal here is to verify the simulated efficiencies. Therefore we fit the peaks in both the experimental and simulated spectra in the exact same way, using a fit function composed of following three elements:

1. a Gaussian: The main component of the peak arising from the electronic response to an otherwise mono-energetic γ ray,
2. a smoothed step function: From Compton scattered γ rays that enter the detector and the escape of scintillator photons from the crystal, using the functional form proposed in RadWare's gf3 [15],
3. an constant background: From the contribution of other peaks and their Compton spectrum.

We attempted to extend the fitting routine for more complicated peak structures, like the double peaks in ^{133}Ba and ^{152}Eu, but could not find a good and consistent way of fitting them. For the comparison in Fig. 3, only fits that converged properly are processed. The full-energy peak efficiencies ϵ_{fe} agree within the fit uncertainties. The analyzed efficiencies ϵ_{fe} in turn are fit as proposed in gf3 [15]:

$$\ln \epsilon_{\mathrm{ph}} = p_0 + p_1 \ln(E_\gamma) + p_2 \ln(E_\gamma)^2. \quad (2)$$

The best-fit values are listed in Table A.2.

4.2. In-beam spectra

The comparison to experimental in-beam spectra provides additional insights, but also challenges to the data processing.

We use particle-γ coincidence measurements from the (p,p')^{28}Si and (p,p')^{12}C reactions, both measured in 2019. Gating on the detected particle energy, we can select γ rays from population of specific excited states and their decay, e.g. the first excited states at 1779 and 4440 keV, respectively. It was not possible to obtain other mono-energetic spectra from ^{28}Si by gaiting on higher excitation, because the particle

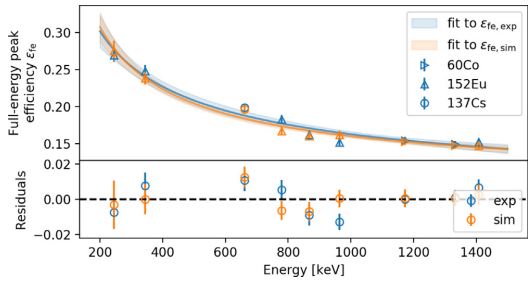

Fig. 3. Full-energy peak efficiency of OSCAR from calibration sources (blue) and simulation (orange). The bottom panel shows the residuals from the fits. (For interpretation of the references to color in this figure legend, the reader is referred to the web version of this article.)

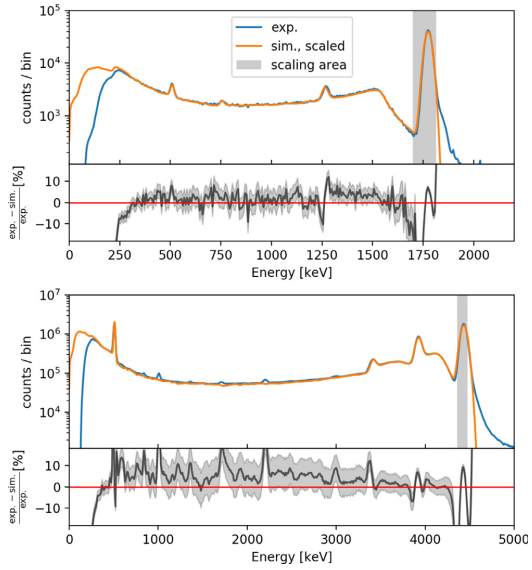

Fig. 4. Experimental in-beam γ-ray spectra (blue) compared to simulations (orange) of mono-energetic incident γ ray of 1779 (top) and 4440 keV (bottom), respectively. The lower panels show the relative difference between experiment and simulation. The area used to scale the simulations to the experiment is highlighted in gray. The discrepancies are explained in the text. (For interpretation of the references to color in this figure legend, the reader is referred to the web version of this article.)

energy resolution was not good enough to clearly distinguish the different states (and separate them from states of ^{29}Si and ^{16}O contaminating the target).

For the in-beam spectra random coincidences with particles from previous beam bursts of the cyclotron are subtracted using two dimensional graphical time-energy cuts. The total number of incident γ rays is not known for the experimental spectra. Therefore, we use the number of detected γ rays that fulfill the coincidence requirements and normalize the simulated and experimental spectra to the same number of counts in the full-energy peak. Naturally, the spectra agree within the close vicinity of the full-energy peak, but from Fig. 4 we can see that they also match well for the single- and double-escape peaks, the annihilation peak and the Compton-spectrum above $E_\gamma \approx 200$ keV.

There are several noteworthy discrepancies. Below $E_\gamma \approx 200$, the simulations seemingly overestimate the experimental spectra significantly. We attribute this to an over-subtraction of the background for low energies in connection with inaccurate graphical time-energy gates. On the contrary, the simulations apparently underestimate the Compton-background for the 4440 keV γ-ray spectrum from ^{12}C. This is however linked to the contamination of γ rays from the aluminum frame of the ^{12}C target, which contaminate the experimental ^{12}C spectrum. This can be identified from the position of the additional aluminum peaks, where the 1014, 1720, and 2212 keV lines are easily visible in Fig. 4. Finally, we observe that the full-energy peak in the experimental spectra is not perfectly Gaussian shaped, but has a tail towards higher energies. Note that this is not visible in the source spectra of Fig. 2. It is beyond the scope of this article to verify whether the tail is due to suboptimal settings during the data acquisition (e.g. different impedances causing a slight ringing in the cables) such that it can be removed in future experiments, or whether it is of permanent nature (e.g. pileup with γ rays or X-rays created from the cyclotron operation, etc.). In the latter case, one could use a non-Gaussian kernel for the smoothing of the simulated spectra, which is described in Section 3.3.

4.3. Response matrix

For the previously used CACTUS γ-ray detectors, the response matrix was obtained from an interpolation and extrapolation of a small number of measured experimental spectra [1]. Given the simulations presented here and their successful verification in Sections 4.1 and 4.2, we now calculate the response of OSCAR for a large grid of incident γ-ray energies E_{in} between 50 keV and 20 MeV. A simulation of 10^6 single incident γ-rays of 5 MeV in the standard setup with the new spherical target chamber takes about 8 cpu-hours on a single Intel E5-2683v4 2.1 GHz core. As most experiments only require the response below 10 MeV, we split the calculations in two parts. Below 10 MeV we use a step-size of 10 keV, removing the need for interpolations; in addition we simulate the response for 12, 15 and 20 MeV. As an additional measure to balance runtime against the accuracy of the results, we increase the number of events from 0.5×10^6 for the low energies to 3×10^6 for the highest incident energies. The total computation time of the response was $\approx$ 17000 cpu-hours and it is available online on github and as dataset Ref. [12] in the matrix format $R(E_{in}, E_{out})$, where E_{out} is the simulated response. Note that we use an isotropic source with multiplicity 1 for all events here, but the source definition can easily be adopted for higher multiplicities and other angular distributions through the GPS macro commands if this is desirable.

In Fig. 5 the total efficiency is plotted, which is given by the ratio of counts detected above a threshold over the number of simulated events. As the most common unfolding technique that is used in the Oslo method [1] requires the full energy, single and double escape, and annihilation probabilities for the so called Compton subtraction method, these probabilities are extracted as well.

5. Lessons learnt

A first version of the OSCAR simulation was developed in 2018 [16], but we encountered several challenges in the model development and the comparison to experiments [17]. In the following, we try to summarize the main lessons learnt which lead to the very good agreement between simulation and experiment.

1. As mentioned in Section 4.1, the full-energy peak efficiency is rather sensitive to the fit function and procedure. In the simulations, it is possible to select only photoeffect interactions and base the full-energy peak efficiency on these. However, this induced a systematic discrepancy and lead to an apparently poorer reproduction of the experimental fits.

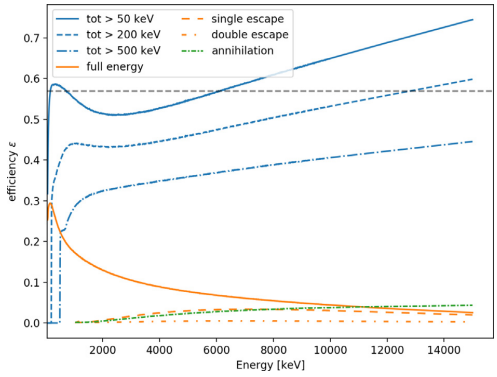

Fig. 5. Simulated efficiencies (see legend), where the total efficiency is given for different lower thresholds. The geometric efficiency of 57% is highlighted (black dashed line), but can be exceeded due e.g. cross-talk between detectors for one and the same gamma event. (For interpretation of the references to color in this figure legend, the reader is referred to the web version of this article.)

2. Several studies have shown that the $LaBr_3$(Ce) detectors have a non-linear energy response, especially at low energies, see e.g. Refs. [18] and references therein. However, during the first benchmarking phase for the simulations, only a subset of the calibration sources was used, which only allowed for a linear energy calibration. This induced an error which was misattributed to the accuracy of the geometry implementation. Ideally, even more calibration sources should be available if one wants to improve the response below $E_\gamma = 200$ keV.
3. Initially, we experienced large problems importing the CAD geometry, with particle tracks getting stuck. This was easily resolved with GUIMesh and the parallel world geometry. Problems with the material definition in GUIMesh v1 were circumvented by grouping the elements of a drawing by material, exporting each group individually, and editing the material through a *search and replace*.

6. Summary

Response functions of the new γ-ray detector array OSCAR at the OCL have been simulated with the Geant4 toolkit up to 20 MeV. The simulations are compared to experimental spectra from calibration sources and in-beam γ-rays, where a good agreement has been achieved. The deviations are below $\approx 5\%$ for γ-ray energies E_γ larger than 200 keV. Additionally, we obtained the total and partial efficiencies for the various components of the γ-ray interaction with the detectors. Finally, we summarized several of the main challenges of the analysis.

CRediT authorship contribution statement

F. Zeiser: Conceptualization, Software, Methodology, Validation, Writing - original draft, Visualization, Formal analysis, Investigation, Data curation, Writing - review & editing. **G.M. Tveten:** Conceptualization, Software, Methodology, Writing - review & editing. **F.L. Bello Garrote:** Formal analysis, Investigation, Writing - review & editing. **M. Guttormsen:** Data curation, Writing - review & editing. **A.C. Larsen:** Writing - review & editing, Funding acquisition. **V.W. Ingeberg:** Data curation. **A. Görgen:** Funding acquisition. **S. Siem:** Funding acquisition.

Table A.1
Labeling of the detectors and the position of the detectors determined by the geometry of the frame. This labeling is used both in the Geant4 simulations and on the actual detector frame of OSCAR. The angles θ and ϕ specify the detector location in spherical coordinates, the distance can be varied by spacers.

Ring	Det. number	θ [deg]	ϕ [deg]
1	1	142.6	0.0
	2	142.6	72.0
	3	142.6	144.0
	4	142.6	216.0
	5	142.6	288.0
2	6	116.6	324.0
	8	116.6	36.0
	10	116.6	108.0
	12	116.6	180.0
	14	116.6	252.0
3	7	100.8	0.0
	9	100.8	72.0
	11	100.8	144.0
	13	100.8	216.0
	15	100.8	288.0
4	16	79.2	324.0
	18	79.2	36.0
	20	79.2	108.0
	22	79.2	180.0
	24	79.2	252.0
5	17	63.4	0.0
	19	63.4	72.0
	21	63.4	144.0
	23	63.4	216.0
	25	63.4	288.0
6	26	37.4	324.0
	27	37.4	36.0
	28	37.4	108.0
	29	37.4	180.0
	30	37.4	252.0

Declaration of competing interest

The authors declare that they have no known competing financial interests or personal relationships that could have appeared to influence the work reported in this paper.

Acknowledgments

The scientific advisory board of the OSCAR project, consisting of Franco Camera, David Jenkins and Pete Jones, have been important for the OSCAR project and we wish to thank them for their valuable advice. We would also like to thank Jan Mierzejewski and C3D for the mechanical design of the frame and Agnese Giaz for spending time transferring knowledge on $LaBr_3$(Ce) scintillator detectors to us at OCL. The fact that the INFN Milan lended us a Labrpro unit was a great help to the project. We would like to thank Kevin C.W. Li for his excellent comments on the Geant4 simulations, and Wanja Paulsen for providing the calibrated experimental ^{12}C spectrum. We wish to thank the OCL engineers, Jan C. Müller, Jon Wikne, Pawel A. Sobas and Victor Modamio for excellent experimental conditions for testing OSCAR. The OSCAR Array is financed by the Research Council of Norway under contract no. 245882. F. Z., V. W. I., A. G. and S. S. acknowledge funding from the Research Council of Norway under contract no. 263030, G. M. T acknowledges funding under contract no. 262952. A. C. L. acknowledges funding from the European Research Council through ERC-STG-2014 under grant agreement no. 637686, and support from the "ChETEC" COST Action (CA16117), supported by COST (European Cooperation in Science and Technology). The grid computations were performed on resources provided by UNINETT Sigma2 the National Infrastructure for High-Performance Computing and Data Storage in Norway.

Appendix. Tables

See Tables A.1 and A.2.

Table A.2
Full-energy peak efficiency fit coefficients, see Eq. (2) and their covariances. Note that the values are strongly correlated, thus the efficiency is better determined as it might seem from the quoted 1σ uncertainties for each parameter.

(a) Optimal parameters

	p_0	p_1	p_2
exp.	1.94(27)	0.75(85)	0.030(66)
sim.	3.0(21)	−1.11(65)	0.058(50)

(b) Covariances for fit to exp.

	p_0	p_1	p_2
p_0	7.2e+00	−2.3e+00	1.8e−01
p_1	−2.3e+00	7.1e−01	−5.6e−02
p_2	1.8e−01	−5.6e−02	4.4e−03

(c) Covariances for fit to sim.

	p_0	p_1	p_2
p_0	4.3e+00	−1.4e+00	1.0e−01
p_1	−1.4e+00	4.2e−01	−3.3e−02
p_2	1.0e−01	−3.3e−02	2.5e−03

References

[1] M. Guttormsen, T. Tveter, L. Bergholt, F. Ingebretsen, J. Rekstad, The unfolding of continuum γ-ray spectra, Nucl. Instrum. Methods Phys. Res. A 374 (3) (1996) 371–376, http://dx.doi.org/10.1016/0168-9002(96)00197-0.

[2] J. Rekstad, A. Henriquez, F. Ingebretsen, G. Midttun, B. Skaali, R. Øyan, J. Wikne, T. Engeland, T.F. Thorsteinsen, E. Hammaren, et al., A study of the nuclear structure at high energy and low spin, Phys. Scr. T5 (1983) 45–50, http://dx.doi.org/10.1088/0031-8949/1983/t5/007.

[3] A. Schiller, L. Bergholt, M. Guttormsen, E. Melby, J. Rekstad, S. Siem, Extraction of level density and γ strength function from primary γ spectra, Nucl. Instrum. Methods Phys. Res. A 447 (3) (2000) 498–511, http://dx.doi.org/10.1016/s0168-9002(99)01187-0.

[4] A.C. Larsen, M. Guttormsen, M. Krtička, E. Běták, A. Bürger, A. Görgen, H.T. Nyhus, J. Rekstad, A. Schiller, S. Siem, et al., Analysis of possible systematic errors in the Oslo method, Phys. Rev. C 83 (3) (2011) 034315, http://dx.doi.org/10.1103/physrevc.83.034315.

[5] V. Blobel, Unfolding, in: Data Analysis in High Energy Physics, Wiley-VCH Verlag GmbH & Co. KGaA, 2013, pp. 187–225, http://dx.doi.org/10.1002/9783527653416.ch6.

[6] G. Choudalakis, Fully Bayesian unfolding, 2012, arXiv:http://arxiv.org/abs/1201.4612v4.

[7] U. Agvaanluvsan, A. Schiller, J.A. Becker, L.A. Bernstein, P.E. Garrett, M. Guttormsen, G.E. Mitchell, J. Rekstad, S. Siem, A. Voinov, et al., Level densities and γ-ray strength functions in Yb 170 , 171 , 172, Phys. Rev. C 70 (5) (2004) http://dx.doi.org/10.1103/physrevc.70.054611.

[8] S. Riboldi, F. Camera, N. Blasi, S. Brambilla, C. Boiano, F.C. Crespi, A. Giaz, B. Million, R. Nicolini, L. Pellegri, O. Wieland, Active voltage divider for improved estimation of interacting radiation energy with photomultiplier tubes coupled to high light yield scintillators, in: 2011 IEEE Nuclear Science Symposium Conference Record, IEEE, 2011, http://dx.doi.org/10.1109/nssmic.2011.6154296.

[9] V.W. Ingeberg, et al., Characterization of the Oslo scintillator array OSCAR, 2020, Manuscript, in preparation.

[10] M. Guttormsen, A. Bürger, T. Hansen, N. Lietaer, The siri particle-telescope system, Nucl. Instrum. Methods Phys. Res. A 648 (1) (2011) 168–173, http://dx.doi.org/10.1016/j.nima.2011.05.055.

[11] T.G. Tornyi, A. Görgen, M. Guttormsen, A.C. Larsen, S. Siem, A. Krasznahorkay, L. Csige, A new fission-fragment detector to complement the CACTUS-SiRi setup at the Oslo Cyclotron Laboratory, Nucl. Instrum. Methods Phys. Res. A 738 (2014) 6–12, http://dx.doi.org/10.1016/j.nima.2013.12.005.

[12] F. Zeiser, G.M. Tveten, oslocyclotronlab/OCL_GEANT4: Geant4 model of OSCAR, 2020, http://dx.doi.org/10.5281/ZENODO.3997010, Zenodo, Version v2.0.0.

[13] M. Pinto, P. Gonçalves, GUIMesh: A tool to import STEP geometries into Geant4 via GDML, Comput. Phys. Comm. (2019) http://dx.doi.org/10.1016/j.cpc.2019.01.024.

[14] R. Brun, F. Rademakers, ROOT — An object oriented data analysis framework, Nucl. Instrum. Methods Phys. Res. A 389 (1–2) (1997) 81–86, http://dx.doi.org/10.1016/s0168-9002(97)00048-x.

[15] D. Radford, Notes on the use of the program gf3, 2020, https://radware.phy.ornl.gov/gf3/. (Accessed 30 July 2020).

[16] F. Zeiser, G.M. Tveten, Oslocyclotronlab/Ocl_Geant4: Geant4 model of oscar, 2018, http://dx.doi.org/10.5281/zenodo.1342610, Zenodo, Version v1.0.4.

[17] F. Zeiser, G.M. Tveten, F.L.B. Garrote, M. Guttormsen, A.C. Larsen, V.W. Ingeberg, A. Görgen, S. Siem, The energy response of the Oslo Scintillator Array OSCAR, version 1, arXiv:2008.06240v1.

[18] G. Gosta, N. Blasi, F. Camera, B. Million, A. Giaz, O. Wieland, F. Rossi, H. Utsunomiya, T. Ari-izumi, D. Takenaka, D. Filipescu, I. Gheorghe, Response function and linearity for high energy γ -rays in large volume LaBr 3 :Ce detectors, Nucl. Instrum. Methods Phys. Res. A 879 (2018) 92–100, http://dx.doi.org/10.1016/j.nima.2017.10.018.

Paper IV

Restricted spin-range correction in the Oslo method: The example of nuclear level density and γ-ray strength function from ^{239}Pu(d, pγ)^{240}Pu

Zeiser, F., Tveten, G. M., Potel, G., Larsen, A. C., Guttormsen, M., Laplace, T. A., Siem, S., Bleuel, D. L., Goldblum, B. L., Bernstein, L. A., Garrote, F. L. Bello, Campo, L. Crespo, Eriksen, T. K., Görgen, A., Hadynska-Klek, K., Ingeberg, V. W., Midtbø, J. E., Sahin, E., Tornyi, T., Voinov, A., Wiedeking, M., Wilson, J.

Published in *Physical Review C*, August 2019, Volume 100, Number 2, Article no. 024305 DOI: 10.1103/physrevc.100.024305.

IV

Restricted spin-range correction in the Oslo method: The example of nuclear level density and γ-ray strength function from ^{239}Pu$(d, p\gamma)^{240}$Pu

F. Zeiser,[1,*] G. M. Tveten,[1] G. Potel,[2] A. C. Larsen,[1] M. Guttormsen,[1] T. A. Laplace,[3] S. Siem,[1] D. L. Bleuel,[4] B. L. Goldblum,[3] L. A. Bernstein,[3] F. L. Bello Garrote,[1] L. Crespo Campo,[1] T. K. Eriksen,[1] A. Görgen,[1] K. Hadynska-Klek,[1] V. W. Ingeberg,[1] J. E. Midtbø,[1] E. Sahin,[1] T. Tornyi,[1] A. Voinov,[5] M. Wiedeking,[6] and J. Wilson[7]

[1]*Department of Physics, University of Oslo, N-0316 Oslo, Norway*
[2]*Facility for Rare Isotope Beams, Michigan State University, East Lansing, Michigan 48824, USA*
[3]*Department of Nuclear Engineering, University of California, Berkeley, California 94720, USA*
[4]*Lawrence Livermore National Laboratory, Livermore, California 94551, USA*
[5]*Department of Physics and Astronomy, Ohio University, Athens, Ohio 45701, USA*
[6]*iThemba LABS, P.O. Box 722, Somerset West 7129, South Africa*
[7]*Institut de Physique Nucléaire d'Orsay, CNRS/Université Paris-Sud, Université Paris Saclay, 91406 Orsay Cedex, France*

(Received 8 April 2019; revised manuscript received 21 June 2019; published 5 August 2019)

The Oslo method has been applied to particle-γ coincidences following the ^{239}Pu(d, p) reaction to obtain the nuclear level density (NLD) and γ-ray strength function (γSF) of ^{240}Pu. The experiment was conducted with a 12 MeV deuteron beam at the Oslo Cyclotron Laboratory. The low spin transfer of this reaction leads to a spin-parity mismatch between populated and intrinsic levels. This is a challenge for the Oslo method as it can have a significant impact on the extracted NLD and γSF. We have developed an iterative approach to ensure consistent results even for cases with a large spin-parity mismatch, in which we couple Green's function transfer calculations of the spin-parity dependent population cross-section to the nuclear decay code RAINIER. The resulting γSF shows a pronounced enhancement between 2–4 MeV that is consistent with the location of the low-energy orbital $M1$ scissors mode.

DOI: 10.1103/PhysRevC.100.024305

I. INTRODUCTION

Accurate knowledge of neutron induced cross sections on actinides is important for many applications. From thermal energies up to several MeVs, there is a considerable competition between fission and neutron absorption. This competition, as well as several other factors like the lack of a monoenergetic neutron source in this energy range and the lifetime of short-lived isotopes, pose a challenge for direct cross-section measurements.

Most designs for next generation nuclear reactors are based on fast-neutron induced fission [1]. Therefore, knowledge of the cross sections for a wider range of incident neutron energies E_n have become important. In particular, more precise measurements of the ^{239}Pu(n, γ) cross section below $E_n \approx$ 1.5 MeV are listed as a high priority request by the Nuclear Energy Agency (NEA) [2]. Calculations for E_n above the resonance region (i.e., above $\approx$10 keV) can be obtained within the statistical Hauser-Feshbach framework [3] and require knowledge of the nuclear level density (NLD) and γ-ray strength function (γSF) of the residual nucleus ^{240}Pu. Furthermore, a better knowledge of NLDs and γSFs in the actinide region has the potential to improve the nuclear-physics related uncertainties introduced to abundance calculations of heavy-element production in extreme astrophysical environments [4].

The Oslo method [5,6] can be used on particle-γ coincidence spectra from transfer reactions to simultaneously extract the NLD and γSF below the neutron separation energy S_n. In a campaign to study actinide nuclei, the method has been applied to the compound nuclei $^{231-233}$Th, ^{232,233}Pa, $^{237-239}$U, ^{238}Np [7–10], and ^{243}Pu [11] using different light-ion reactions. So far, all observed NLDs are consistent with a constant temperature [12] level density formula. The γSF of these heavy and well-deformed systems show a pronounced enhancement between about 2–4 MeV, which is in the energy range [13] of a low-energy orbital $M1$ scissors resonance (SR).

The nuclear data community has recently started to take into account these strong $M1$ SRs, and in two recent studies by Ullmann *et al.* [14,15], a significant impact of the SR on the cross sections calculated for uranium isotopes has been shown. An extraction of the NLD and γSF of ^{240}Pu will facilitate similar calculations for ^{239}Pu(n, γ). They can be validated by comparison to updated direct measurement by Mosby *et al.* [16] between 10 eV and 1.3 MeV.

Larsen *et al.* [6] have shown that the population of a limited spin range make it necessary to correct the slopes of γSFs extracted with the Oslo method. In the previous experimental studies on actinides [7–11], first indications of the impact of a low spin transfer using the (d, p) reaction mechanism were observed and an improvised procedure for the correction was

*fabio.zeiser@fys.uio.no

developed. More recently, we have presented a systematic analysis of the effect of a realistic spin distribution on both the NLD and γSF for the ^{239}Pu$(n,\gamma)^{240}$Pu reaction [17].

In this article, we will present the NLD and γSF of ^{240}Pu analyzed with the Oslo method. We develop an iterative procedure to correct for the bias introduced in the Oslo method for (d,p) reactions on heavy nuclei due to a spin-parity population mismatch.

II. EXPERIMENTAL METHODS AND DATA ANALYSIS

The ^{239}Pu$(d,p)^{240}$Pu experiment was conducted using a 12 MeV deuteron beam extracted from the MC-35 Scanditronix Cyclotron at the Oslo Cyclotron Laboratory (OCL). The 0.4 mg/cm^2 thick ^{239}Pu target was purified by an anion-exchange resin column procedure [18] prior to electroplating it onto a 2.3 mg/cm^2 beryllium backing. A γ-ray assay of the resulting target revealed the ^{239}Pu purity to be $>99.9\%$.

Particle-γ coincidences were measured with the SiRi particle telescopes [19] and CACTUS γ-ray detector array [20]. SiRi consists of 64 silicon particle telescopes with a thickness of 130 μm for the front (ΔE) and 1550 μm for the back (E) detectors. In this experiment they were placed in a backward position with respect to the beam direction, covering azimuthal angles from 126° to 140°. Compared to the forward direction, this configuration reduces the contribution of elastically scattered deuterons and populates a broader and higher spin-range. The CACTUS array was composed of 26 lead collimated 5 in. $\times$ 5 in. NaI(Tl) crystals with a total efficiency of 14.1(2)% at $E_\gamma = 1.33$ MeV (measured with a ^{60}Co source) that surrounded the target chamber and the particle telescopes. Additionally, four parallel plate avalanche counters (PPAC) [21] were used to detect fission events. The back detectors of SiRi were used as master gates for a time-to-digital converter (TDC). The NaI(Tl) detectors were delayed by $\approx$400 ns and individually served as stop signals. The signals were processed by a leading edge discriminator and the resulting time walk was corrected for by the procedure given in Ref. [19]. The prompt particle-γ coincidences were sorted event-by-event from a 28 ns wide time-window and the background from random coincidences was subtracted. The amount of deposited energy depends on the outgoing particle type, which facilitated the selection of (d,p) events by setting proper gates in a ΔE-E matrix. The spectra were calibrated using reaction kinematics, which also allowed translation of the deposited particle energy to the initial excitation energy E_x of the residual nucleus ^{240}Pu. The γ-ray spectra for each excitation energy E_x were unfolded following the procedure of Ref. [22], however using new response functions measured in 2012 [23]. In this work we used the Oslo method software v1.1.2 [24].

To select the γ decay channel, only excitation energies E_x below the neutron separation energy ($S_n = 6.534$ MeV [25]) were considered. The energy range was further constrained by pile-up of γ rays and the onset of fission events at $E_x \approx 4.5$ MeV. The latter was previously identified as sub-barrier fission [26,27]. A more detailed analysis of the prompt fission γ rays can be found in Ref. [28]. The final extraction regions were $E_\gamma^{\min} = 1.2$ MeV, $E_x^{\min} = 2.5$ MeV, $E_x^{\max} = 4.0$ MeV.

We applied an iterative subtraction technique to obtain the energy spectrum of the primary (also called first generation) γ rays from the initial spectrum, which includes all γ decay cascades. The principal assumption of the first-generation method [29] is that the γ decay from any excited state is independent of its formation. The branching ratio is an inherent property of a state. Thus, the assumption is automatically fulfilled if levels have the same probability to be populated by the decay of higher-lying states as directly by nuclear reactions [e.g., via the (d,p) reaction]. As we consider the quasicontinuum, we can relax the strict conditions and apply statistical considerations so we only require that in a given excitation energy bin all levels with the same spin-parity are populated approximately equally (instead of specific states). In addition, the population probability of levels with a given spin-parity should be approximately constant as a function of the excitation energy. In Sec. V we will show that this condition is not satisfied and we propose a procedure to minimize the impact of the violation of this assumption. For a thorough discussion of other possible errors and uncertainties

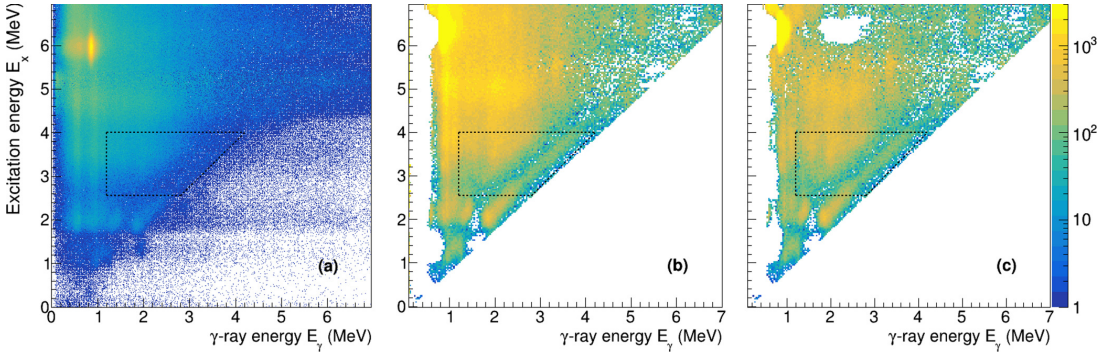

FIG. 1. The raw particle-γ coincidences for ^{240}Pu (a), the unfolded spectra (b), and the extracted primary-γ rays (c). The dotted lines display the region used for the extraction of the NLD and γSF. Before unfolding, all events with $E_\gamma > E_x + \delta E_\gamma$ have been removed as they only represent noise, where δE_γ is the detector resolution.

TABLE I. Parameters used to extract the initial level density and γ-strength function (see text).

S_n [MeV]	a [MeV^{-1}]	E_1 [MeV]	$\sigma(S_n)$	D_0 [eV]	$\rho(S_n)$ [10^6 MeV^{-1}]	$T_{\rm CT}$ [MeV]	$\langle\Gamma_\gamma(S_n)\rangle$ [MeV]
6.53420(23)[a]	25.16(20)[b]	0.12(8)[b]	8.43(80)[d]	2.20(9)[c]	32.7(66)	0.415(10)	43(4)[c]

[a]Reference [25]; [b]Reference [39]; [c]Reference [38]; [d]Assuming a 10% uncertainty.

in this method, see Ref. [6]. The coincidence matrices are displayed in Fig. 1.

III. EXTRACTION OF NLD AND γSF

According to Fermi's golden rule, the decay rate from an initial state to a final state can be decomposed into the transition matrix element and the level density $\rho(E_{\rm f})$ at the final state $E_{\rm f} = E_i - E_\gamma$ [30,31]. In the regime of statistical γ rays, we consider ensembles of initial and final states, thus probing decay properties averaged over many levels. We assume that any decay mode can be build on the ground and excited state in the same way, i.e., there is no spin-parity or excitation energy dependence, which is a generalized version of the Brink-Axel hypothesis [32,33]. Thus, the decay properties do not depend on the specific levels, but only on the energy difference between them. Consequently, the dependence on initial and final states is reduced to a single dependence on the energy difference given by the γ-ray energy E_γ. The decay probability corresponding to the first-generation matrix $P(E_i, E_\gamma)$ can therefore be factorized into the level density of the final excitation energy $\rho(E_{\rm f})$ and the transmission coefficient $\mathcal{T}(E_\gamma)$ [5]:

$$P(E_i, E_\gamma) \propto \rho(E_{\rm f})\mathcal{T}(E_\gamma). \tag{1}$$

The validity of the Brink-Axel hypothesis in the quasicontinuum has recently been shown for several nuclei [34,35], amongst them the actinide nucleus ^{238}Np [36]. The level density $\rho(E_{\rm f})$ and transmission coefficient $\mathcal{T}(E_\gamma)$ were obtained by a fit to $P(E_i, E_\gamma)$ [5]. Note that this procedure does not require any initial assumptions on the functional form of ρ and $\mathcal{T}$. However, any transformation $\tilde{\rho}$ and $\tilde{\mathcal{T}}$ with the parameters α, A, and B gives identical fits to the matrix $P(E_i, E_\gamma)$ [5]:

$$\tilde{\rho}(E_i - E_\gamma) = A\exp[\alpha\,(E_i - E_\gamma)]\,\rho(E_i - E_\gamma), \tag{2}$$

$$\tilde{\mathcal{T}}(E_\gamma) = B\exp[\alpha\,E_\gamma]\,\mathcal{T}(E_\gamma). \tag{3}$$

The determination of the transformation parameters corresponding to the correct physical solution, i.e., the normalization of the NLD and γSF, is discussed in the next section.

IV. INITIAL EXTRACTION OF THE LEVEL DENSITY AND TRANSMISSION COEFFICIENT

For the normalization of the level density, ρ, we need at least two reference points, such that we can determine the parameters A and α in Eq. (2). At low excitation energies, our data are matched to discrete levels [37] up to the critical energy $E_{\rm crit} \approx 1.3$ MeV, where we expect the low-lying level scheme to be complete. At the neutron separation energy S_n, we calculate $\rho(S_n)$ under the assumption of equal parity distribution from the average neutron resonance spacing for s waves, D_0, taken from RIPL-3 [38] following Ref. [5]:

$$\rho(S_n) = \frac{2\sigma^2}{D_0}\frac{1}{(J_t+1)\exp[-(J_t+1)^2/2\sigma^2] + J_t\exp\left[-J_t^2/2\sigma^2\right]}. \tag{4}$$

Here, J_t is the ground-state spin of the target nucleus ^{239}Pu.

We use the spin distribution $g(E_x, I)$ proposed by Ericson [12, Eq. (3.29)][1] together with the rigid-body moment of inertia approach for the spin cut-off parameter σ from 2005 by von Egidy and Bucurescu [39]:

$$g(E_x, I) = \frac{2I+1}{2\sigma^2(E_x)}\exp[-(I+1/2)^2/2\sigma^2], \tag{5}$$

$$\sigma^2(E_x) = 0.0146A^{2/3}\frac{1+\sqrt{4aU(E_x)}}{2a}, \tag{6}$$

where A is the mass number of the nucleus, a is the level density parameter, $U(E_x) = E_x - E_1$ is the intrinsic excitation energy, and E_1 is the back-shift parameter. All parameters are listed in Table I.

Since there is a gap of approximately 3.5 MeV between the highest excitation energy of the extracted level densities and the neutron separation energy S_n, an interpolation is used to connect the data sets. In accordance with the findings for other actinides [8], we use the constant temperature (CT) level density formula [12]

$$\rho_{\rm CT}(E_x) = \frac{1}{T_{\rm CT}}\exp\frac{E_x - E_0}{T_{\rm CT}} \tag{7}$$

with the shift in excitation energy E_0 given by

$$E_0 = S_n - T_{\rm CT}\ln[\rho(S_n)T_{\rm CT}]. \tag{8}$$

The best fit is obtained for a constant temperature of $T_{\rm CT} = 0.415(10)$ MeV. Only a limited number of data points are available for the fit which are well above $E_{\rm crit}$. This makes a proper interpretation of the uncertainty on the fit parameters difficult. This is the main contribution to the systematic error, which is shown as an error band in the results in Fig. 2.

For the transmission coefficient $\mathcal{T}$, the remaining parameter B is determined by normalization to the average total radiative width $\langle\Gamma_\gamma(S_n)\rangle$ from (n, γ) experiments [38], under

[1]The same spin distribution is often attributed to the subsequent work of Gilbert and Cameron [40].

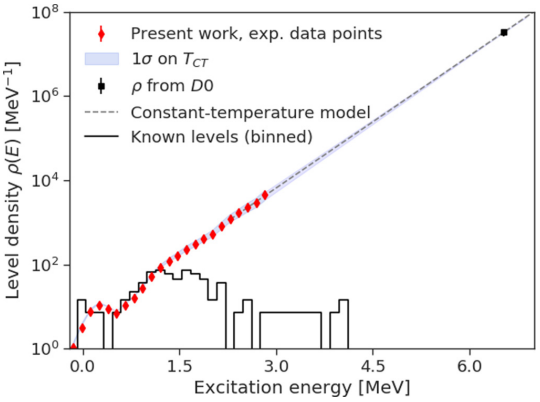

FIG. 2. Initial analysis of the total NLD for ^{240}Pu. The NLD is normalized to the discrete levels (in 140 keV bins) [37] at low excitation energies and to $\rho(S_n)$ calculated from D_0 [38], using a constant temperature interpolation with $T_{\rm CT} = 0.415(10)$.

the assumption of equal parity using [41,42]

$$\langle \Gamma_\gamma(S_n, J_t \pm 1/2, \pi_t)\rangle = \frac{B}{4\pi\,\rho(S_n, J_t \pm 1/2, \pi_t)} \int_0^{S_n} dE_\gamma\, \mathscr{T}(E_\gamma)\rho(S_n - E_\gamma) \times \sum_{j=-1}^{1} g(S_n - E_\gamma, J_t \pm 1/2 + j), \quad (9)$$

where π_t is the ground-state parity of the target nucleus ^{239}Pu. Note that the sum in Eq. (9) runs over all available final states of ^{240}Pu, where we consider only spins $J_t \pm 1/2 + j$ that can be reached by one primary dipole transition after neutron capture, i.e., $j = -1, 0, 1$. The γ-ray strength function f is obtained under the same assumption of a dominance of dipole strength, L=1, so $f \simeq f_{E1} + f_{M1}$, and

$$f(E_\gamma) = \frac{\mathscr{T}(E_\gamma)}{2\pi E^{2L+1}} \simeq \frac{\mathscr{T}(E_\gamma)}{2\pi E_\gamma^3}. \quad (10)$$

To specify the integral in Eq. (9) completely, we use a log-linear extrapolation in the γSF below $E_\gamma^{\rm min}$ and a log-linear extrapolation in $\mathscr{T}$ between $E_\gamma^{\rm max}$ and S_n.

V. CORRECTIONS DUE TO SPIN-PARITY MISMATCH

A. Overview

First indications that a limited spin-range of the levels populated in a given reaction has an impact on the Oslo method have been discussed in Ref. [6]. Due to the low angular momentum transfer expected for light-ion reactions, and in particular the (d, p) transfer reaction, the higher spin states that are already available at $E_x \approx 2$ to 6 MeV in heavy nuclei may not be populated. In Ref. [7] an ad hoc method was developed to correct for observations that were attributed to the limited angular momentum transfer. This correction has subsequently been applied to other heavy nuclei [8–11,43]. In a recent analysis on systematic errors for $(d, p)^{240}$Pu we have demonstrated that the application of the Oslo method produces consistent results when the spin-parity dependent population probability $g_{\rm pop}$ equals the theoretically expected distribution of the intrinsic levels $g_{\rm int}$. However, when there is a large mismatch in the spin-parity distributions we have also shown that the aforementioned ad-hoc method lead to significant distortions in the NLD and γSF [17]. We will denote the extracted quantities as the *apparent* NLD and γSF, and distinguish them from the *true* NLD and γSF that would have been observed with an ideal, bias-free method. In absence of an ideal method, our goal is to find a consistent set of NLD and γSF, where we define consistency as follows: if we provide this set as input to a nuclear decay code like RAINIER [44], the generated synthetic data should match the experimentally obtained coincidences. This grantees at the same time that the analysis of the synthetic data yields the same *apparent* NLD and γSF as those determined from the *naive*[2] experimental analysis. In this section we extend the analysis of Ref. [17] in order to retrieve a consistent set of NLD and γSF for ^{240}Pu for the same reaction. This approach is, however, easily generalizable to other target nuclei and in principle also applicable for other light-ion reactions.

We will start with a brief overview of the procedure and then discuss each step in more detail:

(1) Calculate the spin-parity distribution of the population probability $g_{\rm pop}$, and the distribution of the intrinsic levels $g_{\rm int}$ for each excitation energy bin E_x.
(2) Generate a synthetic coincidence data set for an artificial nucleus resembling ^{240}Pu, given the spin distributions, and the trial NLD and γSF.
(3) Analyze and compare the *apparent* NLD and γSF from the synthetic data set and experimental coincidences using the Oslo method.
(4) Adjust the trial NLD and γSF and repeat steps 2 and 3. Adopt the solution with the smallest difference between experimental and synthetic coincidence spectra.

B. Spin-parity calculations

To calculate the population probability $g_{\rm pop}$ for each J^π in the residual nucleus following a (d, p) reaction, we have to distinguish between two reaction mechanisms. First, we consider direct processes, i.e., the breakup of a deuteron with emission of a proton, followed by the formation of a compound nucleus with the remaining neutron and the target. Spin-parity dependent cross section are calculated for the angles covered in the experiment within the Green's function transfer formalism described in Refs. [45,46]. The neutron-nucleus interactions are modeled by the dispersive optical model potential (OMP) of Capote *et al.* [47] implemented through potential no. 2408 listed in RIPL-3 [38]. The usage of a dispersive OMP improves the predictive power for $E_x < S_n$. Note that we did not use the OMP in the context of full coupled-channels calculations, which would have explicitly accounted for the coupling to rotational states. We expect that

[2]In the sense that the experimental analysis does not inherently take into account a spin-parity mismatch.

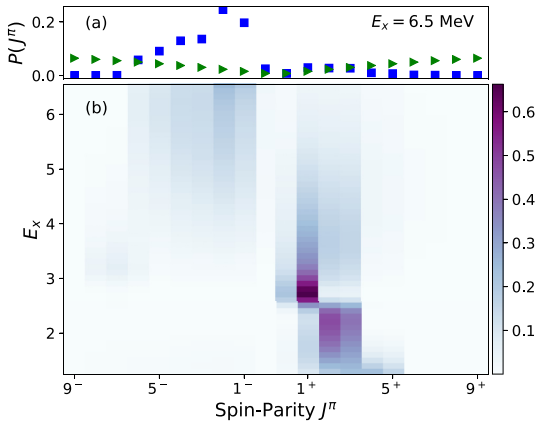

FIG. 3. Population probability $g_{\rm pop}(E_x, J, \pi)$ of levels in the ^{239}Pu$(d, p)^{240}$Pu reaction as a function of excitation energy E_x, and spin-parity J^π. (a) Projection of $g_{\rm pop}(E_x)$ (blue squares) for the highest excitation energy, $E_x = 6.5$ MeV, which reveals a strong asymmetry in the populated parities. We observe that $g_{\rm int}$ (green triangles) is much broader then $g_{\rm pop}$ (blue squares). Note that the distributions are normalized to 1 summing over all J^π in each E_x bin, but the plot ranges only between $J^\pi = 9^\pm$.

this will lead to an underestimation of the absorption cross section of about 20%; however the relative population of the different spins and parities should essentially be unaffected. We normalize the population cross sections to 1 for each E_x bin, thus obtaining the probability distribution $g_{\rm pop}$. Figure 3 shows the results for the population spin-parity distribution $g_{\rm pop}(E_x, J, \pi)$.

Compound reactions are the second mechanism leading to ^{240}Pu as a residual nucleus: proton evaporation after fusion of the deuteron and target nucleus and the inelastic excitation of the target to energies above the proton emission threshold. The spin-parity integrated cross section for these processes has been estimated to be ≈0.5 mb/(MeV sr) using the statistical framework of the TALYS nuclear reactions code v1.8 [48]. This is an order of magnitude smaller than for the direct process and therefore neglected. The low cross sections are reasonable as the deuteron beam energy of 12 MeV is below the Coulomb barrier of about 14.46 MeV, where the latter is calculated with a radius parameter $r_0 = 1.26$ fm [49].

C. Synthetic data

To study the effect on the extracted NLD and γSF, we generate a synthetic data set with the statistical nuclear decay code RAINIER v1.4.1 [44,50]. This code uses a Monte Carlo approach to generate levels of an artificial nucleus and simulate γ-emission cascades via $E1$, $M1$, or $E2$ transitions. The analysis library facilitates the extraction of the γ-ray spectra (first or all generations) emitted from each initial excitation energy bin E_x. The matrix including the γ-ray spectra of all generations substitutes for the experimental particle-γ coincidence in the further analysis. The input parameters have been chosen to resemble the ^{240}Pu nucleus and the analysis in the previous section. The initial settings are summarized below, and a comprehensive list including the analysis code can be found online:[3]

(i) Discrete levels up to 1.037 MeV (18 levels).
(ii) Above 1.037 MeV: Generated levels from the NLD extracted in Sec. IV with the nearest-neighbor spacing according to the Wigner distribution [51].
(iii) Intrinsic spin distribution $g_{\rm int}(E_x, J)$ following Eq. (5), with a spin-cut parameter σ of Eq. (6) (assumes equiparity).
(iv) Spin-parity dependent population probabilities $g_{\rm pop}(J, \pi)$ from our calculations.[4]
(v) γSF as extracted in Sec. IV, fitted by two $E1$ constant temperature Generalized Lorentzians (GLO) [42], two $M1$ Standard Lorentzians (SLO), and including Porter-Thomas fluctuations [52]. The $E2$ component was assumed to be negligible.
(vi) Internal conversion model: BrIcc frozen orbital approximation [53].

Due to the strong parity dependence of $g_{\rm pop}$, the generated simulated coincidence spectra depend on the decomposition of the γSF into its $E1$ and $M1$ components. We performed a χ^2 fit of the centroid, the peak cross section and width of each resonance of the γSF simultaneously using the differential evolution algorithm by Storn and Price [54]. In addition to our data $\boldsymbol{Y}_{\rm sum}$, which measures only the summed γSF $(M1 + E1)$, we include the data $\boldsymbol{Y}_{E1/M1}$ of Kopecky *et al.* [55,56] around S_n, which resolve the $E1$ and $M1$ components. There are no measurements for the giant dipole resonance (GDR) of ^{240}Pu. However, as the GDR is expected to vary little between the plutonium isotopes, we also include ^{239}Pu$(\gamma, {\rm abs})$ measurements (again included in $\boldsymbol{Y}_{\rm sum}$) by De Moraes and Cesar [57] and Gurevich *et al.* [58]. A third data set by Berman *et al.* [59] yields systematically lower cross sections than the first two measurements, which are consistent within the error-bars. Therefore we did not include the data of Berman *et al.* [59] in the fit. Each term is weighted by the experimental uncertainty of the datapoint. The total χ^2 is then given as the sum over the χ^2s for the summing data $\boldsymbol{Y}_{\rm sum}$ $(E1 + M1)$ and data $\boldsymbol{Y}_{E1/M1}$ that resolve the $M1$ and $E1$ contributions:

$$\chi^2 = \sum_{i \in \boldsymbol{Y}_{\rm sum}} \chi^2_{\rm sum} + \sum_{i \in \boldsymbol{Y}_{E1}} \chi^2_{E1} + \sum_{i \in \boldsymbol{Y}_{M1}} \chi^2_{M1}. \qquad (11)$$

D. Analysis of an iteration

The generated coincidence data are analyzed with the Oslo method and the results are displayed in Fig. 4. We can quantify how consistent the input NLD and γSF are by construction of the ratio r of the apparent NLD and γSF analyzed from synthetic data to the experimental analysis (see Sec. IV). We extract this ratio for each iteration. For the NLD this means that below 3 MeV we compare to the data points, whereas

[3] https://github.com/fzeiser/240Pu_article_supplement.

[4] Note that we did not include the excitation energy dependence of the population cross-section for this analysis, although it could in principle be included to give a more stringent test of the first generation method.

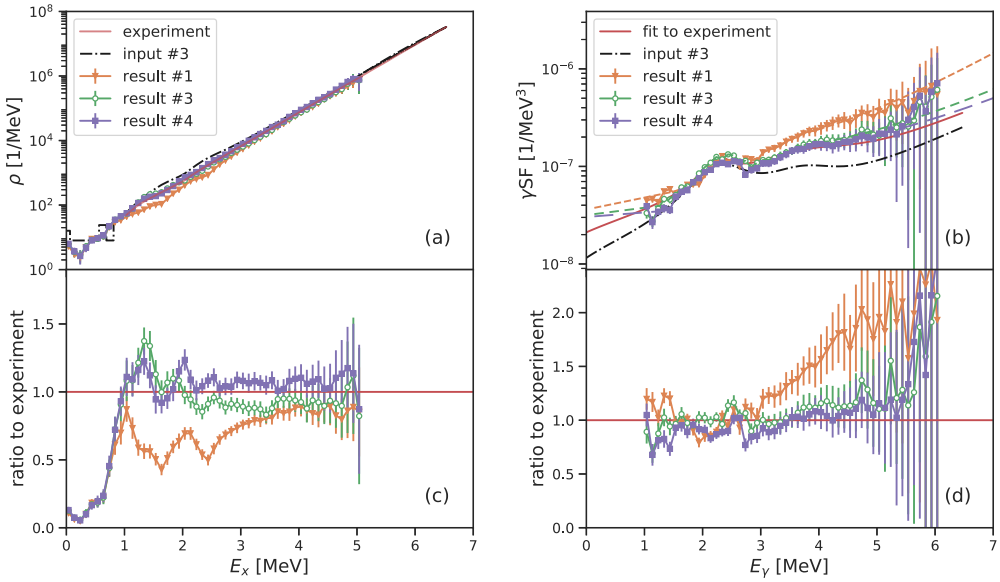

FIG. 4. Upper panels: NLD (a) and γSF (b) extracted with the Oslo method from synthetic data (iterations 1, 3, and 4) compared to those extracted from the experimental coincidence data in Sec. IV. The γSFs are compared to the fit of the experimental data points. As a guide to the eye, the data are connected by solid lines and dashed lines denote the extrapolations assumed for the Oslo method. Lower panels: Ratios of the NLD (c) and γSF (d) extracted from synthetic data to those from the experimental coincidence data. The error bars are a combination of statistical and proposed systematic error (mostly due to potential nonstatistical decay at high E_γ) as retrieved from the Oslo method when analyzing the synthetic data. Note that the analysis of synthetic data created from iteration 3 (input is displayed) results in a NLD and γSF that closely resemble the experimental analysis.

above 3 MeV we use the CT extrapolation. In case of the γSF, we compare to its fit, so the sum of the 2 GLOs and 2 SLOs. The inverse of the ratio r is used as a bin-by-bin correction $z = (1/r) - 1$ to the input NLD and γSF of iteration n, such that we generate the input for the next iteration, $n + 1$:

$$I_{n+1} = I_n\left(1 + \frac{1}{2}z\right), \tag{12}$$

where I is the input NLD or γSF, respectively. We introduced an additional factor of $1/2$, which can be seen as reduction of the step-size of the correction z. This increased the stability of the solution. As an example, looking at the first iteration, we find that the analyzed NLD from the synthetic data at 2.5 MeV is only 50% of the experimentally observed NLD. We would therefore increase the input NLD for the next iteration by 25% in this bin (and process all other bins of the NLD and γSF in the same manner). For the first iterations we observe that the changes impact $\langle\Gamma_\gamma\rangle$ by about 25%. As $\langle\Gamma_\gamma\rangle_{\rm exp}$ is determined from independent measurements, we enforce a match by rescaling the predicted input γSF. Note that this does not affect the generated coincidence spectra.

E. Results

After only 3 to 4 iterations, we observe that the γSF and NLD have approximate converged, with the exception of the higher energy region of the γSF. The reproduction of the γSF above $E_\gamma^{\rm max} = 4.0$ MeV remains challenging. The corresponding fit region in the first-generation matrix is formed by non-statistical decays, thus it is not obvious that the Oslo method should be applicable in this regime. In addition, the comparison in this regime is sensitive to the choice of the extrapolation of the initial γSF.

In Fig. 5 we compare the experimental coincidence data with the synthetic data from different iterations. All spectra have been normalized to obtain the probability $P(E_\gamma)$ for the emission of a γ ray with energy E_γ in the decay cascade from a level in the excitation energy bin E_x. This removes any dependence on the simulated vs. measured number of γ rays and of a potential mismatch of the population cross section as a function of the excitation energy E_x. The χ^2 differences over whole extraction region (see Sec. II) are displayed for each iteration in Fig. 6. We find that iteration 3 improves the reproduction of the experimental coincidence spectra by about 50%, compared to the initial analysis, iteration 1. Higher iterations give a reasonable reproduction of the first generation spectra, but show an increased deviation of the (all generations) coincidence spectra. This might be explained by an overcompensation for $E_\gamma > 4$ MeV as discussed above. Additionally, a closer analysis of the first vs. all generations spectra indicate a too high probability to decay through a specific state, or set of states, with $E_x \approx 1.3$ MeV. This is already visible for iteration 3 in Fig. 5, but the mismatch increases for the higher iterations.

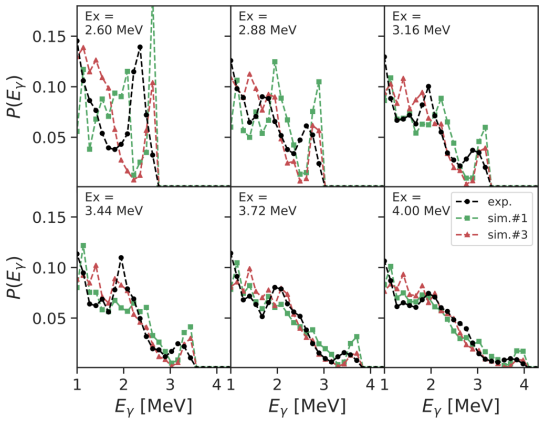

FIG. 5. Comparison of experimental coincidence data with the synthetic data from iterations 1 and 3. In general, the results of iteration 3 match the data quite well, but they fail to reproduce the spectra for the lowest excitation energy bin. The comparison region was chosen in accordance with the extraction region specified in Sec. II.

In the described procedure, we used a Monte Carlo approach to simulate the nucleus and its behavior, therefore, the results may vary between different realizations from the same input parameters. However, we found that in the case of a heavy nucleus the level density was so high that the effects could be neglected for this analysis.

VI. DISCUSSION

As noted in Ref. [17], the Oslo method does not intrinsically account for differences in the spin-parity distributions g_{pop} and g_{int}; when there is a significant spin-parity mismatch the resulting *apparent* NLD and γSF will be distorted compared to the *a priori true* NLD and γSF. This effect can be observed in Fig. 4 by comparing the input for iteration

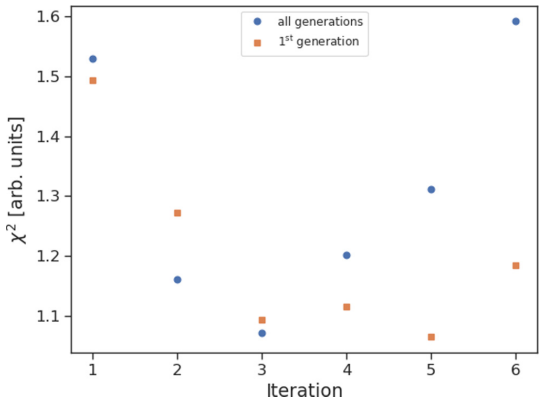

FIG. 6. χ^2 between the synthetic and experimental coincidence and first generation data for each iteration.

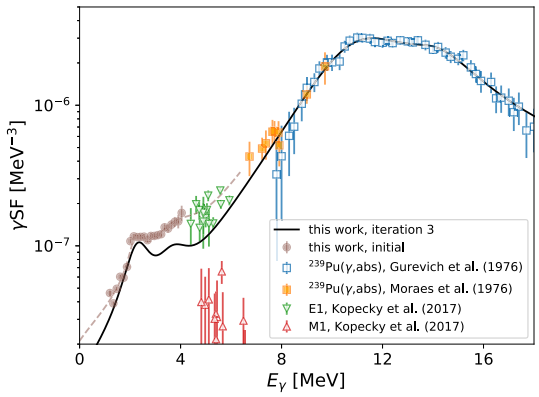

FIG. 7. Proposed γSF (iteration 3) compared to the initial analysis (see Sec. IV) and measurements by Kopecky *et al.* [55,56], De Moraes and Cesar [57], and Gurevich *et al.* [58].

3 to RAINIER to the results after application of the Oslo method. The presented method takes into account g_{pop} and g_{int} and generates synthetic coincidence data sets. As the *apparent* NLD and γSF extracted with the Oslo method from synthetic and experimental coincidences data suffer the same distortions, we can identify a consistent set of NLD and γSF from those simulations that lead to an *apparent* NLD and γSF that match the results from the experimentally obtained coincidences (Sec. IV). In Fig. 4 it can be observed that this is the case for the input NLD and γSF to the third iteration. Future studies are recommended to establish the sensitivity of the current approach. It is, for example, possible to find other suitable decompositions and other empirical models to describe the γSF in the fitting procedure in Sec. V. This would effect the γSF and NLD derived from this method. Ideally, one could couple the RAINIER simulations with a Monte Carlo Markov chain code [60,61] directly (without iterating through the Oslo method) and find the posterior probability of different NLD and γSF combinations to match the experimental observations. However, for a heavy nucleus such as ^{240}Pu each iteration takes about 50 h on a single core Intel E5-2683v4 2.1 GHz, such that the computational costs quickly render a full-scale parameter search unfeasible.

In Fig. 7, we compare the input γSF of the third iteration to the result of the initial analysis (see Sec. IV) and the measurements of Kopecky *et al.* [55], De Moraes and Cesar [57], and Gurevich *et al.* [58]. The absolute scale of the proposed γSF is lower than in the initial analysis, which is attributed to the increased NLD (see Fig. 4, left panels), as can be seen from Eq. (9).

Around 6 MeV, the derived γSF is significantly lower than the measurements by Kopecky *et al.* [55,56]. However, there are two ways to resolve the apparent discrepancy: First, according to the original analysis [56], the data of Kopecky *et al.* [55,56] have a systematic normalization uncertainty of 30% (only the statistical errors are plotted). Second, our results have little sensitivity to the γSF above approximately 4 MeV. Thus, we could add another resonance at ≈6–8 MeV

without changing any other observables, like the shape of the extracted γSF or $\langle\Gamma_\gamma\rangle$.

The retrieved γSF reveals an excess strength between 2–4 MeV on the hypothetically smooth tail of the GDR. This is consistent with the location of the low-energy orbital $M1$ SR [13]. Several other studies in the actinide region using (d, p) reactions and the Oslo method have observed a similar excess [7–11]. However, we expect that the spin-parity distributions may also have biased the NLD and γSF obtained in those experiments, and therefore plan to reanalyze the extracted strength with the present method.

VII. CONCLUSIONS

We have developed an iterative procedure to correct for the bias introduced in the Oslo method when the spin-parity dependent population probability $g_{\rm pop}$ differs significantly from the spin-parity distribution of the intrinsic levels $g_{\rm int}$. We have calculated $g_{\rm pop}$ for the ^{239}Pu$(d, p)^{240}$Pu experiment performed at the OCL within the Green's function transfer formalism. Using the nuclear decay code RAINIER, we have simultaneously retrieved a NLD and γSF of ^{240}Pu which are consistent with the experimental analysis. The γSF reveals excess strength between 2–4 MeV, which can be identified as the orbital $M1$ SR. The results have been compared to other measurements and the origin of the differences has been addressed.

ACKNOWLEDGMENTS

We would like to thank J. C. Müller, E. A. Olsen, A. Semchenkov, and J. C. Wikne at the Oslo Cyclotron Laboratory for providing the stable and high-quality deuteron beam during the experiment. We are indebted to R. Capote for discussions on the implementation of the OMP and L. E. Kirsch for his help explaining and extending the of capabilities of RAINIER. This work was supported by the Research Council of Norway under project Grants No. 263030 and No. 262952, and by the National Research Foundation of South Africa. A.C.L. gratefully acknowledges funding from the European Research Council, ERC-STG-2014 Grant Agreement No. 637686. We gratefully acknowledge support of the US Department of Energy by Lawrence Livermore National Laboratory under Contract No. DE-AC52-07NA27344 and by the Lawrence Berkeley National Laboratory under Contract No. DE-AC02-05CH11231. This work was supported by the US Department of Energy (DOE), National Nuclear Security Administration (NNSA) under Awards No. DE-NA0002905 and No. DE-NA0003180, the latter via the Office of Defense Nuclear Nonproliferation Research and Development (DNN R&D) through the Nuclear Science and Security Consortium. We acknowledge support by DOE Office of Science, Office of Nuclear Physics, under the FRIB Theory Alliance award no. DE-SC0013617. This work was supported by the National Research Foundation of South Africa Grant No. 118846.

[1] I. Pioro, in *Handbook of Generation {IV} Nuclear Reactors*, Woodhead Publishing Series in Energy, edited by I. L. Pioro (Woodhead Publishing, Cambridge, 2016), pp. 37–54.
[2] Nuclear data high priority request list of the nea (req. id: H.32), http://www.oecd-nea.org/dbdata/hprl/hprlview.pl?id=451.
[3] W. Hauser and H. Feshbach, Phys. Rev. **87**, 366 (1952).
[4] M. Arnould, S. Goriely, and K. Takahashi, Phys. Rep. **450**, 97 (2007).
[5] A. Schiller, L. Bergholt, M. Guttormsen, E. Melby, J. Rekstad, and S. Siem, Nucl. Instrum. Methods Phys. Res. A **447**, 498 (2000).
[6] A. C. Larsen, M. Guttormsen, M. Krtička, E. Běták, A. Bürger, A. Görgen, H. T. Nyhus, J. Rekstad, A. Schiller, S. Siem, H. K. Toft, G. M. Tveten, A. V. Voinov, and K. Wikan, Phys. Rev. C **83**, 034315 (2011).
[7] M. Guttormsen, L. A. Bernstein, A. Bürger, A. Görgen, F. Gunsing, T. W. Hagen, A. C. Larsen, T. Renstrøm, S. Siem, and M. Wiedeking, Phys. Rev. Lett. **109**, 162503 (2012).
[8] M. Guttormsen, B. Jurado, J. N. Wilson, M. Aiche, L. A. Bernstein, Q. Ducasse, F. Giacoppo, A. Görgen, F. Gunsing, T. W. Hagen, A. C. Larsen, M. Lebois, B. Leniau, T. Renstrom, S. J. Rose, S. Siem, T. Tornyi, G. M. Tveten, and M. Wiedeking, Phys. Rev. C **88**, 024307 (2013).
[9] M. Guttormsen, L. A. Bernstein, A. Görgen, B. Jurado, S. Siem, M. Aiche, Q. Ducasse, F. Giacoppo, F. Gunsing, T. W. Hagen, A. C. Larsen, M. Lebois, B. Leniau, T. Renstrom, S. J. Rose, T. G. Tornyi, G. M. Tveten, M. Wiedeking, and J. N. Wilson, Phys. Rev. C **89**, 014302 (2014).
[10] T. G. Tornyi, M. Guttormsen, T. K. Eriksen, A. Görgen, F. Giacoppo, T. W. Hagen, A. Krasznahorkay, A. C. Larsen, T. Renstrøm, S. J. Rose, S. Siem, and G. M. Tveten, Phys. Rev. C **89**, 044323 (2014).
[11] T. A. Laplace, F. Zeiser, M. Guttormsen, A. C. Larsen, D. L. Bleuel, L. A. Bernstein, B. L. Goldblum, S. Siem, F. L. Bello Garrote, J. A. Brown, L. Crespo Campo, T. K. Eriksen, F. Giacoppo, A. Gorgen, K. Hadynska-Klek, R. A. Henderson, M. Klintefjord, M. Lebois, T. Renstrom, S. J. Rose, E. Sahin, T. G. Tornyi, G. M. Tveten, A. Voinov, M. Wiedeking, J. N. Wilson, and W. Younes, Phys. Rev. C **93**, 014323 (2016).
[12] T. Ericson, Adv. Phys. **9**, 425 (1960).
[13] K. Heyde, P. von Neumann-Cosel, and A. Richter, Rev. Mod. Phys. **82**, 2365 (2010).
[14] J. L. Ullmann, T. Kawano, T. A. Bredeweg, A. Couture, R. C. Haight, M. Jandel, J. M. O'Donnell, R. S. Rundberg, D. J. Vieira, J. B. Wilhelmy, J. A. Becker, A. Chyzh, C. Y. Wu, B. Baramsai, G. E. Mitchell, and M. Krtička, Phys. Rev. C **89**, 034603 (2014).
[15] J. L. Ullmann, T. Kawano, B. Baramsai, T. A. Bredeweg, A. Couture, R. C. Haight, M. Jandel, J. M. O'Donnell, R. S. Rundberg, D. J. Vieira, J. B. Wilhelmy, M. Krtička, J. A. Becker, A. Chyzh, C. Y. Wu, and G. E. Mitchell, Phys. Rev. C **96**, 024627 (2017).
[16] S. Mosby, T. Bredeweg, A. Couture, M. Jandel, T. Kawano, J. Ullmann, R. Henderson, and C. Wu, Nucl. Data Sheets **148**, 312 (2018).
[17] F. Zeiser, G. Potel, G. M. Tveten, A. C. Larsen, M. Guttormsen, T. A. Laplace, S. Siem, D. L. Bleuel, B. L. Goldblum, L. A. Bernstein, F. L. Bello Garrote, L. Crespo Campo, T. K. Eriksen, A. G. K. Hadynska-Klek, J. E. Midtbø, T. Renstrøm, E. Sahin, T. Tornyi, A. Voinov, and M. Wiedeking, Proceedings of

the Compund Nuclear Reactions Workshop, Berkeley, 2018, (2018), arXiv:1902.02966.
[18] R. Henderson, J. Gostic, J. Burke, S. Fisher, and C. Wu, Nucl. Instrum. Methods Phys. Res. A **655**, 66 (2011).
[19] M. Guttormsen, A. Bürger, T. Hansen, and N. Lietaer, Nucl. Instrum. Methods Phys. Res. A **648**, 168 (2011).
[20] M. Guttormsen, A. Atac, G. Løvhøiden, S. Messelt, T. Ramsøy, J. Rekstad, T. F. Thorsteinsen, T. S. Tveter, and Z. Zelazny, Phys. Scr. **T32**, 54 (1990).
[21] T. G. Tornyi, A. Görgen, M. Guttormsen, A. C. Larsen, S. Siem, A. Krasznahorkay, and L. Csige, Nucl. Instrum. Methods Phys. Res. A **738**, 6 (2014).
[22] M. Guttormsen, T. Tveter, L. Bergholt, F. Ingebretsen, and J. Rekstad, Nucl. Instrum. Methods Phys. Res. A **374**, 371 (1996).
[23] L. Crespo Campo, F. L. Bello Garrote, T. K. Eriksen, A. Görgen, M. Guttormsen, K. Hadynska-Klek, M. Klintefjord, A. C. Larsen, T. Renstrøm, E. Sahin, S. Siem, A. Springer, T. G. Tornyi, and G. M. Tveten, Phys. Rev. C **94**, 044321 (2016).
[24] M. Guttormsen, F. Zeiser, J. E. Midtbø, V. W. Ingeberg, and A. C. Larsen, doi: 10.5281/zenodo.2318646 (2018).
[25] B. Singh and E. Browne, Nucl. Data Sheets **109**, 2439 (2008), data extracted from the ENSDF database, version November 2010.
[26] B. B. Back, O. Hansen, H. C. Britt, and J. D. Garrett, Phys. Rev. C **9**, 1924 (1974).
[27] M. Hunyadi, D. Gassmann, A. Krasznahorkay, D. Habs, P. Thirolf, M. Csatlós, Y. Eisermann, T. Faestermann, G. Graw, J. Gulyás *et al.*, Phys. Lett. B **505**, 27 (2001).
[28] S. J. Rose, F. Zeiser, J. N. Wilson, A. Oberstedt, S. Oberstedt, S. Siem, G. M. Tveten, L. A. Bernstein, D. L. Bleuel, J. A. Brown, L. Crespo Campo, F. Giacoppo, A. Görgen, M. Guttormsen, K. Hadyńska, A. Hafreager, T. W. Hagen, M. Klintefjord, T. A. Laplace, A. C. Larsen, T. Renstrøm, E. Sahin, C. Schmitt, T. G. Tornyi, and M. Wiedeking, Phys. Rev. C **96**, 014601 (2017).
[29] M. Guttormsen, T. Ramsøy, and J. Rekstad, Nucl. Instrum. Methods Phys. Res. A **255**, 518 (1987).
[30] P. A. M. Dirac, Proc. Royal Soc. A: Math., Phys. Eng. Sci. **114**, 243 (1927).
[31] E. Fermi, *Nuclear Physics* (University of Chicago Press, Chicago, 1950).
[32] D. M. Brink, Ph.D. thesis, Some aspects of the interaction of light with matter, University of Oxford, 1955, https://ora.ox.ac.uk/objects/uuid:334ec4a3-8a89-42aa-93f4-2e54d070ee09.
[33] P. Axel, Phys. Rev. **126**, 671 (1962).
[34] A. C. Larsen, M. Guttormsen, N. Blasi, A. Bracco, F. Camera, L. Crespo Campo, T. K. Eriksen, A. Görgen, T. W. Hagen, V. W. Ingeberg, B. V. Kheswa, S. Leoni, J. E. Midtbø, B. Million, H. T. Nyhus, T. Renstrøm, S. J. Rose, I. E. Ruud, S. Siem, T. G. Tornyi, G. M. Tveten, A. V. Voinov, M. Wiedeking, and F. Zeiser, J. Phys. G: Nucl. Part. Phys. **44**, 064005 (2017).
[35] L. C. Campo, M. Guttormsen, F. L. Bello Garrote, T. K. Eriksen, F. Giacoppo, A. Görgen, K. Hadynska-Klek, M. Klintefjord, A. C. Larsen, T. Renstrøm, E. Sahin, S. Siem, A. Springer, T. G. Tornyi, and G. M. Tveten, Phys. Rev. C **98**, 054303 (2018).
[36] M. Guttormsen, A. C. Larsen, A. Görgen, T. Renstrøm, S. Siem, T. G. Tornyi, and G. M. Tveten, Phys. Rev. Lett. **116**, 012502 (2016).
[37] Data extracted from the endsf database using nndc's chart of nuclides, http://www.nndc.bnl.gov/chart/, accessed 10.05.2015.
[38] R. Capote, M. Herman, P. Obložinský, P. Young, S. Goriely, T. Belgya, A. Ignatyuk, A. Koning, S. Hilaire, and V. Plujko, Nucl. Data Sheets **110**, 3107 (2009), data extracted from RIPL-3 online database https://www-nds.iaea.org/RIPL-3/, accessed 10.05.2015.
[39] T. von Egidy and D. Bucurescu, Phys. Rev. C **72**, 044311 (2005).
[40] A. Gilbert and A. G. W. Cameron, Can. J. Phys. **43**, 1446 (1965).
[41] A. Voinov, M. Guttormsen, E. Melby, J. Rekstad, A. Schiller, and S. Siem, Phys. Rev. C **63**, 044313 (2001).
[42] J. Kopecky and M. Uhl, Phys. Rev. C **41**, 1941 (1990).
[43] F. Giacoppo, F. L. B. Garrote, L. A. Bernstein, D. L. Bleuel, R. B. Firestone, A. Görgen, M. Guttormsen, T. W. Hagen, M. Klintefjord, P. E. Koehler, A. C. Larsen, H. T. Nyhus, T. Renstrøm, E. Sahin, S. Siem, and T. Tornyi, Phys. Rev. C **91**, 054327 (2015).
[44] L. E. Kirsch and F. Zeiser, doi: 10.5281/zenodo.2540342 (2019).
[45] G. Potel, F. M. Nunes, and I. J. Thompson, Phys. Rev. C **92**, 034611 (2015).
[46] G. Potel, G. Perdikakis, B. V. Carlson, M. C. Atkinson, W. H. Dickhoff, J. E. Escher, M. S. Hussein, J. Lei, W. Li, A. O. Macchiavelli, A. M. Moro, F. M. Nunes, S. D. Pain, and J. Rotureau, Eur. Phys. J. A **53**, 12371 (2017).
[47] R. Capote, S. Chiba, E. S. Soukhovitskiĭ, J. M. Quesada, and E. Bauge, J. Nucl. Sci. Technol. **45**, 333 (2008).
[48] A. J. Koning, S. Hilaire, and M. C. Duijvestijn, in *Proceedings of the International Conference on Nuclear Data for Science and Technology 2007*, edited by O. Bersillon, F. Gunsing, E. Bauge, R. Jacqmin, and S. Leray (EDP Sciences, Les Ulis, 2008), p. 211.
[49] E. S. Soukhovitskii, S. Chiba, J.-Y. Lee, O. Iwamoto, and T. Fukahori, J. Phys. G: Nucl. Part. Phys. **30**, 905 (2004).
[50] L. Kirsch and L. Bernstein, Nucl. Instrum. Methods Phys. Res. A **892**, 30 (2018).
[51] E. P. Wigner, ORNL Report No. 2309, 59 (1957).
[52] C. Porter and R. Thomas, Phys. Rev. **104**, 483 (1956).
[53] T. Kibédi, T. Burrows, M. Trzhaskovskaya, P. Davidson, and C. Nestor, Nucl. Instrum. Methods Phys. Res. A **589**, 202 (2008).
[54] R. Storn and K. Price, J. Global Optim. **11**, 341 (1997).
[55] J. Kopecky, S. Goriely, S. Péru, S. Hilaire, and M. Martini, Phys. Rev. C **95**, 054317 (2017).
[56] R. Chrien, J. Kopecky, H. Liou, O. Wasson, J. Garg, and M. Dritsa, Nucl. Phys. A **436**, 205 (1985).
[57] M. A. P. V. De Moraes and M. F. Cesar, Phys. Scr. **47**, 519 (1993).
[58] G. Gurevich, L. Lazareva, V. Mazur, G. Solodukhov, and B. Tulupov, Nucl. Phys. A **273**, 326 (1976).
[59] B. L. Berman, J. T. Caldwell, E. J. Dowdy, S. S. Dietrich, P. Meyer, and R. A. Alvarez, Phys. Rev. C **34**, 2201 (1986).
[60] A. E. Gelfand and A. F. M. Smith, J. Am. Stat. Assoc. **85**, 398 (1990).
[61] C. Robert and G. Casella, Stat. Sci. **26**, 102 (2011).

Paper VI

Energy dependence of the prompt γ-ray emission from the (d, p)-induced fission of ^{234}U* and ^{240}Pu*

Rose, S. J.†, Zeiser, F.†, Wilson, J. N., Oberstedt, A., Oberstedt, S., Siem, S., Tveten, G. M., Bernstein, L. A., Bleuel, D. L., Brown, J. A., Crespo Campo, L., Giacoppo, F., Görgen, A., Guttormsen, M., Hadyńska, K., Hafreager, A., Hagen, T. W., Klintefjord, M., Laplace, T. A., Larsen, A. C., Renstrøm, T., Sahin, E., Schmitt, C., Tornyi, T. G., Wiedeking, M.

Published in *Physical Review C*, July 2017, Volume 96, Number 1, Article no. 014601 DOI: 10.1103/PhysRevC.96.014601.
†Corresponding authors with equal contributions.

Energy dependence of the prompt γ-ray emission from the (d,p)-induced fission of ^{234}U* and ^{240}Pu*

S. J. Rose,[1,*] F. Zeiser,[1,†] J. N. Wilson,[2] A. Oberstedt,[3] S. Oberstedt,[4] S. Siem,[1] G. M. Tveten,[1] L. A. Bernstein,[5,6] D. L. Bleuel,[7] J. A. Brown,[5] L. Crespo Campo,[1] F. Giacoppo,[1,‡] A. Görgen,[1] M. Guttormsen,[1] K. Hadyńska,[1] A. Hafreager,[1] T. W. Hagen,[1] M. Klintefjord,[1] T. A. Laplace,[6,7] A. C. Larsen,[1] T. Renstrøm,[1] E. Sahin,[1] C. Schmitt,[8] T. G. Tornyi,[1] and M. Wiedeking[9]

[1]*Department of Physics, University of Oslo, 0316 Oslo, Norway*
[2]*Institut de Physique Nucléaire d'Orsay, CNRS/ Univ. Paris-Sud, Université Paris Saclay, 91406 Orsay Cedex, France*
[3]*Extreme Light Infrastructure - Nuclear Physics (ELI-NP) / Horia Hulubei National Institute for Physics and Nuclear Engineering (IFIN-HH), 077125 Bucharest-Magurele, Romania*
[4]*European Commission, Joint Research Centre, Directorate for Nuclear Safety and Security, Unit G.2 Standards for Nuclear Safety, Security and Safeguards, 2440 Geel, Belgium*
[5]*Lawrence Berkeley National Laboratory, Berkeley, California 94720, USA*
[6]*University of California - Berkeley Dept. of Nuclear Engineering, Berkeley California 94720, USA*
[7]*Lawrence Livermore National Laboratory, Livermore, California 94551, USA*
[8]*Grand Accélérateur National d'Ions Lourd, Bd Henri Becquerel, BP 55027 - 14076 CAEN Cedex 05, France*
[9]*iThemba LABS, P.O. Box 722, 7129 Somerset West, South Africa*

(Received 19 December 2016; published 5 July 2017)

Prompt-fission γ rays are responsible for approximately 5% of the total energy released in fission, and therefore important to understand when modeling nuclear reactors. In this work we present prompt γ-ray emission characteristics in fission as a function of the nuclear excitation energy of the fissioning system. Emitted γ-ray spectra were measured, and γ-ray multiplicities and average and total γ energies per fission were determined for the ^{233}U(d,pf) reaction for excitation energies between 4.8 and 10 MeV, and for the ^{239}Pu(d,pf) reaction between 4.5 and 9 MeV. The spectral characteristics show no significant change as a function of excitation energy above the fission barrier, despite the fact that an extra ~5 MeV of energy is potentially available in the excited fragments for γ decay. The measured results are compared with model calculations made for prompt γ-ray emission with the fission model code GEF. Further comparison with previously obtained results from thermal neutron induced fission is made to characterize possible differences arising from using the surrogate (d,p) reaction.

DOI: 10.1103/PhysRevC.96.014601

I. INTRODUCTION

Nuclear fission was discovered some 70 years ago [1–3], but still there remain some intriguing mysteries about this complex process. One of the least measured parts of the energy that is released in fission is the contribution that is carried away via prompt γ-ray emission. This accounts for roughly 8 MeV [4,5], which is around 5% of the total energy released in fission. In addition, prompt energy is dissipated via the Coulomb repulsion of the fragments, and the emission of prompt neutrons. Prompt-fission γ rays (PFGs) are typically emitted within a few nanoseconds of scission of the fragments; about 70% of the prompt PFGs are emitted within 60 ps [6], about 95% within 3 ns [7]. PFGs are one of the least understood parts of the fission process [8].

The investigation of PFG emission addresses questions in nuclear structure and reaction physics. One question deals with the deexcitation of nuclei through the emission of neutrons and γ rays. The theoretical description of the deexcitation of neutron-rich isotopes, as being produced in neutron-induced fission, shows significant deficits in describing the neutron and γ-ray spectral shape [8]. To some extent this deficiency seems to be related to a limited understanding of the competing process of prompt neutron and γ emission. Prompt-fission γ-ray spectral (PFGS) data, measured as a function of excitation energy of the compound nucleus may provide important information to benchmark different models, allowing eventually arrival at a consistent description of prompt-fission neutron and γ-ray emission. Furthermore, PFGs are certainly among the most sensitive observables for studying angular-momentum generation in fission [8,9].

Understanding PFG emission is not only useful for complete modeling of the fission process, but it also has some important practical applications for nuclear reactors. In recent years, requests for more accurate PFGS data have motivated a series of measurements to obtain new precise values of the γ-ray multiplicities and mean photon energy release per fission in the thermal-neutron-induced fission of ^{235}U [10,11] and ^{239}Pu [11,12]. With the development of advanced Generation-IV nuclear reactors, the need of new PFGS data becomes important. Since four out of six contemplated Generation-IV reactors require a fast-neutron spectrum, a wider range of incident neutron energies has to be considered [13]. Modeling of the geometrical distribution of γ heating, in and around the reactor core, shows local deviations up to 28% as compared

*sunniva.rose@fys.uio.no
†fabio.zeiser@fys.uio.no
‡Present address: (a) Helmholtz Institute Mainz, 55099 Mainz, Germany; (b) GSI Helmholtzzentrum für Schwerionenforschung, 64291 Darmstadt, Germany.

TABLE I. Target and beam characteristics as used in this work. Fission barrier heights are taken from Ref. [24].

Target	^{233}U (A)	^{239}Pu (B)
Chemical composition	Metallic	Metallic
Active diameter	1 cm	1 cm
^{9}Be backing (mg/cm^2)	2.3	1.8
Total area density (mg/cm^2)	0.2	0.4
Reaction	(d,pf)	(d,pf)
Beam energy (MeV)	12.5	12
Inner fission barrier, $B_{\mathrm{F,a}}$ (MeV)	4.80	6.05
Outer fission barrier, $B_{\mathrm{F,b}}$ (MeV)	5.50	5.15

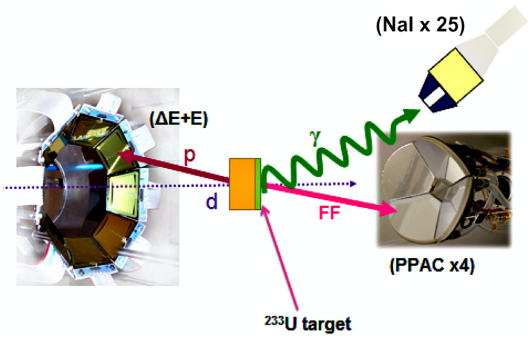

FIG. 1. Schematic view of the experimental setup for experiment (A), showing the SiRi ($\Delta E + E$) telescope, and the NIFF (PPAC) detectors, inside the reaction chamber, surrounded by the CACTUS NaI array. SiRi measures the energy of the outgoing charged particles; NIFF detects fission fragments (FF), and CACTUS detects γ rays all in coincidence, within a time interval of 20 ns. The ^{233}U target (0.2 mg/cm^2, green), on the ^{9}Be backing (2.3 mg/cm^2, orange) was facing NIFF, and SiRi was in the backward direction relative to the beam direction (dotted, purple arrow). The setup for the ^{239}Pu experiment was identical, except for CACTUS having 26 crystals instead of 25.

with measured heat distributions, whereas accuracy within 7.5% is mandatory [14]. These deviations remain mainly, despite experiment campaigns in the 1970s [4,15–17], due to the uncertainties on the existing PFGs data [10,18,19]. For ^{240}Pu*, this work also responds to the high-priority request published through the Nuclear Energy Agency (NEA) of the Organisation for Economic Co-operation and Development (OECD) [14].

In this paper we report measurements of PFG emission from ^{234}U* in the ^{233}U(d,pf) reaction, and ^{240}Pu* in the ^{239}Pu(d,pf) reaction. Both target nuclei represent the fissile key nuclei for the thorium-uranium and uranium-plutonium fuel cycles, respectively. The (d,pf) reaction serves hereby as a surrogate for the neutron-induced fission [20]. Charged-particle-induced reactions allow measurements of fission observables for isotopes not easily accessible to neutron beam experiments or for excitation energies below the neutron binding energy. They also facilitate the study of PFG characteristics as a function of compound nucleus excitation energy. We study the dependence of PFG characteristics on compound nucleus excitation energy and possible differences between surrogate and neutron-induced fission reactions.

II. EXPERIMENTAL DETAILS

Two experiments, denoted (A) and (B), were carried out at the Oslo Cyclotron Laboratory (OCL) of the University of Oslo, using deuteron beams, delivered by a MC-35 Scanditronix cyclotron. The γ-detector array CACTUS [21] together with the SiRi charged-particle detectors [22] and the NIFF detector [23] were used to detect triple coincident events of a proton, one of the two fission fragments (FFs), and γ rays.

Experiment (A) utilized a 12.5 MeV beam incident on a ^{233}U target, and experiment (B) had a 12 MeV beam on a ^{239}Pu target (detailed target specifications are listed in Table I). The targets were cleaned from decay products and other chemical impurities with an anion-exchange resin column procedure [25], and then electroplated on a backing made of ^{9}Be.

For these particular experiments, the SiRi detectors were mounted in the backward direction, and the NIFF detectors in the forward direction, relative to the beam direction (see Fig. 1). This setup was chosen for several reasons: Due to the thick beryllium backing, the targets had to face NIFF to enable detection of any fission events, thereby also avoiding FFs in the SiRi detector. However, the light, outgoing particles could easily penetrate the beryllium and be detected in SiRi. The backward direction of SiRi also reduces the intensity of the elastic peak and minimizes the exposure to protons from deuteron breakup in the target. SiRi was covered by a 21-μm-thick aluminum foil, to attenuate δ electrons in the telescopes.

SiRi consists of 64 ΔE (front) and 8 E (back) silicon detectors with thicknesses of 130 and 1550 μm, respectively. The detectors cover eight angles from $\theta \simeq 126^\circ$ to 140° relative to the beam axis, in a lampshade geometry facing the target at a distance of 5 cm at an angle of 133°. The total solid angle coverage is about 9% of 4π. In experiment (A) twenty-five, and in experiment (B) twenty-six, 12.7 cm × 12.7 cm ($5'' \times 5''$) NaI(Tl) crystals were mounted on the spherical CACTUS frame, 22 cm away from the target. At a γ-ray energy of 1.33 MeV, the crystals detect γ rays with a total efficiency of 13.6(1)% (A), and 14.2(1)% (B). To reduce the amount of Compton scattering, the detectors were collimated with lead cones. NIFF, consisting of four parallel plate avalanche counters (PPACs), covering 41% of 2π, were used for tagging of fission events. For this, it is sufficient to detect one of the two fission fragments, which are emitted back to back. The PPACs are placed at an angle of 45° with respect to the beam axis, at a distance of about 5 cm from the center of the target. Taking into account angular anisotropy effects in the center-of-mass system, Ref. [26] found a total efficiency of about 48%. The particle and fission detectors were mounted in the reaction chamber, surrounded by the CACTUS array (Fig. 1). The experiments ran for one week each, with a typical beam current of 1 nA.

The experimental setup enables particle-FF-γ coincidences that, together with energy and time information, are sorted event by event. In the present work, we focused on the ^{233}U(d,pf) and the ^{239}Pu(d,pf) reactions. The detection of

a charged particle in SiRi was the event trigger. In a timing interval of ∼20 ns we require a γ signal in CACTUS and a FF in NIFF.

From kinematics, the measured energy of the outgoing charged particle is converted into initial excitation energy E_x of the fissioning system. In our cases, we measure the deposited energy of the proton in the particle telescope, thereby selecting ^{234}U* and ^{240}Pu* as the fissioning system, for experiments (A) and (B), respectively. The excitation energy was reconstructed event by event from the detected proton energy and emission angle, and accounting for energy losses in the target and backing. For each energy bin in E_x, a correction for the neutron contribution to the γ-ray spectrum is performed, which is detailed in the next section. Finally, the raw γ spectra are corrected for the detector response to produce a set of unfolded PFGS. The applied unfolding process, which has the advantage that the original statistical fluctuations are preserved, is fully described in Ref. [27]. NaI response functions are based on in-beam γ lines from excited states in ^{56,57}Fe, ^{28}Si, ^{17}O, and ^{13}C, which were remeasured in 2012 [28].

A. Correction for neutron contribution

In the fission process, both neutrons and γ rays are emitted. Neutrons can interact with the NaI crystals of CACTUS, depositing energy mostly in the form of γ rays from $(n,n'\gamma)$ reactions. Unfortunately, the timing gate (20 ns) of the current setup (Fig. 1) only allows for discrimination between γ rays and neutrons via time of flight (TOF) for the slowest neutrons, i.e., with energies lower than 600 keV. However, the majority of prompt neutrons emitted in fission have higher energy than this. To obtain PFGS, a correction for the neutron component needs to be made, with subtraction of counts arising from energy deposition by neutrons.

Our neutron correction method relies on using a neutron response spectrum of a NaI detector, which is most representative of that for fission neutrons. Normalizing this to the known average neutron multiplicity emitted in fission for a particular compound nucleus excitation energy allows estimation of the neutron component in the total measured PFGS at this energy. This component is then subtracted. In this work we used a spectrum [29] for 2.3 MeV neutrons, which is close to the average fission neutron energy.

The response of 7.6 cm × 7.6 cm (3″ × 3″) NaI detectors to incident neutrons at energies between 0.4 and 10 MeV has been measured by Häusser *et al.* [29] by using TOF discrimination with quasimonoenergetic neutrons produced in the ^{7}Li(p,n) and ^{197}Au(p,n) reactions. They find that the neutron response is dominated by $(n,n'\gamma)$ reactions. For the energies most prominent from fission neutrons, 1–2.5 MeV, most counts in the NaI detectors are observed between 0.4 and 1 MeV. For 2.3 MeV neutrons, they report 0.13(5) triggers per incident neutron. Since the CACTUS detectors are longer (12.5 cm), we scale the number of triggers to 0.21(8) triggers per incident neutron. We assume that the intrinsic detection efficiency $\epsilon_{\rm int}$ for γ rays from fission is the same as those created in the detector by $(n,n'\gamma)$ reactions. The γ-ray multiplicity $\bar{M}$ for neutron contribution correction purposes is taken as 6.31 for ^{234}U* [17] and 7.15 for ^{240}Pu* [30].

TABLE II. Parameters to scale the excitation-energy dependence of the average total neutron multiplicity relative to the neutron separation energy S_n extracted from Ref. [31] (^{234}U*) and Ref. [33] (^{240}Pu*).

	^{234}U*	^{240}Pu*
a (n/MeV)	0.1	0.14
b ($\bar{\nu}$ @ thermal fission)	2.5	2.9
S_n (MeV)	6.85	6.53

The relative contribution f of neutrons to the measured data $N_{\rm tot}(E_x,E_\gamma)$ for each excitation energy E_x and γ-ray-energy bin E_γ can be estimated by the detection efficiencies. Taking into account the ratio of neutron and γ-ray multiplicities we find

$$f = \frac{\epsilon_{\rm int,n}\bar{\nu}}{\epsilon_{\rm int,n}\bar{\nu} + \bar{M}}. \quad (1)$$

The neutron multiplicity $\bar{\nu}$ is known to vary approximately linearly as a function of the incident neutron energy E_n [31–33]. Taking into account the neutron separation energy S_n, the same dependence is assumed for the compound nucleus excitation energy E_x with the parameters given in Table II, such that $\bar{\nu}(E_x) = a(E_x - S_n) + b$. The total contribution to the data caused by neutrons is estimated as a fraction of counts, $f(E_x)$, that is weighted as a function of E_γ by Häusser's neutron spectrum $H(E_\gamma)$, i.e.,

$$N_n(E_x,E_\gamma) = N_{\rm tot}(E_x) f(E_x) H(E_\gamma), \quad (2)$$

where $N_{\rm tot}(E_x)$ is the projection of the γ matrix onto E_x:

$$N_{\rm tot}(E_x) = \sum_{E_\gamma} N_{\rm tot}(E_x,E_\gamma). \quad (3)$$

$N_{\rm tot}(E_x,E_\gamma)$ is the matrix element in the γ matrix. $H(E_\gamma)$ is normalized so that $\sum_{E_\gamma} H(E_\gamma) = 1$. The γ-ray spectrum $N_\gamma(E_x,E_\gamma)$ is obtained by subtracting the neutron contribution $N_n(E_x,E_\gamma)$ from the measured data $N_{\rm tot}(E_x,E_\gamma)$:

$$N_\gamma(E_x,E_\gamma) = N_{\rm tot}(E_x,E_\gamma) - N_n(E_x,E_\gamma). \quad (4)$$

The results of the subtraction procedure can be seen graphically in Fig. 2, where the raw spectrum, neutron contribution, and corrected spectrum are shown. Since inelastic scattering is the main energy-deposition mechanism for neutrons, which occurs mostly on low-lying states in sodium and iodine nuclei, the neutron contribution is largest in the low-energy part of the spectrum. However, overall, the correction for the neutron contribution in our experiments remains small (see Table III).

B. Extrapolation of spectra towards zero energy

Detectors used in experiments that attempt to measure PFGS will always have an energy threshold to prevent rapid triggering on noise. Below this threshold, γ-ray detection is impossible, so the lowest energy γ rays emitted in fission will not be detected. As a consequence, this will introduce a systematic uncertainty in the deduction of average spectral quantities: Measured multiplicities $\bar{M}$ and total γ energy $E_{\rm tot}$ will thus be lower, and measured average γ-ray energy $E_{\rm av}$

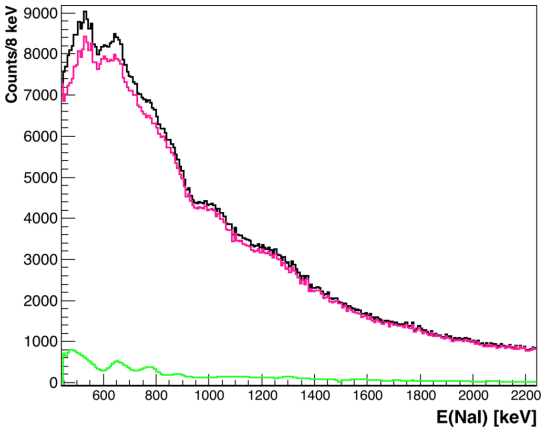

FIG. 2. The total (summed over all E_x) raw PFGS detected in the ^{233}U(d,pf) reaction (black) and the calculated spectral contribution due to interactions of prompt-fission neutrons in the NaI detector (green). The corrected γ spectrum is also shown (pink).

released per fission will be higher than their actual values. In fact, such systematic uncertainties from threshold effects may explain discrepancies between previous PFG experimental results [10,35]. To account for the undetected γ rays below threshold, it is necessary to make an extrapolation towards zero energy, such as, e.g., that performed in Ref. [36]. In our case the detection threshold was rather high, at 450 keV. As the shape of the γ-ray spectrum is not known for the low γ-ray energies, we chose a constant value for the bins below threshold. A reasonable extrapolation of each spectrum was made by averaging over the first three γ-ray bins above the threshold. The uncertainty was estimated by the minimum and maximum values in these bins, including their uncertainties. This results in an average value of about 5.5 ± 2 photons per fission per MeV (^{234}U*) below threshold. By assuming a nonzero value for this energy bin, the extrapolation reduces the uncertainty, but it does not eliminate it entirely. In our case it is still the dominant source of uncertainty on the absolute values

TABLE III. Values used for calculating the neutrons in the CACTUS detectors. The average neutron energies were calculated from ENDF/B VII.1 [34]. Neutron multiplicities $\bar{\nu}$ are taken from Ref. [31,33] and γ-ray multiplicities $\bar{M}$ from Ref. [17] (^{234}U*) and Ref. [30] (^{240}Pu*).

	A (^{234}U*)	B (^{240}Pu*)
Average neutron energy (MeV)	2.0	2.1
Intrinsic neutron efficiency (triggers/neutron)	0.21(8)	0.21(8)
Neutron multiplicities (@ thermal fission)	2.5	2.9
γ-ray multiplicities	6.31(30)	7.15(9)
Relative contribution (@ thermal fission)	0.0768	0.078

of the average spectral quantities deduced. Since we compare our data with thermal-neutron-induced fission experiments, we chose the same cutoff of the PFGS as Ref. [15], of $E_\gamma = 140$ keV.

III. PREDICTIONS WITH THE GENERAL FISSION MODEL CODE

We compare our data to predictions from the semi-empirical general fission model (GEF) [37]. GEF is based on the observation of a number of regularities in fission observables, revealed by experimental studies, combined with general laws of statistical and quantum mechanics. It provides a general description of essentially all fission observables (fission-fragment yields and kinetic energies, prompt and delayed neutrons and γ rays, and isomeric ratios) in a consistent way while preserving the correlations between all of them. GEF has been shown to be able to explain in an unprecedented good manner fission-fragment and neutron properties over a wide range, running from spontaneous fission to induced fission up to an excitation energy of about 100 MeV for $Z = 80$ to $Z = 112$ [37]. Modeling of γ rays in fission has been implemented most recently. In contrast to other existing codes in the field, GEF provides also reliable predictions for nuclei for which no experimental data exist. This is particularly important in our case, since no experimental data on the fragment properties exist for the majority of the excitation energies that we are investigating.

Calculations were performed for fission of both ^{234}U* and ^{240}Pu*, applying the same cutoff of the PFGS as for the experimental data, of 140 keV, as described in Sec. II B. The total angular momentum $J = I_0 + L_{\text{trans}}$ is the sum of the target nucleus ground-state spin I_0 and the angular momentum L_{trans} transferred in the (d,p) reaction. The distribution in the GEF v.2016/1.1 calculations is given by

$$\rho(J) \propto (2J+1)\exp[-J(J+1)/J_{\text{rms}}^2], \qquad (5)$$

where we used the root mean square (rms) of the total angular momentum[1] J_{rms} and the excitation energy to describe the fissioning system as input. The maximum value for J_{rms} of 12 was obtained from $J_{\text{rms}} = \sqrt{2T\mathcal{I}}/\hbar$ [38], where the nuclear temperature was chosen to be $T \approx 0.45$ MeV in line with other actinide nuclei [39,40]. The rigid body moment of inertia $\mathcal{I}$ is given by $\frac{2}{5}m_A(r_0A^{1/3})^2(1+0.31\beta_2) \approx 160(\hbar c)^2/\text{MeV}$, where we used the isotope mass m_A, the mass number A, the quadrupole deformation β_2 from Ref. [24], and radius parameter $r_0 \lesssim 1.3$. The results are compared with an intermediate value of $J_{\text{rms}} = 8$, and to the lower limit, $J_{\text{rms}} = 0$, where the latter facilitates the comparison to neutron-induced reactions, which transfer little angular momentum. Additionally we performed calculations for an energy-dependent J_{rms}, which was adopted from the systematics of Ref. [41]:

$$J_{\text{rms}}^2(E_x) = 2 \times 0.0146A^{5/3}\frac{1+\sqrt{1+4a(E_x-E_1)}}{2a}, \qquad (6)$$

[1] J_{rms} can be expressed in terms of the spin cutoff parameter σ by $J_{\text{rms}} = \sqrt{2}\sigma$.

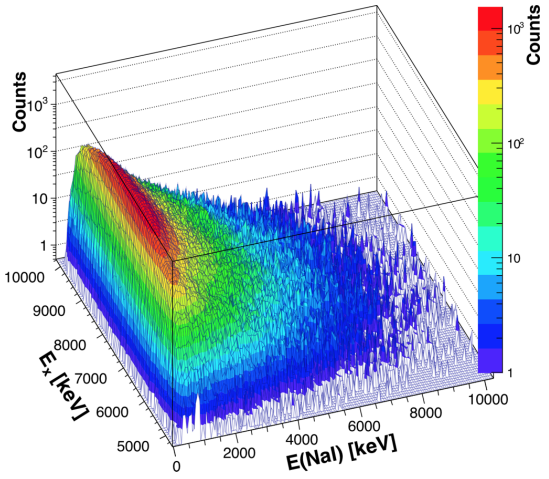

FIG. 3. Matrix of the fission and proton-gated raw γ data from the ^{233}U(d,pf) reaction (after subtraction of the contribution from neutrons). The x axis gives the deduced compound nucleus excitation energy E_x. The y axis gives the detected γ-ray energy, and the z axis gives the number of counts recorded during the experiment (not efficiency corrected). The bin width is 64 keV for E_x and E_γ.

where the level-density parameter a and the energy backshift E_1 are obtained from a fit to experimental data [41].

IV. EXPERIMENTAL RESULTS

A. The ^{234}U* case

Figure 3 shows a three-dimensional overview of the data set where, for a given compound nucleus excitation energy, the corresponding raw detected PFGS (prior to unfolding the response function) is displayed with the neutron contribution subtracted. The excitation energy range, over which the data are collected, can be seen more closely in Fig. 4, which histograms the double coincidences of protons and fission fragments (d,pf) and triple coincidences of protons, fission fragments, and γ rays $(d,pf\gamma)$ as a function of E_x. In the case of ^{234}U*, only a very few subthreshold fission events occur below the inner fission barrier [24] at $E_x = 4.8$ MeV, which is 2 MeV below the neutron separation energy at 6.85 MeV [42]. The ^{233}U(d,pf) reaction at 12.5 MeV incident energy populates compound-nuclear excitation energies up to a maximum of 10 MeV in this case.

The E_x range is divided into 8 bins, each with a width of 650 keV to obtain a sufficient statistics PFGS for each bin. Each spectrum is unfolded for the CACTUS response and normalized to the number of fission events detected in that excitation energy bin. The set of eight normalized spectra is overlaid in Fig. 5, and they exhibit similar spectral shapes.

The average spectral quantities after extrapolation to zero energy are then deduced and plotted as a function of the excitation energy. These results are plotted in Fig. 6 with their corresponding statistical error bars and compared with calculations from the GEF code. The wider band denoted by the dash-dotted lines indicates the sum of the statistical uncertainties on each data point plus the systematic uncertainty on the absolute values due to the presence of the detection threshold.

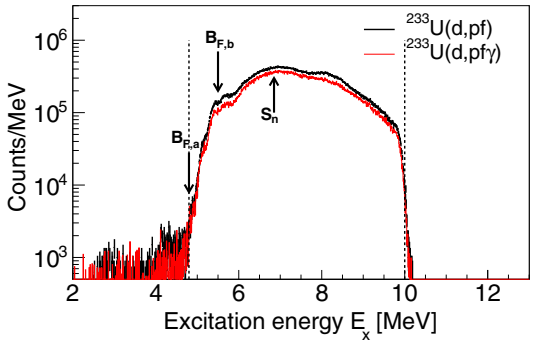

FIG. 4. The total number of ^{233}U(d,pf) and ^{233}U(d,pfγ) events recorded during the experiment histogrammed as a function of the deduced compound-nuclear excitation energy of ^{234}U* for each event. The inner and outer fission barriers $B_{F,a}$ at 4.80 MeV and $B_{F,b}$ at 5.50 MeV, respectively, and the neutron separation energy S_n at 6.85 MeV are shown. The dotted lines indicate the minimum and maximum E_x of the analyzed area. The lower limit on E_x is the inner fission barrier.

B. The ^{240}Pu* case

The same analysis was performed for the ^{239}Pu(d,pf) reaction. The (d,pf) and the $(d,pf\gamma)$ reactions are histogrammed as functions excitation energy (Fig. 7). In the ^{240}Pu* case, there appears to be a significant amount of subbarrier fission, which is in accordance with observations in Refs. [43,44]. This can be explained in the double-humped fission barrier picture; by the resonant population of states in the second potential minimum

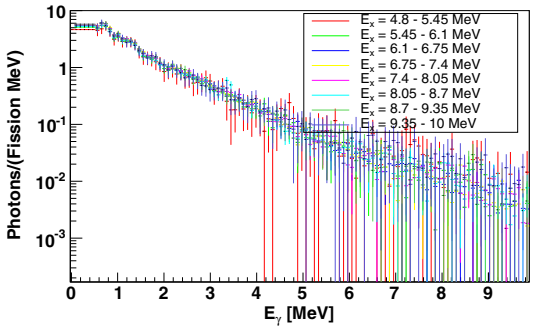

FIG. 5. Overlay of the eight ^{233}U(d,pf) PFGS for different excitation-energy bins in compound-nucleus excitation energy E_x. The spectra are normalized to the number of photons per fission and per MeV to provide a comparison of the spectral shapes. The extrapolation from the detector threshold at 450 keV towards zero energy is explained in the text.

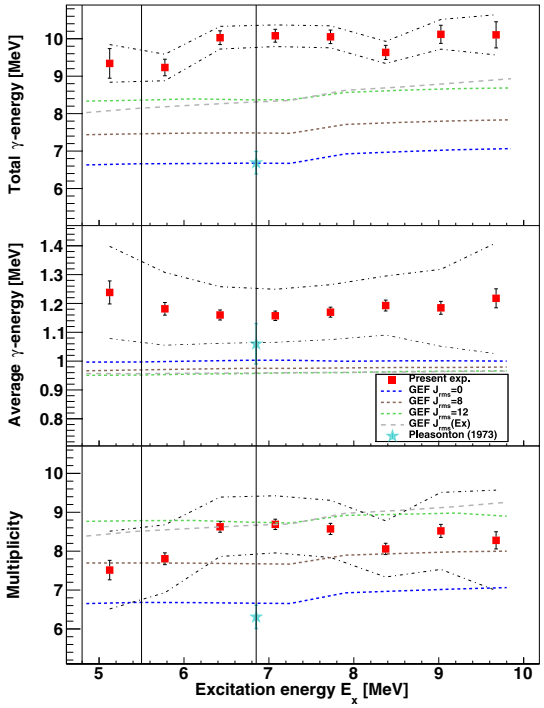

FIG. 6. Energy dependence of the ^{233}U(d,pf) average PFG spectral quantities compared with calculations from the GEF code for different $J_{\rm rms}$ of the ^{234}U* nucleus. In addition, results from Pleasonton [17] are shown. Multiplicity, average γ-ray energy, and total γ-ray energy as function of excitation energy of ^{234}U* are shown. The error bars represent the statistical uncertainty of the measurement. The dash-dotted lines represent the total uncertainty, which is the sum of the systematic uncertainty on the absolute values due to the detector threshold, and the extrapolation towards zero energy plus the statistical uncertainty. Vertical lines mark the inner and outer fission barriers ($E_{\rm x} = 4.8$ MeV and $E_{\rm x} = 5.40$ MeV) and the neutron separation energy ($E_{\rm x} = 6.85$ MeV), respectively.

of the ^{240}Pu* nucleus and a tunneling through the outer fission barrier.

The overlay of the unfolded PFGS for the ^{239}Pu(d,pf) reaction is shown in Fig. 8. The spectral shapes are all observed to be similar. However, the PFGS for the two lowest compound-nucleus excitation-energy bins starting at 4.65 and 5.45 MeV appear to be significantly lower than the others. This effect also manifests itself in the average photon multiplicity $\bar{M}$ and total energy $E_{\rm tot}$ release at this energy (see Fig. 9). We note that this is the region below the fission barrier and, hence, originates from subbarrier fission. Otherwise, the trends for the spectral characteristics seem to have no significant trend and are fairly constant, i.e., independent of excitation energy and thus consistent with the predictions of the GEF code.

Finally, we compare the measured PFGS at excitation energy of 6.5 MeV, which corresponds to the thermal-neutron-

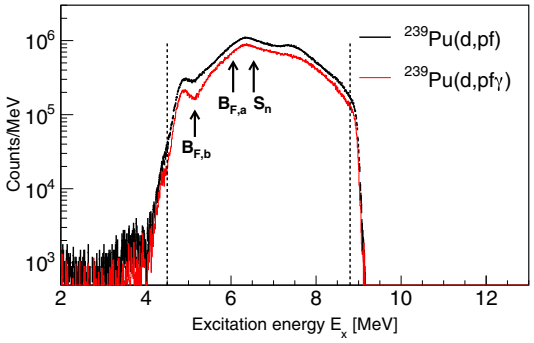

FIG. 7. The total number of ^{239}Pu(d,pf) and ^{239}Pu$(d,pf\gamma)$ events recorded during the experiment histogrammed as a function of the ^{240}Pu* deduced excitation energy event by event. The inner and outer fission barriers $B_{\rm F,a}$ at 6.05 MeV and $B_{\rm F,b}$ at 5.15 MeV, respectively, and the neutron separation energy S_n at 6.53 MeV are shown. The dotted lines indicate the minimum and maximum $E_{\rm x}$ of the analyzed area. The lower limit of $E_{\rm x}$ is at 4.8 MeV, which is more than 1 MeV below the fission barrier due to subbarrier fission.

induced fission reaction for ^{239}Pu, with the measured PFGS of Verbinski *et al.* [15] for thermal-neutron-induced fission. Figure 10 shows this comparison along with a spectrum from the GEF code. An excess of counts is observed between 2 and 4 MeV for our surrogate PFGS measured in the ^{239}Pu(d,pf) reaction as compared with the neutron-induced reaction.

V. DISCUSSION

In this study, both experiments reveal an approximately constant behavior of average γ-ray energy $E_{\rm av}$, $\bar{M}$, and $E_{\rm tot}$, as a function of $E_{\rm x}$ of the fissioning system; shown in Fig. 6 for uranium and in Fig. 9 for plutonium. The constant trend

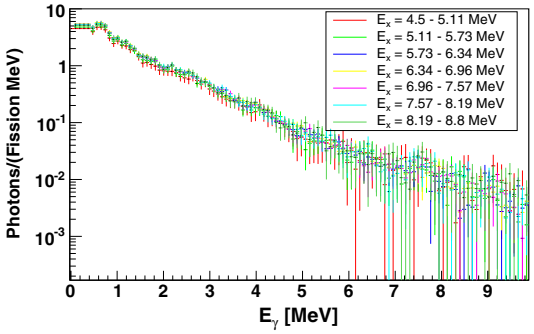

FIG. 8. Overlay of the six ^{239}Pu(d,pf) unfolded PFG gamma spectra for different excitation-energy bins in compound-nucleus excitation energy E_x. The spectra are normalized to the number of photons per fission and per MeV to provide a comparison of the spectral shapes. The extrapolation between 140 keV energy and the detector threshold at 450 keV is explained in the text.

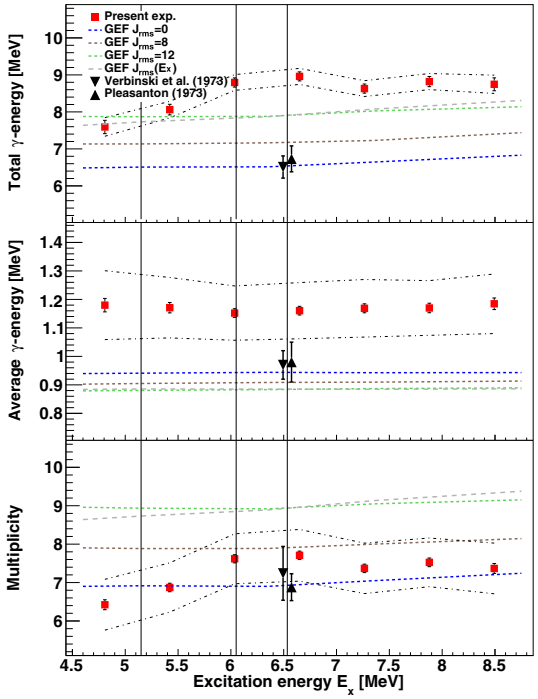

FIG. 9. Energy dependence of the ^{239}Pu(d,pf) PFG average spectral quantities from the GEF code for different $J_{\rm rms}$ of the ^{240}Pu* nucleus. The thermal neutron data of Pleasonton (1973) [17] and Verbinski *et al.* (1973) [15] are shifted slightly around S_n for better visibility. Multiplicity, average γ-ray energy, and total γ-ray energy, as function of excitation energy of ^{240}Pu* are shown. The error bars represent the statistical uncertainty of the measurement. The dash-dotted lines represent the systematic uncertainty on the absolute values due to the detector threshold and the necessary extrapolation to zero energy. Vertical lines mark the inner and outer fission barriers ($E_{\rm x} = 6.05$ MeV and $E_{\rm x} = 5.15$ MeV) and the neutron separation energy ($E_{\rm x} = 6.5$ MeV), respectively.

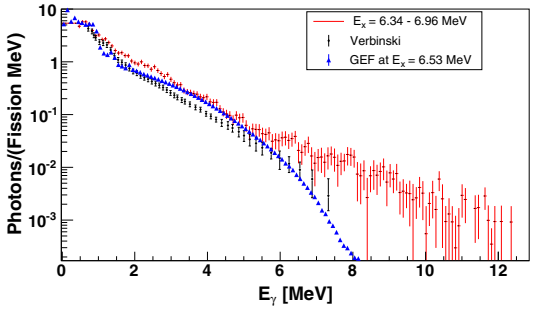

FIG. 10. A comparison of the ^{239}Pu(d,pf) PFGS measured at $E_x \sim S_n$ (red), the PFGS for thermal-neutron-induced fission ^{239}Pu$(n_{\rm th},f)$ from Verbinski *et al.* [15] (black points), and the calculations by GEF for $J_{\rm rms} = 8$ and $E_{\rm x} = 6.35$ (blue).

(although not the absolute value) in spectral characteristics that we observe is broadly in line with the predictions of GEF.

There seems to be a slight decrease in $\bar{M}$ below S_n for both nuclei, but more clearly seen in the plutonium data. Although up to 5 MeV of extra excitation energy for the hot fission fragments is available, this energy is clearly more efficiently dissipated by the evaporation of prompt-fission neutrons. The prompt-fission neutron multiplicity is well known to increase linearly with excitation energy. One could expect that the total angular momentum J of the fissioning nucleus should increase with increasing $E_{\rm x}$. Our experimental data exhibit a flat trend, which is compatible to GEF calculations for a constant or energy-dependent $J_{\rm rms}$ in the studied excitation-energy range.

An excess of counts is observed when comparing the surrogate (d,p) PFG and thermal-neutron-induced PFGS. Such a discrepancy might arise from differences in the surrogate and neutron-induced reactions. The spectrum (Fig. 10) predicted with the GEF code lies in between the two experimental cases in the region in which the deviation is observed. For γ rays above 8 MeV, significantly fewer photons are predicted in comparison with our data. The spectrum by Verbinski *et al.* [15] is reported only up to $E_\gamma = 7.5$ MeV.

It is expected that reactions involving charged particles will on average introduce more angular momentum $L_{\rm trans}$ into the reaction than thermal-neutron-induced reactions. The distribution of the angular momentum J will have a tail, which extends higher, the greater the mass difference is between the ingoing and outgoing charged particles in the reaction. It may, therefore, be possible that the excess counts observed in the PFGS of the surrogate reaction is an angular-momentum effect introduced by using the (d,p) reaction to induce fission instead of neutrons.

It is consistent that, for $\bar{M}$ and $E_{\rm tot}$, our (d,p) PFG data are in better agreement with larger $J_{\rm rms}$, whereas the thermal-neutron-induced data are in all cases in good agreement with low $J_{\rm rms}$. For $E_{\rm av}$ the results of the GEF calculation are in both reactions less sensitive to $J_{\rm rms}$, and there the discrepancy between our experimental results and the calculations increases.

The absolute values of $E_{\rm tot}$ and $\bar{M}$ are higher for the ^{234}U* than the ^{240}Pu*. Comparison with the results from GEF, and a slightly higher deuteron beam energy, indicates a higher angular momentum in the uranium case. Average higher angular momentum of the fission fragments might result in neutron emission being partially hindered from odd fission fragments up to 1 MeV above their S_n. In such a case γ-ray emission will compete with neutron emission, also above S_n. This would result in an increased total γ energy and higher $\bar{M}$.

Recently, surrogate measurements have demonstrated that radiative capture and fission cross sections [45] can be used to get quantitative insight into the angular momentum $L_{\rm trans}$ imparted to the compound nucleus following a specific transfer reaction. A detailed review of both theory, experimental results, and challenges can be found in Ref. [46]. The connection between these cross sections and $L_{\rm trans}$ involves sophisticated Hauser–Feshbach calculations [47]. On the other hand, it is established that prompt-fission γ multiplicity $\bar{M}$ is the most direct probe of the angular momentum of the fission fragments.

The latter is influenced by the angular momentum of the fissioning system, i.e., L_{trans} in the presented GEF calculations. The present work shows that the measured $\bar{M}$ is indeed sensitive to L_{trans}. Hence, it can be used as an alternative observable, complementary to cross sections [45], to quantify L_{trans}.

Above the neutron binding energy S_n there is no significant increase in average PFG energy and total PFG energy released per fission with increasing excitation E_{x}. This observation is important for applications, since γ rays from fission are responsible for a large part of the heating that occurs in reactor cores. The observed result implies that passing from current Generation-III thermal reactors to fast Generation-IV reactor concepts will not require significant changes in the modeling of γ heat transport from the fast-neutron-induced fission process. Since ^{233}U is the main fissile isotope in the thorium cycle, and ^{239}Pu is the main fissile isotope in the plutonium-uranium cycle, and the flat trend is observed in both these nuclei, effects of γ heating from fission in both cycles are expected to be similar.

VI. CONCLUSION

Emission of prompt γ rays from nuclear fission induced via the ^{233}U(d,pf) and ^{239}Pu(d,pf) reactions have been studied. PFGS have been extracted as functions of the compound-nucleus excitation energy for both nuclei. The average spectral characteristics have been deduced and trends as a function of excitation energy have been studied and compared with calculations by the GEF code.

We observe an approximately constant behavior of the spectral properties as a function of energy for both nuclei. However, a much lower multiplicity is seen in the subbarrier fission of ^{240}Pu*. More detailed studies are needed to understand why subbarrier fission results in emission of low multiplicities of prompt γ rays from the excited fission fragments. Furthermore, we observe an excess of γ rays above 2 MeV emitted in the surrogate ^{239}Pu(d,pf) reaction when comparing with the neutron-induced PFGS measured by Verbinski *et al.* This effect is not yet understood, but may be as due to higher angular momenta involved in the transfer-induced reactions as compared with the neutron-induced one, over the energy range of our study. This conjecture is supported by GEF calculations.

Our measured γ-ray multiplicities and total γ energies are higher than those observed for the neutron-induced reactions from Verbinski *et al.* and Pleasonton. This difference may be explained as due to higher J by comparing with the GEF calculations.

In the future we hope to revisit these types of measurements with the OSCAR array of 26 large volume $LaBr_3$ detectors currently being constructed at the Oslo Cyclotron Laboratory. These will not only provide a much better γ-ray-energy resolution and lower energy thresholds, but an excellent timing resolution which will allow for discrimination of neutrons from γ rays via time of flight.

ACKNOWLEDGMENTS

We would like to thank J. Müller, E. A. Olsen, and A. Semchenkov for providing excellent beams during the experiments. We would also like to thank Beatriz Jurado and Karl-Heinz Schmidt for fruitful discussions. A.C.L. gratefully acknowledges funding through ERC-STG-2014, Grant Agreement No. 637686. G.M.T. and S. Siem gratefully acknowledge funding through the Research Council of Norway, Project No. 222287 and Grant No. 210007, respectively. We would like to thank Lawrence Livermore National Laboratory for providing the ^{233}U and ^{239}Pu targets. This work was performed under the auspices of the University of California Office of the President Laboratory Fees Research Program under Award No. 12-LR-238745, the U.S. Department of Energy by Lawrence Livermore National Laboratory under Contract DE-AC52-07NA27344, Lawrence Berkeley National Laboratory under Contract No. DE-AC02-05CH11231, and the National Research Foundation of South Africa under Grants No. 92789 and No. 83671. M.W. acknowledges funding from the National Research Foundation of South Africa under Grants No. 92989 and No. 83867.

[1] L. Meitner and O. R. Frisch, Nature (London) **143**, 239 (1939).
[2] O. Hahn and F. Strassmann, Naturwissenschaften **27**, 11 (1939).
[3] N. Bohr and J. A. Wheeler, Phys. Rev. **56**, 426 (1939).
[4] F. Pleasonton, R. L. Ferguson, and H. W. Schmitt, Phys. Rev. C **6**, 1023 (1972).
[5] H. R. Bowman and S. G. Thompson, The prompt radiations in the spontaneous fission of ^{252}Cf, Tech. Rep. UCRL-5038(Rev.) (California University, Livermore, Radiation Laboratory, 1958).
[6] H. Albinsson, Phys. Scr. **3**, 113 (1971).
[7] P. Talou, T. Kawano, I. Stetcu, J. P. Lestone, E. McKigney, and M. B. Chadwick, Phys. Rev. C **94**, 064613 (2016).
[8] I. Stetcu, P. Talou, T. Kawano, and M. Jandel, Phys. Rev. C **90**, 024617 (2014).
[9] R. Schmitt, G. Mouchaty, and D. Haenni, Nucl. Phys. A **427**, 614 (1984).
[10] A. Oberstedt, T. Belgya, R. Billnert, R. Borcea, T. Bryś, W. Geerts, A. Göök, F.-J. Hambsch, Z. Kis, T. Martinez, S. Oberstedt, L. Szentmiklosi, K. Takàcs, and M. Vidali, Phys. Rev. C **87**, 051602(R) (2013).
[11] A. Chyzh, C. Y. Wu, E. Kwan, R. A. Henderson, J. M. Gostic, T. A. Bredeweg, A. Couture, R. C. Haight, A. C. Hayes-Sterbenz, M. Jandel, H. Y. Lee, J. M. O'Donnell, and J. L. Ullmann, Phys. Rev. C **87**, 034620 (2013).
[12] A. Gatera, T. Belgya, W. Geerts, A. Göök, F.-J. Hambsch, M. Lebois, B. Maróti, A. Moens, A. Oberstedt, S. Oberstedt, F. Postelt, L. Qi, L. Szentmiklósi, G. Sibbens, D. Vanleeuw, M. Vidali, and F. Zeiser, Phys. Rev. C **95**, 064609 (2017).
[13] I. L. Pioro, *Handbook of Generation IV Nuclear Reactors* (Woodhead Publishing, Cambridge, 2016), Chap. 2, pp. 37–54.
[14] Nuclear Data High Priority Request List of the NEA (Req. ID: H.3); http://www.oecd-nea.org/dbdata/hprl/hprlview.pl?id=421.
[15] V. Verbinski, H. Weber, and R. Sund, Phys. Rev. C **7**, 1173 (1973).

[16] R. W. Peelle and F. C. Maienschein, Phys. Rev. C **3**, 373 (1971).
[17] F. Pleasonton, Nucl. Phys. A **213**, 413 (1973).
[18] M. Salvatores *et al.*, *Uncertainty and Target Accuracy Assessment for Innovative Systems using Recent Covariance Data Evaluations* (OECD/NEA WPEC, Greece, Hungary, Iceland, 2008), Vol. 26.
[19] R. Billnert, F.-J. Hambsch, A. Oberstedt, and S. Oberstedt, Phys. Rev. C **87**, 024601 (2013).
[20] J. D. Cramer and H. C. Britt, Nucl. Sci. Eng. **41**, 177 (1970).
[21] M. Guttormsen, A. Atac, G. Løvhøiden, S. Messelt, T. Ramsøy, J. Rekstad, T. Thorsteinsen, T. Tveter, and Z. Zelazny, Phys. Scr. **1990**, 54 (1990).
[22] M. Guttormsen, A. Bürger, T. Hansen, and N. Lietaer, Nucl. Instrum. Methods Phys. Res., Sect. A **648**, 168 (2011).
[23] T. G. Tornyi, A. Görgen, M. Guttormsen, A.-C. Larsen, S. Siem, A. Krasznahorkay, and L. Csige, Nucl. Instrum. Methods Phys. Res., Sect. A **738**, 6 (2014).
[24] R. Capote, M. Herman, P. Obložinský, P. Young, S. Goriely, T. Belgya, A. Ignatyuk, A. J. Koning, S. Hilaire, V. A. Plujko *et al.*, Nucl. Data Sheets **110**, 3107 (2009).
[25] R. Henderson, J. Gostic, J. Burke, S. Fisher, and C. Wu, Nucl. Instrum. Methods Phys. Res., Sect. A **655**, 66 (2011).
[26] Q. Ducasse, B. Jurado, M. Aïche, P. Marini, L. Mathieu, A. Görgen, M. Guttormsen, A. Larsen, T. Tornyi, J. Wilson *et al.*, Phys. Rev. C **94**, 024614 (2016).
[27] M. Guttormsen, T. Tveter, L. Bergholt, F. Ingebretsen, and J. Rekstad, Nucl. Instrum. Methods Phys. Res., Sect. A **374**, 371 (1996).
[28] L. Crespo Campo, F. L. Bello Garrote, T. K. Eriksen, A. Görgen, M. Guttormsen, K. Hadynska-Klek, M. Klintefjord, A. C. Larsen, T. Renstrøm, E. Sahin, S. Siem, A. Springer, T. G. Tornyi, and G. M. Tveten, Phys. Rev. C **94**, 044321 (2016).
[29] O. Häusser, M. Lone, T. Alexander, S. Kushneriuk, and J. Gascon, Nucl. Instrum. Methods Phys. Res. **213**, 301 (1983).
[30] J. Ullmann, E. Bond, T. Bredeweg, A. Couture, R. Haight, M. Jandel, T. Kawano, H. Lee, J. M. O'Donnell, A. Hayes *et al.*, Phys. Rev. C **87**, 044607 (2013).
[31] ENDF/B-VII.1 Evaluated Nuclear Data Files, ZA=92233, NSUB=10(N), MT=456, http://www.nndc.bnl.gov/exfor/endf02.jsp (2011).
[32] D. Madland, Nucl. Phys. A **772**, 113 (2006).
[33] ENDF/B-VII.1 Evaluated Nuclear Data Files, ZA=94239, NSUB=10(N), MT=456, http://www.nndc.bnl.gov/exfor/endf02.jsp (2011).
[34] M. Chadwick, M. Herman, P. Obložinský, M. E. Dunn, Y. Danon, A. Kahler, D. L. Smith, B. Pritychenko, G. Arbanas, R. Arcilla *et al.*, Nucl. Data Sheets **112**, 2887 (2011).
[35] A. Chyzh, C. Wu, E. Kwan, R. Henderson, J. Gostic, T. Bredeweg, R. Haight, A. Hayes-Sterbenz, M. Jandel, J. M. O'Donnell *et al.*, Phys. Rev. C **85**, 021601 (2012).
[36] M. Lebois, J. Wilson, P. Halipré, A. Oberstedt, S. Oberstedt, P. Marini, C. Schmitt, S. Rose, S. Siem, M. Fallot *et al.*, Phys. Rev. C **92**, 034618 (2015).
[37] K.-H. Schmidt, B. Jurado, C. Amouroux, and C. Schmitt, Nucl. Data Sheets **131**, 107 (2016).
[38] T. Ericson, Adv. Phys. **9**, 425 (1960).
[39] M. Guttormsen, B. Jurado, J. Wilson, M. Aiche, L. Bernstein, Q. Ducasse, F. Giacoppo, A. Görgen, F. Gunsing, T. Hagen *et al.*, Phys. Rev. C **88**, 024307 (2013).
[40] M. Guttormsen, L. Bernstein, A. Görgen, B. Jurado, S. Siem, M. Aiche, Q. Ducasse, F. Giacoppo, F. Gunsing, T. Hagen *et al.*, Phys. Rev. C **89**, 014302 (2014).
[41] D. Bucurescu and T. von Egidy, J. Phys. G **31**, S1675 (2005).
[42] E. Browne and J. Tuli, Nucl. Data Sheets **108**, 681 (2007).
[43] M. Hunyadi, D. Gassmann, A. Krasznahorkay, D. Habs, P. Thirolf, M. Csatlós, Y. Eisermann, T. Faestermann, G. Graw, J. Gulyás *et al.*, Phys. Lett. B **505**, 27 (2001).
[44] P. Glässel, H. Rösler, and H. Specht, Nucl. Phys. A **256**, 220 (1976).
[45] G. Boutoux, B. Jurado, V. Méot, O. Roig, L. Mathieu, M. Aïche, G. Barreau, N. Capellan, I. Companis, S. Czajkowski *et al.*, Phys. Lett. B **712**, 319 (2012).
[46] J. E. Escher, J. T. Burke, F. S. Dietrich, N. D. Scielzo, I. J. Thompson, and W. Younes, Rev. Mod. Phys. **84**, 353 (2012).
[47] W. Hauser and H. Feshbach, Phys. Rev. **87**, 366 (1952).

Appendices

Appendix A

Derivations of the photo-excitation strength function

The photo-excitation strength function $\vec{f}$ was derived from the photo-absorption cross-section σ by Axel [42, 43] starting from the Breit-Wigner cross section for the population of an isolated level at excitation energy E_r, [18, 237]

$$\sigma^{(r)}_{0\to f}(E^{(r)}_{\Gamma}) = \pi g \left(\frac{\hbar c}{E_\gamma}\right)^2 \frac{\Gamma^{(r)}_0 \Gamma^{(r)}_f}{(E_\gamma - E_r)^2 + (\Gamma^{(r)}/2)^2} \tag{A.1}$$

$$\begin{aligned}\sigma^{(r)}_{0\to abs} &= \sum_f \sigma^{(r)}_{0\to f} = \pi g \left(\frac{\hbar c}{E_\gamma}\right)^2 \frac{\Gamma^{(r)}_0 \Gamma^{(r)}}{(E_\gamma - E_r)^2 + (\Gamma^{(r)}/2)^2} \\ &= g''\pi \left(\frac{\hbar c}{E_\gamma}\right)^2 \frac{\Gamma^{(r)}_0}{\Gamma^{(r)}} \frac{1}{\left(\frac{2(E_\gamma - E_r)}{\Gamma^{(r)}}\right)^2 + 1}\end{aligned} \tag{A.2}$$

where $\sigma^{(r)}_{0\to f}$ is the cross section to go from the ground state, 0, to *a specific* excited state f through the resonance r. Further, we denote the cross section for the subsequent decay to *any* accessible state by $\sigma^{(r)}_{0\to abs}$, and

$$g = \frac{2J_r + 1}{2(2J_0 + 1)} = \frac{g'}{2} = \frac{g''}{4} \tag{A.3}$$

is the statistical weight for an unpolarized photon beam accounts for the degeneracy of the levels [18, p. 423 & 436]. The decay widths are labeled $\Gamma^{(r)}_0$ and $\Gamma^{(r)}_f$ for the decay back to the ground state, and the decay to an excited state f, respectively. The total width is given by $\Gamma^{(r)} = \sum_j \Gamma^{(r)}_j$. Note that we for brevity dropped the subscript γ indicating γ-ray decay on the cross section and decay widths.

The original approach taken by Kinsey [41] and Axel [42] is to integrate $\sigma^{(r)}_{0\to abs}$ in order to get an average cross section. The equation written in Refs. [41, 42], $\int \sigma^{(r)}_{0\to abs}$, does not converge due to the $1/E^2$ behavior at low energies. However, from the context of the calculations, one may implicitly assume the presence of a somewhat narrow photon energy beam with a beam spread ΔE that cuts off the lowest energies of the cross section (see also Ref. [238, Eq. 30] and Ref. [239, p. 22]). For simplicity, let us assume that the photon flux $N_\gamma(E_\gamma)$ is 1 in a region ΔE around E_r. Despite the beam being narrow, it is still much larger than the width of the resonance, $\Gamma^{(r)} \ll \Delta E$, such that we can calculate the effective

integrated cross section (which is closely related to the interaction rate),

$$\begin{aligned}\int \sigma^{(r)}_{0\to abs,\mathrm{eff}}(E_\gamma)\,\mathrm{d}E_\gamma &= \int N_\gamma(E_\gamma)\sigma^{(r)}_{0\to abs}(E_\gamma)\,\mathrm{d}E_\gamma \\ &= \int_{E_r-\Delta E/2}^{E_r+\Delta E/2} \sigma^{(r)}_{0\to abs}(E_\gamma)\,\mathrm{d}E_\gamma \\ &= \int_{E_r-\Delta E/2}^{E_r+\Delta E/2} g''\pi \left(\frac{\hbar c}{E_\gamma}\right)^2 \frac{\Gamma_0^{(r)}}{\Gamma^{(r)}} \frac{1}{\left(\frac{2(E_\gamma-E_r)}{\Gamma^{(r)}}\right)^2+1}\,\mathrm{d}E_\gamma.\end{aligned} \tag{A.4}$$

As $1/E^2$ varies little in vicinity of E_r in comparison to $1/(1+(E_\gamma-E_r)^2)$, it can regarded as approximately constant in the region of the resonance, thus

$$\begin{aligned}&\int_{E_r-\Delta E/2}^{E_r+\Delta E/2} g''\pi \left(\frac{\hbar c}{E_\gamma}\right)^2 \frac{\Gamma_0^{(r)}}{\Gamma^{(r)}} \frac{1}{\left(\frac{2(E_\gamma-E_r)}{\Gamma^{(r)}}\right)^2+1}\,\mathrm{d}E_\gamma \\ &\approx g''\pi \left(\frac{\hbar c}{E_r}\right)^2 \Gamma_0^{(r)} \int_{E_r-\Delta E/2}^{E_r+\Delta E/2} \frac{1}{\Gamma^{(r)}} \frac{1}{\left(\frac{2(E_\gamma-E_r)}{\Gamma^{(r)}}\right)^2+1}\,\mathrm{d}E_\gamma \\ &\approx g''\pi^2 \left(\frac{\hbar c}{E_r}\right)^2 \Gamma_0^{(r)} \int \frac{1}{\pi\Gamma^{(r)}} \frac{1}{\left(\frac{2(E_\gamma-E_r)}{\Gamma^{(r)}}\right)^2+1}\,\mathrm{d}E_\gamma \\ &= g''\pi^2 \left(\frac{\hbar c}{E_r}\right)^2 \frac{1}{2}\Gamma_0^{(r)} = \frac{2J_r+1}{2J_0+1}\pi^2 \left(\frac{\hbar c}{E_r}\right)^2 \Gamma_0^{(r)},\end{aligned} \tag{A.5}$$

where the last integral is equal to the integral over a Cauchy distribution after the substitution $E = 2E_\gamma$, so $\mathrm{d}E_\gamma = \mathrm{d}E/2$.

The average integrated cross section $\langle\sigma^{(J_r)}\rangle$ for the interval ΔE containing n isolated level of spin J_r is then given by [41–43]

$$\begin{aligned}\langle\sigma^{(J_r)}\rangle &= \frac{1}{\Delta E}\sum_r^n \int \sigma^{(r)}_{0\to abs,\mathrm{eff}}(E_\gamma)\,\mathrm{d}E_\gamma = g'\pi^2 \left(\frac{\hbar c}{E_r}\right)^2 \frac{\sum_r \Gamma_0^{(r)}}{\Delta E} \\ &= g'\pi^2 \left(\frac{\hbar c}{E_r}\right)^2 \frac{n\langle\Gamma_0\rangle}{\Delta E} = \frac{2J_r+1}{2J_0+1}\pi^2 \left(\frac{\hbar c}{E_r}\right)^2 \langle\Gamma_0\rangle\rho(E_x\approx E_r, J_r).\end{aligned} \tag{A.6}$$

The average decay width to the ground-state $\langle\Gamma_0\rangle$ for the n resonances is expected to converge for a large enough n; the Breit-Wigner cross section is still a good approximation as the widths $\Gamma^{(r)}$ are still assumed to be much smaller than the level spacing $D = 1/p$. Finally, we realize that Eq. (A.6) holds for all narrow beams with the mean energy E_γ (that may excite into the quasi-continuum), such we can get the energy dependence of the average cross-section by the substitution $E_r \to E_\gamma$,

$$\langle\sigma^{(J_r)}\rangle(E_\gamma) = g'\pi^2 \left(\frac{\hbar c}{E_\gamma}\right)^2 \langle\Gamma_0\rangle\rho(E_x\approx E_\gamma, J_r). \tag{A.7}$$

Using the definition of the strength function, Eq. (2.10), we can write this as

$$\vec{f}_{XL}(E_\gamma, E_i = 0, J_i^\pi, J_f^\pi) = \frac{\langle \sigma_{XL}^{(J_f)} \rangle}{g'(\pi\hbar c)^2 E_\gamma^{2L-1}}. \tag{A.8}$$

If the γ-ray strength function is spin-independent, in line with the Brink-Axel hypothesis, the absorption cross-section $\langle\sigma\rangle$ to all levels close to E_γ can be simplified as

$$\langle\sigma\rangle_{XL} = \sum_{J_f} g'(\pi\hbar c)^2 E_\gamma^{2L-1} \vec{f}_{XL} = (2L+1)(\pi\hbar c)^2 E_\gamma^{2L-1} \vec{f}_{XL}, \tag{A.9}$$

or equivalently,

$$\vec{f}_{XL}(E_\gamma) = \frac{\langle \sigma_{XL} \rangle}{(2L+1)(\pi\hbar c)^2 E_\gamma^{2L-1}}, \tag{A.10}$$

where we have used $\sum g' = 2L + 1$, which is obvious for $J_0 = 0$ due to the selection rules, but can be shown to hold for arbitrary J_0.

On a historical note it is interesting to see that the same type of calculations have been performed by Kinsey [41] for the neutron capture cross-section already 5 years before Axel.

Appendix B

Supplement to Paper II

This appendix provides a small supplement to Paper II on the response of the OSCAR detector array. Here, we verify the simulated efficiencies for higher γ-ray energies than those published in the article.

As mentioned in the paper, there are two approaches in determining the full-energy peak efficiency ϵ_{fe}:

1. The "optimal" fit: This requires a careful selection of the fit-model (a linear, constant or no background; single or double peak, ...) and fit regions for each γ-ray transition individually.

2. A consistent/automatic fit: If the equivalence of the experimental and simulated spectra (and efficiencies) is to be shown, both spectra should be fitted with the exact same routine to rule out a confirmation bias.

In Fig. B.1 we show the full-energy peak efficiency ϵ_{fe} that was extracted for the "optimal" fit to each transition. In contrast, Fig. B.2a compares efficiencies for the simulated and experimental spectra, where we put an emphasis on the consistency of the fit procedures. The ^{133}Ba source was excluded there, as the double lines were badly reproduced by the automatic procedure.[1] The good agreement between the fits adds confidence in that the simulations truthfully reproduce γ-ray interactions.

Both approaches are displayed in Fig. B.2b together with the efficiency ϵ_{fe} that was extracted from the simulations directly, i.e. before smoothing the spectrum with a Gaussian so that peak fitting was not necessary. The agreement of the "optimal" fit with the efficiency directly obtained from Geant4 is remarkable, as the former were performed by F. L. Bello Garrote only on the experimental data and *without* any knowledge of the Geant4 simulations.

In her Master thesis, W. Paulsen adopted another approach to estimate efficiencies [232]. She determines the full-energy peak efficiency ϵ_{fe} from the ratio of detected particle to γ-rays in in-beam coincidence measurements of ^{28}Si and ^{12}C and shows that internal conversion is negligible for the selected transitions. The results are also displayed in Fig. B.2b and agree well with the efficiencies directly extracted from Geant4 and the "optimal" fit to the source spectra. This verifies the simulated efficiencies also for higher energy γ-rays which were not accessible with the available calibration sources.

[1] Of course, it is in principle possible to develop a more elaborate automatic routine, but this was not the goal of the article.

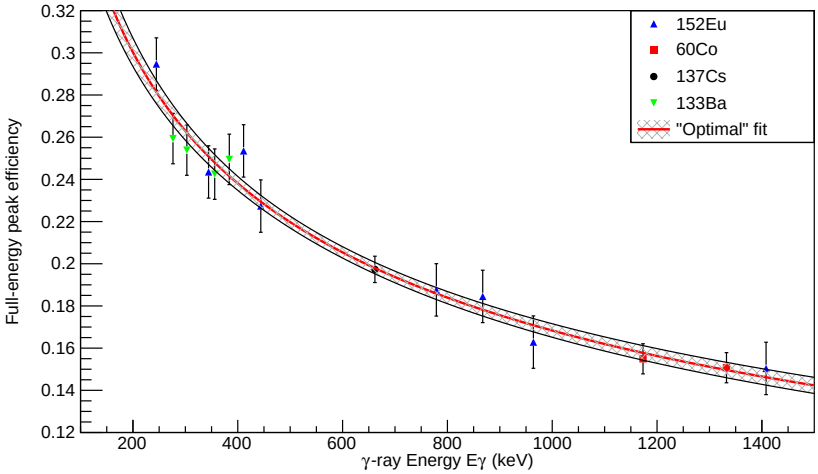

Figure B.1: Full-energy peak efficiency of OSCAR, where the transitions for each calibration source have been fitted "optimally". Courtesy to F. L. Bello Garrote.

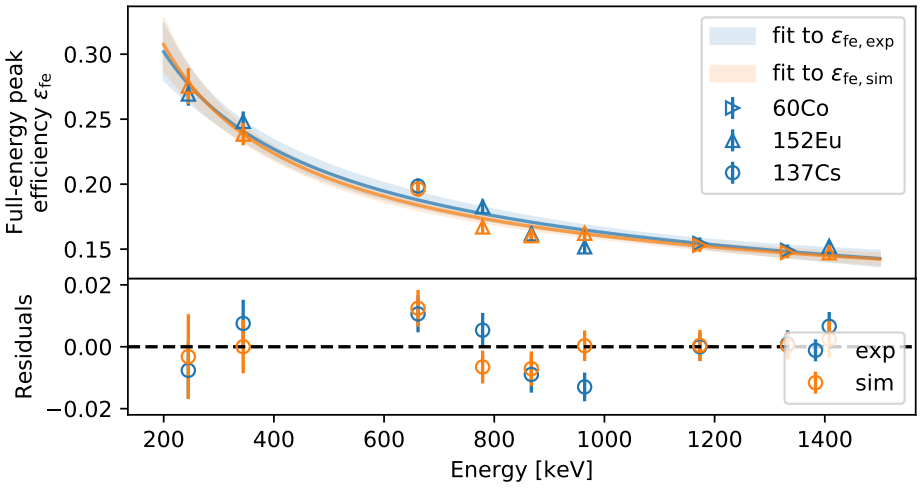

(a)

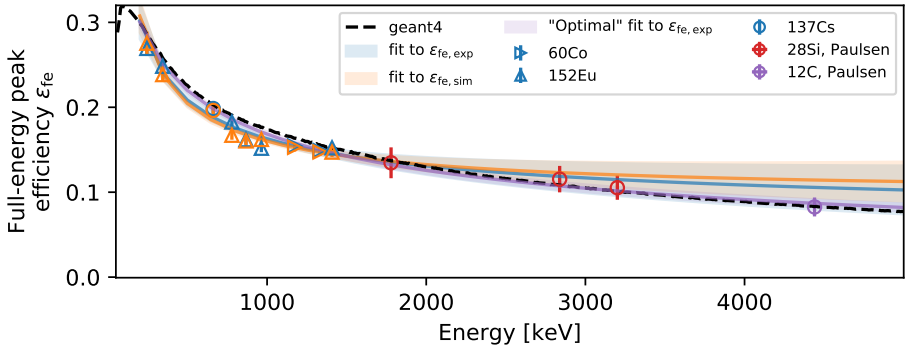

(b)

Figure B.2: Pannel (a): Full-energy peak efficiency of OSCAR from selected calibration sources and from simulation. The bottom panel shows the residuals from the fits. Reprinted from Ref. [240] (Paper II) with permission from Elsevier. Pannel (b): As above, but also with the efficiency as extracted the Geant4 simulations directly and the "optimal" fit to the calibration source data. Additional experimental in-beam data of Paulsen [232] are not included in the fit, but verify the extracted efficiency for higher γ-ray energies.

Bibliography

[1] Rekstad, J., Henriquez, A., Ingebretsen, F., Midttun, G., Skaali, B., Øyan, R., Wikne, J., Engeland, T., Thorsteinsen, T. F., Hammaren, E., and Liukkonen, E. "A Study of the Nuclear Structure at High Energy and Low Spin". In: *Phys. Scr.* Vol. T5 (Jan. 1983), pp. 45–50. DOI: 10.1088/0031-8949/1983/t5/007.

[2] Henden, L., Bergholt, L., Guttormsen, M., Rekstad, J., and Tveter, T. "On the relation between the statistical γ-decay and the level density in 162Dy". In: *Nuclear Physics A* vol. 589, no. 2 (July 1995), pp. 249–266. DOI: 10.1016/0375-9474(95)00133-l.

[3] Schiller, A., Bergholt, L., Guttormsen, M., Melby, E., Rekstad, J., and Siem, S. "Extraction of level density and γ strength function from primary γ spectra". In: *Nucl. Instrum. Methods Phys. Res. A* vol. 447, no. 3 (June 2000), pp. 498–511. DOI: 10.1016/s0168-9002(99)01187-0.

[4] Larsen, A. C., Guttormsen, M., Krtička, M., Běták, E., Bürger, A., Görgen, A., Nyhus, H. T., Rekstad, J., Schiller, A., Siem, S., and al., et. "Analysis of possible systematic errors in the Oslo method". In: *Phys. Rev. C* vol. 83, no. 3 (Mar. 2011), p. 034315. DOI: 10.1103/physrevc.83.034315. Corrected in Larsen, A. C. et al. "Enhanced low-energy γ-decay strength of Ni70 and its robustness within the shell model". In: *Physical Review C* vol. 97, no. 5 (May 2018). DOI: 10.1103/physrevc.97.054329.

[5] Tveter, T., Bergholt, L., Guttormsen, M., Melby, E., and Rekstad, J. "Observation of Fine Structure in Nuclear Level Densities and γ-Ray Strength Functions". In: *Physical Review Letters* vol. 77, no. 12 (Sept. 1996), pp. 2404–2407. DOI: 10.1103/physrevlett.77.2404.

[6] Melby, E., Bergholt, L., Guttormsen, M., Hjorth-Jensen, M., Ingebretsen, F., Messelt, S., Rekstad, J., Schiller, A., Siem, S., and Ødegård, S. W. "Observation of Thermodynamical Properties in the ^{162}Dy, ^{166}Er, and ^{172}Yb Nuclei". In: *Physical Review Letters* vol. 83, no. 16 (Oct. 1999), pp. 3150–3153. DOI: 10.1103/physrevlett.83.3150.

[7] Schiller, A., Bjerve, A., Guttormsen, M., Hjorth-Jensen, M., Ingebretsen, F., Melby, E., Messelt, S., Rekstad, J., Siem, S., and Ødegård, S. W. "Critical temperature for quenching of pair correlations". In: *Physical Review C* vol. 63, no. 2 (Jan. 2001). DOI: 10.1103/physrevc.63.021306.

[8] Voinov, A., Algin, E., Agvaanluvsan, U., Belgya, T., Chankova, R., Guttormsen, M., Mitchell, G. E., Rekstad, J., Schiller, A., and Siem, S. "Large Enhancement of Radiative Strength for Soft Transitions in the

Quasicontinuum". In: *Physical Review Letters* vol. 93, no. 14 (Sept. 2004). DOI: 10.1103/physrevlett.93.142504.

[9] Voinov, A., Guttormsen, M., Melby, E., Rekstad, J., Schiller, A., and Siem, S. "γ-ray strength function and pygmy resonance in rare earth nuclei". In: *Physical Review C* vol. 63, no. 4 (Mar. 2001), p. 044313. DOI: 10.1103/physrevc.63.044313.

[10] *Nuclear Data High Priority Request List of the NEA (Req. ID: H.33), http://www.oecd-nea.org/dbdata/hprl/hprlview.pl?ID=452.* 2018. URL: http://www.oecd-nea.org/dbdata/hprl/hprlview.pl?ID=452 (visited on 11/01/2020).

[11] *Nuclear Data High Priority Request List of the NEA (Req. ID: H.32), http://www.oecd-nea.org/dbdata/hprl/hprlview.pl?ID=451.* 2018. URL: http://www.oecd-nea.org/dbdata/hprl/hprlview.pl?ID=451 (visited on 11/01/2020).

[12] Dupont, E. et al. "HPRL – International cooperation to identify and monitor priority nuclear data needs for nuclear applications". In: *EPJ Web of Conferences* vol. 239 (2020). Ed. by Ge, Z., Shu, N., Chen, Y., Wang, W., and Zhang, H., p. 15005. DOI: 10.1051/epjconf/202023915005.

[13] Liddick, S. N. et al. "Experimental Neutron Capture Rate Constraint Far from Stability". In: *Physical Review Letters* vol. 116, no. 24 (June 2016). DOI: 10.1103/physrevlett.116.242502.

[14] Liddick, S. N. et al. "Benchmarking the extraction of statistical neutron capture cross sections on short-lived nuclei for applications using the β-Oslo method". In: *Physical Review C* vol. 100, no. 2 (Aug. 2019). DOI: 10.1103/physrevc.100.024624.

[15] Larsen, A., Spyrou, A., Liddick, S., and Guttormsen, M. "Novel techniques for constraining neutron-capture rates relevant for r-process heavy-element nucleosynthesis". In: *Progress in Particle and Nuclear Physics* vol. 107 (July 2019), pp. 69–108. DOI: 10.1016/j.ppnp.2019.04.002.

[16] LIGO Scientific Collaboration and Virgo Collaboration et al. "GW170817: Observation of Gravitational Waves from a Binary Neutron Star Inspiral". In: *Physical Review Letters* vol. 119, no. 16 (Oct. 2017). DOI: 10.1103/physrevlett.119.161101.

[17] Weisskopf, V. and Wigner, E. "Berechnung der natürlichen Linienbreite auf Grund der Diracschen Lichttheorie". In: *Zeitschrift für Physik* vol. 63, no. 1-2 (Jan. 1930), pp. 54–73. DOI: 10.1007/bf01336768.

[18] Blatt, J. M. and Weisskopf, V. F. *Theoretical Nuclear Physics*. New York: Wiley [u.a.], 1952. XIV, 864.

[19] Capote, R., Herman, M., Obložinský, P., Young, P., Goriely, S., Belgya, T., Ignatyuk, A., Koning, A., Hilaire, S., Plujko, V., and al., et. "RIPL – Reference Input Parameter Library for Calculation of Nuclear Reactions and Nuclear Data Evaluations". In: *Nuclear Data Sheets* vol. 110, no. 12 (Dec. 2009). Data extraced from RIPL-3 online database https://www-nds.iaea.org/RIPL-3/, accessed 10.05.2015., pp. 3107–3214. DOI: 10.1016/j.nds.2009.10.004.

[20] Bethe, H. A. "An Attempt to Calculate the Number of Energy Levels of a Heavy Nucleus". In: *Physical Review* vol. 50, no. 4 (Aug. 1936), pp. 332–341. DOI: 10.1103/physrev.50.332.

[21] Kaneko, K., Hasegawa, M., Agvaanluvsan, U., Algin, E., Chankova, R., Guttormsen, M., Larsen, A. C., Mitchell, G. E., Rekstad, J., Schiller, A., Siem, S., and Voinov, A. "Breaking of nucleon Cooper pairs at finite temperature in $^{93-98}$Mo". In: *Physical Review C* vol. 74, no. 2 (Aug. 2006). DOI: 10.1103/physrevc.74.024325.

[22] Goriely, S. "A new nuclear level density formula including shell and pairing correction in the light of a microscopic model calculation". In: *Nuclear Physics A* vol. 605, no. 1 (July 1996), pp. 28–60. DOI: 10.1016/0375-9474(96)00162-5.

[23] Bardeen, J., Cooper, L. N., and Schrieffer, J. R. "Theory of Superconductivity". In: *Physical Review* vol. 108, no. 5 (Dec. 1957), pp. 1175–1204. DOI: 10.1103/physrev.108.1175.

[24] Gilbert, A. and Cameron, A. G. W. "A Composite Nuclear-level Density Formula With Shell Corrections". In: *Canadian Journal of Physics* vol. 43, no. 8 (Aug. 1965), pp. 1446–1496. DOI: 10.1139/p65-139.

[25] Egidy, T. von and Bucurescu, D. "Systematics of nuclear level density parameters". In: *Phys. Rev. C* vol. 72, no. 4 (Oct. 2005), p. 044311. DOI: 10.1103/physrevc.72.044311. Corrected in Egidy, T. von and Bucurescu, D. "Erratum: Systematics of nuclear level density parameters [Phys. Rev. C 72, 044311 (2005)]". In: *Physical Review C* vol. 73, no. 4 (Apr. 2006). DOI: 10.1103/physrevc.73.049901.

[26] Ignatyuk, A., Smirenkin, G., and Tishin, A. "Phenomenological description of energy dependence of the level density parameter". In: *Yadernaya Fizika* vol. 21, no. 3 (1975), pp. 485–490.

[27] Ericson, T. "A statistical analysis of excited nuclear states". In: *Nuclear Physics* vol. 11 (May 1959), pp. 481–491. DOI: 10.1016/0029-5582(59)90291-3.

[28] Gilbert, A., Chen, F. S., and Cameron, A. G. W. "Level Densities In Lighter Nuclei". In: *Canadian Journal of Physics* vol. 43, no. 7 (July 1965), pp. 1248–1258. DOI: 10.1139/p65-120.

[29] Guttormsen, M., Aiche, M., Bello Garrote, F. L., Bernstein, L. A., Bleuel, D. L., Byun, Y., Ducasse, Q., Eriksen, T. K., Giacoppo, F., Görgen, A., and al., et. "Experimental level densities of atomic nuclei". In: *The European Physical Journal A* vol. 51, no. 12 (Dec. 2015). DOI: 10.1140/epja/i2015-15170-4.

[30] Guttormsen, M., Jurado, B., Wilson, J. N., Aiche, M., Bernstein, L. A., Ducasse, Q., Giacoppo, F., Görgen, A., Gunsing, F., Hagen, T. W., and al., et. "Constant-temperature level densities in the quasicontinuum of Th and U isotopes". In: *Phys. Rev. C* vol. 88, no. 2 (Aug. 2013), p. 024307. DOI: 10.1103/physrevc.88.024307.

[31] Moretto, L. G., Larsen, A. C., Giacoppo, F., Guttormsen, M., and Siem, S. "Experimental First Order Pairing Phase Transition in Atomic Nuclei". In: *Journal of Physics: Conference Series* vol. 580 (Feb. 2015), p. 012048. DOI: 10.1088/1742-6596/580/1/012048.

[32] Hilaire, S., Girod, M., Goriely, S., and Koning, A. J. "Temperature-dependent combinatorial level densities with the D1M Gogny force". In: *Physical Review C* vol. 86, no. 6 (Dec. 2012). DOI: 10.1103/physrevc.86.064317.

[33] Nyhus, H. T., Siem, S., Guttormsen, M., Larsen, A. C., Bürger, A., Syed, N. U. H., Tveten, G. M., and Voinov, A. "Radiative strength functions in Dy 163, 164". In: *Physical Review C* vol. 81, no. 2 (Feb. 2010). DOI: 10.1103/physrevc.81.024325.

[34] Koning, A., Hilaire, S., and Goriely, S. *TALYS 1.9, User Manual*. 2017.

[35] Koning, A. J., Hilaire, S., and Duijvestijn, M. C. "TALYS-1.0". In: *Proceedings of the International Conference on Nuclear Data for Science and Technology 2007*. Ed. by Bersillon, O., Gunsing, F., Bauge, E., Jacqmin, R., and Leray, S. Les Ulis: EDP Sciences, Apr. 2008, p. 211. DOI: 10.1051/ndata:07767.

[36] Bethe, H. A. "Nuclear Physics B. Nuclear Dynamics, Theoretical". In: *Reviews of Modern Physics* vol. 9, no. 2 (Apr. 1937), pp. 69–244. DOI: 10.1103/revmodphys.9.69.

[37] Egidy, T. von and Bucurescu, D. "Experimental energy-dependent nuclear spin distributions". In: *Phys. Rev. C* vol. 80, no. 5 (Nov. 2009), p. 054310. DOI: 10.1103/physrevc.80.054310.

[38] Zhongfu, H., Ping, H., Zongdi, S., and Chunmei, Z. In: *Chin. J. Nucl. Phys.* (13 1991), p. 147. As referenced in Egidy, T. von and Bucurescu, D. "Systematics of nuclear level density parameters". In: *Phys. Rev. C* vol. 72, no. 4 (Oct. 2005), p. 044311. DOI: 10.1103/physrevc.72.044311. Corrected in Egidy, T. von and Bucurescu, D. "Erratum: Systematics of nuclear level density parameters [Phys. Rev. C 72, 044311 (2005)]". In: *Physical Review C* vol. 73, no. 4 (Apr. 2006). DOI: 10.1103/physrevc.73.049901.

[39] Bartholomew, G. A., Earle, E. D., Ferguson, A. J., Knowles, J. W., and Lone, M. A. "Gamma-Ray Strength Functions". In: *Advances in Nuclear Physics* (1973), pp. 229–324. DOI: 10.1007/978-1-4615-9044-6_4.

[40] Lone, M. A. "Photon Strength Functions". In: *Neutron Capture Gamma-Ray Spectroscopy*. Ed. by Chrien, R. E. and Kane W., R. Springer US, 1979, pp. 161–180. DOI: 10.1007/978-1-4613-2940-4_9.

[41] Kinsey, B. B. "Nuclear Reactions, Levels, and Spectra of Heavy Nuclei". In: *Nuclear Reactions I / Kernreaktionen I*. Springer Berlin Heidelberg, 1957, pp. 202–372. DOI: 10.1007/978-3-642-45875-0_2.

[42] Axel, P. "Electric Dipole Ground-State Transition Width Strength Function and 7-Mev Photon Interactions". In: *Phys. Rev.* Vol. 126, no. 2 (Apr. 1962), pp. 671–683. DOI: 10.1103/physrev.126.671.

[43] Axel, P. "Simple Nuclear Excitations Distributed among Closely Spaced Levels". In: *Nuclear Structure: Dubna Symposium 1968. Invited Papers from the International Symposium. Organized by the Joint Institute for Nuclear Research, Dubna, and Held in Dubna, 4-11 July, 1968*. Vol. 189. International Atomic Energy Agency. 1968, p. 299.

[44] Porter, C. and Thomas, R. "Fluctuations of Nuclear Reaction Widths". In: *Phys. Rev.* Vol. 104, no. 2 (Oct. 1956), pp. 483–491. DOI: 10.1103/physrev.104.483.

[45] Bollinger, L. M., Coté, R. E., Carpenter, R. T., and Marion, J. P. "Distribution of Partial Radiation Widths". In: *Physical Review* vol. 132, no. 4 (Nov. 1963), pp. 1640–1662. DOI: 10.1103/physrev.132.1640.

[46] Jackson, H. E., Julien, J., Samour, C., Bloch, A., Lopata, C., Morgenstern, J., Mann, H., and Thomas, G. E. "Properties of Partial Radiation Widths in Pt196". In: *Physical Review Letters* vol. 17, no. 12 (Sept. 1966), pp. 656–658. DOI: 10.1103/physrevlett.17.656.

[47] Coceva, C., Corvi, F., Giacobbe, P., and Stefanon, M. "High-energy dipole radiation from resonance neutron capture in 105Pd". In: *Nuclear Physics A* vol. 170, no. 1 (July 1971), pp. 153–176. DOI: 10.1016/0375-9474(71)90689-0.

[48] Wasson, O. A., Chrien, R. E., Slaughter, G. G., and Harvey, J. A. "Distribution of Partial Radiation Widths in $^{238}\mathrm{U}(n,\gamma)^{239}\mathrm{U}$". In: *Physical Review C* vol. 4, no. 3 (Sept. 1971), pp. 900–912. DOI: 10.1103/physrevc.4.900.

[49] Garg, J. B., Tikku, V. K., Harvey, J. A., Macklin, R. L., and Halperin, J. "Statistical properties of complex states of $^{67}_{30}\mathrm{Zn}$". In: *Physical Review C* vol. 24, no. 5 (Nov. 1981), pp. 1922–1939. DOI: 10.1103/physrevc.24.1922.

[50] Weidenmüller, H. A. and Mitchell, G. E. "Random matrices and chaos in nuclear physics: Nuclear structure". In: *Reviews of Modern Physics* vol. 81, no. 2 (May 2009), pp. 539–589. DOI: 10.1103/revmodphys.81.539.

[51] Koehler, P. E., Reifarth, R., Ullmann, J. L., Bredeweg, T. A., O'Donnell, J. M., Rundberg, R. S., Vieira, D. J., and Wouters, J. M. "Abrupt Change in Radiation-Width Distribution for ^{147}Sm Neutron Resonances". In: *Physical Review Letters* vol. 108, no. 14 (Apr. 2012). DOI: 10.1103/physrevlett.108.142502.

[52] Koehler, P. E., Larsen, A. C., Guttormsen, M., Siem, S., and Guber, K. H. "Extreme nonstatistical effects in γ decay of 95Mo neutron resonances". In: *Physical Review C* vol. 88, no. 4 (Oct. 2013). DOI: 10.1103/physrevc.88.041305.

[53] Fanto, P., Alhassid, Y., and Weidenmüller, H. A. "Statistical-model description of γ decay from compound-nucleus resonances". In: *Physical Review C* vol. 101, no. 1 (Jan. 2020). DOI: 10.1103/physrevc.101.014607.

[54] Brink, D. M. "Some Aspects of the Interaction of Fields with Matter". PhD thesis. University of Oxford, 1955. URL: https://ora.ox.ac.uk/objects/uuid:334ec4a3-8a89-42aa-93f4-2e54d070ee090.

[55] Hughes, D. J. and Harvey, J. A. "Radiation-Widths of Nuclear Energy-Levels". In: *Nature* vol. 173, no. 4411 (May 1954), pp. 942–943. DOI: 10.1038/173942a0.

[56] Bečvář, F. "Simulation of γ cascades in complex nuclei with emphasis on assessment of uncertainties of cascade-related quantities". In: *Nuclear Instruments and Methods in Physics Research Section A: Accelerators, Spectrometers, Detectors and Associated Equipment* vol. 417, no. 2-3 (Nov. 1998), pp. 434–449. DOI: 10.1016/s0168-9002(98)00787-6.

[57] Kirsch, L. and Bernstein, L. "RAINIER: A simulation tool for distributions of excited nuclear states and cascade fluctuations". In: *Nuclear Instruments and Methods in Physics Research Section A: Accelerators, Spectrometers, Detectors and Associated Equipment* vol. 892 (June 2018), pp. 30–40. DOI: 10.1016/j.nima.2018.02.096.

[58] Johnson, C. W. "Systematics of strength function sum rules". In: *Physics Letters B* vol. 750 (Nov. 2015), pp. 72–75. DOI: 10.1016/j.physletb.2015.08.054.

[59] Renstrøm, T., Utsunomiya, H., Nyhus, H. T., Larsen, A. C., Guttormsen, M., Tveten, G. M., Filipescu, D. M., Gheorghe, I., Goriely, S., Hilaire, S., Lui, Y.-W., Midtbø, J. E., Péru, S., Shima, T., Siem, S., and Tesileanu, O. "Verification of detailed balance for γ absorption and emission in Dy isotopes". In: *Physical Review C* vol. 98, no. 5 (Nov. 2018). DOI: 10.1103/physrevc.98.054310.

[60] Guttormsen, M., Larsen, A. C., Görgen, A., Renstrøm, T., Siem, S., Tornyi, T. G., and Tveten, G. M. "Validity of the Generalized Brink-Axel Hypothesis in ^{238}Np". In: *Physical Review Letters* vol. 116, no. 1 (Jan. 2016). DOI: 10.1103/physrevlett.116.012502.

[61] Crespo Campo, L., Guttormsen, M., Bello Garrote, F. L., Eriksen, T. K., Giacoppo, F., Görgen, A., Hadynska-Klek, K., Klintefjord, M., Larsen, A. C., Renstrøm, T., Sahin, E., Siem, S., Springer, A., Tornyi, T. G., and Tveten, G. M. "Test of the generalized Brink-Axel hypothesis in ^{64,65}Ni". In: *Physical Review C* vol. 98, no. 5 (Nov. 2018). DOI: 10.1103/physrevc.98.054303.

[62] Krtička, M., Bečvář, F., Honzátko, J., Tomandl, I., Heil, M., Käppeler, F., Reifarth, R., Voss, F., and Wisshak, K. "Evidence for M1 Scissors Resonances Built on the Levels in the Quasicontinuum of ^{163}Dy". In: *Physical Review Letters* vol. 92, no. 17 (Apr. 2004). DOI: 10.1103/physrevlett.92.172501.

[63] Valenta, S., Baramsai, B., Bredeweg, T. A., Couture, A., Chyzh, A., Jandel, M., Kroll, J., Krtička, M., Mitchell, G. E., O'Donnell, J. M., Rusev, G., Ullmann, J. L., and Walker, C. L. "Examination of photon strength functions for ^{162,164}Dy from radiative capture of resonance neutrons". In: *Physical Review C* vol. 96, no. 5 (Nov. 2017). DOI: 10.1103/physrevc.96.054315.

[64] Martin, D. et al. "Test of the Brink-Axel Hypothesis for the Pygmy Dipole Resonance". In: *Physical Review Letters* vol. 119, no. 18 (Nov. 2017). DOI: 10.1103/physrevlett.119.182503.

[65] Bečvář, F., Cejnar, P., Chrien, R. E., and Kopecký, J. "Test of photon strength functions by a method of two-step cascades". In: *Physical Review C* vol. 46, no. 4 (Oct. 1992), pp. 1276–1287. DOI: 10.1103/physrevc.46.1276.

[66] Kopecky, J. and Chrien, R. "Observation of the $M1$ giant resonance by resonance averaging in ^{106}Pd". In: *Nuclear Physics A* vol. 468, no. 2 (1987), pp. 285–300. DOI: 10.1016/0375-9474(87)90518-5.

[67] Angell, C. T., Hammond, S. L., Karwowski, H. J., Kelley, J. H., Krtička, M., Kwan, E., Makinaga, A., and Rusev, G. "Evidence for radiative coupling of the pygmy dipole resonance to excited states". In: *Physical Review C* vol. 86, no. 5 (Nov. 2012). DOI: 10.1103/physrevc.86.051302.

[68] Isaak, J., Savran, D., Löher, B., Beck, T., Bhike, M., Gayer, U., Krishichayan, Pietralla, N., Scheck, M., Tornow, W., Werner, V., Zilges, A., and Zweidinger, M. "The concept of nuclear photon strength functions: A model-independent approach via ($\vec{\gamma}$,γ'γ") reactions". In: *Physics Letters B* vol. 788 (Jan. 2019), pp. 225–230. DOI: 10.1016/j.physletb.2018.11.038.

[69] Goriely, S., Dimitriou, P., Wiedeking, M., Belgya, T., Firestone, R., Kopecky, J., Krtička, M., Plujko, V., Schwengner, R., Siem, S., Utsunomiya, H., Hilaire, S., Péru, S., Cho, Y. S., Filipescu, D. M., Iwamoto, N., Kawano, T., Varlamov, V., and Xu, R. "Reference database for photon strength functions". In: *The European Physical Journal A* vol. 55, no. 10 (Oct. 2019), p. 172. DOI: 10.1140/epja/i2019-12840-1.

[70] Bassauer, S., Neumann-Cosel, P. von, and Tamii, A. "γ strength function and level density of Pb208 from forward-angle proton scattering at 295 MeV". In: *Physical Review C* vol. 94, no. 5 (Nov. 2016). DOI: 10.1103/physrevc.94.054313.

[71] Kinsey, B. B. and Bartholomew, G. A. "Dipole and Quadrupole Transition Probabilities in Neutron-Capture Gamma Radiation". In: *Physical Review* vol. 93, no. 6 (Mar. 1954), pp. 1260–1278. DOI: 10.1103/physrev.93.1260.

[72] Kopecky, J. *Quadrupole radiation strength in neutron capture*. Tech. rep. ECN–99. Netherlands, 1981, p. 24. URL: https://inis.iaea.org/search/search.aspx?orig_q=RN:13649709 (visited on 10/26/2020).

[73] Chrien, R. and Kopecky, J. "The nuclear structure of 239U". In: *Nuclear Physics A* vol. 414, no. 2 (Feb. 1984), pp. 281–300. DOI: 10.1016/0375-9474(84)90645-6.

[74] Winter, C. and Lieb, K. P. "Strength functions of primary transitions following thermal neutron capture in strontium". In: *Zeitschrift für Physik A - Atomic Nuclei* vol. 332, no. 4 (Dec. 1989), pp. 397–405. DOI: 10.1007/bf01292425.

[75] Vennink, R., Kopecky, J., Endt, P., and Glaudemans, P. "Investigation of the 56Fe(n,γ)57Fe and 58Fe(n,γ)59Fe reactions". In: *Nuclear Physics A* vol. 344, no. 3 (Aug. 1980), pp. 421–445. DOI: 10.1016/0375-9474(80)90400-5.

[76] Jones, M. D. et al. "Examination of the low-energy enhancement of the γ -ray strength function of Fe56". In: *Physical Review C* vol. 97, no. 2 (Feb. 2018). DOI: 10.1103/physrevc.97.024327.

[77] Rusev, G., Tsoneva, N., Dönau, F., Frauendorf, S., Schwengner, R., Tonchev, A. P., Adekola, A. S., Hammond, S. L., Kelley, J. H., Kwan, E., Lenske, H., Tornow, W., and Wagner, A. "Fine Structure of the Giant $M1$ Resonance in ^{90}Zr". In: *Physical Review Letters* vol. 110, no. 2 (Jan. 2013). DOI: 10.1103/physrevlett.110.022503.

[78] Larsen, A. C., Blasi, N., Bracco, A., Camera, F., Eriksen, T. K., Görgen, A., Guttormsen, M., Hagen, T. W., Leoni, S., Million, B., Nyhus, H. T., Renstrøm, T., Rose, S. J., Ruud, I. E., Siem, S., Tornyi, T., Tveten, G. M., Voinov, A. V., and Wiedeking, M. "Evidence for the Dipole Nature of the Low-Energy γ Enhancement in ^{56}Fe". In: *Physical Review Letters* vol. 111, no. 24 (Dec. 2013). DOI: 10.1103/physrevlett.111.242504.

[79] Larsen, A. C. et al. "Low-energy enhancement and fluctuations of γ-ray strength functions in ^{56,57}Fe: test of the Brink–Axel hypothesis". In: *Journal of Physics G: Nuclear and Particle Physics* vol. 44, no. 6 (Apr. 2017), p. 064005. DOI: 10.1088/1361-6471/aa644a.

[80] Simon, A., Guttormsen, M., Larsen, A. C., Beausang, C. W., Humby, P., Burke, J. T., Casperson, R. J., Hughes, R. O., Ross, T. J., Allmond, J. M., Chyzh, R., Dag, M., Koglin, J., McCleskey, E., McCleskey, M., Ota, S., and Saastamoinen, A. "First observation of low-energy γ-ray enhancement in the rare-earth region". In: *Physical Review C* vol. 93, no. 3 (Mar. 2016). DOI: 10.1103/physrevc.93.034303.

[81] Steinwedel, H. and Jensen, J. H. D. "Hydrodynamik von Kerndipolschwingungen". In: *Z. Naturfoschg.* Vol. 5a (1950), p. 413.

[82] Plujko, V. A., Kadenko, I. M., Gorbachenko, O. M., and Kulich, E. V. "The Simplified Description Of Dipole Radiative Strength Function". In: *International Journal of Modern Physics E* vol. 17, no. 01 (Jan. 2008), pp. 240–244. DOI: 10.1142/s0218301308009744.

[83] Kopecky, J. and Uhl, M. "Test of gamma-ray strength functions in nuclear reaction model calculations". In: *Physical Review C* vol. 41, no. 5 (May 1990), pp. 1941–1955. DOI: 10.1103/physrevc.41.1941.

[84] Kopecky, J., Goriely, S., Péru, S., Hilaire, S., and Martini, M. "E1 and M1 strength functions from average resonance capture data". In: *Phys. Rev. C* vol. 95 (5 May 2017), p. 054317. DOI: 10.1103/PhysRevC.95.054317.

[85] Kadmenskiı, S., Markushev, V., and Furman, V. "Radiative width of neutron resonances. Giant dipole resonances". In: *Sov. J. Nucl. Phys.* Vol. 37 (1983). Yadernaya Fizika v. 37(2); p. 277-283, p. 165.

[86] Kopecky, J. and Uhl, M. "Calculations of Capture Cross Sections and Gamma-Ray Spectra with Different Strength Function Models". In: American Institute of Physics, 1991. DOI: 10.1063/1.41227.

[87] Mughabghab, S. and Dunford, C. "A dipole–quadrupole interaction term in E1 photon transitions". In: *Physics Letters B* vol. 487, no. 1-2 (Aug. 2000), pp. 155–164. DOI: 10.1016/s0370-2693(00)00792-9.

[88] Plujko, V. "An investigation of interplay between dissipation mechanisms in heated Fermi systems by means of radiative strength functions". In: *Nuclear Physics A* vol. 649, no. 1-4 (Mar. 1999), pp. 209–213. DOI: 10.1016/s0375-9474(99)00063-9.

[89] Plujko, V. A. "A new closed-form thermodynamic approach for radiative strength functions". In: *AcPPB* vol. 31, no. 2 (2000), p. 435.

[90] Plujko, V. A., Ezhov, S., Kavatsyuk, M., Grebenyuk, A., and Yermolenko, R. "Testing and Improvements of Gamma-Ray Strength Functions for Nuclear Model Calculations". In: *Journal of Nuclear Science and Technology* vol. 39, no. sup2 (Aug. 2002), pp. 811–814. DOI: 10.1080/00223131.2002.10875222.

[91] Popov, Y. P. "Decay of highly excited states by α-particle emission". In: *Physics and Applications (Proc. Europhysics Topical Conference, Smolenice, 1982) vol.* Vol. 10. 1982.

[92] Szeflíński, Z., Szeflińska, G., Wilhelmi, Z., Rząca-Urban, T., Klapdor, H., Anderson, E., Grotz, K., and Metzinger, J. "Experimental test of the brink hypothesis". In: *Physics Letters B* vol. 126, no. 3-4 (June 1983), pp. 159–163. DOI: 10.1016/0370-2693(83)90582-8.

[93] Weisskopf, V. F. "Radiative Transition Probabilities in Nuclei". In: *Physical Review* vol. 83, no. 5 (Sept. 1951), pp. 1073–1073. DOI: 10.1103/physrev.83.1073.

[94] Bohr, A. and Mottelson, B. R. *Nuclear structure: 1 : Single-particle motion*. eng. Vol. 1. New York: Benjamin, 1969.

[95] Greiner, W. and Maruhn, J. A. *Nuclear Models*. Springer Berlin Heidelberg, 1996. DOI: 10.1007/978-3-642-60970-1.

[96] Simbirtseva, N., Krtička, M., Casten, R. F., Couture, A., Furman, W. I., Knapová, I., O'Donnell, J. M., Rusev, G., Ullmann, J. L., and Valenta, S. "Examination of photon strength functions and nuclear level density in Pt196 from the γ -ray spectra measured at the DANCE facility". In: *Physical Review C* vol. 101, no. 2 (Feb. 2020). DOI: 10.1103/physrevc.101.024302.

[97] Plompen, A. J. M. et al. "The joint evaluated fission and fusion nuclear data library, JEFF-3.3". In: *The European Physical Journal A* vol. 56, no. 7 (July 2020). DOI: 10.1140/epja/s10050-020-00141-9.

[98] Shibata, K., Iwamoto, O., Nakagawa, T., Iwamoto, N., Ichihara, A., Kunieda, S., Chiba, S., Furutaka, K., Otuka, N., Ohasawa, T., and al., et. "JENDL-4.0: A New Library for Nuclear Science and Engineering". In: *Journal of Nuclear Science and Technology* vol. 48, no. 1 (Jan. 2011), pp. 1–30. DOI: 10.1080/18811248.2011.9711675.

[99] *Handbook for Calculations of Nuclear Reaction Data Reference Input Parameter Library*. Tech. rep. IAEA-TECDOC-1034. Vienna, 1998. URL: https://www.iaea.org/publications/5331/handbook-for-calculations-of-nuclear-reaction-data-reference-input-parameter-library.

[100] Goriely, S., Khan, E., and Samyn, M. "Microscopic HFB + QRPA predictions of dipole strength for astrophysics applications". In: *Nuclear Physics A* vol. 739, no. 3-4 (July 2004), pp. 331–352. DOI: 10.1016/j.nuclphysa.2004.04.105.

[101] Goriely, S., Hilaire, S., Péru, S., Martini, M., Deloncle, I., and Lechaftois, F. "Gogny-Hartree-Fock-Bogolyubov plus quasiparticle random-phase approximation predictions of the M1 strength function and its impact on radiative neutron capture cross section". In: *Physical Review C* vol. 94, no. 4 (Oct. 2016). DOI: 10.1103/physrevc.94.044306.

[102] Goeppert Mayer, M. "On Closed Shells in Nuclei". In: *Physical Review* vol. 74, no. 3 (Aug. 1948), pp. 235–239. DOI: 10.1103/physrev.74.235.

[103] Goeppert Mayer, M. "On Closed Shells in Nuclei. II". In: *Physical Review* vol. 75, no. 12 (June 1949), pp. 1969–1970. DOI: 10.1103/physrev.75.1969.

[104] Haxel, O., Jensen, J. H. D., and Suess, H. E. “On the "Magic Numbers" in Nuclear Structure”. In: *Physical Review* vol. 75, no. 11 (June 1949), pp. 1766–1766. DOI: 10.1103/physrev.75.1766.2.

[105] Caurier, E., Martınez-Pinedo, G., Nowacki, F., Poves, A., and Zuker, A. P. “The shell model as a unified view of nuclear structure”. In: *Reviews of Modern Physics* vol. 77, no. 2 (June 2005), pp. 427–488. DOI: 10.1103/revmodphys.77.427.

[106] Lanczos, C. “An iteration method for the solution of the eigenvalue problem of linear differential and integral operators”. In: *Journal of Research of the National Bureau of Standards* vol. 45, no. 4 (Oct. 1950), p. 255. DOI: 10.6028/jres.045.026.

[107] Otsuka, T., Honma, M., Mizusaki, T., Shimizu, N., and Utsuno, Y. “Monte Carlo shell model for atomic nuclei”. In: *Progress in Particle and Nuclear Physics* vol. 47, no. 1 (Jan. 2001), pp. 319–400. DOI: 10.1016/s0146-6410(01)00157-0.

[108] Togashi, T., Tsunoda, Y., Otsuka, T., Shimizu, N., and Honma, M. “Novel Shape Evolution in Sn Isotopes from Magic Numbers 50 to 82”. In: *Physical Review Letters* vol. 121, no. 6 (Aug. 2018). DOI: 10.1103/physrevlett.121.062501.

[109] Schwengner, R., Frauendorf, S., and Larsen, A. C. “Low-Energy Enhancement of Magnetic Dipole Radiation”. In: *Physical Review Letters* vol. 111, no. 23 (Dec. 2013). DOI: 10.1103/physrevlett.111.232504.

[110] Schwengner, R. et al. “Electric and magnetic dipole strength in Fe54”. In: *Physical Review C* vol. 101, no. 6 (June 2020). DOI: 10.1103/physrevc.101.064303.

[111] Brown, B. A. and Larsen, A. C. “Large Low-Energy $M1$ Strength for Fe56,57 within the Nuclear Shell Model”. In: *Physical Review Letters* vol. 113, no. 25 (Dec. 2014). DOI: 10.1103/physrevlett.113.252502.

[112] Brown, B. and Rae, W. “The Shell-Model Code NuShellX@MSU”. In: *Nuclear Data Sheets* vol. 120 (June 2014), pp. 115–118. DOI: 10.1016/j.nds.2014.07.022.

[113] Brown, B. A. “The Nuclear Configuration Interations Method”. In: *Springer Proceedings in Physics*. Springer International Publishing, 2019, pp. 3–31. DOI: 10.1007/978-3-030-22204-8_1.

[114] Midtbø, J. E., Larsen, A. C., Renstrøm, T., Garrote, F. L. B., and Lima, E. “Consolidating the concept of low-energy magnetic dipole decay radiation”. In: *Physical Review C* vol. 98, no. 6 (Dec. 2018). DOI: 10.1103/physrevc.98.064321.

[115] Larsen, A. C. et al. “Enhanced low-energy γ-decay strength of Ni70 and its robustness within the shell model”. In: *Physical Review C* vol. 97, no. 5 (May 2018). DOI: 10.1103/physrevc.97.054329.

[116] Koonin, S., Dean, D., and Langanke, K. "Shell model Monte Carlo methods". In: *Physics Reports* vol. 278, no. 1 (Jan. 1997), pp. 1–77. DOI: 10.1016/s0370-1573(96)00017-8.

[117] Alhassid, Y. "Quantum Monte Carlo Methods For Nuclei At Finite Temperature". In: *International Journal of Modern Physics B* vol. 15, no. 10n11 (May 2001), pp. 1447–1462. DOI: 10.1142/s0217979201005945.

[118] Alhassid, Y., Fang, L., and Nakada, H. "Heavy Deformed Nuclei in the Shell Model Monte Carlo Method." In: *Physical Review Letters* vol. 101, no. 8 (Aug. 2008). DOI: 10.1103/physrevlett.101.082501.

[119] Alhassid, Y., Fang, L., and Nakada, H. "Shell model Monte Carlo approach: the heavy nuclei". In: *Journal of Physics: Conference Series* vol. 267 (Jan. 2011), p. 012033. DOI: 10.1088/1742-6596/267/1/012033.

[120] Alhassid, Y., Bonett-Matiz, M., Liu, S., and Nakada, H. "Direct microscopic calculation of nuclear level densities in the shell model Monte Carlo approach". In: *Physical Review C* vol. 92, no. 2 (Aug. 2015). DOI: 10.1103/physrevc.92.024307.

[121] Alhassid, Y. "The shell model Monte Carlo approach to level densities: Recent developments and perspectives". In: *The European Physical Journal A* vol. 51, no. 12 (Dec. 2015). DOI: 10.1140/epja/i2015-15171-3.

[122] Demetriou, P. and Goriely, S. "Microscopic nuclear level densities for practical applications". In: *Nuclear Physics A* vol. 695, no. 1-4 (Dec. 2001), pp. 95–108. DOI: 10.1016/s0375-9474(01)01095-8.

[123] Hilaire, S. and Goriely, S. "Global microscopic nuclear level densities within the HFB plus combinatorial method for practical applications". In: *Nuclear Physics A* vol. 779 (Nov. 2006), pp. 63–81. DOI: 10.1016/j.nuclphysa.2006.08.014.

[124] Hilaire, S., Delaroche, J. P., and Girod, M. "Combinatorial nuclear level densities based on the Gogny nucleon-nucleon effective interaction". In: *The European Physical Journal A* vol. 12, no. 2 (Oct. 2001), pp. 169–184. DOI: 10.1007/s100500170025.

[125] Hilaire, S., Delaroche, J., and Koning, A. "Generalized particle-hole state densities within the equidistant spacing model". In: *Nuclear Physics A* vol. 632, no. 3 (Mar. 1998), pp. 417–441. DOI: 10.1016/s0375-9474(98)00003-7.

[126] Goriely, S., Hilaire, S., Girod, M., and Péru, S. "First Gogny-Hartree-Fock-Bogoliubov Nuclear Mass Model". In: *Physical Review Letters* vol. 102, no. 24 (June 2009). DOI: 10.1103/physrevlett.102.242501.

[127] Goriely, S. "Nuclear Reaction Data Relevant to Nuclear Astrophysics". In: *Journal of Nuclear Science and Technology* vol. 39, no. sup2 (Aug. 2002), pp. 536–541. DOI: 10.1080/00223131.2002.10875157.

[128] Goriely, S. and Khan, E. “Large-scale QRPA calculation of E1-strength and its impact on the neutron capture cross section”. In: *Nuclear Physics A* vol. 706, no. 1-2 (July 2002), pp. 217–232. DOI: 10.1016/s0375-9474(02)00860-6.

[129] Martini, M., Péru, S., Hilaire, S., Goriely, S., and Lechaftois, F. “Large-scale deformed quasiparticle random-phase approximation calculations of theγ-ray strength function using the Gogny force”. In: *Physical Review C* vol. 94, no. 1 (July 2016). DOI: 10.1103/physrevc.94.014304.

[130] Kamerdzhiev, S., Speth, J., and Tertychny, G. “Extended theory of finite Fermi systems: collective vibrations in closed shell nuclei”. In: *Physics Reports* vol. 393, no. 1 (Mar. 2004), pp. 1–86. DOI: 10.1016/j.physrep.2003.11.001.

[131] Avdeenkov, A., Goriely, S., Kamerdzhiev, S., and Krewald, S. “Self-consistent calculations of the strength function and radiative neutron capture cross section for stable and unstable tin isotopes”. In: *Physical Review C* vol. 83, no. 6 (June 2011). DOI: 10.1103/physrevc.83.064316.

[132] Achakovskiy, O. I., Kamerdzhiev, S. P., and Tselyaev, V. I. “Radiative strength function and the pygmy dipole resonance in 208Pb and 70Ni”. In: *JETP Letters* vol. 104, no. 6 (Sept. 2016), pp. 374–379. DOI: 10.1134/s0021364016180053.

[133] Tselyaev, V. I. “Quasiparticle time blocking approximation within the framework of generalized Green function formalism”. In: *Physical Review C* vol. 75, no. 2 (Feb. 2007). DOI: 10.1103/physrevc.75.024306.

[134] Kawano, T. et al. “IAEA Photonuclear Data Library 2019”. In: *Nuclear Data Sheets* vol. 163 (Jan. 2020), pp. 109–162. DOI: 10.1016/j.nds.2019.12.002.

[135] Huizenga, J. R. and Moretto, L. G. “Nuclear Level Densities”. In: *Annual Review of Nuclear Science* vol. 22, no. 1 (Dec. 1972), pp. 427–464. DOI: 10.1146/annurev.ns.22.120172.002235.

[136] Richter, A. In: *Proceedings of the International Conference on Nuclear Physics, Florence, 1983*. Ed. by Blasi, P. and Ricci, R. A. Vol. 2. Tipografia Compositori, 1983.

[137] Box, G. E. and Draper, N. R. *Empirical model-building and response surfaces*. eng. Wiley series in probability and mathematical statistics. Applied probability and statistics. New York: Wiley, 1987.

[138] Bothe, W. and Gentner, W. “Atomumwandlungen durch γ-Strahlen”. In: *Zeitschrift für Physik* vol. 106, no. 3-4 (Mar. 1937), pp. 236–248. DOI: 10.1007/bf01340320.

[139] Baldwin, G. C. and Klaiber, G. S. “Photo-Fission in Heavy Elements”. In: *Physical Review* vol. 71, no. 1 (Jan. 1947), pp. 3–10. DOI: 10.1103/physrev.71.3.

[140] Goldhaber, M. and Teller, E. "On Nuclear Dipole Vibrations". In: *Physical Review* vol. 74, no. 9 (Nov. 1948), pp. 1046–1049. DOI: 10.1103/physrev.74.1046.

[141] Krtička, M., Bečvář, F., Tomandl, I., Rusev, G., Agvaanluvsan, U., and Mitchell, G. E. "Two-step γ cascades following thermal neutron capture in ^{95}Mo". In: *Phys. Rev. C* vol. 77 (5 May 2008), p. 054319. DOI: 10.1103/PhysRevC.77.054319.

[142] Krtička, M. and Bečvář, F. "What do we really know about photon strength functions?" In: *Journal of Physics G: Nuclear and Particle Physics* vol. 35, no. 1 (Dec. 2007), p. 014025. DOI: 10.1088/0954-3899/35/1/014025.

[143] Sheets, S. A., Agvaanluvsan, U., Becker, J. A., Bečvář, F., Bredeweg, T. A., Haight, R. C., Jandel, M., Krtička, M., Mitchell, G. E., O'Donnell, J. M., Parker, W., Reifarth, R., Rundberg, R. S., Sharapov, E. I., Ullmann, J. L., Vieira, D. J., Wilhelmy, J. B., Wouters, J. M., and Wu, C. Y. "Test of the statistical model in Mo96 with the BaF2 γ calorimeter DANCE array". In: *Physical Review C* vol. 79, no. 2 (Feb. 2009). DOI: 10.1103/physrevc.79.024301.

[144] Wiedeking, M., Bernstein, L. A., Krtička, M., Bleuel, D. L., Allmond, J. M., Basunia, M. S., Burke, J. T., Fallon, P., Firestone, R. B., Goldblum, B. L., Hatarik, R., Lake, P. T., Lee, I.-Y., Lesher, S. R., Paschalis, S., Petri, M., Phair, L., and Scielzo, N. D. "Low-Energy Enhancement in the Photon Strength of Mo95". In: *Physical Review Letters* vol. 108, no. 16 (Apr. 2012). DOI: 10.1103/physrevlett.108.162503.

[145] Midtbø, J. E. "The low-energy enhancement. An experimental and theoretical study of nuclear level densities and γ-ray strength functions". PhD thesis. University of Oslo, 2019. URL: http://urn.nb.no/URN:NBN:no-79895.

[146] Ingeberg, V. W. et al. "First application of the Oslo method in inverse kinematics". In: *The European Physical Journal A* vol. 56, no. 2 (Feb. 2020). DOI: 10.1140/epja/s10050-020-00070-7.

[147] Spyrou, A., Liddick, S. N., Larsen, A. C., Guttormsen, M., Cooper, K., Dombos, A. C., Morrissey, D. J., Naqvi, F., Perdikakis, G., Quinn, S. J., and al., et. "Novel technique for Constraining r-Process (n, γ) Reaction Rates". In: *Physical Review Letters* vol. 113, no. 23 (Dec. 2014). DOI: 10.1103/physrevlett.113.232502.

[148] Guttormsen, M., Ramsøy, T., and Rekstad, J. "The first generation of γ-rays from hot nuclei". In: *Nucl. Instrum. Methods Phys. Res. A* vol. 255, no. 3 (Apr. 1987), pp. 518–523. DOI: 10.1016/0168-9002(87)91221-6.

[149] Bohr, N. "Neutron Capture and Nuclear Constitution". In: vol. 137 (1936), pp. 344–348. DOI: 10.1038/137344a0.

[150] Guttormsen, M., Chankova, R., Agvaanluvsan, U., Algin, E., Bernstein, L. A., Ingebretsen, F., Lönnroth, T., Messelt, S., Mitchell, G. E., Rekstad, J., and al., et. "Radiative strength functions in $^{93-98}$Mo". In: *Physical Review C* vol. 71, no. 4 (Apr. 2005). DOI: 10.1103/physrevc.71.044307.

[151] Guttormsen, M., Bagheri, A., Chankova, R., Rekstad, J., Siem, S., Schiller, A., and Voinov, A. "Thermal properties and radiative strengths in ^{160,161,162}Dy". In: *Physical Review C* vol. 68, no. 6 (Dec. 2003). DOI: 10.1103/physrevc.68.064306.

[152] Agvaanluvsan, U., Schiller, A., Becker, J. A., Bernstein, L. A., Garrett, P. E., Guttormsen, M., Mitchell, G. E., Rekstad, J., Siem, S., Voinov, A., and al., et. "Level densities and γ-ray strength functions in ^{170,171,172}Y". In: *Physical Review C* vol. 70, no. 5 (Nov. 2004). DOI: 10.1103/physrevc.70.054611.

[153] Guttormsen, M., Bernstein, L. A., Görgen, A., Jurado, B., Siem, S., Aiche, M., Ducasse, Q., Giacoppo, F., Gunsing, F., Hagen, T. W., and al., et. "Scissors resonance in the quasicontinuum of Th, Pa, and U isotopes". In: *Phys. Rev. C* vol. 89, no. 1 (Jan. 2014), p. 014302. DOI: 10.1103/physrevc.89.014302.

[154] Tornyi, T. G., Guttormsen, M., Eriksen, T. K., Görgen, A., Giacoppo, F., Hagen, T. W., Krasznahorkay, A., Larsen, A. C., Renstrøm, T., Rose, S. J., Siem, S., and Tveten, G. M. "Level density and γ-ray strength function in the odd-odd ^{238}Np nucleus". In: *Phys. Rev. C* vol. 89, no. 4 (Apr. 2014), p. 044323. DOI: 10.1103/physrevc.89.044323.

[155] Laplace, T. A., Zeiser, F., Guttormsen, M., Larsen, A. C., Bleuel, D. L., Bernstein, L. A., Goldblum, B. L., Siem, S., Bello Garrote, F. L., Brown, J. A., and al., et. "Statistica properties of ^{243}Pu, and ^{242}Pu(n,γ) cross section calculation". In: *Physical Review C* vol. 93, no. 1 (Jan. 2016), p. 014323. DOI: 10.1103/physrevc.93.014323.

[156] Belgya, T., Szentmiklósi, L., Massarczyk, R., Schwengner, R., Junghans, A. R., and Grosse, E. "High-resolution study of the 113Cd(n,γ) spectrum by statistical decay model with discrete levels and transitions". In: *EPJ Web of Conferences* vol. 146 (2017). Ed. by Plompen, A., Hambsch, F.-J., Schillebeeckx, P., Mondelaers, W., Heyse, J., Kopecky, S., Siegler, P., and Oberstedt, S., p. 05009. DOI: 10.1051/epjconf/201714605009.

[157] Massarczyk, R., Schramm, G., Belgya, T., Schwengner, R., Beyer, R., Bemmerer, D., Elekes, Z., Grosse, E., Hannaske, R., Junghans, A. R., Kis, Z., Kögler, T., Lorenz, C., Schmidt, K., Szentmiklósi, L., Wagner, A., and Weil, J. L. "Role of electric and magnetic dipole strength functions in the ^{114}Cd(γ,γ') and ^{113}Cd(n,γ) reactions". In: *Phys. Rev. C* vol. 93 (1 Jan. 2016), p. 014301. DOI: 10.1103/PhysRevC.93.014301.

[158] Honzátko, J., Konečný, K., Tomandl, I., Vacík, J., Bečvář, F., and Cejnar, P. "Facility and method for studying two-step γ cascades in thermal neutron capture". In: *Nuclear Instruments and Methods in Physics Research Section A: Accelerators, Spectrometers, Detectors and Associated Equipment* vol. 376, no. 3 (July 1996), pp. 434–442. DOI: 10.1016/0168-9002(96)81753-0.

[159] Krtička, M., Goriely, S., Hilaire, S., Péru, S., and Valenta, S. "Constraints on the dipole photon strength functions from experimental multistep cascade spectra". In: *Physical Review C* vol. 99, no. 4 (Apr. 2019). DOI: 10.1103/physrevc.99.044308.

[160] Jandel, M., Bredeweg, T., Couture, A., Fowler, M., Bond, E., Chadwick, M., Clement, R., Esch, E.-I., O'Donnell, J., Reifarth, R., Rundberg, R., Ullmann, J., Vieira, D., Wilhelmy, J., Wouters, J., Macri, R., Wu, C., and Becker, J. "GEANT4 simulations of the DANCE array". In: *Nuclear Instruments and Methods in Physics Research Section B: Beam Interactions with Materials and Atoms* vol. 261, no. 1-2 (Aug. 2007), pp. 1117–1121. DOI: 10.1016/j.nimb.2007.04.252.

[161] Walker, C. L., Krtička, M., Baramsai, B., Bečvář, F., Bredeweg, T. A., Chyzh, A., Haight, R. C., Jandel, M., Kroll, J., Mitchell, G. E., O'Donnell, J. M., Rundberg, R. S., Ullmann, J. L., Valenta, S., and Wilhelmy, J. B. "Measurement of the ^{97}Mo(n,γ) reaction with the DANCE γ calorimeter array". In: *Phys. Rev. C* vol. 92 (1 July 2015), p. 014324. DOI: 10.1103/PhysRevC.92.014324.

[162] Kneissl, U., Pitz, H., and Zilges, A. "Investigation of nuclear structure by resonance fluorescence scattering". In: *Progress in Particle and Nuclear Physics* vol. 37 (Jan. 1996), pp. 349–433. DOI: 10.1016/0146-6410(96)00055-5.

[163] Berg, U. E. P. and Kneissl, U. "Recent Progress on Nuclear Magnetic Dipole Excitations". In: *Annual Review of Nuclear and Particle Science* vol. 37, no. 1 (Dec. 1987), pp. 33–69. DOI: 10.1146/annurev.ns.37.120187.000341.

[164] Metzger, F. R. "Resonance fluorescence in nuclei". In: *Prog Nucl Phys* vol. 7 (1959), pp. 54–88.

[165] Pietralla, N., Isaak, J., and Werner, V. "Photonuclear reactions: Achievements and perspectives". In: *The European Physical Journal A* vol. 55, no. 12 (Dec. 2019). DOI: 10.1140/epja/i2019-12857-4.

[166] Isaak, J. "Investigation of Decay Properties of the Pygmy Dipole Resonance and Photon Strength Functions on Excited States in $(\gamma,\gamma'\gamma'')$ Reactions". PhD thesis. Universitätsbibliothek Mainz, 2016.

[167] Agostinelli, S. et al. "Geant4—a simulation toolkit". In: *Nuclear Instruments and Methods in Physics Research Section A: Accelerators, Spectrometers, Detectors and Associated Equipment* vol. 506, no. 3 (July 2003), pp. 250–303. DOI: 10.1016/s0168-9002(03)01368-8.

[168] Massarczyk, R. et al. “Electromagnetic dipole strength of136Ba below the neutron separation energy”. In: *Physical Review C* vol. 86, no. 1 (July 2012). DOI: 10.1103/physrevc.86.014319.

[169] Löher, B. “Probing the decay characteristics of the Pygmy Dipole Resonance in the semi-magic nucleus 140Ce with γ–γ coincidence measurements”. PhD thesis. Johannes Gutenberg-Universität Mainz, 2014. URL: https://openscience.ub.uni-mainz.de/handle/20.500.12030/2863.

[170] Mughabghab, S. F. *Atlas of neutron resonances : resonance parameters and thermal cross sections Z=1-100*. Vol. 6th Edition. Amsterdam: Elsevier, 2018.

[171] Midtbø, J. E., Zeiser, F., Lima, E., Larsen, A.-C., Tveten, G. M., Guttormsen, M., Bello Garrote, F. L., Kvellestad, A., and Renstrøm, T. “A new software implementation of the Oslo method with rigorous statistical uncertainty propagation”. In: (2020). arXiv: 1904.13248 [physics.comp-ph].

[172] Bollinger, L. M. “Gamma Rays From Neutron Capture In Resonances”. In: *Experimental Neutron Resonance Spectroscopy*. Elsevier, 1970, pp. 235–345. DOI: 10.1016/b978-0-12-329850-8.50010-0.

[173] Mughabghab, S. F. “Nonstatistical Effects in Radiative Neutron Capture”. In: *Nuclear Structure Study with Neutrons*. Springer US, 1974, pp. 167–195. DOI: 10.1007/978-1-4613-4499-5_7.

[174] McCullagh, C. M., Stelts, M. L., and Chrien, R. E. “Dipole radiative strength functions from resonance neutron capture”. In: *Physical Review C* vol. 23, no. 4 (Apr. 1981), pp. 1394–1403. DOI: 10.1103/physrevc.23.1394.

[175] Kopecky, J. *Revision and Update of experimental Gamma-Ray Strength Functions Derived from the Discrete Neutron Resonance Capture*. Tech. rep. INDC(NDS)–0772. International Atomic Energy Agency (IAEA), 2018, p. 49. URL: http://inis.iaea.org/search/search.aspx?orig_q=RN:51035041.

[176] Kopecky, J. and Goriely, S. *Strength Functions Derived from The Discrete And Average Neutron Resonance Capture*. Tech. rep. INDC(NDS)–0790. International Atomic Energy Agency (IAEA), 2019, p. 82. URL: http://inis.iaea.org/search/search.aspx?orig_q=RN:51052829.

[177] Kopecky, J. *Atlas of Average Resonance Capture Data (Starter File)*. Tech. rep. INDC(NDS)–0738. International Atomic Energy Agency (IAEA), 2017, p. 46. URL: http://inis.iaea.org/search/search.aspx?orig_q=RN:49059860.

[178] Kopecky, J. *Present Status of Experimental Gamma-ray Strength Functions Derived from Neutron Capture*. Tech. rep. INDC(NED)-013. International Atomic Energy Agency (IAEA), 2016. URL: https://www-nds.iaea.org/publications/indc/indc-ned-0013/.

[179] Chrien, R. E. “Neutron Resonance Averaging with Filtered Beams”. In: *Neutron Induced Reactions*. Springer Netherlands, 1986, pp. 200–220. DOI: 10.1007/978-94-009-4636-1_24.

[180] Chrien, R. E. “Principles of resonance-averaged gamma-ray spectroscopy”. In: *Neutron-capture gamma-ray spectroscopy and related topics 1981*. BNL–30177. Jan. 1982, pp. 342–355. URL: https://www.osti.gov/servlets/purl/5967196.

[181] Kopecky, J. and Uhl, M. *Present status of experimental gamma-ray strength functions*. Tech. rep. ECN-RX–94-103. Netherlands, 1994, p. 26. URL: http://inis.iaea.org/search/search.aspx?orig_q=RN:27033357.

[182] Kopecky, J. *Photon Strength Functions in Thermal Neutron Capture*. Tech. rep. INDC(NDS)–0799. International Atomic Energy Agency (IAEA), 2020, p. 90. URL: http://inis.iaea.org/search/search.aspx?orig_q=RN:51052838.

[183] Hauser, W. and Feshbach, H. “The Inelastic Scattering of Neutrons”. In: *Physical Review* vol. 87, no. 2 (July 1952), pp. 366–373. DOI: 10.1103/physrev.87.366.

[184] Vonach, H. “Extraction Of Level Density Information From Non-resonant Reactions”. In: *Proceedings of the IAEA Advisory Group Meeting on Basic and Applied Problems of Nuclear Level Densities, Upton, NY, 1983*. BNL Report No. BNL-NCS-51694. 1983, p. 247.

[185] Voinov, A. V., Grimes, S. M., Brune, C. R., Hornish, M. J., Massey, T. N., and Salas, A. “Test of nuclear level density inputs for Hauser-Feshbach model calculations”. In: *Physical Review C* vol. 76 (2007). DOI: 10.1103/physrevc.76.044602.

[186] Byun, Y., Ramirez, A. P. D., Grimes, S. M., Voinov, A. V., Brune, C. R., and Massey, T. N. “Deuteron-induced reactions on ^{89}Y and nuclear level density of ^{90}Zr”. In: *Physical Review C* vol. 90, no. 4 (Oct. 2014). DOI: 10.1103/physrevc.90.044303.

[187] Ramirez, A. P. D., Voinov, A. V., Grimes, S. M., Byun, Y., Brune, C. R., Massey, T. N., Akhtar, S., Dhakal, S., and Parker, C. E. “Level density and mechanism of deuteron-induced reactions on ^{54,56,58}Fe”. In: *Physical Review C* vol. 92, no. 1 (July 2015). DOI: 10.1103/physrevc.92.014303.

[188] Ramirez, A. P. D., Voinov, A. V., Grimes, S. M., Schiller, A., Brune, C. R., Massey, T. N., and Salas-Bacci, A. “Nuclear level densities of ^{64,66}Zn from neutron evaporation”. In: *Physical Review C* vol. 88, no. 6 (Dec. 2013). DOI: 10.1103/physrevc.88.064324.

[189] Voinov, A. V., Grimes, S. M., Agvaanluvsan, U., Algin, E., Belgya, T., Brune, C. R., Guttormsen, M., Hornish, M. J., Massey, T., Mitchell, G. E., and al., et. “Level density of Fe56 and low-energy enhancement of γ-strength function”. In: *Physical Review C* vol. 74, no. 1 (July 2006). DOI: 10.1103/physrevc.74.014314.

[190] Voinov, A. V., Grimes, S. M., Larsen, A. C., Brune, C. R., Guttormsen, M., Massey, T., Schiller, A., Siem, S., and Syed, N. U. H. "Level densities of Sc44 and Ti47 from different experimental techniques". In: *Physical Review C* vol. 77, no. 3 (Mar. 2008). DOI: 10.1103/physrevc.77.034613.

[191] Santra, R., Dey, B., Roy, S., Laskar, M., Palit, R., Pai, H., Rajbanshi, S., Ali, S., Bhattacharjee, S., Babra, F., Mukherjee, A., Jadhav, S., Naidu, B. S., Vazhappilly, A. T., and Pal, S. "Nuclear level density of 69Zn from gamma gated particle spectrum and its implication on 68Zn(n, γ)69Zn capture cross section". In: *Physics Letters B* vol. 806 (July 2020), p. 135487. DOI: 10.1016/j.physletb.2020.135487.

[192] Ericson, T. "Fluctuations of Nuclear Cross Sections in the "Continuum" Region". In: *Physical Review Letters* vol. 5, no. 9 (Nov. 1960), pp. 430–431. DOI: 10.1103/physrevlett.5.430.

[193] Ericson, T. "A theory of fluctuations in nuclear cross sections". In: *Annals of Physics* vol. 23, no. 3 (Sept. 1963), pp. 390–414. DOI: 10.1016/0003-4916(63)90261-6.

[194] Ericson, T. and Mayer-Kuckuk, T. "Fluctuations in Nuclear Reactions". In: *Annual Review of Nuclear Science* vol. 16, no. 1 (Dec. 1966), pp. 183–206. DOI: 10.1146/annurev.ns.16.120166.001151.

[195] Mishra, V., Boukharouba, N., Grimes, S. M., Doctor, K., Pedroni, R. S., and Haight, R. C. "Determination of the level density of Si29 from Ericson fluctuations". In: *Physical Review C* vol. 44, no. 6 (Dec. 1991), pp. 2419–2425. DOI: 10.1103/physrevc.44.2419. Corrected in "Erratum: Determination of the level density of Si29 from Ericson fluctuations". In: *Physical Review C* vol. 47, no. 5 (May 1993), pp. 2426–2426. DOI: 10.1103/physrevc.47.2426.

[196] Salas-Bacci, A., Grimes, S. M., Massey, T. N., Parpottas, Y., Wheeler, R. T., and Oldendick, J. E. "Level widths and level densities in Si28, Ti46, Cr52, and Ni60 from Ericson fluctuations". In: *Physical Review C* vol. 70, no. 2 (Aug. 2004). DOI: 10.1103/physrevc.70.024311.

[197] Kawano, T., Capote, R., Hilaire, S., and Huu-Tai, P. C. "Statistical Hauser-Feshbach theory with width-fluctuation correction including direct reaction channels for neutron-induced reactions at low energies". In: *Physical Review C* vol. 94, no. 1 (July 2016). DOI: 10.1103/physrevc.94.014612.

[198] Moldauer, P. A. "Why the Hauser-Feshbach formula works". In: *Physical Review C* vol. 11, no. 2 (Feb. 1975), pp. 426–436. DOI: 10.1103/physrevc.11.426. Corrected in "Erratum: Why the Hauser-Feshbach formula works". In: *Physical Review C* vol. 13, no. 5 (May 1976), pp. 2093–2093. DOI: 10.1103/physrevc.13.2093.

[199] Hansen, P., Jonson, B., and Richter, A. "Applications of statistical nuclear physics to nuclear spectroscopy". In: *Nuclear Physics A* vol. 518, no. 1-2 (Nov. 1990), pp. 13–34. DOI: 10.1016/0375-9474(90)90532-q.

[200] Neumann-Cosel, P. von and Tamii, A. "Electric and magnetic dipole modes in high-resolution inelastic proton scattering at 0°". In: *The European Physical Journal A* vol. 55, no. 7 (July 2019). DOI: 10.1140/epja/i2019-12781-7.

[201] Kalmykov, Y., Özen, C., Langanke, K., Martínez-Pinedo, G., Neumann-Cosel, P. von, and Richter, A. "Spin- and Parity-Resolved Level Densities from the Fine Structure of Giant Resonances". In: *Physical Review Letters* vol. 99, no. 20 (Nov. 2007). DOI: 10.1103/physrevlett.99.202502.

[202] Descouvemont, P. and Baye, D. "The R-matrix theory". In: *Reports on Progress in Physics* vol. 73, no. 3 (Feb. 2010), p. 036301. DOI: 10.1088/0034-4885/73/3/036301.

[203] Lane, A. M. and Thomas, R. G. "R-Matrix Theory of Nuclear Reactions". In: *Rev. Mod. Phys.* Vol. 30, no. 2 (Apr. 1958), pp. 257–353. DOI: 10.1103/revmodphys.30.257.

[204] Wigner, E. P. "Resonance Reactions". In: *Physical Review* vol. 70, no. 9-10 (Nov. 1946), pp. 606–618. DOI: 10.1103/physrev.70.606.

[205] Wigner, E. P. and Eisenbud, L. "Higher Angular Momenta and Long Range Interaction in Resonance Reactions". In: *Physical Review* vol. 72, no. 1 (July 1947), pp. 29–41. DOI: 10.1103/physrev.72.29.

[206] Rochman, D., Goriely, S., Koning, A., and Ferroukhi, H. "Radiative neutron capture: Hauser Feshbach vs. statistical resonances". In: *Physics Letters B* vol. 764 (Jan. 2017), pp. 109–113. DOI: 10.1016/j.physletb.2016.11.018.

[207] Brown, D. et al. "ENDF/B-VIII.0: The 8 th Major Release of the Nuclear Reaction Data Library with CIELO-project Cross Sections, New Standards and Thermal Scattering Data". In: *Nuclear Data Sheets* vol. 148 (Feb. 2018), pp. 1–142. DOI: 10.1016/j.nds.2018.02.001.

[208] Kullmann, I. K. B., Larsen, A. C., Renstrøm, T., Beckmann, K. S., Garrote, F. L. B., Campo, L. C., Görgen, A., Guttormsen, M., Midtbø, J. E., Sahin, E., Siem, S., Tveten, G. M., and Zeiser, F. "First experimental constraint on the Os191(n,γ) reaction rate relevant to s -process nucleosynthesis". In: *Physical Review C* vol. 99, no. 6 (June 2019). DOI: 10.1103/physrevc.99.065806.

[209] Utsunomiya, H., Goriely, S., Kondo, T., Iwamoto, C., Akimune, H., Yamagata, T., Toyokawa, H., Harada, H., Kitatani, F., Lui, Y.-W., Larsen, A. C., Guttormsen, M., Koehler, P. E., Hilaire, S., Péru, S., Martini, M., and Koning, A. J. "Photoneutron cross sections for Mo isotopes: A step toward a unified understanding of (γ,n) and (n,γ) reactions". In: *Physical Review C* vol. 88, no. 1 (July 2013). DOI: 10.1103/physrevc.88.015805.

[210] Kheswa, B., Wiedeking, M., Giacoppo, F., Goriely, S., Guttormsen, M., Larsen, A., Bello Garrote, F., Eriksen, T., Görgen, A., Hagen, T., Koehler, P., Klintefjord, M., Nyhus, H., Papka, P., Renstrøm, T., Rose, S., Sahin, E., Siem, S., and Tornyi, T. "Galactic production of ^{138}La: Impact of ^{138,139}La statistical properties". In: *Physics Letters B* vol. 744 (May 2015), pp. 268–272. DOI: 10.1016/j.physletb.2015.03.065.

[211] Crespo Campo, L., Bello Garrote, F. L., Eriksen, T. K., Görgen, A., Guttormsen, M., Hadynska-Klek, K., Klintefjord, M., Larsen, A. C., Renstrøm, T., Sahin, E., Siem, S., Springer, A., Tornyi, T. G., and Tveten, G. M. "Statistical γ-decay properties of Ni64 and deduced (n,γ) cross section of the s-process branch-point nucleus Ni63". In: *Physical Review C* vol. 94, no. 4 (Oct. 2016), p. 044321. DOI: 10.1103/physrevc.94.044321.

[212] Larsen, A. C. et al. "Experimentally constrained (p,γ)Y89 and (n,γ)Y89 reaction rates relevant top-process nucleosynthesis". In: *Physical Review C* vol. 93, no. 4 (Apr. 2016). DOI: 10.1103/physrevc.93.045810.

[213] Spyrou, A., Larsen, A. C., Liddick, S. N., Naqvi, F., Crider, B. P., Dombos, A. C., Guttormsen, M., Bleuel, D. L., Couture, A., Campo, L. C., Lewis, R., Mosby, S., Mumpower, M. R., Perdikakis, G., Prokop, C. J., Quinn, S. J., Renstrøm, T., Siem, S., and Surman, R. "Neutron-capture rates for explosive nucleosynthesis: the case of 68Ni(n,γ)69Ni". In: *Journal of Physics G: Nuclear and Particle Physics* vol. 44, no. 4 (Feb. 2017), p. 044002. DOI: 10.1088/1361-6471/aa5ae7.

[214] Malatji, K. et al. "Re-estimation of 180Ta nucleosynthesis in light of newly constrained reaction rates". In: *Physics Letters B* vol. 791 (2019), pp. 403–408. DOI: https://doi.org/10.1016/j.physletb.2019.03.013.

[215] Tveten, G. M. et al. "Completing the nuclear reaction puzzle of the nucleosynthesis of Mo92". In: *Physical Review C* vol. 94, no. 2 (Aug. 2016). DOI: 10.1103/physrevc.94.025804.

[216] Bauge, E. et al. "Coherent investigation of nuclear data at CEA DAM: Theoretical models, experiments and evaluated data". In: *The European Physical Journal A* vol. 48, no. 8 (Aug. 2012). DOI: 10.1140/epja/i2012-12113-7.

[217] Chadwick, M., Herman, M., Obložinský, P., Dunn, M., Danon, Y., Kahler, A., Smith, D., Pritychenko, B., Arbanas, G., Arcilla, R., and al., et. "ENDF/B-VII.1 Nuclear Data for Science and Technology: Cross Sections, Covariances, Fission Product Yields and Decay Data". In: *Nuclear Data Sheets* vol. 112, no. 12 (Dec. 2011), pp. 2887–2996. DOI: 10.1016/j.nds.2011.11.002.

[218] Nobre, G. P., Sonzogni, A. A., and Brown, D. A. *Assessment of the current status of cross-section evaluations of plutonium minor isotopes*. Tech. rep. May 2019. DOI: 10.2172/1513540.

[219] Escher, J. E., Burke, J. T., Hughes, R. O., Scielzo, N. D., Casperson, R. J., Ota, S., Park, H. I., Saastamoinen, A., and Ross, T. J. "Constraining Neutron Capture Cross Sections for Unstable Nuclei with Surrogate Reaction Data and Theory". In: *Physical Review Letters* vol. 121, no. 5 (July 2018). DOI: 10.1103/physrevlett.121.052501.

[220] Ratkiewicz, A., Cizewski, J. A., Escher, J. E., Potel, G., Burke, J. T., Casperson, R. J., McCleskey, M., Austin, R. A. E., Burcher, S., Hughes, R. O., Manning, B., Pain, S. D., Peters, W. A., Rice, S., Ross, T. J., Scielzo, N. D., Shand, C., and Smith, K. "Towards Neutron Capture on Exotic Nuclei: Demonstrating (d,pγ) as a Surrogate Reaction for (n,γ)". In: *Physical Review Letters* vol. 122, no. 5 (Feb. 2019). DOI: 10.1103/physrevlett.122.052502.

[221] Escher, J. E., Burke, J. T., Dietrich, F. S., Scielzo, N. D., Thompson, I. J., and Younes, W. "Compound-nuclear reaction cross sections from surrogate measurements". In: *Rev. Mod. Phys.* Vol. 84, no. 1 (Mar. 2012), pp. 353–397. DOI: 10.1103/revmodphys.84.353.

[222] Potel, G., Perdikakis, G., Carlson, B. V., Atkinson, M. C., Dickhoff, W. H., Escher, J. E., Hussein, M. S., Lei, J., Li, W., Macchiavelli, A. O., Moro, A. M., Nunes, F. M., Pain, S. D., and Rotureau, J. "Toward a complete theory for predicting inclusive deuteron breakup away from stability". In: *The European Physical Journal A* vol. 53, no. 9 (Sept. 2017). DOI: 10.1140/epja/i2017-12371-9.

[223] Enders, J., Neumann-Cosel, P. von, Rangacharyulu, C., and Richter, A. "Parameter-free description of orbital magnetic dipole strength". In: *Physical Review C* vol. 71, no. 1 (Jan. 2005). DOI: 10.1103/physrevc.71.014306.

[224] Iudice, N. L. and Palumbo, F. "New Isovector Collective Modes in Deformed Nuclei". In: *Physical Review Letters* vol. 41, no. 22 (Nov. 1978), pp. 1532–1534. DOI: 10.1103/physrevlett.41.1532.

[225] Iachello, F. "Electron scattering in the interacting boson model". In: *Nuclear Physics A* vol. 358 (Apr. 1981), pp. 89–112. DOI: 10.1016/0375-9474(81)90308-0.

[226] Bohr, A. and Mottelson, B. R. *Nuclear structure: 2: Nuclear deformations*. eng. Vol. 2. New York: Benjamin, 1975.

[227] Bohle, D., Richter, A., Steffen, W., Dieperink, A., Iudice, N. L., Palumbo, F., and Scholten, O. "New magnetic dipole excitation mode studied in the heavy deformed nucleus 156Gd by inelastic electron scattering". In: *Physics Letters B* vol. 137, no. 1-2 (Mar. 1984), pp. 27–31. DOI: 10.1016/0370-2693(84)91099-2.

[228] Krtička, M., Wiedeking, M., Bečvář, F., and Valenta, S. "Consistency of photon strength function models with data from the ^{94}Mo(d,p$\gamma\gamma$) reaction". In: *Physical Review C* vol. 93, no. 5 (May 2016). DOI: 10.1103/physrevc.93.054311.

[229] Scholz, P., Guttormsen, M., Heim, F., Larsen, A. C., Mayer, J., Savran, D., Spieker, M., Tveten, G. M., Voinov, A. V., Wilhelmy, J., Zeiser, F., and Zilges, A. "Primary γ-ray intensities and γ-strength functions from discrete two-step γ-ray cascades in radiative proton-capture experiments". In: *Physical Review C* vol. 101, no. 4 (Apr. 2020). DOI: 10.1103/physrevc.101.045806.

[230] Wiedeking, M., Guttormsen, M., Larsen, A. C., Zeiser, F., Görgen, A., Liddick, S. N., Mücher, D., Siem, S., and Spyrou, A. "Independent Normalization for γ-ray Strength Functions: The Shape Method". In: (Oct. 24, 2020). submitted to PRC. arXiv: 2010.15696 [physics.data-an].

[231] Mücher, D. et al. "A novel approach for extracting model-independent nuclear level densities far from stability". In: (Nov. 2, 2020). submitted to PRL. arXiv: 2011.01071 [nucl-ex].

[232] Paulsen, W. "Reassessment of the radiative width of the Hoyle state from gamma ray spectroscopy using OSCAR". MA thesis. University of Oslo, Aug. 10, 2020.

[233] Martinez, G. D., McKay, J., Farmer, B., Scott, P., Roebber, E., Putze, A., and Conrad, J. "Comparison of statistical sampling methods with ScannerBit, the GAMBIT scanning module". In: *The European Physical Journal C* vol. 77, no. 11 (Nov. 2017). DOI: 10.1140/epjc/s10052-017-5274-y.

[234] Athron, P. et al. "GAMBIT: the global and modular beyond-the-standard-model inference tool". In: *The European Physical Journal C* vol. 77, no. 11 (Nov. 2017). DOI: 10.1140/epjc/s10052-017-5321-8.

[235] Gerbaudo, D., Helsens, C., and Rubbo, F. *PyFBU*. 2020. URL: https://github.com/pyFBU/fbu (visited on 11/09/2020).

[236] Choudalakis, G. "Fully Bayesian Unfolding". In: (Jan. 22, 2012). arXiv: 201.4612v4 [physics.data-an].

[237] Breit, G. and Wigner, E. "Capture of Slow Neutrons". In: *Physical Review* vol. 49, no. 7 (Apr. 1936), pp. 519–531. DOI: 10.1103/physrev.49.519.

[238] Axel, P. "Giant Resonances And Some Related Gamma-ray Decay Rates: A 1979 Status Report". In: *Transactions of the New York Academy of Sciences* vol. 40, no. 1 Series II (Sept. 1980), pp. 20–39. DOI: 10.1111/j.2164-0947.1980.tb02997.x.

[239] Carpenter, R. T. *The Electric-dipole Gamma-ray Strength Function For Heavy Even-even Nuclei*. Tech. rep. Aug. 1962. DOI: 10.2172/4787158.

[240] Zeiser, F., Tveten, G. M., Bello Garrote, F. L., Guttormsen, M., Larsen, A. C., Ingeberg, V. W., Görgen, A., and Siem, S. "The γ-ray energy response of the Oslo Scintillator Array OSCAR". In: *Nuclear Instruments and Methods in Physics Research Section A: Accelerators, Spectrometers, Detectors and Associated Equipment* (Sept. 2020), p. 164678. DOI: 10.1016/j.nima.2020.164678.